The ADEMA project comprised a programme of integrated research seeking to enhance mining exploration and planning capability. The main topics studied were seismic processing, radio imaging, drilling parameter analysis, micro-seismic activity and predictive analysis.

Oil industry techniques have been adapted to the coal environment. 3D seismic data have been reprocessed for inversion and modelling projects and refined for lithology classification schemes. Additionally, a new seismic inversion method, known as ADAPS, which uses pattern recognition to extract the seismic wavelet, has been developed and applied. The AVP inversion method has been developed enabling derivation of rock properties. Software has been developed to generate impedance data which, when correlated with boreholes, provide a lithology indicator.

Radio imaging methods have been analysed. An extensive appraisal of electromagnetic propagation in coal seams has been completed, prototype transmitting equipment built and the parameters of the coal seam medium measured, using several different types of equipment.

Drilling parameters have been defined from drilling equipment. They have been combined to obtain a specific energy and drilling exponent, which can be correlated with mechanical properties of the rock mass. An increase in specific energy with the rock quality was observed.

A 64-channel, flameproof seismic observation system, incorporating new low-frequency geophones, has been installed in a Polish coalmine. Evolutionary tomographic algorithms have allowed the construction of velocity images for the surrounding rocks, providing a method for the location of seismic hazard zones in coalmines.

A programme of cored underground boreholes, samples and geological observations has been undertaken to validate the sedimentary model generated from the re-processed seismic volume.

KI-NA-24217-EN-C

Price (excluding VAT) in Luxembourg: EUR 7

Publications Office

ISBN 978-92-79-14549-0

9 789279 145490

EC

ADEMA: Advances in exploration methods and applications

EUR 24217

EUROPEAN COMMISSION

European Research Area

ADEMA: Advances in exploration methods and applications

Research Fund for Coal & Steel

Interested in European research?

RTD info is our quarterly magazine keeping you in touch with main developments (results, programmes, events, etc.). It is available in English, French and German. A free sample copy or free subscription can be obtained from:

Directorate-General for Research
Information and Communication Unit
European Commission
B-1049 Brussels
Fax (32-2) 29-58220
E-mail: research@ec.europa.eu
Internet: http://ec.europa.eu/research/rtdinfo/index_en.html

How to obtain EU publications

Free publications:

- via EU Bookshop (http://bookshop.europa.eu);
- at the European Commission's representations or delegations. You can obtain their contact details by linking http://ec.europa.eu or by sending a fax to +352 2929-42758.

Publications for sale:

- via EU Bookshop (http://bookshop.europa.eu);
- Priced subscriptions (Official Journal of the EU, Legal cases of the Court of Justice as well as certain periodicals edited by the European Commission) can be ordered from one of our sales agents. You can obtain their contact details by linking http://bookshop.europa.eu, or by sending a fax to +352 2929-42758.

EUROPEAN COMMISSION
Directorate-General for Research
Research Fund for Coal and Steel Unit

Contact: RFCS publications
Address: European Commission, CDMA 0/124, B-1049 Brussels
Fax (32-2) 29-65987; e-mail: rtd-steel@ec.europa.eu

European Commission

Research Fund for Coal and Steel

ADEMA: Advances in exploration methods and applications

J. Wilson, T. Jowitt ([1]), J. Galera, C. Muñoz ([2]), A. Lurka, G. Mutke ([3]),
S. Lavu, R. Limacher, R. McHugh, P. Olden, R. Westerman ([4]),
M. Bedford, D. Brenkley, J. Ford, D. Gibson ([5]), A. Fogg ([6]),
T. Benedictus, S. Dortland, B. Orlic, F. van Bergen, B. Wassing, P. Winthaegen ([7])

([1]) **UK Coal Mining Ltd —** Harworth Park, Blyth Road, Harworth, Doncaster DN11 8DB, UNITED KINGDOM
([2]) **Geocontrol SA —** Cristóbal Bordiú 19-21 5 °, 28003 Madrid, SPAIN
([3]) **Glowny Instytut Gornictwa —** Jednostka Badawczo-Rozwojowa, Plac Gwarków 1, 40 166 Katowice, POLAND
([4]) **Heriot-Watt University —** Riccarton, Edinburgh EH14 4AS, UNITED KINGDOM
([5]) **Mines Rescue Service Ltd —** Leeming Lane South, Mansfield Woodhouse, Mansfield NG19 9AQ, UNITED KINGDOM
([6]) **Seismic Image Processing —** Crossweys, 28–30 High Street, Guildford GU1 3EL, UNITED KINGDOM
([7]) **Nederlandse Organisatie voor Toegepast Natuurwetenschappelijk Onderzoek (TNO) —** Princetonlaan 6, 3584 CB Utrecht, NETHERLANDS

Contract No RFCR-CT-2005-00001
1 July 2006 to 30 June 2008

Final report

Directorate-General for Research

2010 EUR 24217 EN

Europe Direct is a service to help you find answers to your questions about the European Union

Freephone number (*)**:**

00 800 6 7 8 9 10 11

(*) Certain mobile telephone operators do not allow access to 00 800 numbers or these calls may be billed.

A great deal of additional information on the European Union is available on the Internet. It can be accessed through the Europa server (http://europa.eu).

Cataloguing data can be found at the end of this publication.

Luxembourg: Publications Office of the European Union, 2010

ISBN 978-92-79-14549-0

doi:10.2777/884

ISSN 1018-5593

Printed in Luxembourg

PRINTED ON WHITE CHLORINE-FREE PAPER

Table of Contents

1 Final Summary

1.1 WP1 Project Set Up

Work Package 1 was associated with initial scoping, set-up and review matters. As such, this work package largely concerns background tasks, and only key points are noted here for brevity.

In Task 1.1 (Literature and state-of-the-art review) work continued throughout the first two years of the ADEMA project with extensive discussions and workshops between partners when significant issues arose. An example here is the knowledge gap in the rock physics properties of coals. Inspection of the legacy database of British Coal Corporation roof rock properties confirmed that there is almost no equivalent data available for coal. This topic was addressed in Work Package 6.

In Task 1.2 (Analysis of current coal versus oil/gas modelling techniques) it was concluded that 'Petrel' was the preferred platform for modelling the case study from existing data, as TNO, HWU and SIP all had access to licenses. UKC and SIP supplied the borehole and post-stack seismic data for the model, which was built and updated as new data became available.

Task 1.3 (Reprocessing and interpretation of 3D seismic dataset) was completed by SIP after discussion of the pre-stack data quality with UKC, HWU & GIG. The reprocessing was completed successfully, serving as the basis for subsequent studies.

Task 1.4 (Build acoustic array technology) was completed and the equipment used to calibrate angle versus- offset (AVO) acoustic effects in coal, sandstone and mud rock core samples.

Task 1.5 (Investigate technical limitations of in-seam radio imaging) focussed on an investigation of the issues limiting the scope of application of seam tomographic radio imaging in the UK and EU. It aimed to identify criteria for image resolution and uncertainty and to report on aspects such as the limiting geo-electrical properties of basinal seam structures, signal acquisition performance limitations, maturity of tomographic reconstruction and interpretation methodologies. Tomographic radio imaging is widely used in the United States and Australia, but it has not been widely deployed in the British and European coal industries. The results of the literature survey were used to obtain an initial view of which factors were likely to affect the deployment of radio imaging methods, and whether practical improvements would be possible, leading to the potential for a wider deployment of the technique in Europe. This work is further reported in Work Packages 5 and 6.

Task 1.6 (Drilling equipment sourcing and setup) was completed by Geocontrol, who acquired logging tools and drilling parameter recorder equipment. This equipment was successfully deployed for the subsequent extensive drilling measurement and characterisation programme.

Task 1.7 (Identification of a suitable site for mine seismicity and rock burst analysis) was completed by GIG. The selected site had a significant history of rock burst activity and provided a representative trial site for all subsequent monitoring activity, resulting eventually in a significant database of recorded micro-seismic events.

1.2 WP2 Acoustic Impedance Inversion

In Task 2.1 (Development of AI inversion to coal exploration using commercially available software) the development of Acoustic Inversion techniques in relation to coal geology was achieved. Analysis of the inversion results for the Daw Mill data has confirmed that post-stack inversion of seismic data is more stable than pre-stack inversion. Additionally a classification of the log properties in terms of impedance has been carried out. This is enabling UK Coal to interpret the Daw Mill impedance volume in terms of dominant roof strata above the main Warwickshire Thick coal seam as either sandstone or mudstone/siltstone. The technique has been successful in identifying increased dirt split within the coal seam where splits greater than 1.5 m were present.

In Task 2.2 (Development of the ADAPS AI inversion technique). The ADAPS software was fully developed and applied to a set of 40 lines of the Daw Mill dataset. The results of the inversion have been supplied to UK Coal for integration with their interpretation of the volume, with specific regard to the identification of faults.

During the life of the project several factors such as layer thickness, impedance contrasts and lateral variations in the velocity models where tested with synthetic data for their effect on the AVP signature. Especially the effect of thin layers is of importance, due to the tuning effect of the Thick Coal Seam. Due to tuning it is difficult to discriminate between AVP effects caused by variations within the coal seam or effects caused by variations in the lithology directly above or below the seam. This work was undertaken in **Task 2.3** (Development of AVP inversion technique).

1.3 WP3 DEVELOPMENT OF MICRO-SEISMIC SYSTEM

In mines with high seismic hazard it is vital to introduce a high quality monitoring system. The overall concept of Work Package 3 was not only to develop equipment to automatically record mining tremors, but also to implement modern software techniques to data analysis. This particularly applied to analysis of the images of P-wave velocity with time, providing an opportunity to assess zones of seismic hazard. The overall goals of the work were therefore to construct a specific tomography algorithm and software to calculate velocity images of the affected rock in underground mines subject to significant rock burst activity. Passive seismic tomography calculations were used to study the locations of dangerous seismic zones in the vicinity of a coalface.

The 64 channel flameproof and low cost micro-seismic hazard monitoring system was designed by GIG, with the specification discussed with partners. The system was intended as a management tool to evaluate rock-burst hazard (**Task 3.1**). The Seismological Observation System 'SOS' provides an efficient tool for transmission, recording and analysis of seismic events that occurred in underground mines. The system comprised an underground and a surface subsystem. The underground subsystem comprised the DLM measuring probes (low frequency geophones) in combination with the signal amplifiers and converters for transmitting seismic signals in the form of current signals via mine transmission lines. The surface subsystem comprised the DLM-SO Receiving Station which is connected with the Seismic Recording System. The hardware implements 'intelligent' automatic triggering and faithfully captures and records mining seismic events. Multilok and Seisgram software are used in respect of the system data acquisition and data processing. This provides information concerning source parameters and the 3D location of the originating seismic events. The software tools were integrated into the SOS seismic system as part of the development work.

The trial real-time seismic monitoring system SOS was installed in Wujek-Slask mine. During continuous measurements taken between July 2007 and 2008, more than 700 strong seismic events have been recorded from the panel of longwall 2JD and between June 2006 and 2007 more than 1000 seismic events from the panel of longwall 8 L (seismic energy: Es > 1 kJ, local magnitude ML > 0.6). Revised software was implemented to analyse the seismic events,including 3D location and seismic source parameters. After testing this was then implemented in the SOS equipment (**Task 3.4**).

The process of passive tomography calculations for the bulk of the recorded data is unstable. To address this an evolutionary algorithms were applied (**Task 3.2**). These algorithms are well adapted to optimisation problems with a large number of variables. The evolutionary algorithm showed itself to be much more efficient and much more accurate than algebraic reconstruction algorithms (ART). There is clear superiority of the velocity images using the evolutionary algorithm. The algorithm was adapted and implemented within the SOS equipment.

Much of the work has been concerned with the analysis of velocity images to assess areas of rock mass instability together with a review of the real-time seismic monitoring system. Hundreds of seismic events collected by the SOS seismic network were used to calculate velocity images in rocks.

The velocity images were used to determine seismic prone area in the test mine and to assess zones of seismic hazard. The first image of P-wave field velocity calculated in December 2007 showed the existence of a few zones with a high velocity value. The zone with the highest value appeared 200 m before line of the coalface. The second image was calculated on 15 April 2008. The highest seismic anomaly appeared just before the line of the coalface and 200 m north-west of the coalface at the boundary between mined and un-mined area near the gallery 1JD. On 16 April 2008 a collapse in the gallery of longwall panel 2JD took place. The rock-burst event provided direct verification of the effectiveness of the tomography forecast process. It turned out that damage appearing in the gallery 1JD was generally in the place associated with the greatest seismic anomaly activity calculated on 15 April 2008. The hypercentre of rock-burst activity took place on the high velocity gradient to the north-east of the area of damage. Study of P-wave velocity in the longwall panel area 2JD has shown that the anomaly of seismic velocity was moving with time. Epicentres of shocks were located in the area of the anomaly of highest velocity calculated in December 2007 and in April 2008. The seismic hazard zones depend on high seismic wave velocity and a high gradient of seismic wave velocity in the area of mining. Backward analysis showed that the passive tomography was maintaining the improved quality in the forecasts of zones subject to seismic hazard. Images of the P-wave velocity and the real-time seismologic monitoring also allow testing and validation to be applied regarding the effectiveness of rock-burst prevention methods. The application of evolutionary algorithms in tomography calculations is a completely novel approach and is undoubtedly an innovation in work safety problems in mines.

1.4 WP4 In Situ Drilling and Geophysical Logging

The research within Work Package 4 has confirmed that recording drilling parameters is a useful and economical technique for acquiring geotechnical information of ground parameters. The drilling equipment monitors, measures and records drilling parameters for analysis of ground conditions.

Within this work package, rock mass properties were investigated extensively; this involved the collection of underground borehole data and samples, and testing was carried out in several boreholes to obtain drilling parameters data. Some results were used to compare geophysical logs to rock mass properties and the linkage to drilling parameters. Equipment was acquired to provide field measurements for analysis and correlation with rock mass properties.

Correlations were investigated between specific energy and the geophysical well logging parameters in relation to the quality of rock mass. Specific energy was the main index related with all drilling parameters. It was analysed in respect of RMR, number of joints per metre, Young's modulus of the rock mass and uni-axial compressive strength of the rock mass.

These correlations showed that specific energy depends strongly on the geomechanical rock mass quality expressed by the RMR and the number of joints per metre. Higher values of specific energy are associated with high rock mass quality. Additionally, RQD gives high scatter in relation to specific energy. This approach is considered a valuable tool for rock mass characterisation. For example, the higher the number of joints per metre, the lower are the values of Esp. A further important observation is the clear influence of the lithology on the values of Esp observed.

From full wave sonic measurements, wave velocity data (Vp and Vs) were obtained that defines the dynamic elastic deformational parameters of the rock, where in this case it was used to obtain the Young's modulus. The dynamic Young's modulus, in relation to the specific energy and RMR, shows good results with the lithologies analysed; the greater the values of this modulus, the greater the values of specific energy. Additionally, the dynamic Young's modulus of the rock mass has been correlated with the static ones obtained from dilatometers used in-situ tests. Finally the correlation obtained between Vp and specific energy provides the basis of a valuable tool and approach for rock characterisation purposes.

1.5 WP5 RADIO IMAGING (SIGNAL TRANSMISSION AND ACQUISITION)

The main objective of this work package was to determine the factors that limited the deployment of the Radio Imaging Method (RIM) for detection of anomalies in coal seams, and whether practical improvements were possible, leading to the possibility for wider deployment. A second, subsidiary topic of research was to study methods of automating the deployment, current injection and signal retrieval from large-array resistivity measurement schemes, with linear or 2D arrays of electrodes.

It should be emphasised that the techniques investigated in this work package are applicable to *any* circumstance where electromagnetic waves are propagating in a conducting medium. The techniques are therefore applicable not only to conventional RIM technology, but to any new development of the technology.

In Task 5.1 (Novel Approaches to Optimise Frequency and Transmission Characteristics) a detailed study of the RIM techniques was undertaken with reference to key papers from past researchers. Studies indicated that the primary factor limiting the definition obtainable from the earlier RIM trials in the UK was that the reduction in the probe frequency caused an increase in the skin depth in the surrounding rock. This resulted in out-of-seam geological structures having an unwanted effect on the received signals. It was therefore concluded that the most significant improvements to the RIM technique would be achieved by means of transmitter optimisation and receiver signal-processing. A number of novel techniques were devised and this resulted in two patent applications, as mentioned below.

Although initial results suggested that there might be some merit in using ferrite or amorphous metal in a transmitting antenna, it was established that the main benefit of this type of antenna would be at the receiver; and only in favourably low-noise conditions. Although not suitable for the present project, it was concluded that amorphous metal could be of considerable benefit where the receiver antenna is of necessity very small (e.g. personnel-mounted communications receivers), and that this could be a fruitful area for further study.

In Task 5.2 (Transmitter Research and Broadband Induction Loop Antenna Design) improvements to the transmitter antenna of a RIM system were investigated. Prior to this, data was collected on contemporary magnetic induction loop antennas used for through-seam transmissions. This data was assessed and used to give an indication of the increase in size and power that might be required to achieve propagation in the high-conductivity environment present in European mines.

It was deduced that there is merit in departing from the conventional view, that the transmitter should be a tuned induction loop, and that an untuned single-turn antenna could be utilised. Various unconventional antennas were investigated, including the anapole (a multi-turn toroid), rotating magnets and current-injection antennas. An analysis of the contact resistance of a rod-shaped electrode, compared with the contact resistance of a flat plate, lead to the novel suggestion of using conductive cushioning foam to form a flat-plate contact antenna. As a further method of utilising electric or current dipoles, it was noted that materials have become readily available with an extremely high relative permittivity (i.e. dielectric constant). A novel antenna was constructed from ceramic tiles and found to perform favourably.

In Task 5.3 (Radio Imaging Receiver and Signal Acquisition Research) several methods of increasing the processing gain at the receiver were investigated and modelled, including the use of wideband signals. It was discovered that correlation techniques could be used to enhance the transmission distance across the coal panel and to achieve system synchronisation. However, it was observed that the reconstruction of the signal using these DSP processes was of questionable use for tomographic purposes because amplitude and phase information was lost during the process. The techniques show promise for low-rate data transmission, but will be difficult to apply to RIM surveying. However, in a novel development, it was realised that the property of dispersion could itself be used for provide data for a tomographic reconstruction. A patent was filed on the use of a dispersion-based technique to

eliminate the need for a synchronisation channel and to provide input for a tomographic reconstruction.

Consideration was given to the unwanted coupling of signals into the metallic mine infrastructure. Methods were devised for testing the conjecture that an infrastructure-guided wave would be difficult to excite even though such parasitic interference is currently perceived to be a significant problem in RIM surveys, requiring expensive counter-measures. The most significant method of eliminating such interference was considered to be the novel use of a current-injection antenna to increase the level of the wanted signals and to help confine them to the coal panel.

In Task 5.4 (Advanced Coding Techniques) the effect of signal dispersion on the cross-correlation product of a transmitted sequence and its inverse was evaluated. There was some indication that, under certain conditions, e.g. seam height, conductivity of the medium, the correlation peaks due to multi-path propagation may be sufficiently well-spaced to permit the data to be fully separated in time, and this could be an area for further study. However, an interim conclusion that multipath effects could be eliminated or perhaps even made use was withdrawn in favour of the recommendations that (i) a non-ideal sequence should be used for sounding or synchronisation purposes only, and (ii) the tomographic measurements should utilise a very narrow bandwidth spot frequency method, rather than the de-spreading of a spread-spectrum sequence. It was concluded that for conventional RIM surveying, using a spot frequency, the two most significant advances are a large transmitter and a narrow-band receiver, with the narrow bandwidth obtained by means of a lengthy sampling time, DSP-based filtering and signal averaging.

In Task 5.5 (Underground Application Considerations), and as an adjunct to research into RIM enhancements, the ADEMA project investigated the use of a multi-electrode array, such as is used for conventional electrical resistivity tomography (ERT). The salient point, which is a novel and important result for this project, is that the proposed ERT system design has converged with that of a RIM system. Essentially, the system would behave in a similar way to RIM, but with the advantage of higher signal levels because the current is injected directly into the coal seam, instead of being coupled inductively from a magnetic loop antenna. A number of additional operational advantages were also cited.

It was envisaged that the electrodes for a multi-electrode ERT network could be constructed of a conductive plastic and left permanently in place in the coal seam, where the cut fragments would eventually be removed during the coal washing process. A patent application covering this and other aspects of the use of ERT electrodes in coal mines was filed during the course of this project.

1.6 WP6 RADIO IMAGING (TOMOGRAPHIC RECONSTRUCTION)

Initial investigations led to the conclusion that gains from enhanced image reconstruction techniques required a fundamental understanding of how the RIM transmission channel was established and how it varied as a function of frequency, seam parameters and type of coal seam anomaly. A decision was made to realign the objectives of WP6; work on RIM tomographic reconstruction algorithms was subsequently redirected to undertake more advanced modelling investigations, designed to better understand the basic imaging problem.

The wave propagation phenomenon of the Radio Imaging method (RIM) through a coal seam was fully modelled to assess the effectiveness of the RIM technique for detecting flaws or anomalies. The range of coal and shale losses (electrical conductivity) for productive use of RIM was determined. For typical ranges of coal and shale conductivity found in European mines, the power dissipation in the coal and shale layers has been reported. For a low loss coalmine scenario RIM signal sensing has been modelled for various flaw types. It was found that RIM signal propagation is severely distorted when high loss coalmine scenarios are modelled or metal work is introduced into the channel boundaries. These distortion effects make tomographic post-processing of RIM data inappropriate. The

conclusions reached from studies of RIM modelling led subsequently to an examination of an alternate strategy for fault detection in coal seams; the GEM (Guided Electro Magnetic wave) technique. A patent application covering this technique was filed during the course of this project.

GEM uses conducting boundaries along coal panel faces in the roadways to form a rectangular waveguide within which a modal pattern is generated. The GEM principle was modelled for a variety of flaw types. Excitation issues for GEM modal formation along with the power levels required to establish resonance were studied. As with the RIM work the range of electrical conductivity of the coal and shale for undistorted GEM operation was determined. The extensive modelling work, conducted with considerable mathematical rigour, has provided a fundamental insight into the application issues surrounding RIM and has also given an insight into the applicability of GEM in deep mine coal panel survey scenarios.

1.7 WP7 MODELLING

A three-dimensional shared earth model of the selected case study site – the Daw Mill Colliery – was constructed with the software application Petrel using the oilfield approach. The model was continuously updated during the lifetime of the project and it was accessible through a shared online workspace. Using a shared earth modelling approach developed in the oil and gas industry proved to be an efficient way for visualisation and communication of the results among the project partners in the current coal mining-related project.

The oilfield-based approach was successfully applied to lithological interpretation and determination of the elastic rock material properties from borehole logs at Daw Mill. Lithological interpretation relying on gamma ray, sonic and bulk density logs was found to be more consistent and accurate than lithological determination based on visual inspection of drilling cuttings. Besides lithology, log data were also utilised to derive elastic properties of the rock along the borehole trajectories. This indirect, non-destructive method for determination of the elastic rock properties complements and strengthens the commonly used direct method, which relies on rock mechanics tests on samples. Lithological interpretation and geomechanical rock characterisation based on borehole logs at Daw Mill was used to develop geomechanical numerical models.

Two geomechanical numerical models were developed to predict mining induced stress changes and associated deformation around a mine cavity in coal. The benchmark models generally resemble the geological setting and rock material properties at Daw Mill. The project partners involved in geomechanical modelling used different numerical tools in simulations. The performance of the tools was assessed by comparing simulation results with an existing empirical solution or with each other. Benchmark 1 – *Subsidence above longwall coal mine* – is a synthetic case of subsidence prediction above a longwall coalmine. In Benchmark 1 the best match was obtained with the subsidence profile calculated with the finite difference code FLAC. Benchmark 2 – *Induced changes in stresses and deformations around mining caverns in coal* – investigated the influence of different roof strata lithologies on stress distribution and deformation around a cavern in coal. The simulation results obtained by using the finite element packages (SavFem and Diana) and the finite difference package FLAC were in this case very similar. It was noted that inhomogeneous roof strata lithology largely affects the extent of plasticity and fractured zones above the cavity. Mudstones, which are generally weaker than sandstones, promote development of more extensive plasticity zones in the roof than sandstones, especially in sequences of coal layers in-between mudstones. The key material properties that largely determine the extent of plasticity and fractured zones around the modelled cavity are the tensile and shear strength of each rock type in the roof strata sequence.

1.8 WP8 GEOLOGICAL VALIDATION

The collection of data from a series of underground and surface boreholes and their collation has allowed a comprehensive database of geological information to be assembled and variations in the coal seam and adjacent strata to be mapped. The mapped geological data has been compared with impedance data derived from a 3D seismic survey. A comparison of the impedance with the geological data has allowed the investigation of coal thickness roof variations, seam splits, small faults and floor rolls. There is a correlation with some geological features and changes in character of the impedance sections. The impedance data has allowed some differentiation between amplitude anomalies observed on the seismic data not otherwise observable. These include an area of major seam split in 300's development, a shear zone around Keatleys Pool borehole where the seam is present twice in the borehole, a major zone, extending through the south of 400's block of seam split, and general changes in the character of roof sedimentation. The impedance data has allowed some differentiation between amplitude anomalies observed on the seismic data not otherwise available although the detection of smaller scale faulting has not been improved.

Laboratory measurement of static rock properties has been carried out on both core material and block samples obtained from the cases study site at Daw Mill

Evaluation of seismic characteristics in relation to gas content: A model was developed to compare the effects of gas content in coal and applied to the conditions at Daw Mill. Characteristics of the model and seismic results were compared to predict variations of gas content in the thick coal, but because either, the expected modelled variations were too small or the seismic inversion resolution too low, no satisfactory variations in gas content were measured. The results obtained from Coal samples taken at Daw Mill showed that the gas content of the coal is generally low

Use acoustic array technology to calibrate AVO: A laboratory system to calculate AVO was developed. However, no valid results were obtained for the rocks tested but the instrumentation and processing techniques were established for future research.

Validate reconstructed coal seam map from RIM: Suitable transmission and receiving test equipment was developed but underground trials could not be facilitated due to the safety rules in place at the mine test site.

1.9 WP9 PROJECT ASSESSMENT AND CONCLUSIONS

The review of information and evaluation of the results of the project are included in WP 9.

2 Scientific and Technical Description of the Results

2.1 OBJECTIVES OF THE PROJECT

2.1.1 WP1 Project Set Up

This package aimed to complete the evaluation of existing research work and techniques to provide the input for the initiation of the different work packages. It was necessary to complete the analysis of coal and oilfield modelling techniques, reprocess the available seismic data and build a 3D model of the case study area, and evaluate the radio imaging method of coal seam surveying. Also a laboratory system was required to investigate the sonic properties of coal measure rocks. A set of drilling and logging equipment and a mine site for seismicity studies was needed.

2.1.2 WP2 Acoustic Impedance Inversion

This task was to investigate methods of deriving acoustic impedance properties of rock using commercially available software, and to investigate the effects of rock properties on seismic data. A new inversion method called ADAPS was to be developed.

2.1.3 WP3 Development of Micro-seismic System

Firstly to develop a low-cost 32 or 64 channel micro seismic network to provide an efficient tool for transmission, recording and analysis of seismic events that occurred in underground mines and to develop algorithms for tomographic analysis using Evolutionary techniques. Analysis of the resulting velocity images enabled the identification of areas of higher potential rock-mass instability. Additionally the development, in real time seismic monitoring, of new software for analysis of induced seismic events.

2.1.4 WP4 In Situ Drilling and Geophysical Logging

A set of commercial drilling equipment was acquired so that methods of combining data from drilling records with geophysical logging tools could be developed and geotechnical information be obtained from open boreholes drilled in the course of mining. Two approaches were developed, using specific drilling energy, and the drilling exponent used in oil exploration. Correlations with rock mass mechanical properties were obtained from drilling parameters and geophysical logs. Methods would then be employed at a case study site and compared with other techniques developed in this project.

2.1.5 WP5 Radio Imaging (Signal Transmission and Acquisition)

The main objective of this work package was to determine the factors that limited the deployment of radio imaging methods, and whether practical improvements were possible, leading to the possibility for wider deployment. A second, subsidiary topic of research was to study methods of automating the deployment, current injection and signal retrieval from large-array resistivity measurement schemes, with linear or 2D arrays of electrodes.

2.1.6 WP6 Radio Imaging (Tomographic Reconstruction Techniques)

Tomographic image reconstruction techniques are used to infer the spatial distribution of conductivity in the measured region of a radio imaging survey. However, geophysical imaging is an under-constrained inverse problem, mainly because of the sparse and limited data coverage. Typically, measurements are not recorded for a complete set of angles due to the physical limitations of access and other logistical constraints. To improve the reconstruction problem, a number of approaches are

possible, which include the use of full wave tomography inversion processing algorithms in reconstruction rather than techniques assuming straight ray path assumptions. Improvements in tomography reconstruction algorithms will lead to improved resolution, and in particular lateral resolution.

2.1.7 WP7 Modelling

The objectives of the modelling package include the development of geomechanical numerical models in order to predict mining induced stress changes and associated deformation around a mine cavity in coal, and to deliver additional information for improved interpretation of seismic data for better geophysical and geomechanical characterisation of the rock. Assessment of the subsurface and surface deformation and related anthropogenic geological hazards is focussed on the three main application areas, conventional long-wall extraction, underground coal gasification and coal bed methane production. The construction of a shared earth model for efficient communication of results among partners was accessible through a shared on line workspace. An additional task was to identify predictive capabilities of radio imaging techniques.

2.1.8 WP8 Geological Validation

To collect geological information in order to calibrate the results of the exploration techniques investigated in the project. Laboratory testing were used for rock burst analysis, evaluation of seismic characteristics, acoustic array calibration, and acoustic impedance inversion.

2.1.9 WP9 Project Assessment and Conclusions

The task aims were to assess the results of the other packages, and to prepare the final report

2.2 COMPARISON OF INITIALLY PLANNED ACTIVITIES AND WORK ACCOMPLISHED

Deviations form the initial project plan occurred in Work Packages 5, 6 and 8, as summarised below.

In Work Package 5 the work that was accomplished broadly followed the initial plan, except where conclusions drawn from earlier work necessitated a change in the direction of the research. For example, in Task 5.3 it was determined that broadband techniques, whilst suited to communications and system identification, could not readily be applied to RIM-based tomography because of the large degree of dispersion of the signals. This resulted in the work of Task 5.4 being re-directed to some extent and the evaluation of the processing gain of a broadband system in Task 5.5 was curtailed. However, the noted dispersion of the radio signals led to a further avenue of work and a proposal for a novel method of system synchronisation. Some changes to Task 5.5 were brought about by the difficulty of finding an appropriate underground location at which to perform experimental tests. In particular, access to a return roadway was not possible due to restrictions on equipment that could be operated in a hazardous atmosphere. However, within the scope of the project it was still possible to draw significant conclusions from the work. In Task 5.5 it was originally proposed that results would incorporate resistivity, P- and S-wave information from samples in Polish, Spanish and UK mines. This pre-supposed that it would be possible to obtain a full set of RIM (or allied) data and to perform a tomographic reconstruction from it. In practice this was not possible due to the restrictions on operation of equipment, explained above.

In Work Package 6 the first phase of work led to the conclusion that any additional gains from enhanced image reconstruction techniques required a fundamental understanding of how the RIM transmission channel was established and how it varied as a function of frequency, seam parameters and type of coal seam anomaly. It was therefore the considered view of the project partners that directing effort to further improving RIM tomographic reconstruction algorithms would not assist in solving RIM operational deficiencies. As a consequence of these findings, the work within WP6 was subsequently redirected to undertake more advanced modelling investigations, designed to better understand the basic imaging problem. This work was extensive in scope; modelling both the RIM channel electrical parameters and signals, together with developing a resonant waveguide imaging technique (which was given the acronym GEM) for an entirely new method of coal seam excitation. The GEM method employs a waveguide technique rather than the transmission line technique of RIM and is considered to offer advantages in coal seams that feature low electrical losses where the necessarily higher excitation frequencies can be sustained.

Task 8.7 was not possible to complete because of the necessary departures from the work programme in Work Packages 5 and 6.

2.3 DESCRIPTION OF ACTIVITIES AND DISCUSSION

2.3.1 WP1 Project Set Up

2.3.1.1 Literature and state-of-the-art review (T1.1)

This task continued to the end of the project, the accumulated database and results were shared among all the project partners.

2.3.1.2 Analysis of modelling techniques (T1.2)

(Analysis of current coal versus oil/gas modelling techniques and construction of initial 3D model at case study site)

The Petrel system was chosen as the preferred platform for modelling.

2.3.1.3 Reprocessing and interpretation of 3D seismic dataset (T1.3)

(Reprocessing and interpretation of 3D seismic dataset at case study site)

This task was completed by SIP and copied to other partners as required

2.3.1.4 Build acoustic array technology (T1.4)

The technical aspect of the triaxial cell modification was successful, the two main problems being ultrasonic attenuation and noise. In order to perform experimental investigations of AVO response in the laboratory a test set was constructed as shown in the *Figure* below. This comprised a 120 mm diameter by 160 mm high test cylinder with thirty (12 degree) spaced hole positions around the perimeter into which 1 MHz acoustic transducers are placed. One transducer acts as a transmitter and the receiving transducer(s) are located at a variety of angular positions relative to the acoustic source. A 1 MHz acoustic frequency was chosen as a compromise between acoustic attenuation and acoustic wavelength in the test material. A bilithic specimen, typically consisting of a coal/shale slice was intended to be used within the cylinder transducer acts as a transmitter and the receiving transducer(s) are located at a variety of angular positions relative to the acoustic source. A 1 MHz acoustic frequency was chosen as a compromise between acoustic attenuation and acoustic wavelength in the test material. A bilithic specimen, typically consisting of a coal/shale slice was intended to be used within the cylinder.

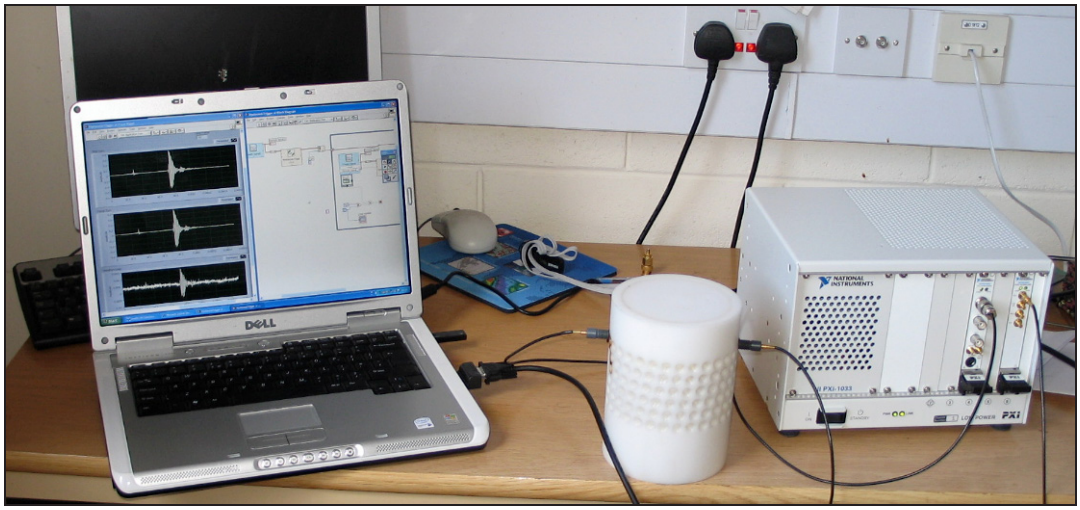

Figure 2.3.1–1 : Laboratory AVO Acoustic Test Set

National Instrument kit with programmed with Labview to improve the Signal to noise ratio by stacking. From right to left, figure shows the NI instrument box for generating and recording the ultrasonic signal, the white sensitive sleeve with a cylindrical blank of the same plastic material as an ideal acoustic medium for reference purposes, the laptop, which triggers the NI box and stacks the output data traces. The screen shows from bottom to top: the recorded single-fold signal; the cumulative stack and the final stack.

SNR improvements are achieved using signal-stacking techniques, as shown in the *Figure* below. SNR improves with the number of records taken in the stack; in practice a 60 dB improvement was achieved using 10,000 records. These results confirm the theory modelled.

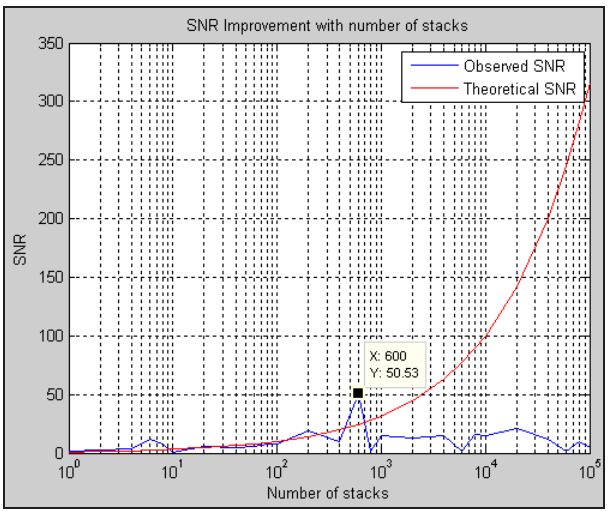

Figure 2.3.1–2 : SNR improvements achieved using signal stacking techniques
An estimate of the signal to noise ratio is plotted as a blue line compared with the theoretical ($\sqrt{}$number of traces stacked) improvement as a red line. The results match the theory up to a fold of stack of 600.

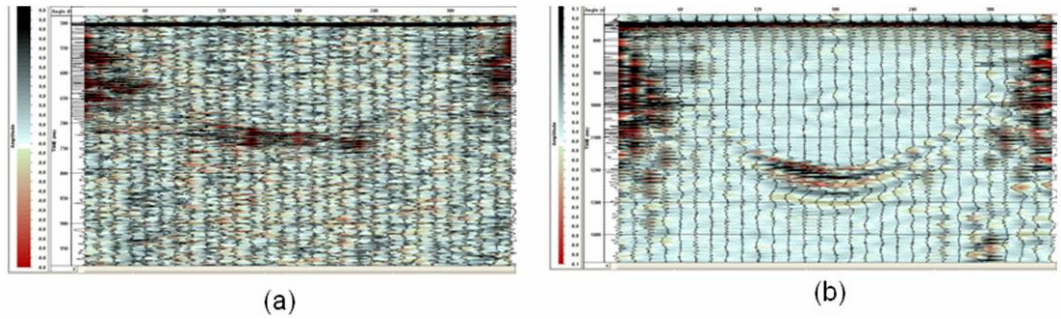

Figure 2.3.1–3 : Triaxial cell records for a saturated coal sample
(a) un-stacked record, (b) stacked record; illustrating the SNR improvement

The size and frequency of the ultrasonic transducers was inevitably a compromise. The custom made transducers overall footprint limited the ultrasonic transmit source level and created a directional transducer with a beam width of approximately 18 degrees.

In experiments with sandstone water injection proved to be insufficient to eliminate air within the voids in the sandstone. The limited ultrasonic transducers source level combined with air voids within the material meant that it was not possible to achieve a successful experiment with sandstone samples. This result was disappointing; however the instrumentation and stacking techniques are established for future research; all that is required is a source of more powerful ultrasonic transducers.

A graphical user interfaced (GUI) Comsol Multiphysics program was developed for three reasons...

- The forward modelling process is repetitive and needs automating.
- The GUI is also easier for both Comsol Multiphysics users and non-users as it provides helpful hints on appropriate parameterisation.
- The model not only computes ultrasonic propagation but also the conversion of strain to electrical signal in each piezo-electric crystal.

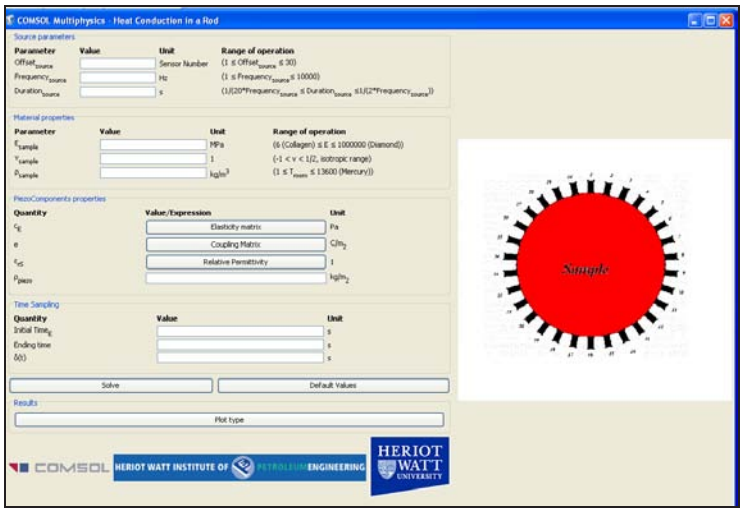

Figure 2.3.1-4 : Comsol Multiphysics GUI

The step of converting from strain to electrical signal could have been neglected, whilst still producing a suite of output traces. However, the angular difference between the polarisation of the acoustic wave particle motion and the orientation of the piezo-electric crystal would not then have been explicitly resolved.

It is now possible to compare the laboratory results with a forward model. That opens the possibility of a future inversion to predict acoustic strain from electrical signal.

2.3.1.5 Investigate technical limitations of in-seam radio imaging (T1.5)

Tomographic radio imaging is widely used in the United States and Australia, but it has not been widely deployed in the British and European coal industries. The results of the literature survey were used to obtain an initial view of which factors were likely to affect the deployment of radio imaging methods, and whether practical improvements would be possible, leading to the potential for a wider deployment of the technique in Europe.

The initial conclusion was that it appeared, on the basis of the information available, that the current generation of equipment (RIM-IV) was certainly capable of producing tomograms that correlated sufficiently well with geological features and anomalies for mine operational planning purposes. However such performance had not been observed in UK trials. A number of reasons for the less favourable performance in the UK (compared to other geographical regions) were identified for further research, which included the geo-electric property of coal-to-rock electrical conductivity ratio and the signal-acquisition requirement of a very low bandwidth. Additionally, the high electrical conductivity of the coal itself was considered to be an issue. A detailed study of these factors was undertaken in Work Packages 5 and 6.

2.3.1.6 Drilling equipment sourcing and set up (T1.6)

This task was completed by GEO, who acquired logging tools and drilling parameter recorder equipment for the purpose.

2.3.1.7 Identification of a suitable site for mine seismicity and rock-burst analysis (T1.7)

This task was completed by GIG.

2.3.2 WP2 Acoustic Impedance Inversion

(Acoustic Impedance inversion and extraction of rock properties from seismic data)

2.3.2.1 Development of AI inversion to coal exploration using commercially available software (T2.1)

Analysis of the inversion results for Daw Mill has confirmed that post-stack inversion of seismic data is more stable than pre-stack inversion. This is due to the limited range of offsets and useable live data fold in the pre-stack data. Pre-stack seismic data conditioning has enabled significantly greater resolution to be achieved from the post-stack seismic inversion when compared with an inversion of the originally processed Daw Mill post-stack volume. Additionally a classification of the log properties in terms of impedance has been carried out. This is enabling UK Coal to interpret the Daw Mill impedance volume in terms of dominant roof strata above the main Warwickshire Thick coal seam as either sandstone or mudstone/siltstone.

Figure 2.3.2-1 depicts a comparison at the EAVES GREEN #1 of recorded borehole data and that predicted by the inversion indicating that the coal and roof strata can be predicted. Six boreholes were used in the inversion parameterisation to ensure the inversion could account for spatial variation.

Figure 2.3.1–2 depicts the inversion result at the EAVES GREEN #1 borehole and the corresponding seismic impedance profile. There is good agreement between the borehole impedance and that of the seismic. Both the thin Half Yard and main Warwickshire Thick coal seam are resolved. Using borehole logs for the six wells used in the inversion study an initial classification scheme has been developed to characterise the Daw Mill *3D* impedance volume in terms rock type: sand, shale/silt/mudstone, and coal. *Figure 2.3.2-4* displays the basis of the classification scheme where the logs have been aligned at the top main coal and cut-off between rock types chosen at 6000 and 9000 mg/scc (see vertical scales).

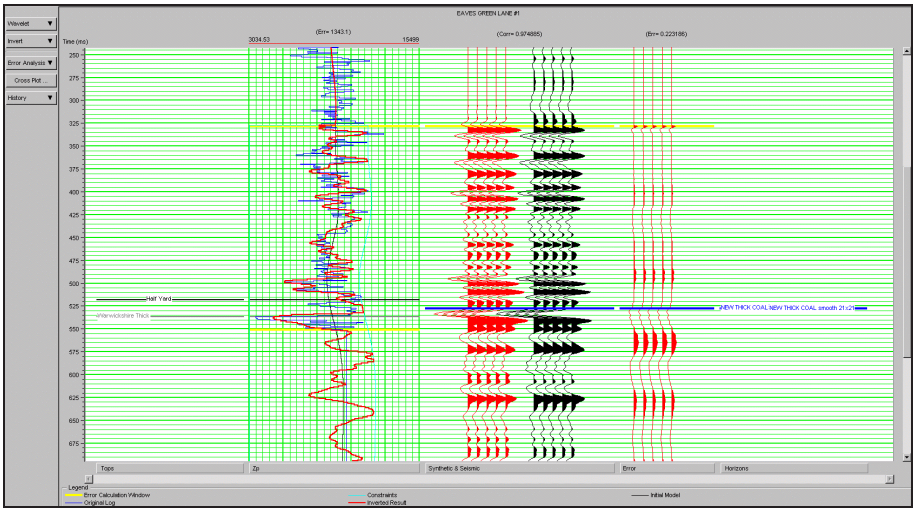

Figure 2.3.2-1 : Borehole logs

Comparison of borehole logs (blue) and inversion results (red) for p-impedance with display of seismic (black) and synthetic based on inversion result (red). There is a good match between the logs indicating the inversion can successfully predict the coal seam and roof.

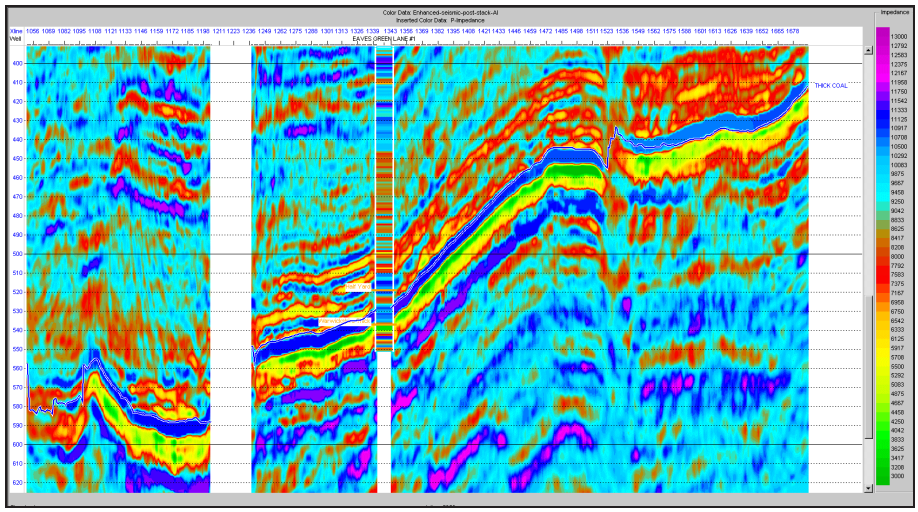

Figure 2.3.2-2 : P-impedance results, Eaves Green #1 borehole
P-impedance results for sub line through the Eaves Green #1 borehole. To the left of the section the coal (rendered yellow/green) is faulted out. To the right of the section the missing coal is a mined panel zone.

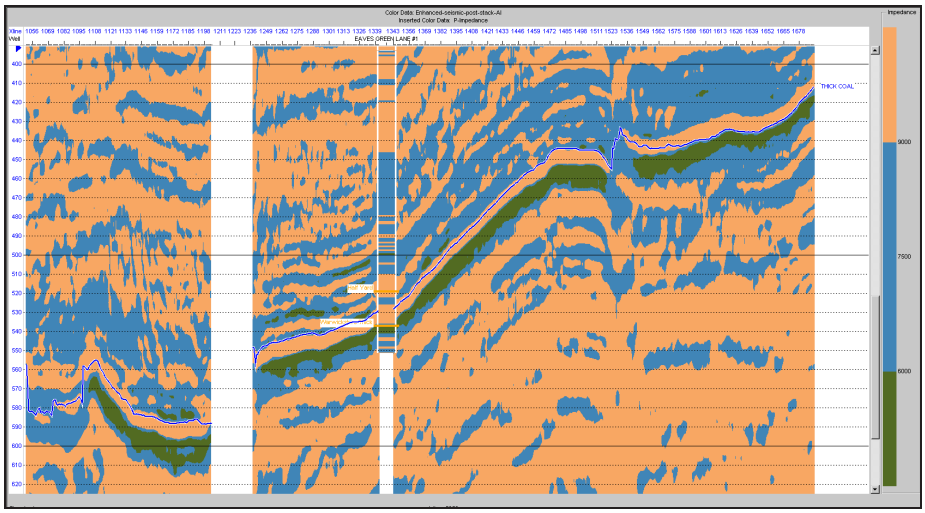

Figure 2.3.2-3 : P-impedance results, Eaves Green #1 borehole
The colour scale is now rendered to represent different rock types as per the nominal classification scheme in Figure 2.3.2-4.

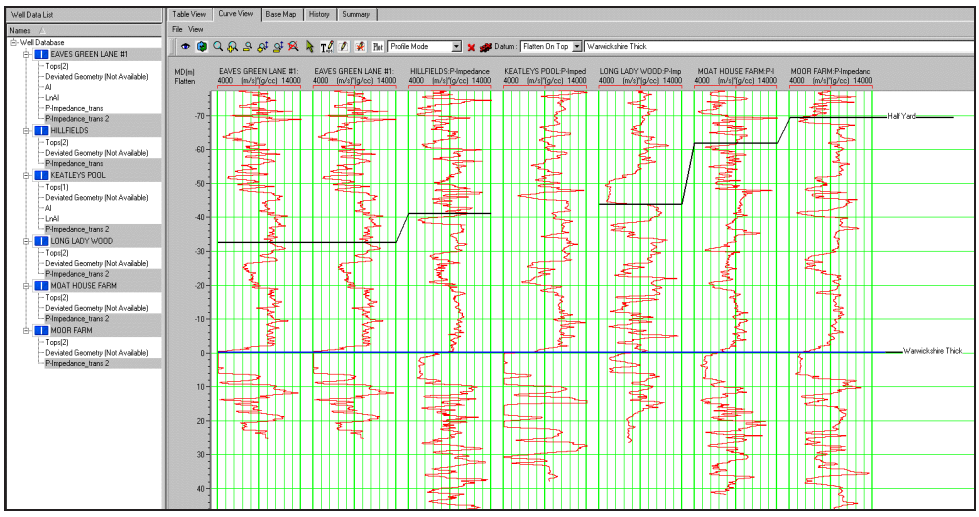

Figure 2.3.2-4 : Lithological classification scheme based on well logs.
Coals show a very low impedance (< 3000 mg/scc), whereas sands show a high impedance (> 6000 mg/scc).

2.3.2.2 Development of the ADAPS AI inversion technique (T2.2)

Software has been fully developed and applied to a set of 40 lines of the Daw Mill dataset. The results of the inversion have been supplied to UK Coal for integration with their interpretation of the volume, with specific regard to the identification of faults.

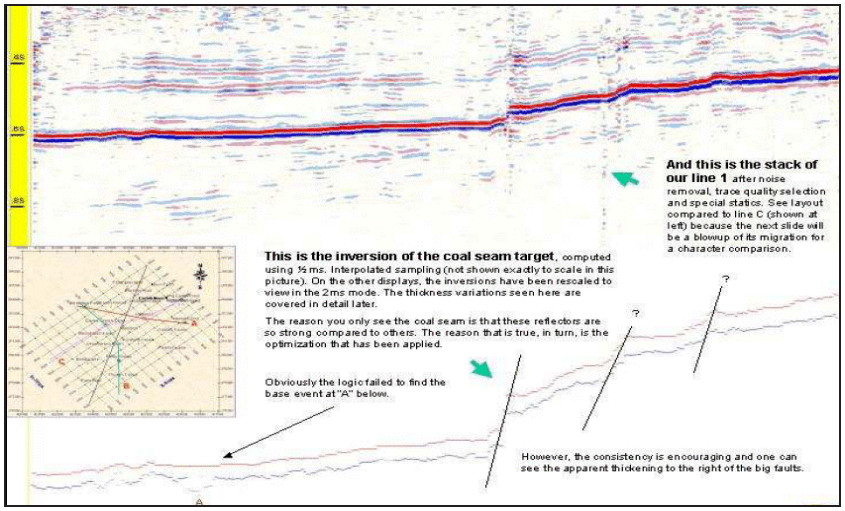

Figure 2.3.2-5 : Application of ADAPS inversion to post-stack seismic data at Daw Mill. The inversion resolves the top and base of the seam (lower part of the display) which is zoomed vertically to indicate potential fault displacement.

2.3.2.3 Development of AVP inversion technique (T2.3)

Amplitude versus Ray parameter (p) is a pre-stack amplitude analysis technique to be used for seismic inversion. The software is intended for R&D and is not commercially available. Several issues occurred when applying this technique to the Daw Mill seismic data: the pre-stack data have a sparse fold; the investigated seismic reflection shows tuning effects of adjacent reflectors, signal to noise is relatively low. Additionally, the coal reflection shows strong variation in depth, which is actually favourable for the AVP technique as it considers the response of reflection points instead of CMP's. Because of irregular spatial sampling and the above mentioned issues the AVP technique did not provided the expected results. By averaging over an area of reflection points (e.g. using the CMP approach) an estimate of the reflection amplitude with ray parameter or angle can be obtained. This should then be followed by elastic impedance inversion. This method strongly depends on the applied velocity model and the tuning effect remains.

During the ADEMA project several factors such as layer thickness, impedance contrasts and lateral variations in the velocity models where tested with synthetic data for their effect on the AVP signature. Especially the effect of thin layers is of importance, due to the tuning effect of the Thick Coal Seam, as was also investigated by SIP (see interim reports). Due to tuning it is difficult to discriminate between AVP effects caused by variations within the coal seam or effects caused by variations in the lithology directly above or below the seam (*Figure 2.3.2-6*).

Therefore, in this task, synthetic seismic data was generated by using a simplified model based on the Hillfields well logs (*Table 2.3.2-1*). This model was also used in WP 8 to investigate the effect of the presence of gas in the Thick Coal Seam on the seismic response. The reflections at the top and bottom of the Thick Coal Seam show a strong interference and show up as one reflection. The reflection at the top of Unnamed 1 is only just visible as separate event from the Thick Coal Seam. This interference influences the AVP as well, shown in *Figure 2.3.2-6*. The curvature and amplitude of the AVP curve changes due to interference (tuning). It therefore also affects the inversion for rock parameters.

Stratigraphy	Z_top (MD in m)	Z_bottom (MD in m)	Thickness (m)	Density (kg/m3)	P-wave (m/s)	S-wave (m/s)
Overburden	0.0	758.0	758.0	2500	3000	1500
Unnamed 1	758.0	799.0	41.0	2600	3810	1905
Thick Coal Seam	799.0	805.0	6.0	1400	2540	1037
Unnamed 2	805.0	-	-	2650	3586	1793

Table 2.3.2-1 : Simplified model based on Hillfields

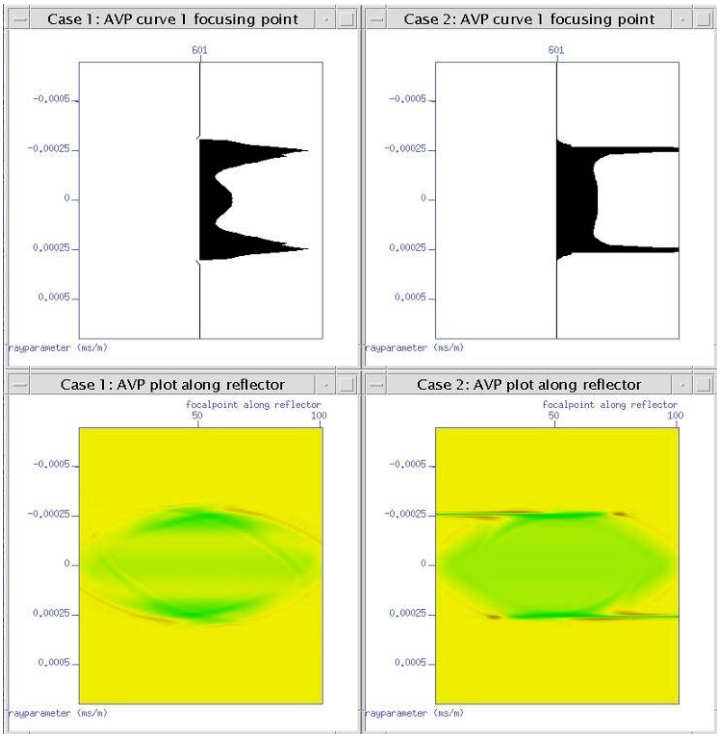

Figure 2.3.2-6 : AVP response

AVP response of the first reflector (top of Unnamed 1) for interfering reflectors (left) and a single reflector (right). All pictures are on the same scale.

2.3.2.4 Extraction of rock properties from seismic data (T2.4)

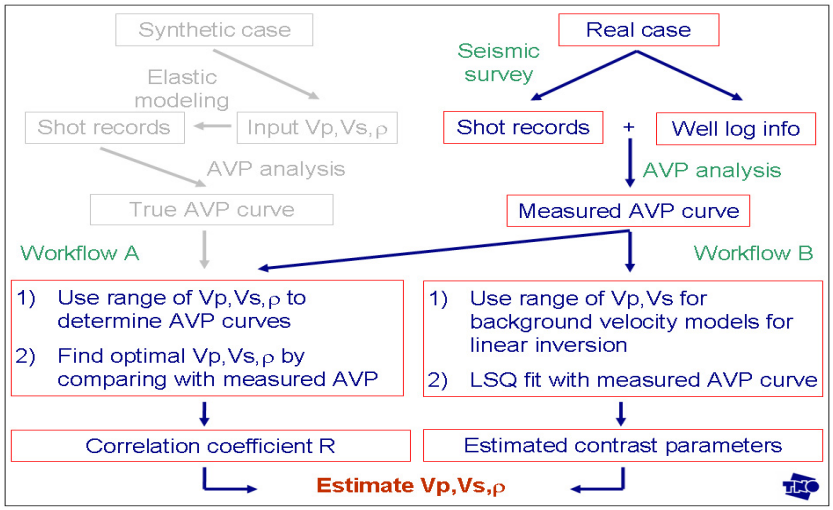

Figure 2.3.2-7 : AVP inversion technique

In the *Figure* above, a schematic overview is given of an approach to extract rock properties from seismic data, using the AVP inversion technique. The approach can be used both on real data and synthetic data. In this report an example is given using synthetic data as a real case.

AVP analysis

The AVP inversion technique can, theoretically, be used to extract rock properties from seismic data (see schematic overview in *Figure 2.3.2-7*). The approach can be used both on real data and synthetic data. Results show that, with some knowledge about velocities in the first layer, the P-wave velocity in the second layer can be estimated within 75 m/s with 90% confidence ($R^2 \geq 0.9$). This is shown in the *Figure* below, in which, in colour is shown the value of the estimated Vp2/Vp1 ratio, derived from the contrast parameters obtained from curve fitting with the average background model based on different combinations of Vp1 and Vp2. Black contour lines show the coefficient of determination R^2 for the correlation between modeled AVP curves with different Vp1-Vp2 combinations and the measured AVP curve, for a p-range of 0 – 0.00030 [ms/m]. The black dot denotes the location of the true model.

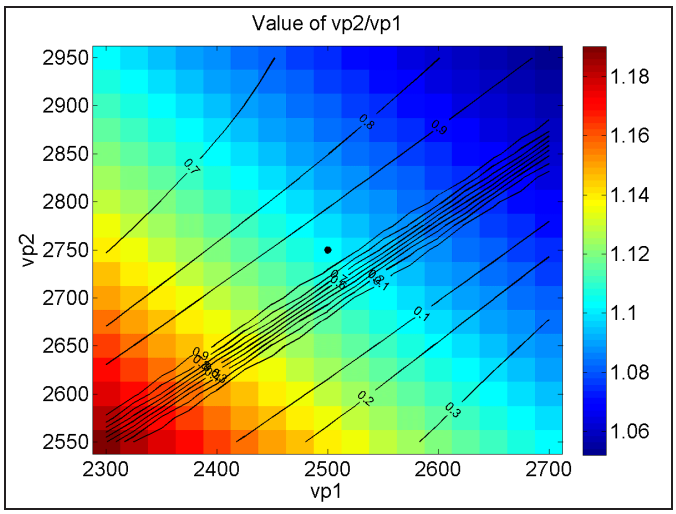

Figure 2.3.2-8 : Estimate of P-wave velocity

2.3.3 WP3 Development of Micro-seismic System

(Development of micro-seismic system for the continuous observation of seismic hazard in the longwall zones on the basis of passive tomography images)

2.3.3.1 Development of low-cost 32 or 64 channel micro-seismic network (T3.1)

The 64 channel Seismic Observation System (SOS) was designed and built in the Central Mining Institute (GIG). The prototype of the SOS system was installed in the Wujek-Slask Mine in the Upper Silesian Basin (Poland). The Seismological Observation System provides a new efficient tool for the transmission, recording and analysis of seismic events that occur in underground mines. The underground components comprise the DLM mobile and low frequency sensor probes and a signal transmitter. These probes replaced the previously used seismometers in coal mines which were expensive and heavy. The surface component of the system comprises the DLM-SO Receiving Station which is connected to the AS-Seisgram Seismic Recording System. The hardware allows automatic triggering and recording of the mining induced seismic events. Multilok and Seisgram software allows the data acquisition and data processing systems to provide source parameters and *3D* locations of seismic events in mines. The software tools were integrated into the SOS seismic system.

Each block of the DLM-SO Receiving Station comprises 16 sensors and seismic receivers, each receiver being connected with one DLM seismic sensor. Two blocks can be connected to 32 channels or four blocks to 64 channels. The seismic events, in the AS-Seisgram seismic recording system, are automatically picked and stored in the computer memory. The Seismic Observation System (SOS) has been designed as flameproof equipment and ATEX certified. Further reporting on this topic is given in an appendix to this report.

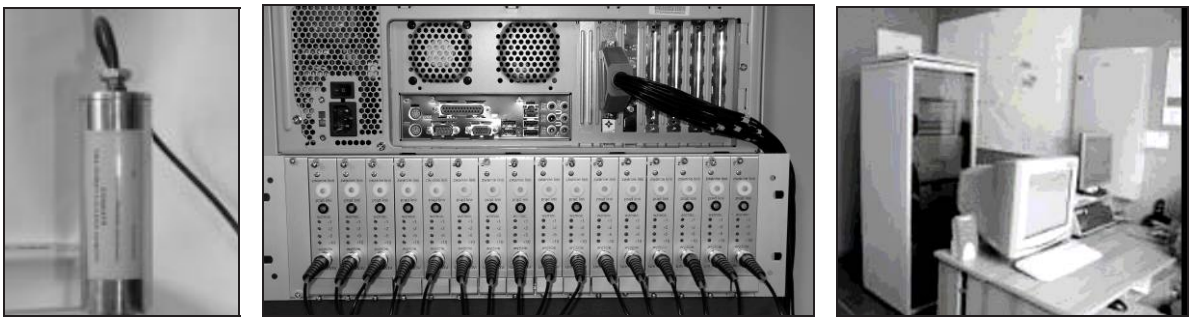

Figure 2.3.3-1 : Low frequency DLM geophone apparatus
Low frequency DLM geophone probe (natural frequency 1 Hz), seismic signal receiver station DLM-SO, and AS-Seisgram seismic recording system, developed during the project.

2.3.3.2 Development of evolutionary algorithms for passive tomography calculations (T3.2)

A new technique to image temporal velocity changes, with passively monitored induced micro seismicity, is proposed to delineate the areas of high seismic hazard. Passive travel-time tomography utilises seismic events as sources in a simultaneous inversion for event locations and velocity structure determination. Good coverage of seismic ray paths from zones of high seismicity induced by mining was obtained from the remote sensors outside the immediate mining area.

An evolutionary algorithm for tomography calculation was developed and the algorithm was adapted to the SOS equipment. The approach to solve passive tomography calculations was performed using a misfit function based on the L1 norm. The L1 norm was selected over the least squares norm L2 as it is much less sensitive to the effects of large errors in outlier data. The number of variables of the tomography misfit function is a few hundred, or more, for typical passive tomography problems. To find the minimum of this function, evolutionary algorithms are used that are well adapted for optimisation problems with a large number of variables (Schwefel, 1995). The evolutionary algorithm

performance was compared with that of algebraic reconstruction algorithms. The velocity images using the evolutionary algorithm are superior to the ART solutions.

The software for tomographic calculation using the evolutionary algorithm was developed and integrated into the SOS seismic system. The application of evolutionary algorithms in tomography calculations is new and represents an innovation in the solution of mine safety problems.

Further reporting on this topic is given in an appendix to this report.

2.3.3.3 Analysis of the velocity images to assess areas of rock mass instability and areas of high seismic hazard (T3.3)

The velocity images were calculated using all of the seismic events recorded from longwall panel 2JD, from 1 July 2007 to 30 April 2008.The software developed using the evolutionary algorithm and L1 norm were used for tomographic calculation. Velocity images were used to predict zones of higher seismicity in Longwall 2JD at the Wujek-Slask mine, assuming that the P-wave velocity increases with higher pressure in the rock . More seismic events being generated in zones of higher pressure!

The first image of the P-wave velocity field, calculated in December 2007, showed the existence of zones with high velocity values (zones I, II, III and IV). The highest velocity values appeared 200 m in advance of the coalface (zone I). The second image was calculated on 15 April 2008. The highest seismic anomalies appeared just before the line of the coalface (zone I) and 200 m north-east of the coalface at the boundary between the mined and un-mined area near the gallery 1JD (zone IV). The velocity images are shown in the *Figure* below. On 16 April 2008 a collapse occurred in gallery 1JD of longwall panel 2JD at the 85 m segment, approximately at the location of the greatest seismic anomaly calculated on 15 April 2008. The rock burst event verified the effectiveness of the tomography forecast. The hypercentre of the rock burst took place on the high velocity gradient located north-east of the area of damage.

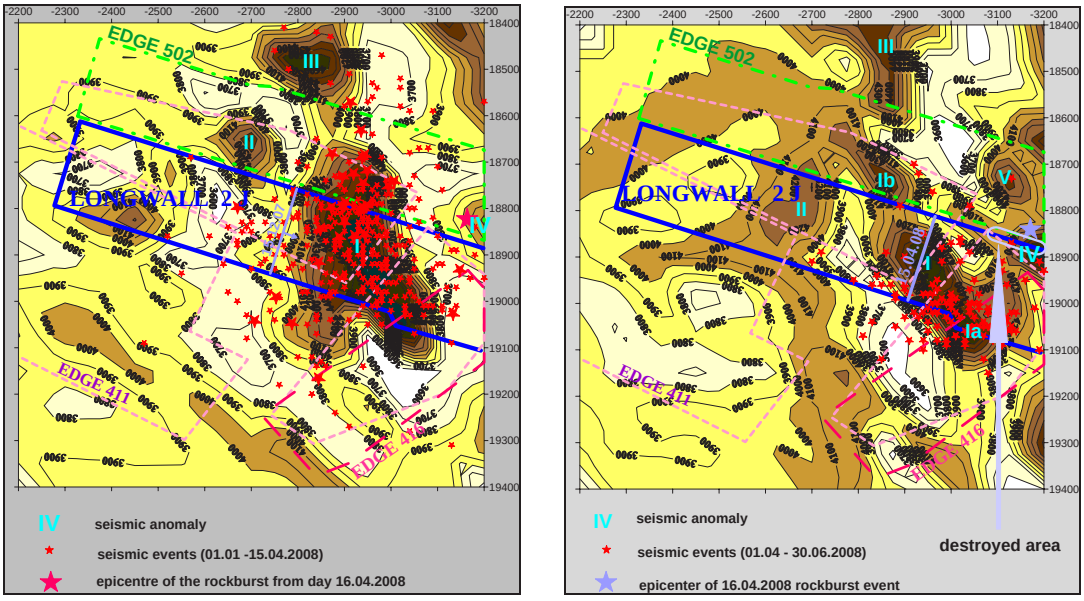

Figure 2.3.3-2 : Velocity image results from passive tomography

Longwall 2JD – velocity image results from passive tomography based on tremors recorded from July to December 2007 (the stars indicate tremors occurred during the next 3 months: January-March 2008) – left site picture and recorded from January to April 2008 (the stars indicate tremors occurred during the next three months: April-Jun 2008) – right site picture

The stars on the pictures indicate tremors that occurred in longwall panel 2JD during the next three months after calculation sessions. It can be seen that seismic activity took place only in the high velocity zones. Backward analysis showed that passive tomography was improving data quality and availability, into predicted zones of potential high seismic hazard.

Further reporting on this topic is given in an appendix to this report.

2.3.3.4 Real time seismic monitoring (T3.4)

(Implementation of real-time seismic monitoring system as a management tool to evaluate rock-burst hazards)

The real-time seismic monitoring system was installed in the Wujek-Slask mine allowing almost two years of continuous measurements. From 1 July 2007 to 30 April 30 2008, more than 700 seismic events from the area of longwall 2JD, seam 502, were recorded. From June 2006 to July 2007 more than 1000 seismic events from the area of longwall 8 L, seam 510. (Seismic Energy: Es > 1 kJ, Local Magnitude M_L > 0.6). The system's database contains co-ordinates of each seismic event, time of origin and seismic energy. All recorded seismic events in the database from longwall 2JD, were used as input data to tomography calculations.

A new method of processing the seismic data was developed and implemented enabling the calculation of source parameters and location of mining tremors. Seisgram, is the software for the acquisition and data processing of seismic signals and MultiLok, the software for the analysis of tremor parameters.

Further reporting on this topic is given in an appendix to this report.

2.3.4 WP4 In Situ Drilling and Geophysical Logging

(Integrated benefit of combining geophysical logging tools and in-situ drilling records)

2.3.4.1 Field measurements of drilling parameters, geophysical logging and comparison of results (T4.1)

Drilling parameters were measured and geophysical logging tools used at the following boreholes...

- PFM-5, 6, 7 and 8 (20, 11, 13.95, 13 m), for set up purposes.
- BH0 (117 m) at a clayly flysch formation, for set up purposes.
- BH-1 (80 m) at a carboniferous formation.
- BH-2 (227.5 m) at a metamorphic formation.
- BH-3 (210 m) at marls, schist and vulcanites.
- BH-4 (64.2 m) at sandstones, shales and coal seams. This borehole is located in the Bierzo Coal Basin at the Union Minera del Norte (UMINSA) which was drilled for this project.

From the available tools, the parameters of acoustic televiewer, full waveform sonic and resistivity were chosen. From these tools the data obtained is useful to characterise discontinuities and natural rock stresses, and to estimate the mechanical rock mass parameters (strength and deformability).

Further reporting on this topic is given in an appendix to this report.

2.3.4.2 Correlation with rock mass mechanical properties (T4.2)

The parameters used are related to the rock masses indexes:

- Rock Mass Rating (RMR)
- Number of Joints per metre.
- Rock Mass Uniaxial Compressive Strength (σ_c^m).

The relationships between the Rock Mass Indexes, Drilling Parameters, and Geophysical Well Logs, have been analyzed in the following correlations:

a) In relation to the data obtained from Drilling Parameters.

Specific Energy (Esp.) is the main index related with drilling parameters. It has been analyzed with respect to RMR, Number Joints per metre, Young Modulus (E.dyn.) and Rock Mass Uniaxial Compressive Strength (σ_c^m). These correlations can be observed below.

Specific Energy (Esp.) with respect to RMR and Number of Joints per metre:

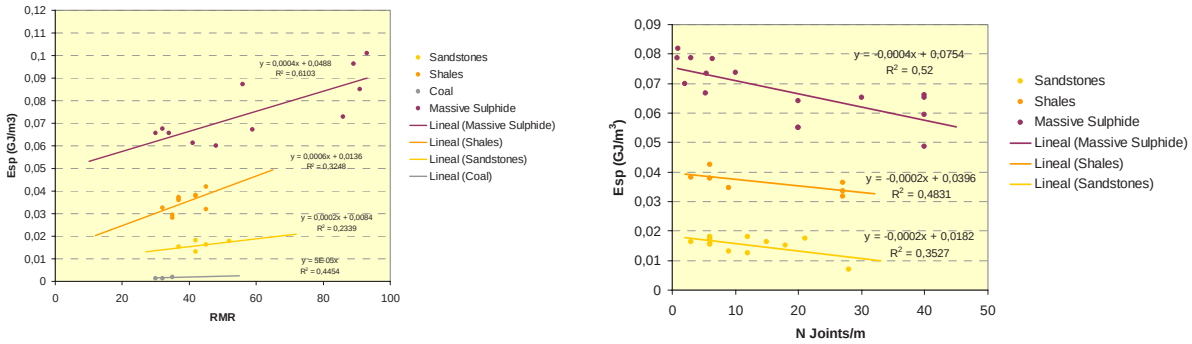

Figure 2.3.4-1 : Correlation between Esp and RMR (left), N Joints/m (right)

In both cases the Specific Energy shows a relationship with respect to the rock mass quality, for higher values of Specific Energy the rock mass quality will be better. It is important to take into account that the number of joints per metre is an important part of the value of RMR, the results indicate the trends when correlations are carried out.

Specific Energy (Esp) with respect to Dynamic Elastic Modulus (Edyn):

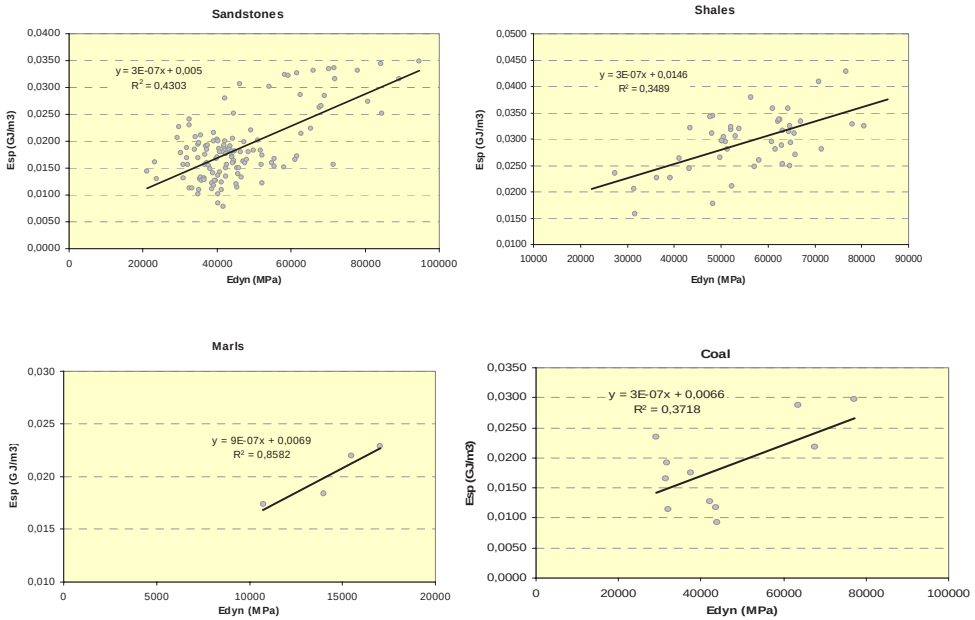

Figure 2.3.4-2 : Correlation between Edyn and Esp

From the Full Wave Sonic P (Vp) and S (Vs) wave velocities are obtained These can be related to dynamic elastic deformational parameters of rock, in this case it is used to obtain Young Modulus, and the trend, for greater values of this modulus, greater values of Specific energy (Esp) are indicated.

Specific Energy (Esp) with respect to Rock Mass Uniaxial Compressive Strength (σcm):

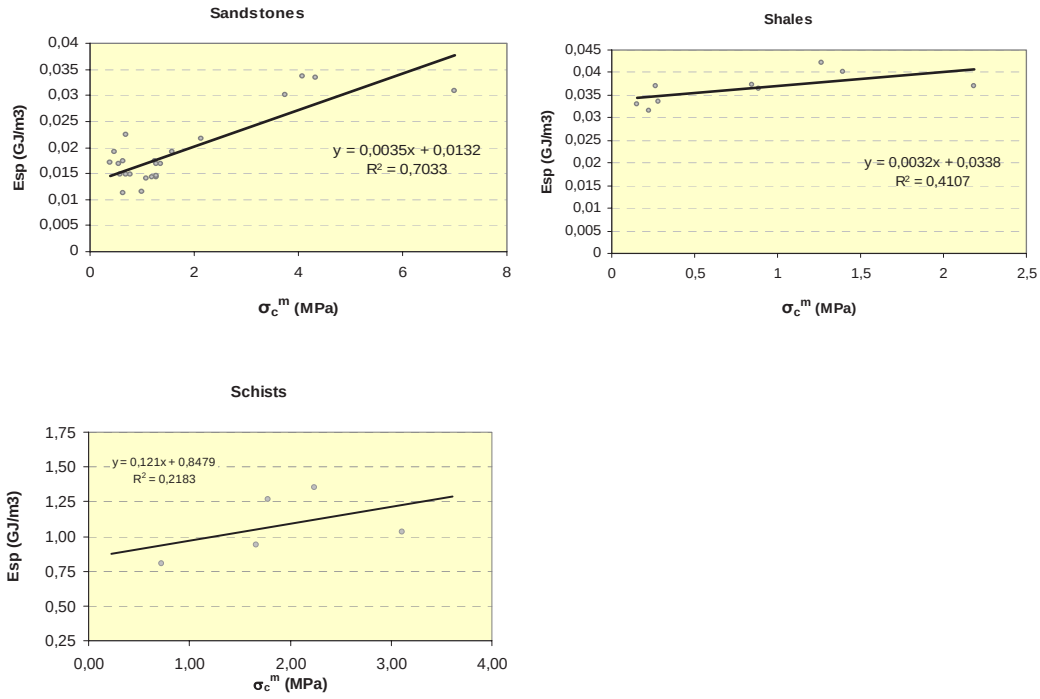

Figure 2.3.4-3 : Correlation between (σ_c^m) and Esp

Rock Mass Uniaxial Compressive Strength (σ_c^m) has been derived from Kalamaras/Bieniawski (1995)'s equation:

$$\sigma_c^m = \sigma_{ci} e^{(RMR-100)/24} \qquad (2.3.4\text{-}1)$$

where σ_{ci} is the uniaxial compressive strength of the intact rock. This indicates that the higher the value of the specific energy (Esp.), the higher the rock mass strength.

b) Geophysical Well Logging

The parameters taken into account from the geophysical well logging are Full Wave Form Sonic and Punctual Resistance. These parameters have been related with...

P wave velocity (Vp) / RMR, and (Vp) / Number of Joints per metre:

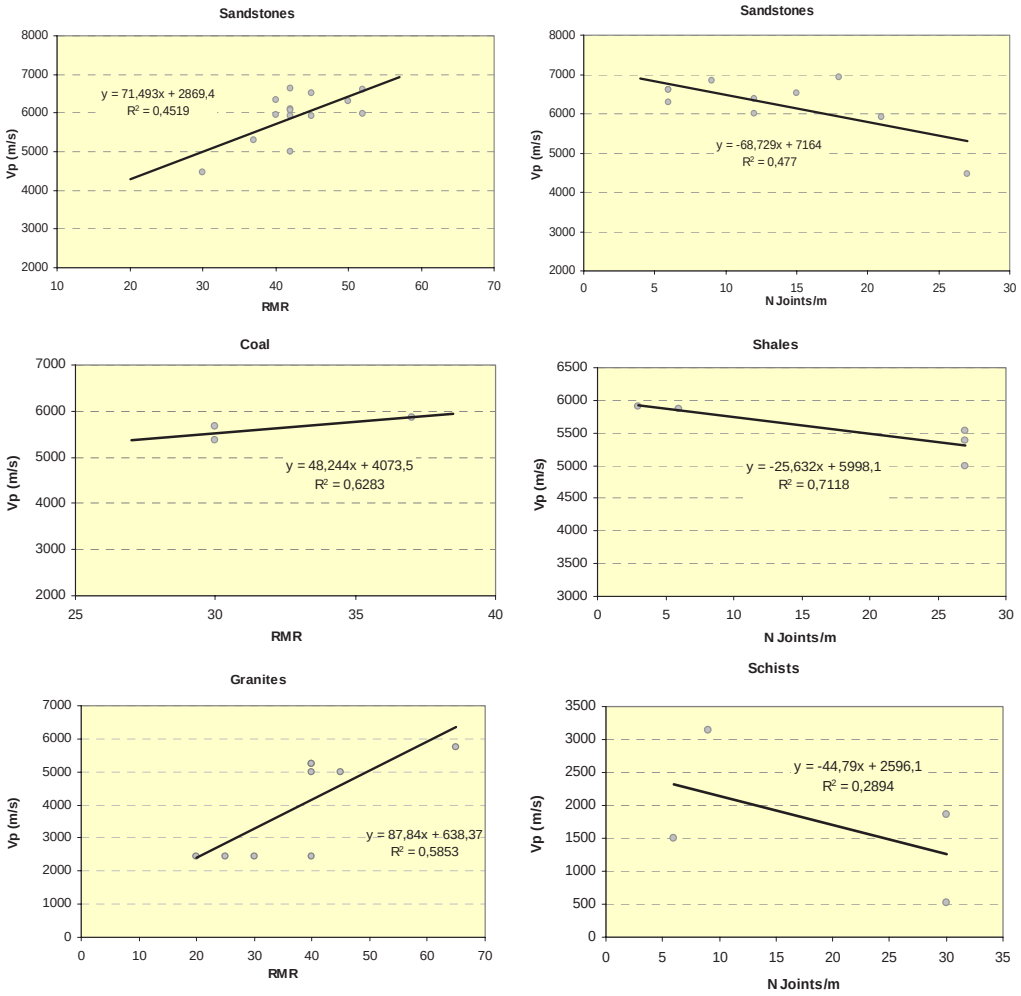

Figure 2.3.4-4 : Correlation between Vp and RMR (left), Joints/m (right)
As the P wave velocity (VP) increases, RMR increases, and the Number Joints per metre decreases.

Dynamic Elastic Modulus (Edyn) / RMR, and Punctual Resistivity (SPR) / RMR:

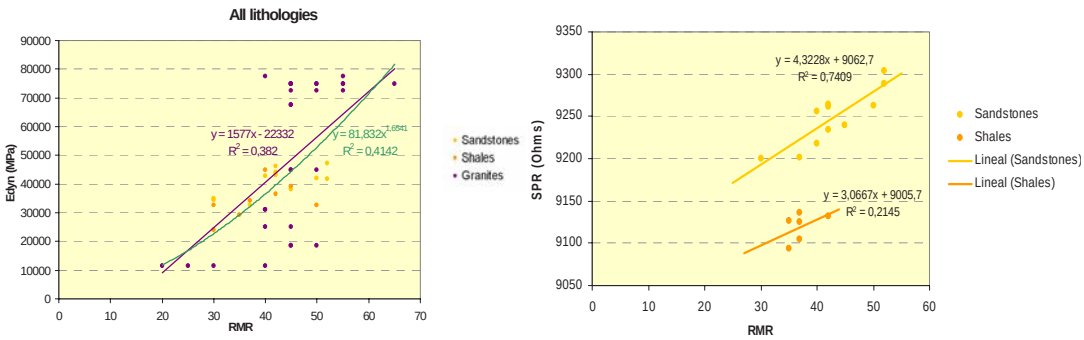

Figure 2.3.4-5 : Correlation between RMR and Edyn (left), SPR (right)
The Dynamic Modulus (Edyn) is obtained from Full Wave Form Sonic (Vp and Vs).

For higher values of Dynamic Elastic Modulus (Edyn), and Punctual Resistivity (SPR), the rock mass quality is better.

Dynamic Elastic Modulus (Edyn) respect to Number Joints per metre:

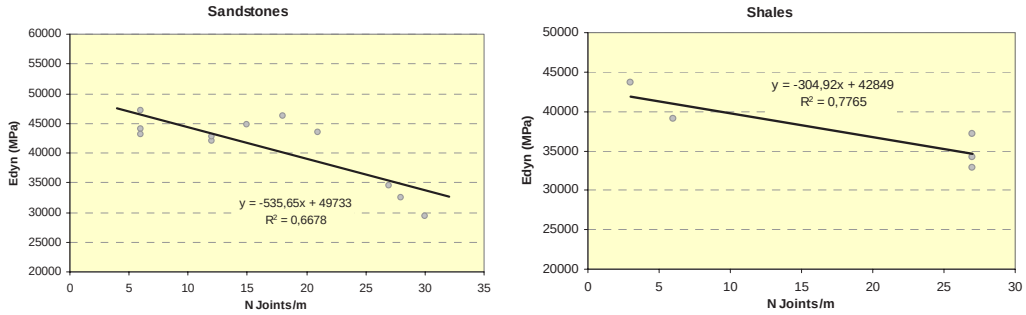

Figure 2.3.4-6 : Correlation between Joints/m and Edyn

As the values of Number Joints per metre increase, the values of Dynamic Elastic Modulus decrease (Edyn).

Punctual Resistivity (SPR) / Number Joints per metre:

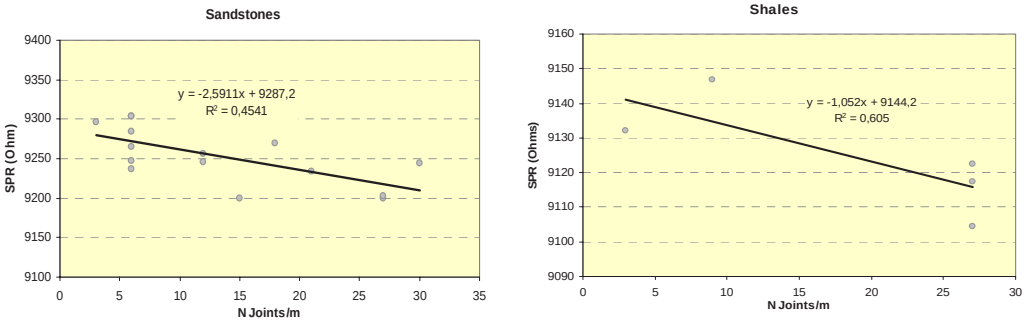

Figure 2.3.4-7 : Correlation between N Joints/m and SPR

As the number joints per metre increase, punctual resistivity (SPR) decreases.

P wave velocity (Vp) / Rock Mass Uniaxial Compressive Strength (σ_c^m):

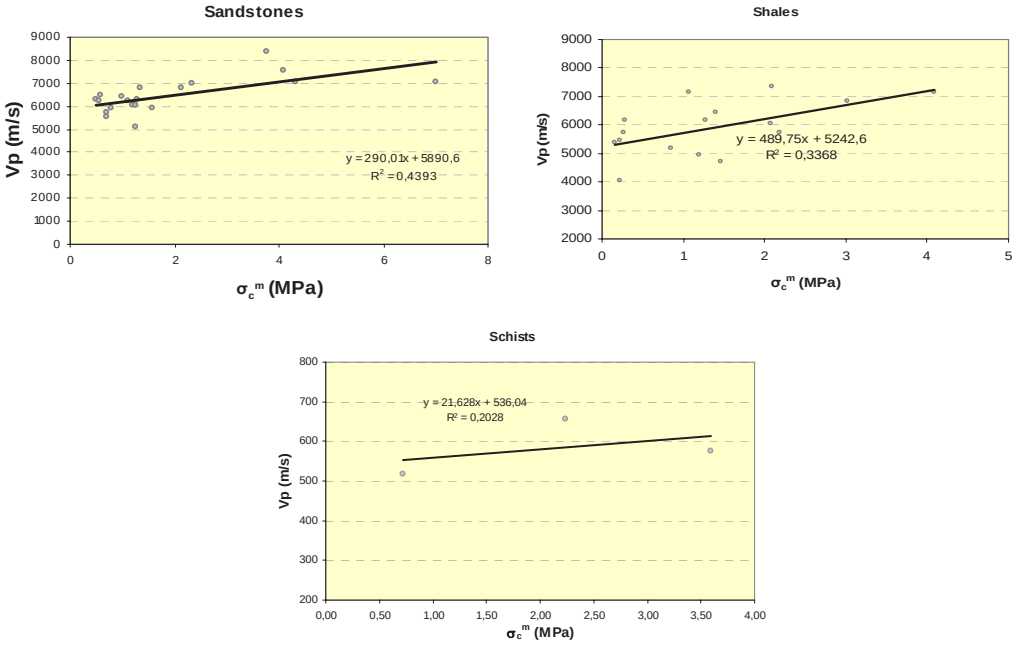

Figure 2.3.4-8 : Correlation between σ_c^m and Vp

A trend was observed between sonic parameters and resistivity, versus RMR index and number of joints per metre.

c) Data obtained from other geophysical methods

Relation between static rock properties and Vp

P-wave velocity in coal and in the surrounding strata was studied using seismic underground measurements in Poland (seismic in seam tomography). The propagation velocity of seismic P-wave in coal varies between 1740 m/s and 1840 m/s. The propagation velocity of seismic P-wave in the surrounding strata varies between 3700 m/s and 4400 m/s. The values of velocities are typical for rocks at depths around 900 m, especially for sandy shales. The floor of the 502 seam consists of shale clay, sandy shale and sandstone (according to boreholes No. G-24/98 and No. G-25/98). The higher values of P-wave velocities (VP) are probably connected with sandy shale.

The static values of the strength parameters, Uniaxial compressive strength (UCS), tensile strength (σt), and compactness index (f) of coal and floor rocks near the 2JD longwall in 502 seam of KWK Wujek-Slask are shown in the *Table* below.

		UCS (MPa)	**σ_t (MPa)**	**f**
Coal in the 2JD longwall (average Vp: 1790 m/s)		30.00	1.90	2.50
Floor of the 502 seam (average Vp: 4050 m/s)	Shale clay	30.51	1.96	2.54
	Sandy shale	38.02	2.44	3.17

Table 2.3.4-1 : Static values of the strength parameters

Natural stress field estimation from borehole ovalisation

Once an acoustic televiewer Mount Sopris SLT ABI-40 was acquired, two lines of research were developed. The first related to the geometry of the borehole while the second related to the discontinuities characterization (structure) in open boreholes. Following, is the borehole ovalisation analysis and its use for the estimation of the existing natural stress field. This utilized some intensive televiewer measurements, carried out at Borehole, BH-8+970 (227.5 m depth) located in the Southeast of Spain (Almería).

This borehole was drilled for a new railway line, in a carboniferous formation. Its depth is 227.5 m, and was logged between 65 and 227.5 m. After a detailed analysis of the travel time data, the following sections were chosen for an ovalisation study: 74.00, 87.00, 96.10, 104.50, 182.40, 217.70 and 218.50 depth. *Figure 2.3.4-9* shows the section at 182.40 m depth.

In ECSC 7220-PR/135 (Improved Rock Stress Measurement and Analysis for Planning of Underground Mines), a specific methodology to determine the natural stress field was developed (Galera, 2006) and its results compared with hydrofrac measurements. Using this methodology the *Table* below contains the maximum radio (r_b), the breakout angle (θ) and the strike of the minimum diameter (S_H). This stress distribution is in agreement with the tectonic framework as well as with the stresses derived from the seismicity, demonstrating the validity of this stress determination methodology.

DEPTH	r_b (mm)	BREAKOUT ANGLE			RATIO $\sigma_{h\text{-}H}/\sigma_V$		STRIKE S_H		
		θ_1 (º)	θ_2 (º)	θ (º)	Ko (S_H)	Ko (Sh)	α_1	α_2	
74.20	52.70	33	35	34	2.52	2.20	33	17	N-155 º-E
87.00	52.20	38	34	36	2.52	2.20	14	15	N-165 º-E
96.10	52.03	47	43	45	1.77	1.56	75	68	N-108 º-E
104.50	51.30	43	44	43	1.77	1.56	60	44	N-128 º-E
182.40	51.40	38	32	35	0.989	0.89	17	19	N-162 º-E
217.70	50.70	41	37	39	0.81	0.73	29	37	N-147 º-E
218.50	51.60	38	44	41	0.80	0.72	50	46	N-132 º-E

Table 2.3.4-2 : Results of the estimation of natural stress field in BH-8+970

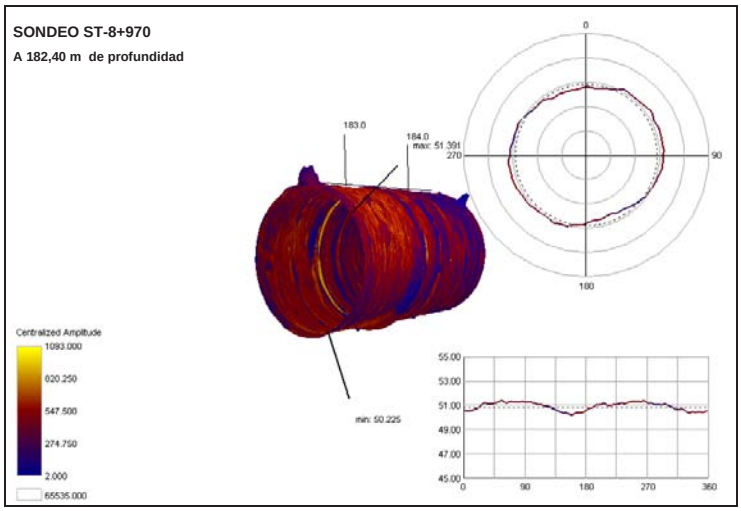

Figure 2.3.4-9 : Borehole 8+970 at 182.40

2.3.4.3 Application of techniques in a working colliery (T4.3)

In order to apply the developed techniques to a real working colliery, an open borehole was drilled at Union Minera del Norte (UMINSA). The results of this application have been included in the respective tasks, at WP.4 (rock mass results) and WP.8 (laboratory). Further reporting on this topic is given in an appendix to this report.

2.3.5 WP5 Radio Imaging (Signal Transmission and Acquisition)

The basis of the radio imaging method (RIM) is the measurement of the attenuation of medium frequency electromagnetic (H field) waves propagating over a number of intersecting paths between transmitters and receivers located in boreholes or mine workings. Typically, several individual frequencies may be used within the range 20 kHz to 1 MHz. Changes in the attenuation indicate coal seam anomalies that can then be related to the geology. Practical deployment problems are caused by the presence of parasitic signal components that arise from unintentional propagation along conductors and other face and roadway metallic infrastructure. In many cases, axial tunnel conductors have had to be periodically disconnected or removed prior to measurement. The goal of this work package was to establish whether these major practical constraints could be overcome.

It should be emphasised that the techniques investigated in this work package are applicable to any circumstance where electromagnetic waves are propagating in a conducting medium. The techniques are therefore applicable not only to conventional RIM technology, but to any new development of the technology.

2.3.5.1 Novel approaches to optimise frequency and transmission characteristics (T5.1)

Task Description: This task covered the scoping and definition of a range of novel approaches to the optimisation of the channel frequency and transmission characteristics of a Radio Imaging (RIM) system. The topics proposed for investigation were...

- Realising an increased magnetic moment from the signal transmitter and antenna
- Realising significant processing gain in the receiver function
- Using advanced channel sounding techniques including spread-spectrum and related codes

Prior to building up a system-level view of Radio Imaging equipment, based on the above points, it was found necessary to re-appraise the RIM technique in order that the salient operational principles could be established.

Principles of RIM technique

An extensive analysis was undertaken of LF and MF propagation within mines. Electromagnetic waves can propagate preferentially in a coal seam in situations where it represents a relatively low conductivity medium ($\sigma \approx 1$ mS/m) bounded by highly-conductive strata ($\sigma \approx 1$ S/m). However, the supposition – often quoted – that a coal seam acts as a waveguide was observed to be not strictly the case. The medium cannot support TE and TM waveguide modes where the frequency is below the waveguide cut-off frequency. In this situation, the medium functions as a transmission line, supporting a zero-order TEM mode, although many papers refer to this mode, casually, as that of a ‘waveguide’.

The results of the analysis were compared and contrasted with previous research. The consensus of earlier research is that coal-seam propagation at low frequencies is that of a transverse magnetic field and an ‘almost transverse’ electric field. The conclusion drawn by [Hill, 1984] was that, because the coal seam supports only a TEM mode of propagation at low frequencies, the system of linear equations to be solved in a tomographic reconstruction was “nearly identical” to that of geophysical tomography. However, Hill also noted that in situations where the seam properties varied rapidly (e.g. in a fault or washout) such a simple reconstruction would not work. The technique was analysed in detail in a PhD thesis [Shope, 1987] in which algorithms for tomographic reconstruction were proposed. Shope’s analysis noted that ‘true’ waveguide modes were possible under certain circumstances, and he analysed the propagation of both TE and TM waves in conditions of varying coal conductivity.

The TEM mode of propagation that characterises the Radio Imaging Method means, essentially, that an electric current is transmitted along the coal/shale boundaries as if the shale formed a parallel-plate transmission line that was periodically ‘shorted out’ by anomalies within the coal. This mode of

propagation extends down to zero-frequency where the method becomes similar to that of electrical resistivity tomography (ERT). However, a significant result of the ADEMA project was to gain an appreciation that European geological conditions differ significantly from those in the USA, and that two notable factors affect the applicability of the technique. These are a) the generally higher conductivity of the coal and b) the generally lower conductivity contrast between the coal seam and the surrounding rock. These are key findings in that they offer, for the first time, a quantitative appreciation of why RIM survey techniques have generally worked favourably in the US and Australia, but have not been applied to great effect in European basinal deposits.

Further reporting on this topic is given in an appendix to this report, *Principles of RIM Technique.*

Signal Transmitter

Magnetic Moment

Several methods of increasing the magnetic moment of the transmitter antenna were considered, and were identified for analysis in the later tasks of this work package. However, it was also realised that the relationship of field strength with distance is such that quite major increases in magnetic moment may result in only moderate or slight increases in range. It was also apparent, from the initial studies, that increasing the power applied to the antenna was not necessarily the best method of increasing the moment. An increase in the size and mass of the antenna was desirable. This has the additional effect that it reduces the Q-factor which, for narrow-band systems, reduces the reactive voltage. With the need to consider intrinsically safe equipment, this was viewed as being an additional benefit of a larger antenna.

Coupling Issues

Two issues of signal coupling were studied. Firstly it was noted from practical and theoretical observations that a low frequency antenna does not need to be placed in extreme close proximity to the rock. This conclusion, supported by [Wait, 1952; 1969], derives in part from the fact that the coupling does not depend on radiation resistance nor on notions of impedance matching. Essentially the antenna is a near-field non-radiating structure.

Secondly, note was taken of the reported influence of secondary signal contributions arising from parasitic coupling into mine electrical cables and continuous metallic infrastructure (such as rails, pipes and braided hoses). This secondary signal contribution is generally considered to be difficult to account for or to remove by signal processing. At present, the practical deployment of cross-panel electromagnetic survey techniques usually requires that cross-panel electrical connections are disconnected over a distance of 25 m or more. An assessment of the problem and proposed methods for handling it are discussed in subsequent tasks. The conclusions are considered to be significant since they could greatly reduce the practical preparations required to undertake a survey.

Receiver Antenna

It is a general principle that there is a maximum size for a receiver antenna beyond which there is no advantage to increasing its size. This arises because of the relative contributions of amplifier noise, antenna noise and ambient (‘background’ or ‘atmospheric’ noise). Typical figures for mine noise were examined, including those published by the US National Bureau of Standards and which were quoted in [Lagace, Cohen, Emslie and Spencer, 1975]. These indicate that the horizontal component of magnetic noise field spectral density has been measured at -10 to -20 dB[μA/m/√Hz] in a representatively noisy area of a coal mine.

With this in mind, it was considered that the main benefits to the receiver would arise from processing gain, rather than from antenna size or materials. The processing gain may arise in two ways – it was originally envisaged that a wideband signal would provide this, but initial studies within this project indicated that there was also merit in considering a narrow-band system where an ultra narrow-band filter was provided using DSP techniques. For example, there is a 60 dB signal/noise advantage in moving from a conventional voltmeter measurement with (say) a 10 Hz bandwidth to a DSP-based

measurement with a bandwidth of 0.01 Hz, although the latter requires, of course, a measurement period of the order of 100 s. The latter would generally be of little consequence in performing a panel survey.

Channel Sounding

It was confirmed that the use of a wideband sequence (e.g. pseudo-random or similar) would be ideal for channel sounding with a wideband antenna. It was also confirmed by simulation that correlating the received signal with its inverse function could provide a useful system identification function. Channel sounding is therefore a useful method of probing the medium to identify an optimum frequency for signal transmission.

However, the appraisal of the RIM technique indicated that the RIM probing frequency could not be lowered without a loss of image definition. (This is due to signal leakage into the surrounding rock; not because of measurement resolution). Neither can the probing frequency be raised, as increased attenuation will result. The practical use of channel sounding is therefore questionable in the given application. The technique of generating a system identification function by cross-correlation at the receiver is, however, of use for synchronisation purposes, as reported later in this work package. This is a useful outcome for design guidance. It was also concluded, from the studies within this project, that a systematic application of channel sounding would be of benefit for generalised communications research.

Optimisation of Transmission Characteristics

Further topics studied in this task included a study of antenna types, resolution v. frequency and optimum frequency. It was concluded that, if induction loop antennas are to be used for RIM applications, the established co-planar horizontal dipole orientation is the most ideal. However, two novel types of antenna have been analysed and are reported later in this work package.

2.3.5.2 Transmitter research and broadband induction loop antenna design (T5.2)

Task description: The aim of this task was to study methods of designing an efficient transmitter power amplifier (PA) and antenna. The topics proposed for investigation were...

- Tuned v. untuned (broadband) antennas; Class C and D power amplifiers
- Proximity and skin effect in air-cored loop antennas
- Use of specialised ferrite and amorphous metal magnetic materials
- Non-conventional antenna configurations (such as the anapole and dielectric disc)

Contemporary RIM Antennas

Prior to investigating antenna improvements, some data was collected on contemporary magnetic induction loop antennas used for through-seam transmissions. This data was assessed and used to give an indication of the increase in size and power that might be required to achieve propagation in a higher-conductivity environment than is evidently present in USA mines. Broadly speaking, it was found that the transmitter antenna needed to provide a magnetic moment ten times greater, which could be achieved by doubling its radius, increasing the number of turns by four times and tripling the power input.

Tuned v. Untuned Antennas

The conventional view is that an induction loop antenna, used with a spot frequency, has to be tuned to resonance for maximum efficiency. Although an untuned antenna could be expected to generate a significantly lower magnetic moment, studies within this project have confirmed that there are possible advantages to such a design. For example, for reasons to do with the presence of an inductive load, an untuned antenna does not benefit from being multi-turn – and as a single turn antenna, it cannot then suffer from the proximity effect. Additionally, in a potentially high-Q resonant antenna, the comparatively low Q-factor of other components in the system (e.g. in a practical tuning arrangement) can significantly reduce the efficiency of the system.

An analysis was also undertaken to compare the merits of switching (class D) amplifiers that have an output stage comprising an H-bridge, with those of class C amplifiers. For reasons of efficiency, the choice would be class D. However, it was noted that if it were necessary to pre-process the digital sequence (e.g. to counteract signal dispersion) then this would dictate an analogue class-C driver. It was determined that, for experimental purposes, an untuned or partially-tuned antenna would be used with a class D driver.

Proximity and Skin Effect in Air-cored Loop Antennas

An initial assumption was that the transmitter would be an air-cored induction loop operating on a single frequency. Such antennas suffer from a 'proximity' effect, which adversely affects their performance, and so one aim of this task was to investigate how this effect might be minimised. Further investigations established that the concept of an optimum wire spacing to reduce the proximity and skin effect only applied when the winding cross-sectional area of the antenna was constrained by design. However, for the purposes of this project, and certainly for a 'development' antenna, there is no such constraint and it was concluded that the optimum form of cross-section was that of a single-layer ribbon.

Use of Magnetic Materials

An air-cored loop antenna is frequently cited as a requirement for magnetic field generation because, unlike a ferrite-cored antenna, it does not saturate at a high flux density. However, there are several classes of ferrite ideally suited to the range of frequencies under consideration in this project. Additionally, a range of materials known as amorphous metals has been developed for use in switched-mode power supplies and similar power devices, which have superior properties to ferrites. Although initial results of the ADEMA studies suggested that there might be some merit in using ferrite or amorphous metal in a transmitting antenna, it was established that the main benefit of this type of antenna would be at the receiver; and only in favourably low-noise conditions. Although not suitable for the present project, it was concluded that amorphous metal could be of considerable benefit where the receiver antenna is of necessity very small (e.g. personnel-mounted communications receivers), and that this could be a fruitful area for further study. Again, this design guidance is of value in survey system specification.

Non-conventional Antenna Configurations

Anapole antenna

There has been some interest, in recent years, in the idea of using a toroid – that is, a solenoid bent into a doughnut shape – as a transmitter. An analysis of such an 'anapole' antenna was undertaken, but it was concluded that the benefits of this topology of antenna were more suited to higher frequency operation than is the case for applications of the RIM technique. However, the merits reported by [Wait, 1995 a; b] could apply to other electric field antennas, such as the dielectric disc or ceramic tile antenna described elsewhere in this report.

Rotating Magnets

A permanent magnet, rotating about an axis perpendicular to its dipole moment will produce a magnetic field that is equivalent to that of two perpendicular current loops driven in phase quadrature. With simple equipment its rotational speed might be limited to 12,000 rpm, which would result in magnetic dipole fields at 200 Hz. Although this is clearly a frequency greatly removed from that used at present for RIM surveys, this novel method of field generation was studied briefly because there are indications that such an antenna would be highly efficient. The only power input to the system is that needed to spin the material using a small motor. A small slab of a neodymium-iron-boron (Nd Fe B) magnet, measuring 50 mm × 25 mm × 12.5 mm, would present a magnetic moment of 15 Am^2.

A further study of this method was curtailed as soon as the results of the propagation modelling indicated that the RIM probing frequency could not be significantly reduced without incurring adverse

effects. Although not suitable for the present project, it was concluded that a rotating magnet antenna could be useful for ELF communications, and that this could be a fruitful area for further study.

J-field antennas

Coal seam imaging using the RIM technique uses the principle that an *E* or *H*-field antenna will couple into the lossy transmission line formed by the low conductivity coal and the high conductivity boundary rocks. A novel approach that was developed within the ADEMA project was to increase the degree of coupling by injecting the current directly into the rock using electrodes. There are various ways of viewing a 'grounded electrode' antenna – one model assumes it is an *E*-field antenna with capacitive ends; another model treats it as a *J*-field; that is, a source of injected current. The latter model is the more appropriate model at low frequency.

Corresponding measurements using a J-field antenna would take place using roving 'top and bottom' electrodes in the roadway, in much the same manner as a conventional RIM survey. However, there is also scope for permanently installing much larger arrays of electrodes as discussed in Task 5.5. A novel development is that such electrodes do not need to be drilled into the rock, but can take the form of conductive pads.

An analysis of the contact resistance of a rod-shaped electrode, compared with the contact resistance of a flat plate lead to the novel suggestion of using a conductive cushioning foam of the type normally used for used for the transport of electronic devices. Vermason (**vermason.co.uk**) manufactures a polyurethane foam impregnated with rigid conductive latex for this purpose. Using this approach a method was investigated for deploying electrodes without needing to drill holes. This uses compressible foam pads as shown in the *Figure* below.

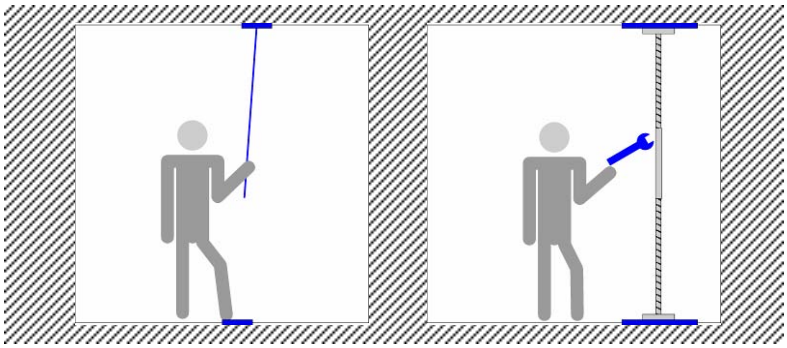

Figure 2.3.5-1 : Using compressible conductive foam pads as a J-field antenna
Exerting a pressure on the pads will allow a good contact to the coal. The use of a current-regulated power amplifier will take up any variability in contact resistance. A larger pad will result in a lower circuit resistance but will require mechanical force to compress it

Further reporting on this topic is given in an appendix to this report, *A Conductive Pad J-field Antenna*.

A Ceramic Tile Antenna

As a further method of utilising electric or current dipoles, it was noted that materials had become available with an extremely high relative permittivity (i.e. dielectric constant). Within the ADEMA project, the advantage of such a 'dielectric disc' antenna is that the voltage stress and size of this electric field antenna can be reduced to the point where it can be operated under acceptable conditions, and generating a signifcant associated magnetic field. An analysis was undertaken, using the concept of 'specific length' [Gibson, 2003], which showed that the performance of the antenna depended on the ratio of the relative permittivity ε_r to the product of mass density ρ and dissipation factor *d*. Following a similar line of argument to that used with induction loop antennas, the performance of the dielectric disc antenna was found to depend on the mass of the dielectric and not

on the area of the plates, nor on their separation. These latter parameters are mere 'operational' constraints that govern the voltage and current that might be required.

Following a search for suitable materials with a high value for ε_r / ρd, a manufacturer was engaged to supply a set of 16 tiles made from a high-permittivity perovskite ceramic based on barium strontium titanate ($Ba_{1-x}Sr_xTiO_3$). Each tile measured 4 mm × 50 mm × 50 mm and the total stack weighed 1 kg. The tiles were metallised top and bottom and were able to be connected in a variety of configurations in order to provide electrical matching to a power amplifier.

Figure 2.3.5-2 : High-permittivity ceramic tiles used to construct a compact E-field antenna

Manufacturing problems delayed the delivery of the tiles by some 12 months, which limited the range of tests that could be performed. However, laboratory tests showed that, for very little power dissipation, the antenna produced a significant magnetic moment, with the absence of the usual losses associated with induction loop antennas. However, the high Q-factor associated with this type of antenna was found to be a problem in two respects. Firstly, the antenna was difficult to drive efficiently; secondly, if tuned to resonance, the relatively low-Q tuning inductance moderated the overall Q-factor with the result that the overall efficiency (magnetic moment v. power drawn) was not improved over a representative induction loop antenna. However, it is considered that these problems can be overcome by further careful design and that the ceramic tile antenna has potential uses not only for RIM surveying, but for communications purposes.

Further reporting on this topic is given in an appendix to this report, *A Novel Ceramic Tile Antenna.*

2.3.5.3 Radio imaging receiver and signal acquisition research (T5.3)

The aim of this task was to undertake research into signal acquisition and the design of a radio imaging receiver. The topics proposed for investigation were...

- Processing gain due to use of spread-spectrum coding and signal averaging
- Methods of system synchronisation including fibre-optic cable, correlation of received signal

Channel Coding and Signal Averaging

Several methods of increasing the processing gain at the receiver were investigated. The most straightforward of these is to use a wideband channel-coding using, for example, a pseudo-random binary (PRB) sequence (or similar) to produce a spread-spectrum signal which is de-spread at the receiver. The effect of such a signal propagating through the rock was modelled algebraically for a uniform medium by deriving a transfer function for antenna–rock–antenna system.

The phase constant β of a signal travelling in a conductive medium varies with frequency. Moreover, because it is a non-linear function of frequency ω, this means that the group velocity ($d\omega/d\beta$) is not constant and so the signal will undergo the phenomenon of dispersion. For a wideband signal, the

effect can be modelled as a type of low-pass filter. The results of modelling using MatLab (**mathworks.co.uk**) indicated that transmission of data over distances greater than two skin depths could result in closure of the signal's eye pattern. However, further investigation indicated that it was possible to use correlation techniques to extract the signal at greater distances, when dispersion had resulted in the eye's closure. This topic is discussed further in Task 5.4.

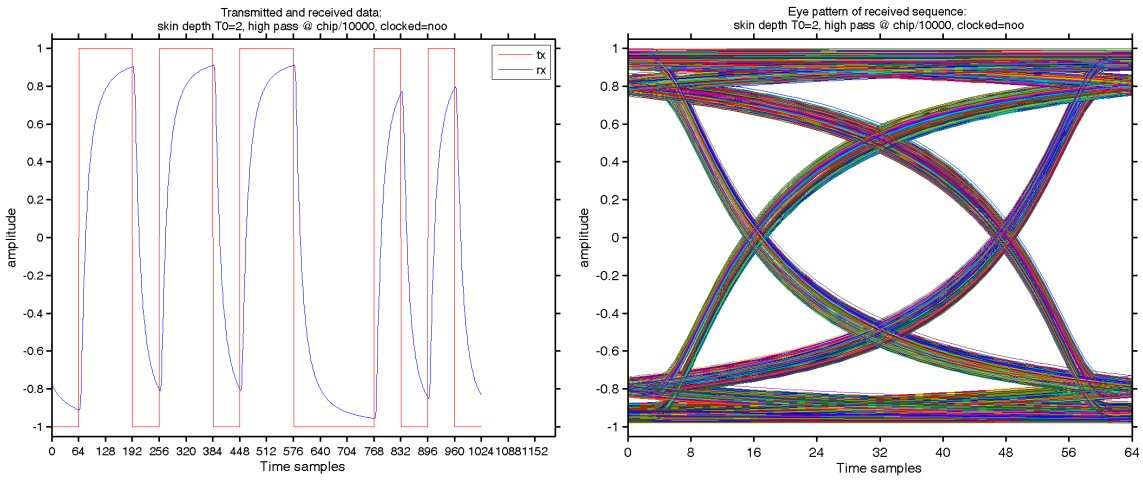

Figure 2.3.5-3 : Modelling the transmission path to investigate dispersion
Left: transmitted and received signals. Right: eye pattern at receiver.

Signal averaging is a method of increasing signal/noise ratio by sampling multiple copies of the same signal. This is a manifestation of a particular type of finite impulse response (FIR) digital filter. An investigation indicated that the combination of a 'spreading code' and signal averaging could result in a significant transmission distance simply because of the narrow bandwidth that results from this. It was noted, though, that it would be difficult to perform the signal-averaging in software in real time and so a hardware-based system would be required. A drawback would then be that hardware signal-averaging precludes the use of non-rectangular windowing functions. However, in a novel development, it was realised that weighting the signal averaging process (i.e. by adding some samples and not others according to a carefully predetermined algorithm) it was possible to modify the filter transfer function. This technique requires further investigation but is considered to offer processing benefits.

Methods of System Synchronisation

Problems arise during the practical deployment of equipment using the radio imaging method (RIM), because of the need to synchronise the transmitter and receiver for the purpose of making measurements of phase shift. Hitherto, this has been a major drawback to deploying RIM-based survey techniques. One method of achieving synchronisation is to transmit a reference signal between the transmitter and receiver using a fibre-optic cable, but this is expensive and difficult to deploy because the cable has to run the entire length of the long-wall coalface and may be readily damaged or otherwise compromised. A copper cable cannot be used because of the danger that parasitic coupling may cause it to convey unwanted signals.

Several methods were investigated, and it was noted that [Stolarczyk, 2004] describes a technique that involves transmitting a reference signal on a 2.5 kHz carrier, which is supposedly low enough not to be affected by the geological structure of the medium. However, one disadvantage of this method is that it requires a separate transmitter and receiver to be set up. The logistical and practical difficulties of co-ordinating dual transmitters and receivers are often significant. As noted above, one novel method that was considered was to extract synchronisation from a sounding sequence.

Another novel method developed within the ADEMA project involves using the property of dispersion and is the subject of a patent application. Any measurement of relative phase shift between two

transmitted signals cannot, by itself, be used to establish a phase reference for synchronisation purposes, because the velocity of propagation through the medium is a function of the conductivity, which is unknown. However, in a novel development, it was discovered that multiple measurements of relative phase shift made at three or more distinct frequencies could be used to deduce the conductivity of the medium and this information used, in turn, to derive an absolute phase measurement, thereby eliminating the need for a synchronisation channel. In effect, it is the dispersion of the medium that is being used to deduce the conductivity. The patent application describes a scheme for realising the related benefits of a) eliminating the need for a synchronisation channel and b) deriving path conductivity as a function of the signal dispersion. In one form, the technique uses three closely-spaced frequencies (e.g. 99, 100 and 101 kHz) thus allowing the signals to be transmitted simultaneously from the same tuned antenna, which is in contrast to earlier systems.

A further development is that a tomographic reconstruction can be obtained from the dispersion information. It is known from recent RIM surveys carried out in the USA that some coal-seam anomalies tend to result in amplitude disturbances whilst others result in phase disturbances. It is therefore reasonable to deduce that anomalies may manifest in a different and distinctive manner with a dispersion-based measurement. The algorithms for such a reconstruction will be different to those used at present and the development of such advanced algorithms was considered to be beyond the scope of Work Packages 5 and 6 of this project.

Assessment of Noise Problems

A further object of study in this task concerned channel noise. It was considered that, as a future object of research, a systematic study of mine noise should be undertaken. As noted in Task 5.1, some typical figures for mine noise were quoted in [Lagace *et al.*, 1975] but a systematic study of modern mines appears not to have been undertaken. Such a survey was not possible within the ADEMA project because of the restrictions on using un-approved equipment in hazardous areas of a mine.

Consideration was also given to the unwanted coupling of signals into the metallic mine infrastructure. [Lagace *et al.*, 1975] were of the view that an infrastructure-guided wave would be difficult to excite and yet extensive and *continuous* infrastructure is perceived to be a significant problem in RIM surveys, requiring expensive counter-measures. Published information on the extent of the problem was not evident from a literature search. Equipment was constructed to attempt to measure the extent of the problem but laboratory tests were inconclusive. However, as noted in Task 5.4, mathematical modelling indicated that in certain conditions of seam height, conductivity and distance, correlation techniques could be used to identify the resultant multi-path propagation across the coal panel.

2.3.5.4 Advanced coding techniques (T5.4)

Task description: Research into techniques of advanced signal coding included an investigation into the possibility of using non-ideal test sequences, together with algorithms for calculating the inverse of an arbitrary sequence under the operation of cross correlation. This would permit synchronisation via a delay-locked or code-locked loop.

Synchronisation Using Non-ideal Sequences

At the outset of this project, it was considered that system identification using a periodic pseudo-random sequence would have useful application. The procedure relies on the perfect (i.e. impulsive) nature of the auto-correlation function of the test sequence. The test signal applied to the system is a periodic sequence of N samples with sampling interval T, represented by $f(nT)$. To obtain the system impulse response it is necessary to cross-correlate the output signal with a time sequence f^{-1} that is an inverse of f in the sense that the cross-correlation product gives rise to a delta function. This result can be extended to non-ideal sequences for which, in certain circumstances, it is still possible to calculate an inverse (which will usually be multi-valued). Simulations using the maths analysis package MatLab confirmed several of the points conjectured at the outset of this project, namely

- Removal of d.c. component of sequence simplifies transmitter design.
- Choice of sequence length simplifies Fourier transform for channel-sounding purposes.
- Choice of sequence to give a specified cross-correlation product aids synchronisation using a code-locked (delay-locked) loop.

Following on from the modelling of Task 5.3, the effect of signal dispersion on the cross-correlation product of a transmitted sequence and its inverse was also evaluated. It was observed that even when the eye pattern was closed and the signal buried in noise, it was still possible to recover a distinguishable correlation peak. In the presence of multi-path effects – e.g. caused by parasitic signals – the output of the correlator shows a peak corresponding to each time-displaced version of the signal. The width of each peak is related to the dispersion and the separation of the peaks is related to the length of each of the multiple signal paths. These latter two results demonstrated the recovery of digital data from noise. However, it was observed that the reconstruction of the signal using these DSP processes was of questionable use for tomographic purposes because amplitude and phase information was lost during the process. The techniques show promise for low-rate data transmission, but would be difficult to apply to RIM surveying; hence the recommendations outlined below.

The modelling of parasitic coupling suggested that the correlation peaks of the wanted and unwanted could be distinguished but, whilst this was so, the overlap of the 'tails' of the functions meant – once again – that the precise amplitude and phase could not be determined. There is some indication that, under certain conditions, e.g. seam height, conductivity of the medium, the correlation peaks may be sufficiently well-spaced to permit the data to be fully separated, and this could be an area for further study. An interim conclusion that multipath effects could be eliminated or perhaps even made use of was therefore withdrawn in favour of the recommendations that

i) a non-ideal sequence should be used for sounding or synchronisation purposes only, and

ii) the tomographic measurements should utilise a very narrow bandwidth spot frequency method, rather than the de-spreading of a spread-spectrum sequence.

and it was therefore concluded that for conventional RIM surveying, using a spot-frequency, the two most significant advances are a large transmitter and a narrow-band receiver, with the narrow bandwidth obtained by means of a lengthy sampling time, DSP-based filtering and signal averaging.

2.3.5.5 Underground application considerations (T5.5)

Task description: The aim of this task was to confirm the feasibility of using the methods investigated in the previous tasks in an underground environment. This task also included an investigation of remotely addressable 'smart switch' nodes to simplify the signal acquisition of a tomographic array. It was also originally proposed that the task would allow the conformation of the processing gain and transmission range for a given range of probe frequencies.

Summary of Work Undertaken

The studies undertaken in this task were modified as a result of the conclusions obtained from previous tasks in this work package. For example, it had been concluded that a broadband system could not be used for obtaining tomographic data so a determination of the processing gain of such a system in this task was curtailed. Additionally, it was found necessary in this task to spend some time studying the use of non-approved electrical apparatus in mines because restrictions on usage affected the range of experiments that could be undertaken.

Resistivity Tomography and 'Smart Switch' Electrodes

As an adjunct to research into RIM enhancements the ADEMA project investigated the use of a multi-electrode array, such as is used for conventional electrical resistivity tomography (ERT). A single ERT measurement uses four electrodes. Current is injected on one pair of electrodes and a voltage is measured on the second pair. Repeating this measurement for many combinations of driving and sensing pairs provides information for the tomographic reconstruction.

Initially, it was considered that to obtain sufficient coverage of the entire coal panel, it would be necessary for the driving pair of electrodes to be situated one on each side of the panel, to allow current to flow across the panel. However, if the coal/rock resistivity contrast is high, this merely results in the current 'shorting' to the seam boundary as shown in the *Figure* below. A further study of this problem led to the proposal that the driving electrodes be situated on the *same* side of the coal panel (e.g. in the intake roadway) where they could be considered to be connected to the top and bottom 'plates' of the transmission line. In this situation, the field will propagate in a similar manner to that of a conventional RIM system, and will therefore provide tomographic coverage of the entire coal panel, although with the provisos regarding choice of frequency

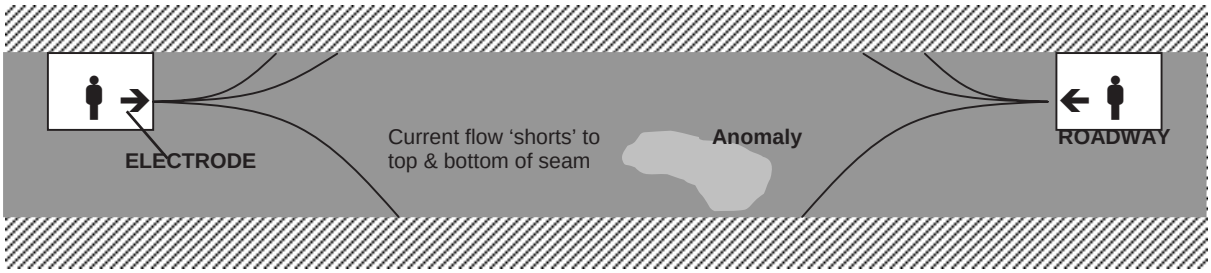

Figure 2.3.5-4 : Conventional ERT, injecting current across the seam
If the seam/rock conductivity has a high contrast then the current may short to the 'plates' of the transmission line. (Elevation across seam).

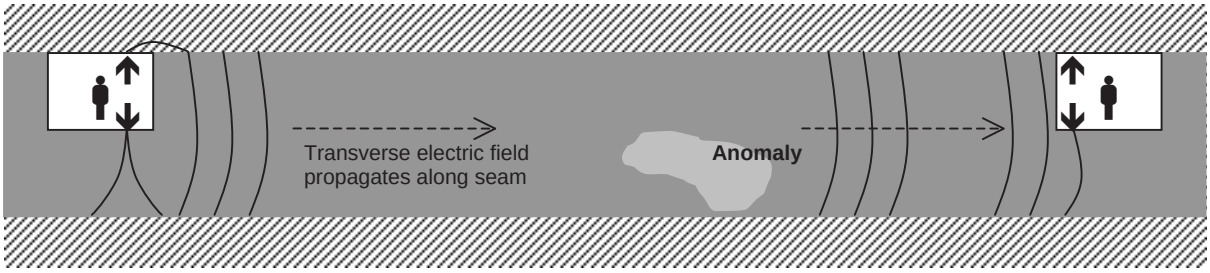

Figure 2.3.5-5 : TEM propagation, injecting current on one side of the seam
A TEM wave will propagate across the seam, in a similar fashion to that of a RIM system. (Elevation across coal seam).

The salient point, which is a novel and important result for this project, is that the proposed ERT system design has converged with that of a RIM system. Essentially, this system will behave in a similar way to RIM, but with the advantage of higher signal levels because the current is injected directly into the coal seam, instead of being coupled inductively from a magnetic loop antenna. It should be noted, however, that the operation of this system – just as with RIM – depends on there being a high conductivity contrast between the coal and the surrounding rock, such that the coal panel can be modelled as a lossy transmission line.

Direct injection of the signal will not only result in a higher signal level, but it will result in less signal being coupled into the metallic infrastructure thus providing a solution to the problem of parasitic coupling of RIM signals.

The question of electrical safety arises, but this problem is addressed by using the results of the earlier tasks, namely synchronous detection, narrow-band systems and the allied signal processing techniques, which can be used to increase the signal/noise ratio of the detected voltage. In this manner, satisfactory operation could be achieved at voltages that are low enough to allow the equipment to be operated in an intrinsically-safe environment.

There are additional operational advantages due to the fact that the entire electrode array would be semi-permanently installed, meaning that the measurement process would not be constrained by time,

allowing a very low bandwidth to be used. It was also considered that the rib-side electrodes would be able to give an early warning of possible collapse of the coal panel – an incident that caused a fatality in the UK in January 2007.

Electrodes
It was envisaged that the electrodes for a multi-electrode ERT network could be constructed of a conductive plastic and left permanently in place in the coal seam, where the cut fragments would eventually be removed during the coal washing process. A patent application covering this, and other aspects of the use of ERT electrodes in coal mines was filed during the course of this project.

Smart Switch Nodes
A further aspect of this Task was to study the deployment of bus-based addressable switches, similar to those already in use in the geophysical industry. It was considered that within a ERT/RIM hybrid system this could give rise to distinct advantages over present methods of deployment of the RIM technique. The use of these so-called 'smart switch nodes' was described in the above-mentioned patent application. The construction of a system of smart switches was not attempted within the ADEMA project as it was considered to be outside the scope of the project. Additionally, it would have been a significant undertaking in terms of hardware design, and would have required the development of specific tomographic techniques to suit. Such techniques are outlined in, for example, [Shope, 1987] and [Stolarczyk, 2003].

Further reporting on this topic is given in an appendix to this report, *Electrodes for Resistivity Tomography in Coal Mines.*

Using Non-Approved Electrical Apparatus in Mines

A document was drawn up, outlining the procedures (in the UK) for the use of non-approved electrical apparatus in the hazardous atmosphere present in underground coal mines. In summary, regulation 19(2) (g) of the UK's Electricity at Work Regulations (1989) allows non-certified, non-approved electrical apparatus to be used underground in a coal mine under certain conditions (commonly referred to as 'Manager's Rules'). The rules usually apply to specific equipment and will name the equipment, although some rules are generic as long as all requirements are met.

Whilst the above safety assessment is essential to satisfy the requirements of the Electricity at Work Act and control the risks of inadvertent ignition of flammable atmospheres and electro-explosive devices, there are also potential issues requiring consideration in regard to occupational safety aspects of low frequency fields. These issues were also examined. The most relevant source of information on exposure limits to electromagnetic fields is considered to be given in [ICNIRP, 1998]. These guidelines, from the International Commission on Non-Ionizing Radiation Protection cover the entire range of test frequencies applicable to the ADEMA project.

The restrictions on the use of non-approved equipment caused considerable difficulties throughout the ADEMA project. For the mine where it was intended to undertake tests, the zones classed as 'Regulation 19(2) exempt' were found to be unsuitable for many of the experiments that had been envisaged. For future projects where underground investigation is a required part of the programme, some early attention will need to be given to the problem of mine access. In the UK, at least, it seems that the use of unapproved equipment underground is extremely restricted.

Experimental Equipment

Several items of experimental equipment were constructed for laboratory-based tests, and some items were submitted to the UK company Health, Safety and Engineering Consultants Limited (HSEC) for inspection prior to being used underground. Initial experiments were undertaken at Daw Mill colliery in the UK. However, as noted above, the restrictions on the use of non-approved equipment still caused considerable difficulties. During initial experiments in Daw Mill colliery, for example, it was not possible to locate exposed areas of coal where the conductive pad electrodes could be properly

deployed. Additionally, none of the areas of the mine where regulations allowed deployment of the equipment were close to the coalface and access to the return roadway was similarly restricted. It was also anticipated that similar prohibitions on the use of non-approved apparatus would apply elsewhere in the European Union. Further reporting on this topic is given in an appendix to this report.

Confirmation of Prospects of High Resolution

Studies have indicated that the primary factor limiting the resolution obtainable from the earlier RIM trials in the UK was that the reduction in the probe frequency caused an increase in the skin depth in the surrounding rock. This resulted in out-of-seam geological structures having an unwanted effect on the received signals. The probe frequency itself does not have an effect on resolution because the sounding is not a Rayleigh system – clearly, zero-frequency resistivity tomography does not have zero resolution.

Because of the leakage of signal into the boundary rock, a reduction in the probe frequency is not desirable. However, the frequency cannot be raised too high because the skin depth in the coal reduces significantly, leading to large losses. The prospect of high resolution is therefore critically dependent on the ability for signals to penetrate the coal seam and be detected with sufficient phase and amplitude accuracy. Whilst it is envisaged that the type of tomographic algorithm will have an influence on the retrieval and identification of geological features from survey data, it is a fundamental requirement that the survey signal should first be recovered faithfully with minimum extraneous noise content, and that a sufficient number of measurements is taken. This reflects the work programme's focus on RIM signal transmission and acquisition in this work package.

2.3.6 WP6 Radio Imaging (Tomographic Reconstruction Techniques)

Initial work investigated the current limitations of tomographic reconstruction techniques. The inverse imaging problem was also addressed in WP5, with regard to enhancements to the signal transmission and acquisition. The initial phase of work also examined the relative gains in the tomographic reconstruction process, primarily in terms of lateral resolution; from employing state of the art forward wave tomography inversion code processing algorithms rather than simple geometric straight ray path reconstruction techniques. This work confirmed that whilst forward wave inversion processing can indeed offer an enhanced ability to resolve multiple complex anomalies, this is only possible where the RIM transmission can be sustained and can be fully-recorded with high-accuracy phase and amplitude determinations. Fundamentally, the results of the initial RIM modelling work using typical European mine electrical parameters showed that signal propagation in the geological channel is subject to complex and severe losses relative to the more favourable electrical seam characteristics in the United States and elsewhere.

As noted in the 'comparison of initially planned activities and work accomplished', the first phase of work in this work package led to the conclusion that any additional gains from enhanced image reconstruction techniques required a more fundamental understanding of the RIM transmission channel and it was therefore the considered view of the project partners that directing effort to further improving RIM tomographic reconstruction algorithms would not assist in solving RIM operational deficiencies.

As a consequence of these findings, the work within WP6 was subsequently redirected to undertake more advanced modelling investigations, designed to better understand the basic imaging problem. The revised work programme has resulted in a major advancement in the modelling, understanding and visualisation of complex transmission behaviour within the coal-seam channel. By way of example, it has confirmed the observations in WP5 that RIM probe frequencies must not be too low and that scattering and loss of confinement of the signal occurs in conditions of low contrast between the seam and the boundary conductivity. Given the highly innovative nature of the revised WP6 research, this is reflected in the focus of the reporting.

2.3.6.1 Investigate current limitations (T6.1)

Task Description: Investigate current limitations on ability to infer spatial distribution of conductivity in the measured region (under-constrained inverse imaging problems, data sparseness, physical limitations of access and other logistical constraints). Undertake tests on specimens taken from opencast coal and deep mine sites. Characterise the frequency-attenuation response of the medium.

The main remit of this work package was to perform *3D* EM modelling for RIM. The main tool in this work was the commercial *3D* full-wave electromagnetic finite element solver HFSS™ from ANSOFT, with additional validation using COMSOL Multiphysics® modeller. The work began with an extensive literature search of RIM techniques and the establishment of a database for typical electrical parameters for coal and associated strata likely to be found in EU and non-EU deep coal mines. The overall goal of this work package had been to develop tomographic enhancements for RIM. However before this work could commence it was necessary to understand through modelling the underground coal channel and its EM characteristics. The conclusions drawn from this initial modelling work lead to an agreed deviation from the work package's task descriptions.

During the literature search it became apparent that conductivity measurements at the frequency of operation of RIM systems were poorly reported in the open literature. Both seismic and electromagnetic imaging techniques rely on the contrast in properties between coal and country rock. Therefore, it became necessary to test relevant coal samples in the Rock Mechanics laboratory at Heriot-Watt University.

The conductivity of coal was found to vary widely dependent on geographical location and in particular moisture levels in the coal and associated strata. The conductivity values quoted in the

literature vary over a wide range from 10 pS/m for dry coal in USA [1] to 100 mS/m for wet Eastern Bituminous coal [2-5]. In the EU region the coal conductivity is quoted [6] as roughly 100 μS/m which varies by a couple of orders depending the geological conditions in a particular area. Similarly the relative permittivity of the coal was given values from about 2.5 [1, 7] to 25 [2, 5, 8-11].

Figure 2.3.6–1 : A coal sample, cored for experiments
The sample was cored for Rock Mechanics laboratory measurements (large orthogonal holes) and also drilled and pinned with pairs of electromagnetic (e-m) measuring probes. At lower front is a pair of e-m probe tops. The pair on the top is coupled to TRASE, then VNA equipment.

Measurements from a UK open cast coal site showed that the relative permittivity of coal in this region is in the range of 7.5 to 12.0 and is highly dependent on moisture levels. Measurements were also made on samples of coal and shale taken from Daw Mill colliery (courtesy of UK Coal Ltd). Core samples were obtained from the roof of a working seam and simple low-frequency measurements of conductivity were made using a modification of the standard geophysical technique of a Wenner array in which the 'traditional' mercury end-caps were replaced by a more effective and safer material, namely the conductive, compressible foam that is used for anti-static protection of electronic components. Calculations demonstrated that the bulk resistivity of this material was adequate to cause the current to be distributed uniformly across the sample's cross-section. Results from the lab tests confirmed the data from a borehole log that was also obtained from UK Coal's Daw Mill mine and is shown in the *Figure* below.

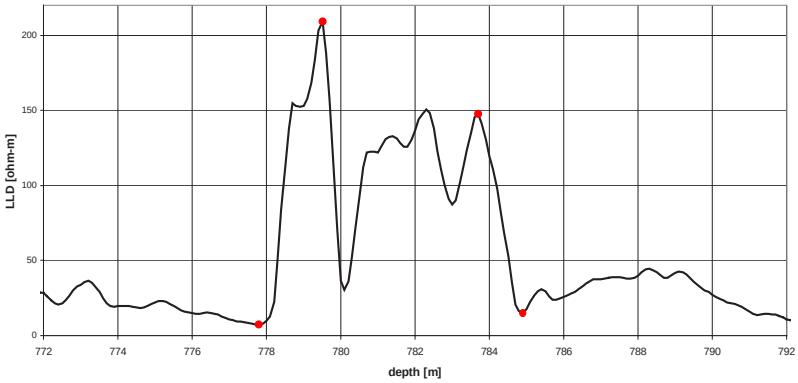

Figure 2.3.6-2 : Borehole Geophysical Log

This data, and typical figures quoted in the literature are summarised in the *Table* below

Source	Coal Conductivity σ_c (mS/m)	Rock Conductivity σ_r (mS/m)	Contrast σ_r / σ_c
Data from Daw Mill seam	5–7	70–140	10–28
Average figures from a range of authors	0.1–10 typ. 0.5	10–100 (max 1000)	typ. >>100

Table 2.3.6-1 : Typical Coal and Rock Conductivity

The Daw Mill figures contrast with those quoted by other authors in three important respects...

- The coal has a much *higher* conductivity than expected. This means that in-seam attenuation will be higher and this may dictate the use of a lower frequency – as borne out by the RIM trials in the UK.
- The surrounding rock has a much *lower* conductivity than expected. The increased skin depth in the rock means that out-of-seam anomalies are more likely to affect the tomographic data.
- The lower conductivity of the boundary layers means that the transmission line or waveguide so formed is likely to be more lossy than expected.

The latter observation is important; the low seam conductivity contrast observed in the UK compared with basinal deposits in the US and elsewhere is a key aspect of explaining the poor results observed in previous electromagnetic tomographic survey tests.

2.3.6.2 Scope possible enhancements to reconstruction process (T6.2)

Task description: Investigate use of full-wave tomography inversion processing algorithms in reconstruction versus straight ray path techniques. Out-of-plane (or seam) geological variability is considered likely to dominate the observed signal and invalidate the narrow assumptions of classical tomography inversion.

The effectiveness of the RIM technique for detecting flaws or anomalies in a coal panel was assessed by examining the wave propagation phenomena through the seam. Extensive modelling was performed to study the applicability of RIM technique for the EU coal mines and this work identified the range of operating conditions in which RIM could be used to detect the presence of seam anomalies. This range is conditioned primarily by the electrical conductivity (i.e. loss) of the coal and shale strata that are assumed to bind the coal panel. The losses are increased by increase in the coal conductivity and/ or decrease in the shale strata conductivity. These conductivity levels are, in turn, related to the wetness of the strata and in particular to the presence of saline minewaters. In the models the dimensions of the coal seam were adjusted to reflect the dimensions of the UK target mine, Daw Mill. The results demonstrated that losses in the coal seam beyond a certain limit introduce not only excessive attenuation but also loss of confinement of the RIM signal across the coal seam. If the RIM signal is available to sense across the coal seam without excessive losses, tomographic inversion can be used to detect the presence of flaws. However if the coal seam channel is more lossy the RIM signal being sensed across the coal seam does not provide constructive input to the tomographic inversion process, as the signal transmission mechanism is less predictable. Moreover, in the lossy scenarios, if more energy is transmitted into the seam in order to achieve the minimum required signal level across the coal seam it can be observed that near the excitation wave port the local source fields (non-modal stored energy fields and radiation fields) are strong enough to affect the RIM signal. Based on the range of coal and shale electrical conductivity and the implications on RIM applicability three scenarios have been defined.

1. **High contrast.** If the coal is realtively non-conductive (< 10 μS/m) and the boundary rock is highly conductive (> 5 S/m) the losses are low and the RIM technique will work for tomographic imaging of hidden anomalies in a coal seam

2. **Medium contrast.** If the coal has a conductivity of about 100 μS/m the boundary rock is moderately conductive (0.1 to 1 S/m) the losses are considerable but the RIM technique is still usable. However, a very high transmitter magnetic moment may be required to achieve detectable signal levels at the sensing points. Moreover, about 40% to 65% of energy that enters the coal seam leaks into the boundary rock.

3. **Low contrast.** If the coal has a higher-than-usual conductivity (> 1 mS/m) and the surrounding rock is less conductive than is normally the case (< 0.1 S/m) the RIM signal through the coal seam is extremely highly attenuated and will leak into the boundary shale layers. In this case the RIM technique may not be applicable. At this level of coal and shale conductivity the effect of a change in the relative permittivity of coal (in the range 2 to 20) and the permittivity of the shale (in the range 10 to 40) is marginal.

The presence of any metal work among the coal seam rib walls also affects adversely the RIM signal propagation across the coal seam. The extent of this depends on the location, area and conductivity of the metal work. If the side walls in the road ways are electrically conducting the direct propagation of a RIM signal across the width of coal seam may no longer be possible.

The RIM imaging capability was investigated for a variety of flaw types over a range of operational conditions.

2.3.6.3 Improvements in tomography reconstruction algorithms (T6.3)

Task Description: Define improvements in tomography reconstruction algorithms in terms of improved resolution, and in particular lateral resolution. Investigate a range of effects of geological uncertainty on the EM response of the evolving ‘shared-earth model’.

The work carried out for this task has been combined with Task 6.4 for reporting purposes.

2.3.6.4 Investigation and testing (T6.4)

Task Description: Investigation and testing of combined gains from enhanced image reconstruction techniques together with improvements to signal transmission and acquisition sub-systems. Constructive evaluation of the experimental phase of the project to ascertain observed and potential technological benefits and future possibilities.

The modelling work that was undertaken established the need for a re-appraisal of radio imaging techniques. According to a standard interpretation of the RIM method, the layers of conducting rock above and below the coal seam form a lossy electrical transmission line and the coal provides further attenuation losses by ‘short-circuiting’ the line. The RIM technique measures the attenuation of the signal between pairs of locations along the coal panel. Above a critical frequency (known as the waveguide cut-off frequency) the conducting boundary layers of rock will allow wave patterns to become established in the space between them. The structure is then identified as a ‘waveguide’ and must be modelled in a different manner. The salient point is that RIM operates below the cut-off frequency, when the structure behaves as a transmission line.

Through further modelling, an alternative strategy to RIM for coal seam imaging was developed which was given the acronym GEM (Guided Electromagnetic Wave). The salient point is that, unlike RIM, GEM operates *above* the waveguide cut-off frequency and relies upon the entire coal panel sustaining a resonant electromagnetic wave.

In comparison to RIM, GEM uses a similar deployment strategy except for three important factors. Firstly, the GEM technique uses conducting boundaries along coal panel faces in the roadways to form a rectangular waveguide. Secondly, GEM does not necessarily operate at any ‘standard’ transmitter frequency; rather it sweeps the input frequency until the waveguide is set into a resonant (evanescent waveguide) mode. Thirdly, in GEM the transmitter is inserted into the coal seam to give maximum coupling. A comparison between RIM and GEM is shown in the *Table* below.

Parameter	Radio Imaging Method (RIM)	Guided Electromagnetic Wave method (GEM)
Principle of operation	**Transmission line** bounded by top and bottom conducting layers	**Waveguide** bounded by top and bottom conducting layers and conducting mesh placed along coal panel and roadways
Operating frequency	*Below* waveguide cut-off Expressly not a 'waveguide' mode Frequency is usually one of several 'spot' values	*Above* waveguide cut-off Frequency is chosen to bring waveguide to resonance
Signal coupling	Roving induction loop transmitters couple only a small amount of energy by induction. Techniques outlined in Work Package 5 may improve this.	Stationary antenna inserted directly into coal seam
Tomographic data	Obtained by making multiple measurements of signal attenuation and phase shift across coal panel	Obtained by measuring signal attenuation and phase shift of the resonant wave established in the structure from a single transmitter

Table 2.3.6-2 : Comparison of RIM and GEM techniques

For the GEM technique there are a number of possible modes (i.e. electromagnetic wave patterns) that can be set up in the waveguide, and each mode is a direct function of the dimensions of the waveguide. The coal seam is continuously excited with a loop antenna embedded into the coal seam to enforce a fundamental TE_{10} mode to be set up in the coal seam. Because the GEM resonance frequency(s) are related to coal seam dimensions, any discontinuity (fault or roof/floor material intrusion into the seam) will change the expected resonance frequency and will thus indicate that a fault exists in the seam. Moreover in GEM, known field modes are set up in the coal panel, permitting the EM field distribution in a flawless scenario to be predicted. Once a deviation in the resonance frequency of the waveguide mode is observed, further sensing of the EM field resonance modes in the coal seam can be performed. A standard tomographic inversion process can then be performed using image construction algorithms similar to those used in RIM, in order to obtain the knowledge of the flaw location, size, shape and its electrical nature.

The GEM principle was modelled for a variety of types of flaw. The model results demonstrate that each different flaw type introduces a unique change in the resonant response and the model (TE_{10} mode) field in the coal seam. Excitation issues such as the influence of the location of the excitation port along the coal seam length and the coupling slot orientation were also studied in detail. Through extensive modelling, the range of electrical conductivity of coal and associated shale strata required to establish an undistorted model field distribution in the coal seam for the GEM technique were determined.

The establishment of modal fields in the coal seam waveguide depends on the electrical conductivity of the coal and the shale layers. TE_{10} mode propagation is predicted to be detectable some 1000 m into a 300 m wide by 6 m high rectangular coal panel for which $\varepsilon_r = 10$ at a frequency $f > 158$ kHz, and at an injected power level of ~1 kW, provided the conductivity of the coal (σ) is less than 100 μS/m ($\tan\delta \approx 1$) and the conductivity of the shale layers forming the coal-seam waveguide is about 5 S/m. This implies that the coal cannot be too wet. When the shale is less conductive, (< 1 S/m) and/or coal seam is more conductive, (> 100 μS/m), the energy losses into the shale and coal layers prevent the formation of the TE_{10} mode. Any increase in the excitation power to compensate for the shale and coal losses introduces distortion by the local non-modal source field near the excitation region.

The modelling evidence is that there is an injected power level 'window' within which a detectable or discernable mode can be set up in a lossy geological stratum such as a coal seam. If the injected power is too low then the modal fields are lost in noise. If they are too high, in order to overcome high

power loss, the modal fields may be undetectable as they are swamped by the local non-modal source fields. For example with a theoretical 1 kW of injected power, for a panel with $\sigma_{coal} > 100$ μS/m and $\sigma_{shale} = 5.0$ S/m, the TE_{10} mode will be distorted at less than 600 m and no longer detectable at more than 900 m.

For a panel with reflecting end walls (e.g. the Daw Mill panel some 300 m wide, by 6 m high and 1000 m long) a longitudinal standing wave pattern is predicted provided that the conductivity of the coal is less than 100 μS/m. This figure will depend on the particular standing wave pattern which is formed. For a coal seam with the above dimensions and for which $\varepsilon_r = 10$ and $\sigma = 100$ μS/m the TE_{10} standing wave resonance will occur at 260 kHz, and at a power level in the range 1 kW to 10 kW

In a very wet or electrically lossy geological layer ($\sigma > 3$ mS/m), TE_{10} mode formation will not occur in a layer which is more than about 50 m wide. Computations indicate that the highly attenuated spreading wave from the electromagnetic wave source essentially disappears at 50 m (about $\lambda/4$) from the source.

Further reporting on this topic is given in an appendix to this report.

2.3.7 WP7 Modelling

2.3.7.1 Construction of geotechnical and numerical models of mining induced changes in stress and deformation (T7.1)

Two benchmark models were defined relevant to two main mining application areas: conventional long-wall extraction and underground coal gasification. The benchmarks are not site-specific; however, the geological settings and the material properties have been inspired by the interpreted data from the Daw Mill Colliery (Task 7.3). Task 7.1 comprises a tool comparison component as each of the three project partners involved in this work package used a different numerical tool for geomechanical simulations.

Case 1 – *Subsidence above longwall coal mine* – is a synthetic case of subsidence prediction above a longwall coal mine based on subsidence prediction example 1 from the Subsidence Engineers' Handbook (SEH; National Coal Board, 1975). SEH provides subsidence solutions based on empirical data from the extensive history of longwall coal mining operations in UK. The existing empirical solutions were used to evaluate the predictive capability of different numerical tools used for subsidence prediction. FLAC*3D* (a finite difference package; FLAC, 2007) simulations, carried out with the large strain hypothesis, resulted in the best match with the SEH/MulPan subsidence profile. Using a Double Yield material model for the caved waste material (goaf), which can cope with significant irreversible compaction, and iteratively changing the input parameters for this material model, it was possible to obtain a good match between the SEH/MulPan and FLA*3D* subsidence profiles. In contrary to FLAC, the finite element simulations (carried out using the SavFem, -, and Diana packages, 2008) and the semi-analytic approach (carried out using the AEsubs package; Fokker and Orlic, 2006) resulted in a much poorer match with the SEH/MulPan subsidence profile. The finite element packages used were inferior to the explicit finite difference code FLAC in simulating large strains-large deformations. The semi-analytic package used assumes elastic response of all the rock surrounding the mine cavity, which is a sound assumption in the oil and gas industry in the case of a compacting hydrocarbon reservoir, but not in the coal mining industry in the case of plastic rock deformation (comprising caving and fracturing) around a mine opening.

Case 2 – *Induced changes in stresses and deformations around mining caverns in coal* – investigated the influence of different roof strata lithologies on stress distribution and deformation around a cavern in coal. In particular it was investigated how the inhomogeneous roof lithology affects the spatial extent of stress perturbation and plastic deformation around a cavern of different size. The roof comprised of a horizontal sequence of alternating, 2 m-thick layers of mudstone, sandstone and coal. The numerical tools used for calculations were the same as in the case of Test case 1. Two reference cases were defined without variations in roof lithology. Other scenarios considered possible combinations of one or two coal layers interlayered between either mudstone or sandstone layers. The simulation results obtained by using the FE packages SavFem and Diana were very similar, while the FLAC results exhibited dissimilarities due to different loading conditions used in calculations. It was noted that inhomogeneous roof strata lithology largely affects the extent of plasticity and fractured zones above the cavity. Mudstones are generally weaker than sandstones and promote development of more extensive plasticity zones in the roof than sandstones, especially in scenarios with sequences of coal layers in-between mudstones. The key material properties that largely determine the extent of plasticity and fractured zones around the modelled cavity are the tensile and shear strength of each rock type in the roof strata sequence.

2.3.7.2 Identify predictive capabilities of enhanced radio imaging technique (T7.2)

As a result of modelling undertaken within the ADEMA project it was identified that the main contributory factor to the limited success of the radio imaging technique in the UK is the higher conductivity of the coal seam, which requires a reduction in the probing frequency, and a corresponding increase in the skin depth in the surrounding rock. This leakage of signal is now believed to be the cause of the limited success of the tomographic reconstruction. Within Work

Package 5, a number of techniques were developed that will remove the need to reduce the probing frequency. However, it is still the case that a reduced conductivity contrast between the coal and the surrounding rock will affect the accuracy of any tomographic reconstruction.

Because the problem appeared to be of geophysical origin rather than one of tomography, resources in Work Package 6 were diverted into obtaining a more thorough understanding of the process of radio imaging. It was originally proposed that, within Task 7.2, the predictive capabilities of an enhanced radio imaging technique would be identified, including a probabilistic models of coal seam washout or fault detection and the localisation accuracy. However, the necessary departures from the original programme have limited the results that could be obtained for this task. The work has, however, established guidelines on the likely operational capability of both a conventional radio imaging system and a novel alternative, referred to as 'guided electromagnetic wave' (GEM). An overview and analysis of RIM is given in Work Package 5, and a description of GEM in Work Package 6.

2.3.7.3 Construction of a 'shared earth' model at the case study site (T7.3)

A *3D* geological model of the selected case study site – the Daw Mill Colliery – was constructed in Petrel (Petrel, 2007) using the oilfield approach of a shared earth model (Olden *et al.*, 2001; Pringle *et al.*, 2004). The model is based on interpretation of *3D* seismic, borehole and geological data from Daw Mill and it was continuously updated during the lifetime of the project. Since the start of the project, the shared earth model of the Daw Mill was accessible through a shared online workspace. Using a shared earth modelling approach developed in the oil and gas industry proved to be an efficient way for visualisation and communication of the results among the project partners also in the current coal mining-related project.

Available data from 50 boreholes from the Daw Mill area were analysed in order to determine characteristic geological settings and rock material properties required for geomechanical benchmarks used in Task 7.1. A representative seismic section was selected and interpreted using geophysical and borehole log data. Six boreholes with the most extensive sets of relevant log types were used for lithological determination and geomechanical characterization. The oilfield-based lithological interpretation relying on gamma ray, sonic and bulk density borehole logs was successfully carried out. This interpretation was found to be more reliable and accurate than lithological determination based on visual inspection of drilling cuttings.

The oilfield-based approach was also successfully pursued in determination of elastic rock material properties from the available borehole logs. For determination of dynamic elastic properties both compressional- (*Vp*) and shear (*Vs*) wave velocities are required. As the shear velocity were not measured in boreholes, *Vs* was estimated using different empirical relationships from the literature (e.g. Castagna *et al.*, 1985; or assuming a constant ratio of *Vp/Vs*=2). Dynamic Young's moduli were calculated using the relationships between the elastic rock properties and wave velocities, which are well-known from the rock physics literature (e.g. Fjær *et al.*, 1992). Since in the geomechanical calculations static Young's moduli are needed, dynamic Young's moduli were converted into static using an empirical relationship (Eissa and Kazi, 1998). The described method for determination of elastic rock parameters from borehole logs performed well in the case of Daw Mill. This indirect method and the direct measurements of rock mechanics properties on samples complement and strengthen each other.

Further reporting on this topic is given in an appendix to this report.

2.3.8 WP8 Geological Validation

(Geological validation and verification of exploration techniques)

2.3.8.1 Collection of geological data at case study sites (T8.1)

During the three years of the project a total of 2347 m of underground roadways were driven. This is substantially lower than envisaged at the start of the project; principally due to changes in the development strategy at the mine due to a fatal accident in January 2007 where part of a roadway side collapsed. This lead to major reduction in development potential as resources were diverted into extensive remedial works to ensure safety in the existing mine infrastructure.

A total of 23 cored underground boreholes were drilled within the period of the project ranging between 5 and 20 m in length. Samples of core from these were provided to partners for analysis and testing in task 8.3. Details of all existing surface boreholes and the geophysical logs relating to these were supplied the relevant partners for use within the project. All available information on stress direction in the case study mine was provided and one new detailed stress measurement was carried out underground at the mine.

2.3.8.2 Collation of geological information from case study sites (T8.2)

Regular underground under ground observations throughout the project period have resulted in the construction of detailed maps and sedimentary models an example of the geological record plan compiled is shown in *Figure 2.3.8–1* below.

Figure 2.3.8–1 : Geological record plan for 302's panel

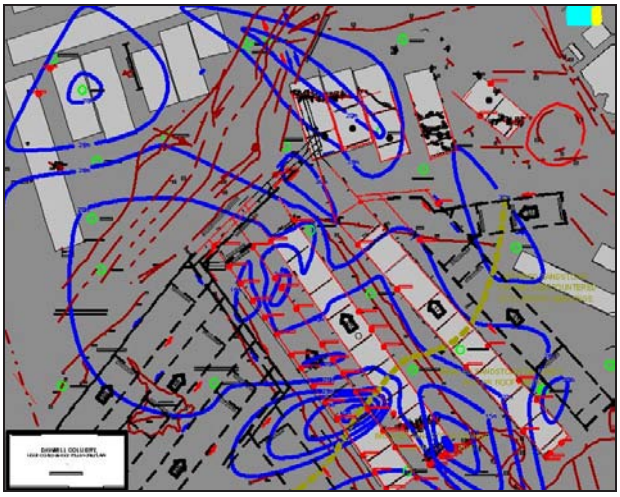

Figure 2.3.8–2 : Location of roof cores to the end of June 2008

The sedimentary variation in the roof measures as determined from the available borehole and underground cores has been modelled, as shown in *Figure 2.3.8–2* above. This shows the location of all the cores taken up to the end of the project period including those completed before the start of the project. The thickness of mudstone roof strata in the roof to the base of stronger siltstone, locally sandstone upper roof is shown in blue. The area at risk from sandstone roof intrusion is shown in gold faulting and structural anomalies are shown in red.

2.3.8.3 Laboratory measurements of static rock properties and failure tests (T8.3)

During the project samples taken from a 20 m cored borehole drilled underground at Daw Mill were tested for geomechanical properties the results are shown in the table below.

Sample No	Height above road-way	Lithology	UCS (MPa)	Modulus (GPa)	Density (g/cc)	Cerchar Index	Abrasivity
1	6.84 m	Siltstone fine sandy laminae	51.05	7.49	2.62	0.6	Slightly abrasive
2	7.40 m	Sandstone fine, silty laminae				0.8	Slightly abrasive
3	8.08 m	Sandstone medium	63.05	6.75	2.59	1.7	Abrasive
5	8.85 m	Mudstone, silty in parts				0.5	Not very abrasive
6	9.38 m	Mudstone, siltstone in parts	52.96	-	2.60	0.4	Not very abrasive
7	10.37 m	Siltstone medium	73.34	5.8	2.64	0.9	Slightly abrasive
8	10.86 m	Mudstone silty				0.5	Not very abrasive
9	12.24 m	Sandstone medium	27.33	9.59	2.40	1.7	Abrasive
12	14.20 m	Sandstone, silty laminae	93.70	8.61	2.45		
13	14.88 m	Sandstone silty laminae	91.48	6.56	2.52		
15	15.61 m	Siltstone fine, sandy laminae	32.20	-	2.56		
17	16.74 m	Siltstone medium, sandy lenses	39.33	-	2.72		

Table 2.3.8-1 : Daw Mill colliery, 300's intake up-bore @1464 mm

2.3.8.4 Evaluation of seismic characteristics in relation to gas content (T8.4)

The goal of this task is to evaluate whether variation of gas content in coal can be shown by means of seismic methods, because there is a clear difference between gas contained by conventional reservoirs and by coal seams.

Background

The gas that is naturally is retained in coal in the subsurface is referred to as coal bed or coal mine methane, because of the high concentration of this gas (> 90%). Most of the methane in a coal is adsorbed on the coal's microstructure. The gas content in the water filled pores and cleats of the coal, is minimal. The gas sorption capacity of coal is generally interpreted to depend on pressure, temperature and coal characteristics. The relationship between pressure and sorption capacity appears to follow a pressure-dependent Langmuir isotherm. This isotherm displays a parabolic increase of the gas-sorption capacity with increasing pressure, until a maximum is reached above 20 MPa. This behaviour reflects mono-layer adsorption on a surface, where the maximum represents a completely saturated surface along which the mono-layer approaches liquid density. The methane content calculated with the Langmuir isotherm is consequently the maximum that the coal seams can contain at the in-situ reservoir pressure. With increasing temperature, the gas-sorption capacity shows a decrease that is reported to be either linear or exponential. Consequently, the opposed effects of pressure and temperature result in a maximum in gas-sorption capacity at a certain depth

Seismic response

Due to the structure of coal, the porosity of coal is usually very small ranging from 0.1 to 10%. Because the majority of the gas is not present in the matrix porosity of a coal seam, but adsorbed onto the surface of micro pores its presence has a limited effect on seismic parameters such as P-wave velocity and density. However, if an opportunistic scenario is assumed, in which the coal has an estimated effective porosity of 10% and the cleats are completely filled with gas instead of water, the change in P-wave velocity and density can be estimated with (Gassman, 1951). This results in a decrease in P-wave velocity of ~8%, and a decrease in density of ~7%, depending on bulk modulus, dry rock parameters, etc.

The previously defined simplified model based on the Hillfields well logs shows a P-wave velocity of 2540 m/s and a density of 1400 kg/m^3 for the Thick Coal Seam. Assuming these values are for a water saturated coal, above mentioned percentage changes in velocity and density, due to the presence of gas instead of water, will give a P-wave velocity of 2335 m/s and a density of 1300 kg/m^3. No change in S-wave velocity is assumed. The seismic response of the water-saturated and gas-saturated Hillfields model is displayed in *Figure 2.3.8-3*. The amplitude of the Thick Coal Seam reflection in the model with gas is higher (roughly 15%) compared to the situation without gas (right of *Figure*). Also, there is a small velocity push down effect due to the above-mentioned decrease in P-velocity. This might slightly influence the estimated amplitude in the difference plot.

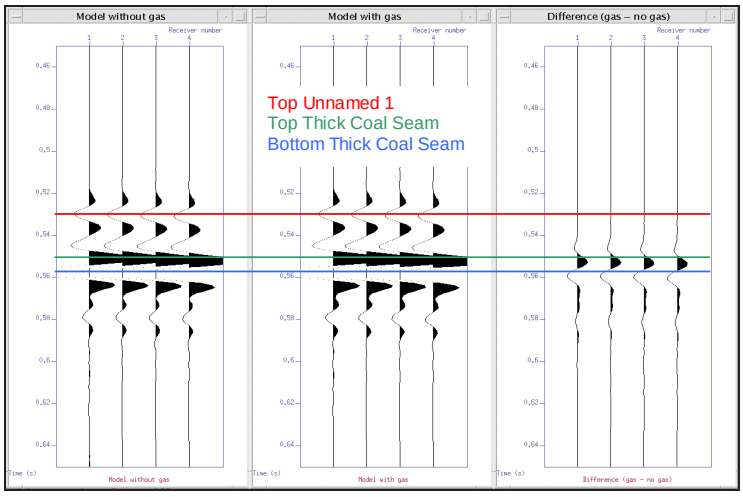

Figure 2.3.8-3 : Seismic response of Hillfields model
First 4 traces of the seismic response of the water-saturated (left) and gas-saturated (middle) Hillfields model together with the difference plot (right).

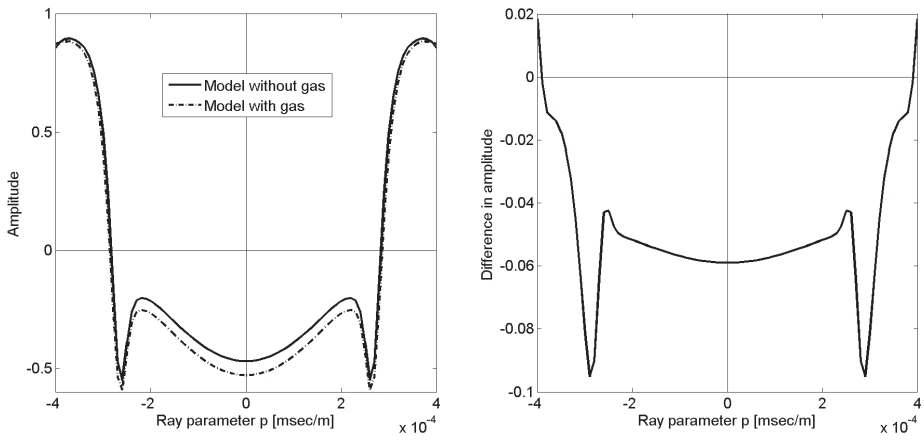

Figure 2.3.8-4 : The AVP response for the Hillfields model
AVP curve: amplitude v. ray parameter. The AVP response of the top of the Thick Coal Seam for the Hillfields model with and without gas (left) and the difference between these two responses (right).

Figure 2.3.8-4 shows the same situation, but now the change in response of the amplitude with ray parameter (AVP). Additional, to amplitude differences only, the shape of the curve can be examined. In this *Figure* it can be seen that, within the critical reflection angles (p = +/- 0.00028 s/m), the predominant effect is a higher seismic amplitude for the model with gas included. However, the change of curvature is small (a few percent).

Results from Daw Mill

Samples of coal were taken from underground for gas content determination. This was achieved by drilling into the rib side of a new roadway. In an attempt to obtain samples as near to the virgin state as possible. It was not practicable to drill at the freshly cut coalface for operational and safety reasons. Because of this it was attempted to drill deep into the coal rib as close to the fresh cut as possible hoping to access coal with original gas content. The results are shown below:

Gas content determination

Mine: **Daw Mill mine, UK-Coal** Coordinates: x-value **427962**
Date of investigation: **01.07.2008** y-value **285421**
Seam: **Ryder/EII/Top nine feet coal** depth (msl): **-544,37 to -544,50** m
Location of sampling: **32´s coal gate** volatile matter: **39,6** % i.daf

No. of application: 1687-1 normal conditions: 1013.0 hPa ; 273.0 K

No. of sample	No. of borehole	Depth of borehole	grain size	gross weight	ash	mass ashfree	Gas portion q1	Gas portion q2	Gas portion q3	total gas content	q1-bar(u)-value	desorbable gas content
		m	mm	g	% by weight	g	m³/t	m³/t	m³/t	m³/t	m³/t	m³/t
1	1	2,0	F	126,3	1,7	124,0	0,0	0,1	0,9	1,0	1,3	**0,0**
2	2	2,0	F	211,6	4,3	201,7	0,0	0,0	1,2	1,2	1,3	**0,0**
5	5	2,0	F	56,8	4,8	53,9	0,0	0,0	1,0	1,0	1,3	**0,0**

F > 2 mm

Gas content determination

Mine: **Daw Mill mine, UK-Coal** Coordinates: x-value **427962**
Date of investigation: **01.07.2008** y-value **285421**
Seam: **Two Yard Coal** depth (msl): **-544,37 to -544,50** m
Location of sampling: **32´s coal gate** volatile matter: **35,0** % i.daf

No. of application: 1687-2 normal conditions: 1013.0 hPa ; 273.0 K

No. of sample	No. of borehole	Depth of borehole	grain size	gross weight	ash	mass ashfree	Gas portion q1	Gas portion q2	Gas portion q3	total gas content	q1-bar(u)-value	desorbable gas content
		m	mm	g	% by weight	g	m³/t	m³/t	m³/t	m³/t	m³/t	m³/t
3	3	2,0	F	214,2	8,2	195,3	0,0	0,0	1,6	1,6	1,4	**0,2**
4	4	1,0	F	188,4	1,6	185,2	0,0	0,2	1,1	1,3	1,4	**0,0**

F > 2 mm

Table 2.3.8-2 : Gas content determination at Daw Mill

It was concluded that the Gas content at Daw Mill is generally low and that the depth of penetration into the solid coal was not sufficient to obtain coal containing original gas content.

2.3.8.5 Task 8.5 Use acoustic array technology to calibrate AVO.

A laboratory system to calculate AVO was developed. No valid results were obtained for the rocks tested due to acoustic source level restrictions .However, the instrumentation and processing techniques were established for future research.

2.3.8.6 Task 8.6 Review AI inversion methods and results]

The goal of this task is to collect geological information of the case study site from the results of the acoustic impedance inversion technique as applied by SIP. Calibration is done by comparing the results from the seismics to lithological descriptions from boreholes.

Properties versus lithologies

In order to determine the specific properties for the main lithologies at Daw Mill, the lithological sequences derived from drilling reports (cutting descriptions) for Hillfields, Long Lady Wood, Eaves Green Lane and Keatleys Pool boreholes were applied. Several indicative properties from well logs are discriminated per lithology (see *Table* below). Whereas the distinction between sandstone and siltstone is ambiguous for acoustic impedance, bulk density and transit time, mudstone and especially coal are easily distinguished based on these properties. Gamma ray characteristics are relatively dispersive, showing high standard deviation values (see *Figure* below).

	Sandstone	**Siltstone**	**Mudstone**	**Coal**
Acoustic impedance (10^6 kg/m^2 s)	10.31	10.19	7.82	3.91
Bulk density (g/cm^3)	2.53	2.55	2.32	1.49
Transit time (us/ft)	75.6	77.4	92.3	117.6
Gamma ray (API units)	76.3	134.4	143.6	40.6

Table 2.3.8-3 : Well log derived properties
as distinguished per lithology (mean values). Based on Hillfields, Long Lady Wood, Eaves Green Lane and Keatleys Pool boreholes.

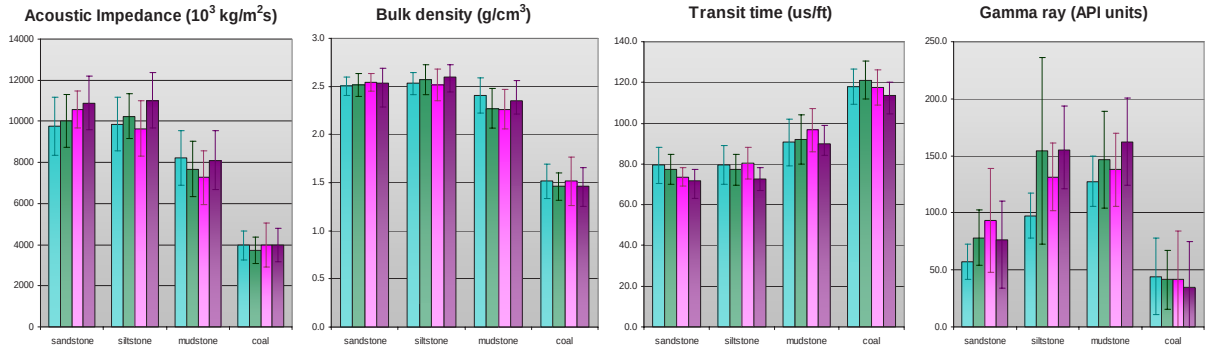

Figure 2.3.8-5 : Property mean values calculated from well logs.
Bars indicate standard deviation. = Hillfields, = Long lady Wood, = Eaves Green Lane, = Keatleys Pool.

Comparison of the acoustic impedance cube for the Daw Mill area in depth domain, provided by SIP, with well logs clearly shows the expected resolution contrast (see *Figure* below). Well log data obviously provides better constraints for detection of coal seams. The impedance cube's resolution amounts approximately 6 metres, which still is sufficient for detection and *3D* tracking of the Thick Coal Seam. However, thinner seams (e.g. Half Yard Seam, bench Seam) are not easily recognizable from the impedance cube.

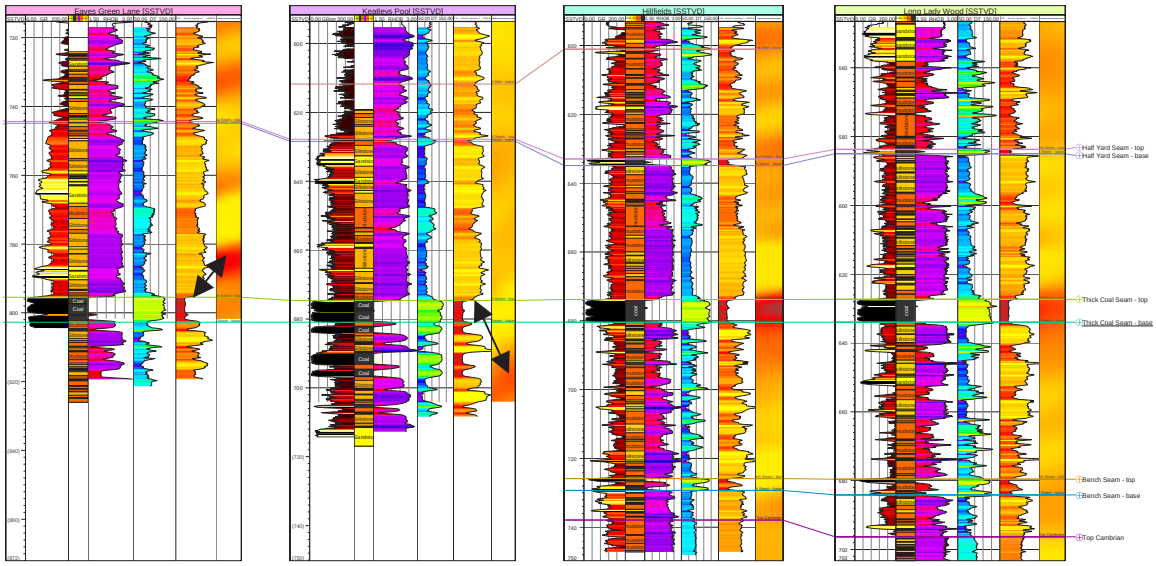

Figure 2.3.8-6 : Well logs compared to acoustic impedance cube sections
for Eaves Green Lane, Keatleys Pool, Hillfields and Long Lady Wood boreholes. Log panel consists of: gamma ray, lithology, density, sonic, acoustic impedance logs and acoustic impedance cube section. Arrows indicate depth mismatch resulting from time-depth conversion of impedance cube.

A comparison between the inverted *3D* seismic volume and lithology from boreholes and mine workings has yielded the following results

Dirt Bands

A 1.2 m dirt split encountered in 31's panel was not clearly interpreted on either the seismic or inverted seismic data. A geological feature was encountered in the access roadways for 300's block. This was proved, by drilling down in the roadway, to be a substantial thickening of the dirt split to around 2.5 m.This feature was unexpected from the previous geological interpretation using the *3D* seismic data but its effect could be seen on images from the inverted volume and its extent estimated.

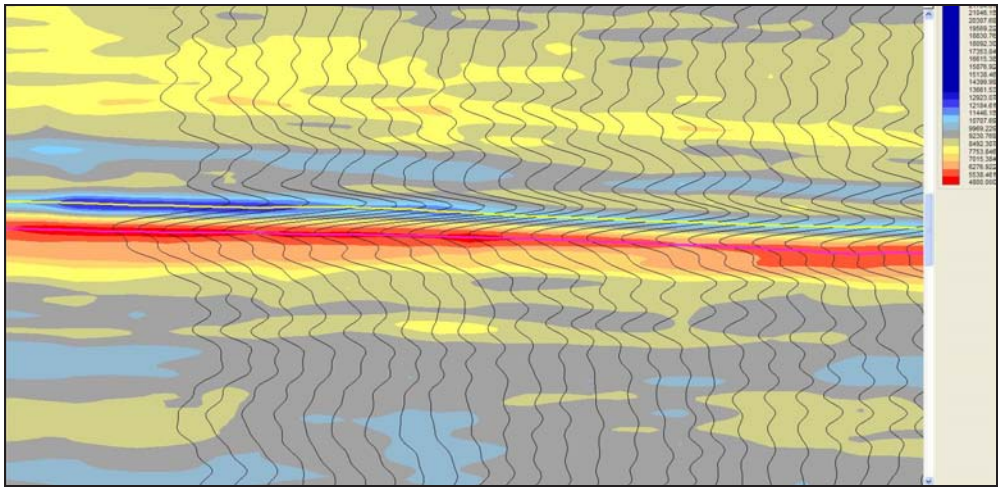

Figure 2.3.8-7 : Section along 300's intake
Using Acoustic impedance data correlates to thicker dirt split in the coal seam

Seam Thickness

Mapping variations in seam thickness using the *3D* seismic data set was not possible. In Keetleys Pool Borehole the thick coal seam is present twice with a 4 m interval caused by a thrust fault. The effect of this could be seen on the inverted data image and its extent estimated but could not be interpreted

from the *3D* seismic data set. Other variations in seam thickness have not been seen, it is estimated the coal section is similar in the area and any local variations are probably caused by seam splitting.

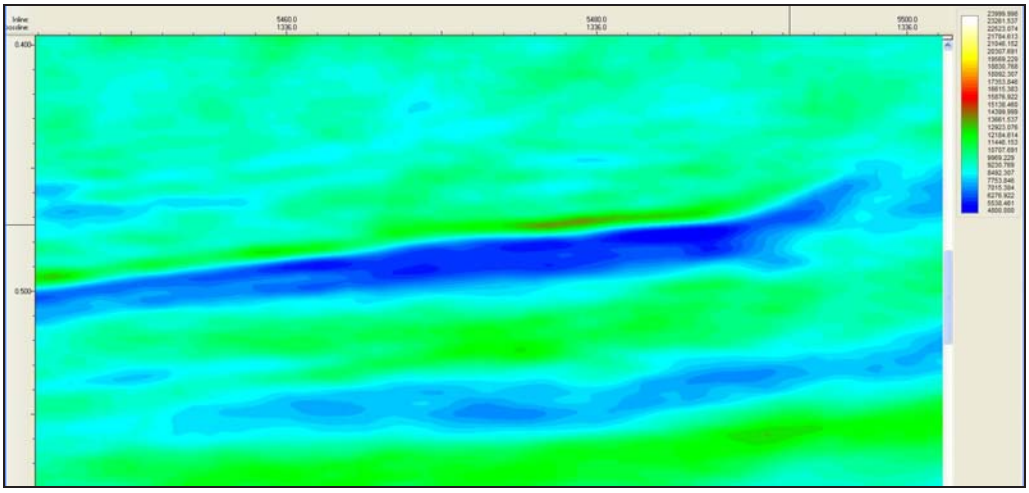

Figure 2.3.8-8 : Acoustic impedance section
correlating with Double seam section in Keatleys Pool surface Borehole

Faulting

Faulting can be mapped using images from the *3D* data set. Faults can be interpreted using images of seismic amplitude variations. There are also variations in the amplitude at the thick coal horizon in images produced from the inverted data set and comparing the two data sets has enabled the presence and size of minor faulting to be more confidently predicted but no new faults have been identified.

Other Results

From the inverted data an event has been mapped in the roof strata close to the seam. This has enabled mapping of zones of possible variations in roof conditions indicating possible problems. In addition a map was produced of the variation in roof acoustic impedance across the area corresponding to an increase in the presence of roof sands.

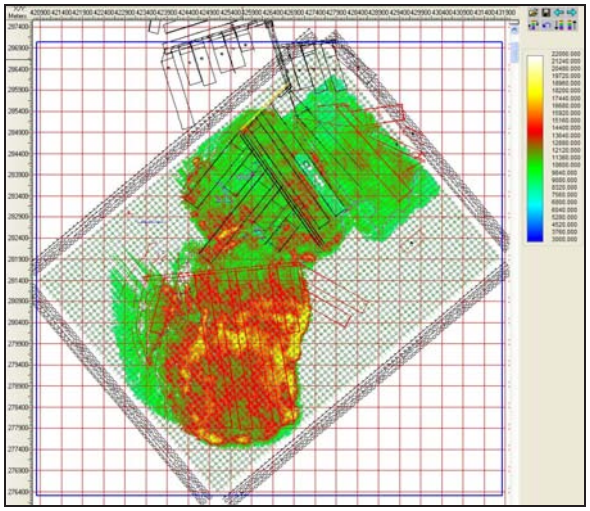

Figure 2.3.8-9 : Variation in Acoustic impedance
corresponding to increased sand content in roof sequence

The geological setting of Daw Mill colliery is deceptive. The northern end of the Midlands micro-craton has a complex, though unspectacular structural history. Strike-slip faulting along craton margins and soft-sediment slides due to block-tilting are well recorded in the nearby Staffordshire Coalfield to the west. the *Figure* below shows similar apparent structures in the Daw Mill *3D* seismic data.

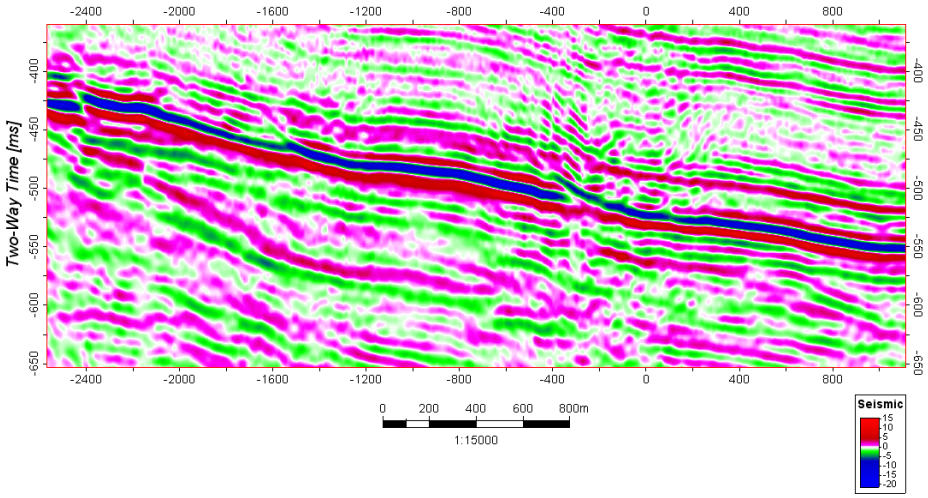

Figure 2.3.8-10 : Inline section through 3D *seismic volume*
showing two possible soft-sediment slides at centre – now over-thrust up dip. Also note a clear reverse fault at the left hand edge of the section.

The structures that may affect mine productivity may be below the resolution of some geophysical methods. In the *Figure* below, the RIM technique achieved a blurred image of small faults across a retreat panel. The panel later proved the faults, but the image had been unconvincing to mine planners. Note that the small faults should extend into the *3D* seismic coverage to east-north-east and west-south-west, but they are not at all resolved by the seismic dip attribute map. The seismic dip map does resolve faults that are parallel to and west of the panel, both as high dips in yellow and red and as an abrupt swing in the structural contours around -470 and -480 ms TWT. Experience recommends that several geophysical techniques be used in combination, since a single technique is often ambiguous.

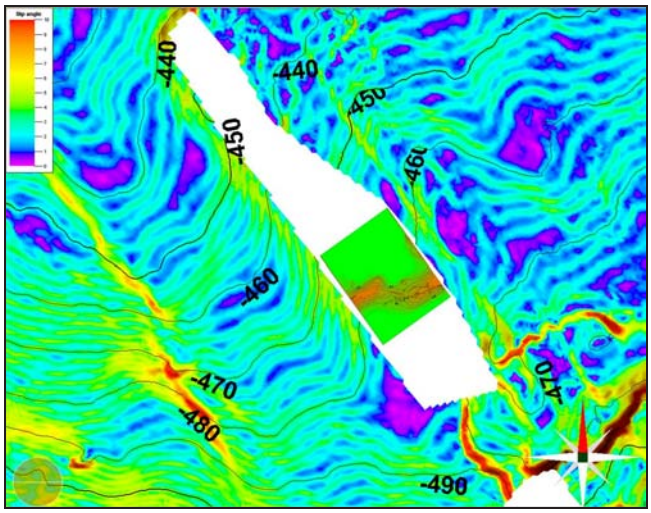

Figure 2.3.8-11 : UK Coal 3D *seismic dip attribute with TWT contours*
The white area is an excised area of the seismic image, badly affected by mining activity. The green and brown rectangle within the panel area is a RIM inversion image of small-scale faulting.

The ADAPS suite of non-linear seismic algorithms was applied in two modes to the Daw Mill *3D* data. First ADAPS removed coherent noise from the pre-stack gathers; see *Figure*s below.

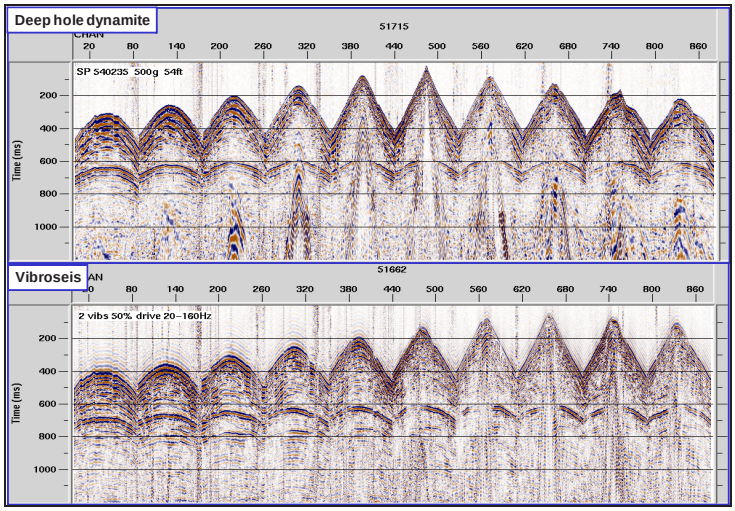

Figure 2.3.8-12 : Serious central noise cone problems on both sources in the Daw Mill 3D *seismic data.*

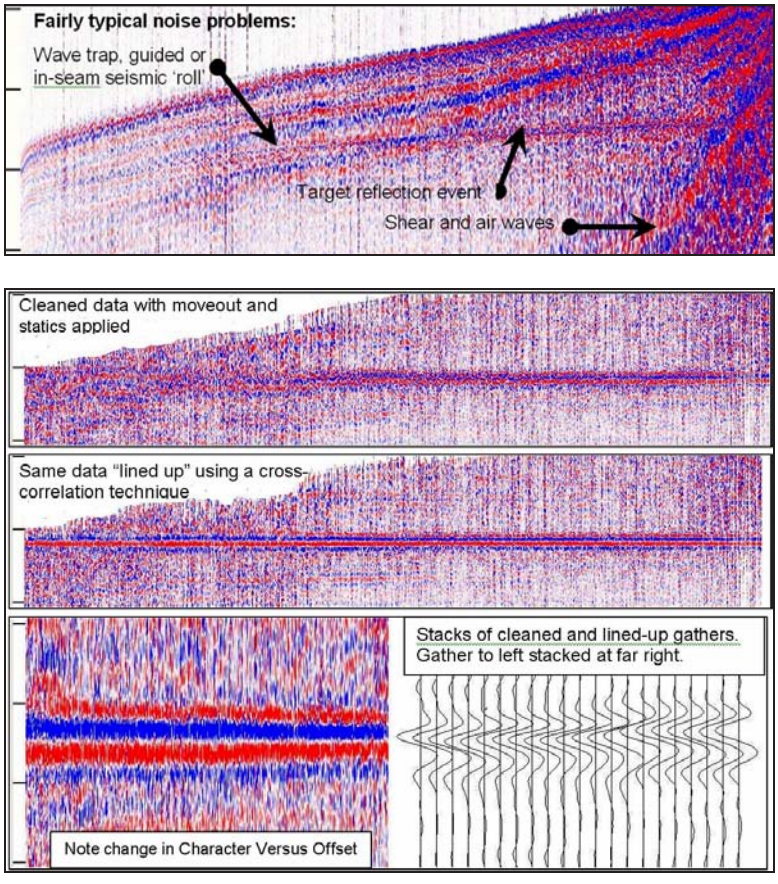

Figure 2.3.8-13 : Non-linear, pattern-based ADAPS pre-processing as applied to Daw Mill 3D *seismic gathers. Top: before processing; bottom after separate stages of processing*

After pre-stack noise removal, an ADAPS inversion technique was applied to the stacked data. It applied another non-linear estimation method to infer a seismic wavelet, which matched that used by a previous study. It then removed the wavelet from each trace to leave a set of spiked, reflection-coefficient time series. The ADAPS, non-linear inversion method started with these advantages: the

target envelope is very strong; the polarity of the two interfaces of interest is known; therefore the first part of the target envelope should duplicate the first part of the wavelet, and a 'guess' can be built. After normalisation, the guessed wavelet is subtracted from the original stack. The process repeats to extract the base reflector. Success is measured by the energy reduction in the target zone (second trace from right in the *Figure* below).

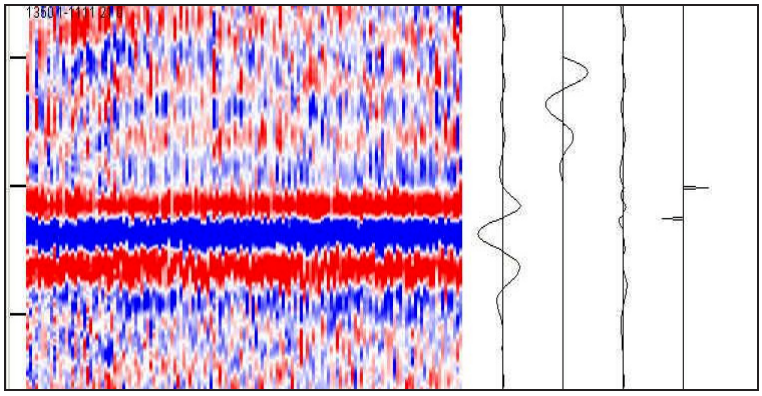

Figure 2.3.8-14 : An illustration of the ADAPS inversion algorithm
the single traces, from left to right are: the stack, the wavelet estimate, the resolved stack and the interfaces

Note that both noise reduction and inversion ADAPS processes work in time, not frequency domain. There is no multi-trace averaging, which can lead to smeared events and loss of spatial resolution.

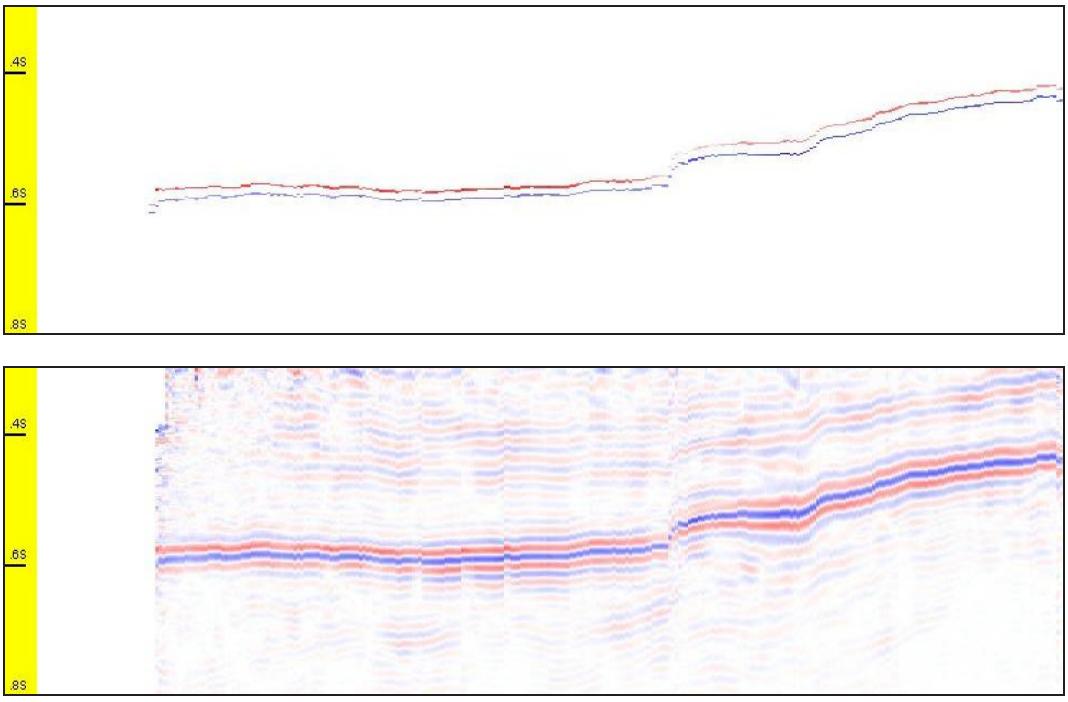

Figure 2.3.8-15 : ADAPS inversion of Daw Mill 3D *seismic data*
A SW-NE random line in colour amplitude display through the Daw Mill 3D *seismic data, above. The ADAPS inversion below – both the roof and the floor of the target seam are resolved. Note the apparent seam thickness change across the fault step*

2.3.8.7 Validate coal seam mappings derived from enhanced radio imaging (T8.7)

It was originally proposed that a reconstructed coal seam mapping would be validated against information derived from other project geophysical methods and from the geological information obtained from mining and the borehole programme. However, necessary departures from the original programme in Work Packages 5 and 6 meant that this task could not be undertaken.

2.3.9 WP9 Project Assessment and Conclusions

2.3.9.1 Review of all techniques in the light of mining experience (T9.1)

Task description: Review the information obtained from all the techniques developed in this project in the light of mining experience at the case study site.

A variety of exploration techniques and methods have been developed and evaluated during the ADEMA project. A good degree of collaboration and transfer of ideas has occurred between the various partners, which is summarised below.

Work Package 2: Acoustic impedance Inversion

The objective of this work package was to improve the resolution of seismic data and to extract additional information from the data. The reprocessing of surface seismic data using several inversion techniques has improved resolution of sedimentary variation within the seismic volume. These techniques are equally applicable to 2D seismic data as well as to the 3D data utilised within the ADEMA project. A new dataset of acoustic impedance data has been generated indicating lateral variation in coal measures stratigraphy. The inversion techniques have enabled the prediction of operationally significant seam variations, such as splitting of the target seam, that were previously not well-resolved in the conventional seismic volume. There is potential for improved accuracy of fault identification although is it noted that in terms of the minimum displacement resolution there is only marginal improvement at the lower end of the scale. The techniques are equally applicable to thick seams and in multi-seam stratigraphy.

Work Package 3: Micro Seismic Monitoring

The deployment of continuous seismic monitoring equipment in a Polish coal mine, together with the development of novel processing software, has provided a mechanism for measuring the frequency and distribution of seismic events around deep mine coal workings enabling the calculation of changes in the velocity field associated with the dynamics of coal extraction. In particular, high stress zones, and the possibility of associated failure, are associated with zones of higher P-wave velocity and rate of change in the velocity. This has resulted in the successful prediction of dangerous rock burst events in high stress mining environments. The equipment and technique has potential for use in other European coalfields. In situations where a suitable array of geophones could be installed, both in surface boreholes and from mine workings, it would be possible to protect an area of several square kilometres in high-risk mines. There is potential to further develop the technique to monitor ground conditions and caving characteristics for underground coal gasification (UCG) projects. This could help to delineate stress fields created around a production burn.

Work Package 4: in situ Drilling and Geophysical Logging

The drilling and logging equipment was sourced and adapted to measure and record drilling parameters, this data was compared to information from geophysical borehole logs in six surface boreholes to provide an assessment of geotechnical characteristics of the rock being drilled. The application of the techniques developed was successful in providing good correlation between the drilling parameters and various characteristics of the in situ rocks. Further development of the equipment for application underground in coal mines is necessary and could see a potential gain if used in association with modern tunnelling machines with on board drill rigs, currently used primarily for placement of ground support. The provision of continuous geotechnical data via the techniques developed in work package 4 from on-board drill rigs could be a very useful tool in assessing roadway stability. This could potentially improve roadway design as a continual process rather than the current practice utilising sporadic spot coring or geotechnical testing. If implemented this has the potential to greatly improve tunnel stability and therefore safety in the underground environment. It should be possible to utilise the techniques extensively in UK and European coalmines.

Work Package 5 and 6: Radio Imaging

Investigation of signal transmission acquisition systems and tomographic reconstruction techniques was used to construct theoretical models to show possible results. Practical results indicate the restrictions associated with the application of the RIM technology are due to the higher electrical conductivity properties of the coal, which limits the transmission properties in the UK and European coal fields. Any further application in Europe depends on the conductivity of the specific target seams and the effective range required to be investigated by RIM. The electromagnetic modelling systems developed in the ADEMA project that investigate the coal seam response for differing geometries are available for further research.

Work Package 7: Modelling

The construction of a shared earth model was a useful tool for integration and presentation of results from various aspects of the research project. The application of the method for understanding stress variations around underground workings in coal mines showed significant potential and there could be equally beneficial gains around the understanding of the stress effects, including the development of the cavity, in underground gasification projects. There is also a potential opportunity for the further application of the GIG micro seismic monitoring method in dynamic monitoring of seismic activity and stress related changes surrounding underground gasification cavities. The application of modelling techniques to coal bed methane exploitation has highlighted the problems of low permeability and porosity in the areas considered. The consideration of the potential of seismic inversion methods to the identification of potential methane sources and CO_2 storage areas in virgin ground proved unsuccessful due to the low porosity. The calibration and processing of geophysical logs to model surface seismic data was achieved and integrated into the 3D shared earth model.

Work package 8: Geological validation

Sedimentary models generated from the seismic inversion data have been used to identify potential changes in the geology at the Daw Mill mine in the UK. During the project the geology encountered underground has been recorded and compared to the sedimentary model produced from the seismic inversion. Roof geology has been investigated using cored boreholes obtained throughout the project. There is a good degree of correlation between sedimentary variation inferred from the seismic inversion data and changes identified in the actual geology underground so far, further development of underground tunnels is required to fully evaluate the results.

2.3.9.2 Evaluation and application of techniques to other areas (T9.2)

Task description: Although most of the work packages in this project have used data collected from deep coal mines, it is thought that there will be applications for these methods in other geographical and technical areas. This work package examines the possibility of applying these techniques to deep coal mines in other parts of the EU, and also investigates their applicability to underground coal gasification, carbon capture, CO_2 sequestration and coal-bed methane exploration projects in the EU.

Underground Coal Gasification (UCG)

In 1989, the European Working Group on UCG recommended trials to evaluate the commercial feasibility of UCG in the thinner and deeper coal seams of Europe. The 1992-1999 trial was undertaken Spain, the UK and Belgium and supported by the European Commission. The site at El Tremedal in Teruel province, northeast Spain had extensive borehole data and a coal seam at a depth of 550 m. The trial was completed successfully, although operating hours were low. It demonstrated the feasibility of gasification at depth using directional drilling for well construction. Heriot-Watt University developed a coal resource under the Firth of Forth, Scotland; since licensed by BCG Energy Ltd.

With this background the ADEMA project assessed the application of the project results. One of the key requirements of a well-managed UCG operation should be to monitor the reaction chamber growth and the flow of reaction products. The burn front, cavity width and roof integrity should all be

monitored during and after each burn. In the former trial at El Tremedal, 'black box' calculations were used and it can be inferred that UCG operation lost a significant proportion of its product gas to overlying strata. The geophysical techniques developed in the ADEMA project could be suitable for monitoring UCG operations as follows

1. AVO with the AI inversion, ADAPS AI inversion and AVP inversion techniques could be used to analyse any 3D surface seismic acquired before or during the development of a UCG operation. As with deep coal mining, the nature of the roof is relevant to the design of a UCG operation. Apart from the issue of product gas losses noted at El Tremedal, some roof collapse helps to direct flow onto the coal wall rock, widening the reaction chamber and improving recovery.
2. GIG's micro-seismic monitoring system could be ideal for monitoring strata movement and velocity changes due to stress relief and gas migration. Aramco is trialling a similar system to monitor reservoir rock decrepitation as cold injection water displaces warm oil.
3. GIG's micro-seismic seismometers could be deployed in boreholes, including development wells not yet used for 'controlled retractable injection point' (CRIP) UCG; In that way, the source-to-receiver distance would be minimised, giving better angular resolution and greater sensitivity to small roof-fall events.
4. Heriot-Watt University's variation on a radio imaging technique, known as GEM, exploits the waveguide properties of a geological resistivity 'sandwich'. A variant has since been conceived that would be tuned to an oil leg in e.g. a North Sea reservoir. In Aramco's Ghawar reservoir the high-resistivity anhydrite cap rock is a better tuning layer and the tuning frequency could be sensitive to the distance between injected water fingers in the reservoir below. GEM instrumentation might also be deployed in boreholes, including development wells not yet used for CRIP UCG; Both vertical and directionally drilled wells are frequently drilled in oilfield exploitation where they are a vital production tool, which also offers an ideal monitoring location for arrays of seismometers or electromagnetic instruments.

Carbon Dioxide Sequestration

Injection of CO_2 into subsurface rock formations is considered to reduce the emission of CO_2 into the atmosphere. At this moment health, safety and environmental CO_2 emission abatement and cost-efficiency issues are the main topics in discussions on the feasibility of subsurface CO_2 storage. For these reasons, it is important to monitor CO_2 injection in a cost-efficient manner. Seismic methods are an established tool for this monitoring, and are, for example, successfully applied in the Sleipner field.

Underground coal seams are also targeted as storage a medium for CO_2. However, coal seams have different characteristics than the porous siliciclastic or carbonate reservoirs that have been monitored so far. Considering the depth of the target coal bed layers, a coal layer thickness of only a few metres, and their impedance contrast, the following parameters become important: the acquired resolution, the signal to noise ratio and the repeatability of the seismic survey to be used. Also important are economic aspects that limit extended monitoring. In an earlier feasibility study, three seismic methods were selected for evaluation: high-resolution seismic (HRS) surface acquisition, Vertical Seismic Profiling (VSP), including reverse-VSP, and cross-well seismology [Winthaegen and Westerhoff, 2002]. With the HRS surface acquisition the source and receivers are positioned at (or near) the surface. For each shot location receivers are positioned at various source-receiver offsets. Hence, the method can be applied in a grid resulting in a 3D coverage of the subsurface. The VSP method uses receivers in a well and the source at the surface. The source is used at various offsets from the well (offset-VSP). The receivers are positioned at various depths. Alternatively, the source is positioned in the well at various depths and the receivers are placed at the surface (reverse-VSP). In the cross-well seismic method two wells are used. The source is applied at various depths in one well, while the receivers are positioned at various depths in the other well.

Resolution, i.e. the ability to distinguish certain objects, is important for monitoring CO_2 storage, because the expected changes in seismic response will be small. Therefore a high resolution is needed for the injection into these thin coal layers. Also the length of the travel paths (measurement length) and the repeatability of a shot experiment are important. Paulsson et al [1996] presented a comparison of different methods for their resolution and measurement length. The obtained resolution of the HRS, VSP and cross-well methods are respectively 20–50 m, 10–70 m (for reverse-VSP: 2–10 m) and 1–5 m. The measurement lengths important for the signal to noise ratio and are respectively 100–10000 m, 100–7500 m (reverse VSP: 100–4000 m), and 10–1000 m.

In a test with a baseline cross-well survey covering the coal layers to be injected and a part of the overburden it appeared that the seismic waves are weak compared to recorded unwanted waves. Possible reasons were: the overburden and coal layers very strongly attenuate the seismic signal, it was not possible to generate sufficient seismic energy into the geological formations, or a combination of the two. It was concluded that further research is required to improve the signal to noise ratio of the acquired data and the results of tomographic inversion and reflection analysis [RECOPOL report, 2005]. Additionally, surface seismic acquisition was applied, having the advantages of being a conventional method and that a structural image can be obtained. Disadvantages are lesser resolution and poorer repeatability. Two partially multi-component seismic surveys were performed at the pilot site in time-lapse. Due to different reasons, among others resolution, the analysis of the time-lapse data set showed limited differences and did not result in conclusive evidence for the migration of gas out of the reservoir [Vandeweijer et al., 2008].

The examples above show that improvements are required to apply seismics as a time-lapse monitoring tool for CO_2 storage in coal seams. The resolution of the seismics as obtained in the ADEMA project give good faith of these future improvements in visualisation of injected CO_2 in geological media, and maybe even in coal seams.

2.3.9.3 Final report (T9.3)

This task covered the compilation of the final report and, as such, requires no further reporting here.

2.4 CONCLUSIONS

This section of the report summarises the conclusions and achievements of the ADEMA project. The material is ordered by subject, rather than by work package, because a number of key observations and opportunities arise from particular techniques that cut across several work packages.

2.4.1 Use of Seismic Techniques for Measuring Rock-burst Activity

This work was mainly concerned with **Work Package 3** (Development of micro-seismic system). The main achievements were connected with designing a modern, relatively cheap and flameproof multi-channel Seismic Observation System (SOS) for detecting mining tremors. The design and optimisation of the system also involved providing software for passive tomography and for analysing field velocity images to permit location of the zones of seismic potential hazard. The concept behind this method involved establishing, analysing and characterising temporal changes in images of P-wave field velocity. This method enables an estimation of the over-stressed zones in the rock strata with time.

The 64 channel micro-seismic hazard monitoring system was installed in Wujek-Ślask mine. Much of the monitoring work was concerned with the analysis of velocity images to assess areas of rock mass instability together with a critical review of the value of the real-time seismic monitoring system as a management tool to evaluate rock-burst hazard. During continuous measurements taken between July 2007-April 2008, more than 700 strong seismic events were recorded from the panel of longwall 2JD and between June 2006-July 2007 more than 1000 seismic events from the panel of longwall 8 L (seismic energy: Es > 1 kJ, local magnitude ML > 0.6). Velocity images were used to determine seismic prone area in this mine. Longwall 2JD had been identified as the hypercentre of seismic events. Approximately 70% of the source locations had been identified to lie beneath the coal seam, whilst 20% lay above the seam. A key conclusion was that damage effects only occur where the tremor source location is within 100 m from a mine opening. The seismic hazard zones depend on high seismic wave velocity, high gradient of seismic wave velocity and the area of mining. There was some evidence that previous mining activity increased seismic velocity, although further work is required to determine whether velocity changes result primarily from stress or lithology changes. The work has developed relationships between P-wave velocity and active strata stress, and has partly answered why some mines display significant seismic activity whilst similar mines are not prone to rock bump. It was collectively considered that the GIG work has made a valuable contribution to hazard monitoring and to understanding the underlying event stimuli and mechanisms. Depending upon the design of the geophone array and availability of suitable locations for their placement up to several square kilometres of ground can be covered by the technique.

2.4.2 Use of Drilling Parameters for Rock Characterisation

This research, undertaken primarily within **Work Package 4 (**Integrated benefit of combining geo-physical logging tools and in-situ drilling records), has confirmed that recording drilling parameters is a useful and economical technique for acquiring geotechnical information of ground parameters. Drilling equipment was adapted to measure and record drilling parameters for analysis of ground conditions. Rock mass properties were investigated, which involved the collection of borehole data and samples, and testing was carried out in several boreholes to obtain drilling parameter data. Geophysical logs were related to rock mass properties and to drilling parameters. Correlations were investigated between specific energy and the geophysical well logging parameters in relation to the quality of rock mass. Specific energy was the main index related with all drilling parameters.

The parameters that were selected for the final correlations were specific energy (Esp), Vp and Vs from FWSL (Edyn), punctual resistance (SPR), rock mass rating (RMR), joints per metre, and rock mass uniaxial compressive strength (scm). Each of the correlations were described and assessed in

turn for their utility as a descriptive measure. Data obtained from partners' other geophysical methods was contrasted. Correlations between the static rock properties with the p-wave velocity were obtained from seam seismic tomography in coal and surrounding floor rocks near the 2JD longwall in 502 seam of KWK Wujek-Ślask mine. As general conclusions, Esp depends strongly on the geomechanical rock mass quality expressed by the RMR and the number of joints per metre. Esp is regarded as a useful tool for rock mass characterisation The higher the number of Joints/m, the lower the values of Esp. Also, a clear influence of the lithology io the values of Esp is observed. The Dynamic Young's Modulus (Edyn), in relation to Esp and RMR also showed good results with the lithologies analysed.

These correlations showed that specific energy depends strongly on the geomechanical rock mass quality expressed by the RMR and the number of joints per metre. Higher values of specific energy are associated with high rock mass quality. Additionally, RQD gives high scatter in relation to specific energy. This approach is considered a valuable tool for rock mass characterisation. For example, the higher the number of joints per metre, the lower are the values of Esp. A further important observation is the clear influence of the lithology on the values of Esp observed.

From full wave sonic measurements, wave velocity data (Vp and Vs) were obtained that defines the dynamic elastic deformational parameters of the rock, where in this case it was used to obtain the Young's modulus. The dynamic Young's modulus, in relation to the specific energy and RMR, shows good results with the lithologies analysed. To conclude, the correlation obtained between Vp and specific energy provides the basis of a valuable tool and approach for rock characterisation purposes.

2.4.3 Electromagnetic Survey Techniques: RIM and GEM

This work was associated principally with **Work Package 5** (Radio imaging; signal transmission and acquisition) and **Work Package 6** (Radio imaging; tomographic reconstruction techniques). The application of the radio imaging method (RIM) of locating anomalies in coal seams has, to date, been difficult in the UK due to adverse geological conditions. The high conductivity of the coal results in a high attenuation of the signal traversing the coal seam, which has, in practical survey situations, necessitated a reduction in the probing frequency. However, the studies demonstrated that with such a reduction in probe frequency the lack of conductivity contrast between the coal seam and the surrounding rocks gives rise to the observed loss of definition of the tomographic image.

It is recognised that the development and implementation of a commercial RIM survey system would be beyond the contractual expectations within ADEMA. However, there are a number of specific design points and design improvements that have been identified, which could be applied to a revised RIM survey system. The following points arising out of the ADEMA research would have major bearing on implementing a commercial survey system:

1. The basinal deposits of the European Union are broadly characterised by higher mean seam conductivity and lower conductivity contrast between the seam and outlying rock than observed elsewhere. This observation must be accepted whatever electromagnetic surveying tool is used.
2. There is therefore a fundamental requirement to use a sufficiently high RIM probe frequency to reduce signal seepage into the surrounding rock. At the same time the signal must be sufficiently low in frequency to reduce attenuation losses. The transmission and signal acquisition arrangements must be designed to support these limitations.
3. The use of broadband methods, except for channel-sounding and synchronisation purposes, does not appear warranted. The technical arrangements supporting this conclusion are not straightforward but they have been considered in the context of best available technology and processing techniques, and as such are considered defensible.

4. Ultra narrowband DSP techniques appear a feasible means of increasing the survey signal to background noise ratio by as much as 60 dB. This will incur a relatively long measurement period, circa 100 seconds, but this is generally considered to be of little consequence.

5. The use of coherent ultra narrowband techniques, as suggested above, requires a stable reference signal to be provided within the RIM receiver. The conventional approach is to transmit a separate pilot signal. An alternative and elegant approach has been devised within the ADEMA project. This involves the transmission of three closely spaced RIM probe frequencies (e.g. 99, 100 and 101 kHz). This importantly requires only a single transmitter-receiver pair with a single tuned antenna at each station. Additionally, and a novel manner, this allows data on dispersion of the radio signal to provide input to a tomographic process. A patent has been applied for that covers these techniques.

6. The conventional notion of using large, tuned air-cored antenna (co-planar magnetic dipoles) has been improved on with the development of novel antenna types. The most promising two variants are an electric field antenna based around high-permittivity ceramic tiles and a current-injection antenna using conductive plastic electrodes or conductive foam to facilitate efficient strata access and current injection. Each of these alternative approaches has been shown to offer significant advantages in terms of signal gain, immunity from parasitic interference and practical implementation. A patent application covers the use of electrodes for resistivity tomography in coal mines.

7. One practical issue that has hitherto greatly impacted on the feasibility of implementing RIM surveys for coal panels that are in production is the possible parasitic signal coupling due to the coalface/roadway conductors and metallic infrastructure that is present. Until now, survey practitioners have advised him that all conductors, pipes, rails and continuous supporting infrastructure are removed for a distance of some 25 m in order to interrupt the possible transmission of unwanted signals between the survey stations. The research within ADEMA has identified that the secondary signal transmission path may not be as severe as speculated and that there are practical measures that can be used to address this.

8. As a final observation, it is evident that the use of non-approved apparatus in the vicinity of coalfaces and, in particular, return airways in gassy mines presents a significant practical difficulty. Indeed, such were the difficulties in gaining access to appropriate test areas underground that several tests could not be undertaken. There are perhaps two possibilities for resolving this problem in future projects...

   (i) Extending the project support period to allow equipment to be I.S. certified or otherwise approved for use, and

   (ii) Identifying at a European level whether there are underground test mine facilities which might lend themselves to experimentation purposes, including providing access for non-approved apparatus to workings that are the equivalent of a modern coalface.

The radio imaging work in **Work Package 6** (Radio imaging; tomographic reconstruction techniques) was redirected to undertake a wide-ranging and substantial electromagnetic modelling programme. This work provided a quantitative, visual appreciation of the complex coal seam signal transmission modes in play. The modelling confirmed the limitations of applying RIM in the UK (and probably European) coal basins arising from high electrical conductivity characteristics and inadequate conductivity contrast between the coal seam and outlying strata layers. It is noted that the enhancements to signal transmission and acquisition evaluated in Work Package 5 offset these limitations to some degree. However, it is recognised that the application of RIM techniques in the EU may have intrinsic limitations, imposed entirely by unfavourable coal seam electrical characteristics and the presence of significant metallic infrastructure. The GEM technique, developed within this project to evaluate and model an alternative coal seam excitation method, is novel. Whilst

GEM requires relatively low loss seam conditions to operate, it does nevertheless offer a promising avenue for future geophysical research.

The work has involved a rigorous analysis of the application of Radio Imaging (RIM) for coal seam and associated over and under burden strata scenarios and has established clear guidelines as to the range of electrical parameters over which the RIM technique is applicable. This insight into electrical channel conditions is not just restricted to coal seam imaging applications but to any application where radio imaging is applied in layered strata. These results are thus useful guidelines in future applications of RIM in other geophysical applications. The novel Guided Electromagnetic Wave (GEM) technique developed within this project has a number of advantages over the RIM technique. The GEM results presented in this work are thus also useful guidelines for possible future applications of GEM in other geophysical areas. One related application that the GEM technique is being considered for lies in the petroleum engineering area. There is a close analogy between the layered structure of a sandwiched coal seam and the layered structure within an oil reservoir. The analogy seems theoretically feasible given the known layered electrical parameter variations in certain oil reservoirs world-wide. However it would be unwise to postulate further until advanced modelling of such a scenario has been performed. However the GEM technique could well be an interesting addition to the monitoring technologies available for use in a petroleum reservoir or a gas field.

2.4.4 Enhanced Resolution and Feature Discrimination from Seismic Surveys

This work collectively cuts across **Work Packages 1, 2, 7 and 8**. A number of specific UK coal mine cases have been analysed based on the results of the advanced seismic inversion and re-interpretation work. This included consideration of layout, major structure, roof horizon, contour structure of thick coal, roof disturbance and mudstone roof thickness contours. Specific examples considered disturbed zones from the inversion process that were not picked previously, several faults both within and outside production panels, and various roof disturbance conditions. Several individual coalfaces were examined and the results contrasted with risk plans derived from current mining exploration and survey processing approaches. The following overall conclusions have been reached:

1. It has been possible to provide an exposition of the processing gains and additional geological detail retrieved from previous UK Coal logs.
2. Overall, it was concluded that the inversion data provided useful gains in resolution of the seam structure.
3. At this point, determination of additional detail of tectonic structure had not yet been achieved and remains a processing goal.
4. The gains from the various methods of inversion of the seismic data set which in the case of the Daw Mill study were derived from 3D seismic, could equally well be applied to conventional 2D data sets from elsewhere, both in the UK and in the European coalfields.

In terms of related studies, a classification scheme of rock type versus impedance was created from the well data and a nominal lithology colour scheme created to assist in the interpretation of the impedance results. The work programme has been critically reviewed in terms of pre-conditioning of seismic data, inversion model definition, inversion parameterisation, inversion results, and lithology classification of impedance data. Testing of the different seismic processing techniques (AI inversion, ADAPS AI inversion, of AVP inversion) showed that some techniques need further development before they can be applied to geological settings comparable to Daw Mill.

In this project a shared earth model was developed for the Daw Mill Colliery with software application Petrel using the approach developed in the oil and gas industry. In the course of the project it was shown that having one platform for most of the geological and geophysical data

provided added value in the communication between partners. It is therefore recommended that a similar approach is followed for similar projects that are facing different sources of data input and formats, whether these are underground coal gasification, carbon capture, CO_2 sequestration and coal-bed methane exploration projects within the EU. Using a shared earth modelling approach proved to be an efficient way for visualisation and communication of the results among the project partners. However, it must be emphasised that all partners should have access to the software to increase its impact.

The shared earth model also enabled the development of a new methodology to deduce geomechanical parameters from logs. This methodology is now applied in a broader context. Also, log data could be linked to the 3D seismic data in the Petrel model. This proved to be a strong calibration and correlation tool, which will be applicable in other projects.

For the extraction of coal bed methane (CBM) from coal seams it would be extremely valuable if the sweet spots (areas with high gas content) could be identified using seismic methods. The evaluation of synthetic data showed that variation in gas content could possibly be observed. However, the observed changes due to variation in gas content are so small that in real case data they would be indistinguishable from the natural variation of coal properties and occurrences and would fall in the noise of the data.

Due to the high resolution of the seismic cube it appeared to be possible to visualize the continuity of the coal seam (in the) underground at distances less than 1000 m away from the borehole at depths less than 1000 m from the surface. This is very important for the production of CBM, because it can give an indication of the acreage that could be exploited by one well. Even more importantly, visualization of the coal seam helps in the planning of horizontal or multilateral wells. It is expected that these kinds of advanced drilling techniques will have to be implied to make the extraction of CBM economically feasible under European conditions. In case this would be combined with the storage of CO_2 (Enhanced CBM). The understanding of the underground structure is crucial to ensure the long-term stability of the injected CO_2. A similar reasoning is valid for the application of underground coal gasification (UCG), where horizontal well drilling is also applied. The application of time lapse seismic with similar resolution would provide information on the development of the cavity. Possibly, also the passive seismic as applied in the coal mine in Poland would be interesting and innovative to follow the evolution of the cavity.

The benchmark between the geomechanical numerical models clearly showed that to model the geomechanical implications of a specific application, whether underground coal gasification, carbon capture, CO_2 sequestration and coal-bed methane exploration, requires a specific approach and modelling tool. The performance of the tools was assessed by comparing simulation results with an existing empirical solution or with each other. Both benchmarks, that is i) subsidence above longwall coal mine and ii) induced changes in stresses and deformations around mining caverns in coal, were synthetic cases of geomechanical response (subsidence prediction and stress distribution and deformation) above a longwall coal mine which could also be representative for a cavity created by the application of UCG. It was shown that the key material properties that largely determine the extent of plasticity and fractured zones around the modelled cavity are the tensile and shear strength of each rock type in the roof strata sequence. For UCG applications, the influence of temperature on these properties should be further investigated.

The benchmark also showed the limitations of the specific numerical tools, which should be taken into account in the future modelling of coal-related activities.

2.5 EXPLOITATION AND IMPACT OF THE RESEARCH RESULTS

2.5.1 Summary of Main Results of Project

Use of seismic techniques for measuring rock-burst activity

- A multi-channel 'Seismic Observation System' (SOS) for detecting mining tremors was designed and installed in a mine.
- Software was developed for passive tomography and location of zones of seismic hazard. This was achieved by monitoring temporal changes in P-wave field velocity using new evolutionary algorithms.

Use of drilling parameters for rock characterisation

- The economic worth was established of recording drilling parameters to determine ground characteristics during coal exploration.
- The correlation obtained between specific energy (a 'figure of merit' derived from drilling parameters) and P-wave velocity was demonstrated to be the basis of a valuable methodology for rock characterisation.

Electromagnetic survey techniques

- Adverse geological conditions in European deposits were identified as the reason for the reported difficulties in applying the radio imaging method (RIM) of locating anomalies in coal seams.
- Recommendations were made for the design of RIM equipment including a consideration of probing frequency and signal processing methods. A novel method was described of utilising the dispersion of radio signals to provide input to a tomographic process electrodes, which is described in a patent application.
- A study of antenna types lead to the development of a novel electric field antenna based around high-permittivity ceramic tiles and a current-injection antenna using conductive plastic electrodes, which is described in a patent application.
- A novel technique, based on guided electromagnetic waves (and given the acronym GEM) was developed for imaging applications within the layered strata of coal seams, and is described in a patent application.

Enhanced Resolution and Feature Discrimination from Seismic Surveys

- Seismic data from several mines was reinterpreted using inversion algorithms and shown to provide a useful increase in resolution of the seam structure. In particular, verification of the inversion data was undertaken using underground boreholes and geological observations
- The ADAPS seismic inversion technique was developed.
- Developing and using a shared earth modelling approach proved to be an efficient way for visualisation and communication of the results among the project partners.
- Geotechnical and numerical models were constructed for analysing mining-induced changes in stress and deformation with application for underground coal gasification. The application of seismic data to the identification of coal-bed methane sources was studied, and the limitations identified.

2.5.2 Actual Applications

The UK company Ikon Science Ltd has expressed an interest in evaluating the ADAPS inversion technique and in re-coding the ADAPS inversion algorithm as part of their oil-industry standard,

RokDoc software package. They believe that this will help them to win significant service contracts. Negotiations on the transfer of IPR will take place in 2009, after the completion of the project.

2.5.3 Further Technical and Economic Potential for the Use of the Results

Coal mining within the EU is characterised by an increasing reliance on mines with single, highly productive coalfaces. This trend towards amalgamation of production units has large commercial risks if geological conditions causes production to be disrupted and so detailed information is required concerning coal seams and surrounding rock properties. In addition, when operating at significant depths, evaluation of mine seismicity and rockburst hazards is essential for safe and productive mining. The ADEMA project has addressed these issues as described below.

The enhanced resolution and feature discrimination from seismic data that has been demonstrated within the project, and the successful use of drilling parameters as an approach to rock characterisation will both contribute to maintaining coal production in adverse geological conditions.

The seismic monitoring equipment developed during this project is considered to have significant potential for the protection against dangerous rock burst events in high-stress mining environments. As noted in the project conclusions, there is potential to further develop the technique for use in underground coal gasification projects.

The deployment of RIM equipment for coal-seam tomography has not been widespread in European coal deposits. There is now a far better quantitative understanding of the associated technical limitations in using previous RIM survey techniques. It is clear that basinal deposits differ from those elsewhere in terms of the coal conductivity and the conductivity contrast with the roof and floor strata. As a result, RIM design guidelines have been produced which will improve current capability. The implementation of these changes is, however, associated with further cost and development. It is intended that the consortium shall undertake discussions with suppliers of electromagnetic survey services, with a view to suggesting adaptations of their equipment for the EU market.

2.5.4 Patent Filing

During the course of the project, the following patent applications were filed

1. **Radio imaging of underground structures: elimination of need for synchronisation channel**
   Applicant Mines Rescue Service Limited
   Application No.: GB0620563.7 Date of Filing: 17 Oct 2006
   Publication No.: GB 2443019 Publication Date: 23 April 2008
   The results of the substantive examination are due on 17 October 2009

2. **Electrodes for resistivity tomography in coal mines**
   Applicant Mines Rescue Service Limited
   Application No.: GB0620860.7 Date of Filing: 20 Oct 2006
   Publication No.: GB 2443246 Publication Date: 30 April 2008
   The results of the substantive examination are due on 20 October 2009

3. **Detection of anomalies within a stratum, structure or seam**
   Applicant Heriot Watt University
   Application No.: GB0802778.1 Date of Filing: 15 Feb 2008
   This application replaces GB0702831.9, which was reported earlier in the project.
   Publication is due in August 2009

2.5.5 Publications / Conference Presentations

A paper, Sangster A J, Lavu S, McHugh R, Westerman R, *Modal Formation of Electromagnetic Fields in a Geological Stratum with Loss Tangent Greater Than Unity*, was submitted to the Journal of Applied Geophysics, June 2008.

A short article, Gibson, D., *Novel Cave Radio Antenna uses Small Ceramic Tiles* was published in the British Cave Research Association's Cave Radio and Electronics Group Journal (ISSN 1361-4800) in June 2008. (CREGJ **71**, pp14-15).

A paper has been prepared for the 7 th International Symposium on Rockburst and Seismicity in Mines (RASIM7) in Dalian (China) in August 2009. The title of the paper is: *Seismic Monitoring and Rock Burst Hazard Assessment in Deep Polish Coal Mines - Case Study of Rock Burst on April 16 th 2008 in Wujek Slask Coal Mine* by Mutke G., Lurka A. and Dubiñski J.

2.5.6 Other Aspects Concerning the Dissemination of Results

The contacts between partners have resulted in several spin-off initiatives, such as the performance of geo-electrical measurements in an open-pit mine in Scotland by partners TNO and HWU.

Parts of the ADEMA coal research project took inspiration from oilfield geophysical methods and techniques. It is gratifying to note that oilfield companies have been quick to appreciate the results of ADEMA. Such recognition should encourage coal-mining companies to evaluate and deploy ADEMA techniques.

Research into optimising RIM antennas has led to several innovations that are applicable to underground communications. In particular, the novel antennas; current injection, dielectric disc and rotating magnets, are considered to have potential in this field. It is intended to make use of the results of this project in current European research including RFCS project EMTECH – Mine Emergency Support Technologies – grant agreement RFCR-CT-2008-00003.

The work on monitoring the source and characteristics of mining micro-seismic activity in three dimensional spaces underground has resulted in a flameproof, relatively inexpensive Seismic Observation System (SOS). This provides two key opportunities:

- Using passive tomography for the assessment of any seismic or rock-burst prone hazards, and possibly mines subject to coalface gas outburst events.
- Assessing safety of the underground excavation under dynamic load.

The seismic monitoring, seismic analysis and passive tomography results may be used in both the spatial-temporal planning of mining operations under predicted high seismicity conditions and the rational choice of geotechnical support and associated preventive actions, ensuring continuity of mine production, and importantly, a significant enhancement in workplace safety.

3 List of Figures and Tables

3.1 FIGURES

3.2 TABLES

4 List of References

The list of references given here includes material from the appendices to this report.

4.1 WP3: DEVELOPMENT OF MICRO-SEISMIC SYSTEM

Aki K., Richards P.G. (1980), "Quantitative Seismology. Theory and Methods". W.H. Freeman, San Francisco.

Andrews D. J., (1986)*:* Objective determination of source parameters and seismicity of earthquakes of different size. In Earthquake Source Mechanics (S. .Das. J. Boutwright and C. H. Sholz, eds) Maurice Ewing, Vol. **6**, Am. Geophys. Union. Washingh D.C.,. 259-267

Ben-Menachem A., Singh S.J. 1981: Seismic waves and sources. Springer-Verlag, New York.

Bjork A., Dahlquist G. (1987), Metody numeryczne - *Numerical methods*, PWN, Warszawa – in Polish

Brady B.G. and Brown E.T. 1985: Rock Mechanics for Underground Mining. George Allen and Unwin

Drzęźla B. (1994), "Zasady projektowania konfiguracji sieci sejsmometrów", Przegląd Górniczy **50** (11), 1-6 – In Polish

Dubiński J. (1995): Metody obliczania energii sejsmicznej wstrząsów górniczych. Biblioteka Szkoły Eksploatacji Podziemnej, Seria Wykłady nr 8, Kraków, 115-142 – In Polish

Findeisen W., Szymanowski J., Wierzbicki A. (1977), Teoria i metody obliczeniowe optymalizacji – *Theory and optimization methods*, PWN, Warszawa – In Polish

Gibowicz J., Kijko A. (1994), "An Introduction to Mining Seismology", Academic Press, San Diego, New York, Boston, London, Tokyo, Toronto.

John C.M.St., Zahrah T.F. (1985): Aseismic design of underground structures. Agbabian Associates, Rep.\No. R-8411-56-16.

Lurka A., (1996), "A certain new method for seismic network optimization and its consequences", Acta Montana, **10**, Praha.

Lurka A. (2000), Analysis of errors of mining tremors using implicite function , PhD thesis, GIG, Katowice – in Polish

Mańczak K., (1976). "Technika planowania eksperymentu – *Planning of experiment*", WNT, Warszawa – In Polish

Mc Garr A., R. W. E. Green and S. M. Spottiswoode, (1981): Strong ground motion of mine tremors: source implications for near-source ground motion parameters, Bull. Seismol. Soc. Am. 71, pp. 295-319

Mc. Garr A., (1991): *„Observation constraining near-source ground motion estimated from locally recorded seismograms"*. J. Geophys. Res., 96, pp. 16.495-16.508.

Press, W. H., Flannery, B. P., Teukolsky, S. A., and Vetterling, W. T. (1990), Numerical Recipes: The Art of Scientific Computing", Cambridge Unversity Press, New York.

Smirnow N.W., Dunin-Barkowski W. "Kurs rachunku prawdopodobieństwa i statystyki matematycznej dla zastosowań technicznych – *Probability and statistics* ", PWN,Warszawa – In Polish

Aki K., Lee W.H.K. (1976).: „Determination of three-dimensional velocity anomalies under a seismic array using first P arrival times from local earthquakes",, J. Geophys. Res. **81**, 4381-4399.

Dębski W. 2004: Application of Monte carlo techniques for solving selected seismological inverse problem. Publ. Inst. Pol. Acad, Sc., Monographic volume, B-34(367)

Dubinski, J. (1989): A seismic method for the monitoring of mine tremors hazard in hard coal mines. *Scientific works of the Central Mining Institute*, Katowice. *(in Polish)*

Dubiński, J. and Dworak, J. (1989): Recognition of the zones of seismic hazard in Polish coal mines by using a seismic method, *PAGEOPH vol. **123,** No. **3.***

Dubiński J., Mutke G. (1996): „Characteristics of mining tremors within the near wave field zone*"* PAGEOPH, Vol. **147,** No. **2**., 251-261.

Dubiński J., Mutke G., Stec K. (1996): „Focal mechanism and source parameters of the rock-bursts in the Upper Silesian Coal Basin" Acta Montana, ser.A, Geodynamics, No.**9** (100), PRAHA, pp.17-27.

Dubiński J. and Mutke G. (1997): „ Characteristics of near-field peak velocity in the Upper Silesian Coal Mines", Rock-bursts and Seismicity in Mines (RaSiM4), Gibowicz & Lasocki (eds), Balkema, Rotterdam, pp. 343-347.

Dubiński J., Lurka A. i Mutke G. (1998): ”Zastosowanie metody tomografii pasywnej do oceny zagrożenia sejsmicznego w kopalniach – *Application of* p*assive tomography in mines*”, Przegląd Górniczy nr. **3**. – In Polish

Dubiński J., Mutke G. (2005). „Study of temporal changes of P-Wave velocity in Polish copper mines in high seismic activity zones”. The 6 th International Symposium on Rock-burst and Seismicity in Mines (RaSiM6). Australia – Perth. 2005.

Dubiński, J., Konopko, W., (2000). Tąpania, ocena, prognoza, zwalczanie, GIG-Katowice – In Polish

Gibowicz, S. J., (1996). Relations between source mechanism and the ratio of the S over P wave energy for seismic events induced by mining, *Acta Montana*, ser. A, No. **9** (100), 7-15.

Glazer S.N., Lurka A., Application of passive seismic tomography to cave mining operations based on experience at Palabora Mining Company, South Africa, 1 st International Symposium on Block and Sub-level Caving, 2007, Cape Town, South Africa, 369-388

Kowalczuk, J. and Szwejkowski, J.(1975): Relation between anomaly of seismic velocity and state of stress around geological structures. *Scientific Bulletins Academy of Mining and Metallurgy*, No **467**, Geology, p.2 - in Polish

Lurka A., (2002) : „Seismic hazard assessment in the Bielszowice coal mine using the passive tomography”, in: Seismogenic Process Monitoring (eds. H. Ogasawara, T. Yanagidani & M. Ando), A.A. Balkema Publishers.

Lurka A. (2004), Zwiększanie informatywności technik tomograficznych w procesach eksploatacji złóż, Archiwum Górnictwa, PAN, Kraków, pp.495-509 - In Polish

Lurka A., Mutke G., (2008): Poprawa dokładności lokalizacji składowej pionowej hipocentrów wstrząsów górniczych (Improvement of accuracy of location vertical component mining tremors foci. Gospodarka Surowcami Mineralnymi (Mineral Resources Management), Vol. 24-2/3. IGSMiE PAN, 261-270 – in Polish

Marcak H. 1993: The use of pattern recognition method for prediction of the rock-burst. Proceedings of the 3 rd International Symposium on Rock-bursts and Seismicity in Mines/ Kingston/ Canada pp. 223-226.

Maxwell S.C.& Young R.P. (1994):” Application of seismic tomography to induced seismicity investigations”, in: Proceedings of Eurock ‘94, Balkema, Rotterdam.

Mendecki A.J. (ed), (1997): „Seismic monitoring in Mines”. Chapmann & Hall, London.

Mutke G. & Stec K. (1997) :Seismicity in the Upper Silesian Coal Basin, Poland: Strong regional seismic events. Proc. 4 th Int. Symp. :Rock-bursts and Seismicity in Mines (RaSiM4), ed. S.J. Gibowicz, Rotterdam, A.A. Balkema, s.213-217.

Mutke G., Lurka A., Mirek A., Bargieł K., Wróbel J. (2001): „ Temporal changes in seismicity and passive tomography images: a case study of Rudna copper ore mine-Poland” . V International Symposium Rock-bursts and Seismicuty in Mines (RaSiM5), The South African Institute of Mining and Metallurgy.

Mutke G. (1999): „Results of ground motion measurements close to the sources of mining tremors”, Publ. Instit. Geophys. Pol. Acad. Sc., **M-22**.

Mutke G. (2007): Charakterystyka drgań wywołanych wstrząsami górniczymi w odległościach bliskich źródła sejsmicznego w aspekcie oceny zagrożenia tąpnięciem (*Characteristics of near-field Grodnu motion resulting from mining tremors to assessing of rock-bursts hazard),* Prace Naukowe GIG , No **87**, s. 145.

Mutke G., 2008: Stability of the underground mine workings in the near-field zone of seismic events. In : 21 st World Mining Congress 2008 – New Challenges and Vision for Mining . Underground Mine Environment. 7-12 September 2008 – Poland – Crocow. University of Since & Technology (AGH), 89-97

Schwefel H.P. (1995): „Evolution and optimum seeking”, John Wiley&Sons

Snoke J.A., 1987: Stable determination of (Brune) stress drops. Bull. of Seismol. Soc. Am. No/ 2, pp. 530-538.

Stec, K., Drzewiecki, J., (2000). Relationship between mine tremor focal mechanism nd local mining and geological conditions. *Acta Montana* ser. A, No. **16 (118),** 189-202.

Tarantola A. (1986) : „Inverse Problem Theory”, Elsevier

4.2 WP4: IN SITU DRILLING AND GEOPHYSICAL LOGGING

Bieniawski, S. T. (1979). *The geomechanics classification in rock engineering applications*. In: Proc. 4 th International Conference on Rock Mechanics. Montreaux. Balkema. Vol. 2.

Galera, J.M. (2006). *Improved rock stress measurement and analysis for planning of underground mines*. ECSC 7220-PR/135

Galera, J. M. (2006). *Natural stress field evaluation using borehole ovalisation analysis and its comparison with hydrofract measurements*. In: Proc. Int. Symp. On In-Situ Stress. Trodheim. Ed. Taylor and Francis, pp241-247.

Kalamaras, G. S. and Bieniawski, Z. T. (1995). *A rock mass strength concept*. In: ISRM International Congress of Rock Mechanics. Tokyo. Japan.

4.3 WP5: RADIO IMAGING (SIGNAL TRANSMISSION AND ACQUISITION)

Burrows, M. L. (1978). *ELF Communications Antennas. [IEE Electromagnetic Waves Series: 5]*. Stevenage: Peter Peregrinus. ISBN 0 906048 00 1

Davidson, C. W. (1978). *Transmission Lines for Communications*. London: Macmillan Press. ISBN 0-333-32738-1

Delogne, P. (1982). *Leaky Feeders and Subsurface Radio Communication. [IEE Electromagnetic Waves Series: 14]*. Stevenage: Peter Peregrinus

Emslie, A. G. and R. L. Lagace (1976). Propagation of Low and Medium Frequency Radio Waves in a Coal Seam. *Radio Science* **11**(4), 253-261

Gibson, D. (2003). Channel Characterisation and System Design for Sub-Surface Communications (PhD Thesis). *School of Electronic and Electrical Engineering*. Leeds: University of Leeds.

Hill, D. A. (1984). Radio Propagation in a Coal Seam and the Inverse Problem. *Journal of Research of the National Bureau of Standards* **89**(5), 385-394

ICNIRP (1998). Guidelines for Limiting Exposure to Time-Varying Electric, Magnetic, and Electromagnetic Fields (up to 300 GHz) [Guidelines of the International Commission on Non-Ionizing Radiation Protection]. *Health Physics* **74**(4), 494-522. ISSN 0017-9078, on-line: 1538-5159. Available at **health-physics.com, icnirp.de.** (Accessed 1 Mar 2007)

Lagace, R. L., M. L. Cohen, A. G. Emslie and R. H. Spencer (1975). *Propagation of Radio Waves in Coal Mines (United State Bureau of Mines, Contract Report H0346045)*. Cambridge, Massachusetts: Arthur D Little

Shope, S. M. (1986). Electromagnetic Coal Seam Tomography. *PhD Thesis*: Pennsylvania State University.

--- (1987). Electromagnetic Coal Seam Tomography (PhD Thesis). *Department of Physics*: Pennsylvania State University.

Stolarczyk, L. G. (2003). Method and System for Radio Imaging Underground Geologic Structures. United States Patent US 6,593,746 B2.

--- (2004). Synchronous Radio-Imaging of Underground Structures. United States patent 6744253

Stolarczyk, L. G. and S. S. Peng (2003). *Advanced Electromagnetic Wave Technologies for the Detection of Abandoned Mine Entries and Delineation of Barrier Pillars*. Geophysical Technologies for Detecting Underground Coal Mine Voids (An Interactive Forum). Lexington, Kentucky: MSHA / OSMRE. July 28-30, 2003. Available at **www .fhwa.dot.gov / engineering / geotech / hazards / mine / workshops / ktwkshp / kentucky.cfm**. (Accessed 24 Feb 2006)

Stolarczyk, L. G. and G. L. Stolarczyk (1999). *Electromagnetic Seam Wave Mapping of Roof Rock Conditions across a Longwall Panel*. 18 th International Conference on Ground Control in Mining. West Virginia University, Morgantown, West Virginia. August 3-5, 1999.

Wait, J. R. (1952). The Magnetic Dipole Immersed in a Conducting Medium. *Proc. IRE* **40**(10), 1244-1245

--- (1969). Electromagnetic Fields of Sources in Lossy Media. In *Antenna Theory - Part 2*. ed. R. E. Collin and F. J. Zucher. New York: McGraw-Hill, pp. 468-471.

--- (1976). Note on the Transmission of Electromagnetic Waves in a Coal Seam. *Radio Science* **11**(4), 263-265

--- (1995 a). Excitation of a Conducting Half-Space by a Toroidal Coil. *IEEE Antennas and Propagation Magazine* **37**(4), 72-74

--- (1995 b). Excitation of a Conducting Half-Space by a Toroidal Coil: Correction. *IEEE Antennas and Propagation Magazine* **37**(5), 43

Williams, H. P. (1951). Subterranean Communication by Electric Waves. *J. of British Institution of Radio Engineers* **11**(3), 101-111

4.4 WP6: RADIO IMAGING (TOMOGRAPHIC RECONSTRUCTION)

1. Mackinnon, A.J., D. Hayward, P.J. Hall, and R.A. Pethrick, Temperature dependent low frequency dielectric and conductivity measurements of Argonne Premium coals. Fuel, 1994. **Vol. 73**(5): p. 731-737.

2. Balanis, C.A., J.L. Jeffrey, and Y.K. Yoon, Electrical Properties of Eastern Bituminous Coal as a Function of Frequency, Polarization and Direction of the Electromagnetic Wave, and Temperature of the Sample. IEEE Transactions on Geoscience Electronics, 1978. **16**(4): p. 316-323.
3. Stolarczyk, L.G., Synchronous radio-imaging of underground structures. 2004. p. US Patent 6744253.
4. Reagor, D. and Q. Jia, Applications of High Temperature Superconductors to Underground Communications and Geophysical Surveys. 2000, DOE Office of Scientific and Technical Information (OSTI).
5. Houck, R.T., Measuring the Electrical Properties of Coal Using Ground-Penetrating Radar. IEEE Transactions on Geoscience and Remote Sensing, 1985. **GE-23**(6): p. 851-854.
6. Chufo, R.L., Medium frequency mine communications. 28 th IEEE Vehicular Technology Conference, 1978. **28**: p. 261-266.
7. Marland, S., Merchant A., and N. Rowson, Dielectric properties of coal Fuel 2001. **Vol 80**(Issue 13): p. 1839-1849.
8. Daniels, D.J., Surface-penetrating radar. Journal of Electronics & Communication Engineering 1996. **8**(4): p. 165-182.
9. Chufo, R.L. and W.J. Johnson, A radar coal thickness sensor. IEEE Transactions on Industry Applications, 1993. **29**(5): p. 834-840.
10. Lester, E., S. Kingman, and C. Dodds, Patrick J., The potential for rapid coke making using microwave energy Fuel, October 2006. **Volume 85**(14-15): p. 2057-2063.
11. Martinez, A. and A.P. Byrnes, Modeling Dielectric-constant values of Geologic Materials: An Aid to Ground-Penetrating Radar Data Collection and Interpretation, Current Research in Earth Sciences, Bulletin 247, part 1 (http://www.kgs.ukans.edu/Current/2001/martinez/martinez1.html).

4.5 WP6 AND WP7 MODELLING

Castagna, J.P., Batzie, M.L. and Eastwood, R.L. (1985). Relationships between compressional-wave and shear-wave velocities in clastic sillicate rocks. *Geophysics*, 1985(**50**), 4, 571-581

Diana Version 9.3 (2008). *Program and User's Documentation*. TNO Diana B.V. (www.tnodiana.com)

Eissa, E.A. and Kazi A. (1988). Relation between static and dynamic Young's moduli of rocks, *Int. J. Rock Mech. Min. Sci. Geomech. Abstr.* 1998*(***25**) 6 479-482

Fjær, E., Holt, R.M., Horsrud, P. and Raaen, A.M. (1992). *Petroleum Related Rock Mechanics*. Developments in Petroleum Science 33, Elsevier ISBN 0-444-88913-2

FLAC3D Version 3.10 (2007). *Program and User's Documentation*. ITASCA (www.itascacg.com/flac3D)

Fokker, P.A. and Orlic, B. (2006). Semi-analytic modelling of subsidence. *Mathematical Geology* 2006(**38**) 5 565-589

MULPAN (Multiple Panel) Ground Movement Prediction System, British Coal HQTD (1987). (A computer program for subsidence calculations following the approach from the *Subsidence Engineers' Handbook* [National Coal Board, 1975])

National Coal Board (NCB) (1975). *Subsidence Engineers' Handbook*, 111 p

Olden, P., Corbett, P., Westerman, R., Somerville, J., Koutsabeloulis, N., and Smart, B. (2001). Modelling combined fluid and stress change effects bin the seismic response of a producing hydrocarbon reservoir, *The Leading Edge*, October 2001

Petrel Version 2007 (2007). *Program and User's Documentation*. Schlumberger (www.slb.com)

Pringle, J.K., Westerman, A.R., Clark, J.D., Drinkwater, N.J., and Gardiner, A.R. (2004). 3D high-resolution digital models of outcrop analogue study sites to constrain reservoir model uncertainty: an example from Alport Castles, Derbyshire, UK. *Petroleum Geoscience* 2004(**10**) 343-352

SavFem, -. *Program and User's Documentation*. Applied Mechanics Inc., Longboat Key, Florida

Wilson, A.H. (1981). *Soft Rock Mechanics*. A Series of Lectures. National Coal Board

Yavuz, H. (2004). An estimation method for cover pressure re-establishment distance and pressure distribution in the goaf of longwall coal mines. *Int. J. Rock Mech. Min. Sci.*, 2004(**41**) 193-205

4.6 WP8: GEOLOGICAL VALIDATION

Gassman, F., 1951, Über die Elastizität porozer Medien. Vierteljahrschr. der Naturforsch. Geselllschaft Zürich, Vol. 96, pp. 1-21.

4.7 WP9: PROJECT ASSESSMENT AND CONCLUSIONS

Paulsson, B.N.P., Cutler, R.P, Kirkendall, G., Chen, S.T., Giles, J.A., 1996, *An advanced seismic source for borehole seismology*, SEG, Expanded abstracts, BG4.2.

RECOPOL report, 2005. Seismic monitoring of CO2 storage in the RECOPOL project, Period: 2003 – 2005. Contract number: ENK-CT-2001-00539. 34 p.

Vandeweijer, V., van Bergen, F., Winthaegen, P., Benedictus, T., Kronimus, A., Krzystolik, P., Jura, B., Skiba, J., 2008. *Monitoring of CO_2 stored in the Enhanced Coalbed Methane pilot site in Kaniów (Poland)*, Proceedings GHGT-9, Washington D.C.

Winthaegen, P.L.A. and Westerhoff, R.S. (2002): *Seismic CO_2 monitoring feasibility study, proceedings of the International Workshop on Present Status and perspective of CO_2 sequestration in coal*, Tokyo, 5 September 2002.

5 Glossary

5.1 Abbreviations and Similar Terms

3D	3-dimensional location of seismic events
A/D	Analogue to Digital
ADAPS	A new seismic inversion method using pattern recognition to extract the seismic wavelet
AI	Acoustic Impedance
ART	Algebraic Reconstruction Technique
ATEX	Flameproof certification
AVP	Amplitude Variation with ray Parameter
BGS	British Geological Survey
BPT	Back-plane Projection Technique
CBM	Coal Bed Methane
CMP	Common Mid-Point
CRIP	Controlled Retractable Injection Point
Diana	A finite element program developed by TNO
DLIS	A file format used for well log curves
DLM	Low frequency geophone probe with transmission developed by GIG
DSP	Digital Signal Processing
ELF	Extra-Low Frequency, 30–300 Hz
EM	Electromagnetic
ERT	Electrical Resistance Tomography
FDP	Frequency-Distance Principle
FE	Finite Element
FIR	Finite Impulse Response
FLAC	An explicit finite difference code developed by Itasca
FWI	Full-Wave Inversion
GEO	Project partner, Geocontrol SA
GIG	Project partner, Glowny Instytut Gornictwa
GUI	Graphical User Interface
HRS	High-Resolution Seismic
HWU	Project partner, Heriot-Watt University
IS	Intrinsic Safety
LF	Low Frequency, 30–300 kHz
MF	Medium Frequency, 300 kHz – 3 MHz
MRSL	Project partner, Mines Rescue Service Ltd
MulPan	(Multiple Panel) Ground Movement Prediction System developed by British Coal
MultiLok	Software for the analysis of tremor parameters
PA	Power Amplifier
Petrel	Schlumberger software intended to aggregate oil reservoir data from multiple sources
PPV	Peak Particle Velocity
PRB, PRBS	Pseudo-Random Binary Sequence
RIM	Radio Imaging Method
RMR	Rock Mass Index
RQD	Rock Quality Designation
SavFem	A finite element program developed by Applied Mechanics Inc.
SEH	Subsidence Engineers Handbook
Seisgram	Software for the analysis of seismic signals
SIP	Project partner, Seismic Image Processing
SIRT	Simultaneous Iterative Reconstruction Technique
SNR	Signal to Noise Ratio
SOS	Seismic Observation System developed by GIG
SPR	Punctual Resistance
TE, TEM, TM	Transverse Electric / Electromagnetic / Magnetic wave
TNO	Project partner Nederlandse Organisatie voor Toegepast Natuurwetenschappelijk Onderzoek
TWT	Two-Way Time
UCS	Unconfined Compressive Strength
UCG	Underground Coal Gasification
UKC	Project partner, UK Coal Mining Ltd
VSP	Vertical Seismic Profiling
WOB	Weight on Bit

5.2 DEFINITIONS

Definitions for Work Packages 5 and 6

Anapole	An electric field antenna comprising a wire wrapped many times around a frame that has the shape of a toroid.
Channel-sounding	The method of measuring the propagation of a signal through a medium (i.e. sounding) at a number of different frequencies (or channels).
Class C	A type of amplifier where the output stage is biased beyond cut-off.
Class D	A digital power amplifier.
Cross-correlation	In signal processing, cross-correlation is a measure of similarity of two waveforms as a function of a time-lag applied to one of them.
Dispersion	The phenomenon caused by waves of different frequency travelling at different speeds.
E-field	Electric field.
External resistance	An electrical resistance similar to radiation resistance, but caused by the induced eddy currents and consequent dissipation of energy in a conductive medium external to the transmitter.
Eye pattern	A method of plotting digital data signals on an oscilloscope. The x-axis represents time and traverses left to right over one signal bit period, and then right to left for a similar period. The eye pattern is formed from the superposition of many such plots.
GEM: Guided Electromagnetic Wave	(GEM). A novel use of electromagnetic waves to image geological anomalies in coal seams, described in Work Package 6 of this report.
H bridge	An arrangement of transistors (or similar devices) that forms the output stage of a bipolar (floating ground) power amplifier.
H-field	Magnetic field.
J-field	Current field.
Manager's rules	Rules drawn up to comply with regulation 19(2) (g) of the UK's Electricity at Work Regulations (1989).
Noise matching	For an amplifier with a given input noise current spectral density, and a given input noise voltage spectral density, the overall noise contribution of these sources is minimised when these parameters have a specified relationship to the source impedance.
Pseudo-random binary sequence	A sequence of binary digits that obeys certain strict mathematical conditions and which can, as a result, be described as 'random' although its useful properties lie beyond this.
Proximity effect	An effect similar to the skin effect, where an electric field is constrained to the outer surface of a bundle of wires.
Q factor	Quality factor. Resonance. The inverse of damping factor.
Radiation resistance	An electrical resistance that appears to be present in a radiating antenna, but which is 'fictitious' and represents the power lost from the antenna by radiation (as opposed to by dissipation, which would manifest as a 'real' resistance).
Radio Imaging Method (RIM)	A well-established method of imaging geological anomalies in coal seams by measuring the propagation of a low-frequency electromagnetic field across a coal seam
Skin effect	An effect whereby an electric field is constrained to the outer surface of a conductor. It arises because fields in conductors obey the diffusion equation – the field diffuses into the conductor and is therefore strongest on its surface.
Specific aperture	A figure of merit that describes the performance of an induction loop antenna in terms of its mass, radius and materials of construction.
Specific length	A figure of merit that describes the performance of an electric field antenna in terms of its mass and materials of construction.
System identification	The process of system identification aims to find a mathematical relationship between the inputs and outputs of a dynamic system without requiring an understanding of the processes inside the system. Specifically, in the context of this project, a cross-correlation of the system input to the system output allows the recovery of synchronisation information.

6 Appendices

6.1 WP1 Project Set Up

There are no appendices to this work package.

6.2 WP2 Acoustic Impedance Inversion

There are no appendices to this work package.

6.3 WP3 Development of Micro-Seismic System

(Development of micro-seismic system for the continuous observation of seismic hazard in the longwall zones on the basis of passive tomography images)

6.3.1 Appendix to Task 3.1

It is important to use relatively low cost equipment to implement with success new micro seismic monitoring method in coalmines. Therefore low costs, low frequency sensor (geophone probe, 1 Hz) was designed by GIG. Until now, the expensive 1 Hz seismometers were used in mining seismological networks in Poland. New sensors are significantly cheaper, smaller and more convenient to install in the mine. A new simplified transmission system was designed to send signals from underground to the surface receivers. Moreover, the 32 and 64 A/D converters were implemented to PC computers with Microsoft Windows operating system as a basis to develop the network. The hardware was connected with seismological software Seisgram and Multilok made by GIG. The software enables specific mining data acquisition and data processing to provide information about source parameters and 3D location of seismic events.

6.3.1.1 Description of the DLM Seismic Sensor

The DLM Measuring Probe is a ground motion velocity measuring unit featuring a combination of the sensor and the transmitter that can be used for passing telecommunication data through transmission lines in the form of current. It can operate with the seismic receivers of the DLM-SO station. The probe comprises the following elements:

Case

The stainless steel case is fastened sing an M20 threaded bolt and sealed at both the cable entry and beneath the top closure. The whole instrument is secured using tamper-proof screws.

Measuring Sensor

Low cost GeoSpace 4–5 Hz geophones have been used to measure ground motion velocity.

Printed Circuit Board

The protection unit uses diodes to limit voltage and prevent polarity reversal.

Printed Circuit Board of the Compensator

On the board are located all elements of the electronic system, including the amplitude / frequency response compensator of the geophone and the transmitter for current or power transmission.

The block diagram of the probe is shown in the *Figure* below.

The voltage signal induced in the geophones coil proportionally to the ground motion velocity is fed to the non-inverting input of the operational amplifier in the characteristic compensator circuit. The

signal, after being amplified there, can further be fed to the input of the FDP low-pass filter of cut-off frequency f = 0.8 Hz built in the operational amplifier. This voltage signal, being properly filter-shaped, can formulate the frequency response of both the compensator and the whole probe.

The signal can further control the current source in the power supply unit. The current variations in the current source can trigger the similar current variations in a transmission line. The current in the transmission line, for the zero input signals from the geophone, can amount to about 12 mA. A change in geophone voltage, proportional to the ground motion velocity, can produce a change in the transmission line current equal to ±6 mA.

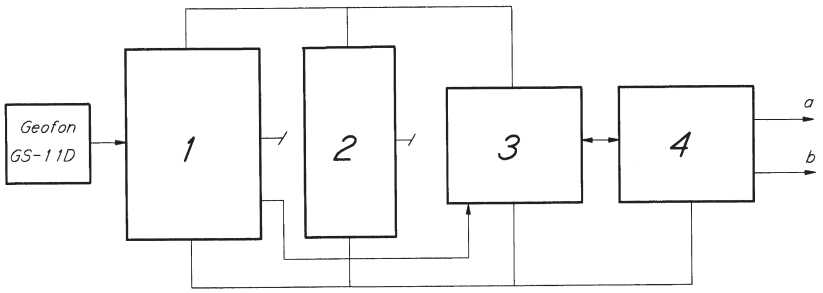

Figure 6.3.1–1 : Block diagram of the seismic probe DLM-2001
This was designed by GIG. 1) amplifier and compensator unit 2) power supply stabilization unit 3) current source controllable 4) the diode circuit of the protection unit

The diode circuit of the protection unit protects the probe against an increase in supply voltage exceeding a value of 43 V and also protects the whole of the electronic circuitry against inadvertently switching on the voltage of reversed polarity.

Functional and Technical Parameters

- Parameter measured: ground motion velocity.
- Type of transmission: current.
- Sensitivity: selection range 50 to 15000 mA·S/m.
- Range of frequency adjustment: 1 to 600 Hz.
- Supply voltage range: 18 to 43 V.
- Power consumption: 12 mA.
- Depth of current modulation in a transmission line: ±6 mA.
- Non-linear distortions: ≤3%.
- Operating Conditions
- Climatic operating conditions:
- humidity: undetermined;
- Operating temperature: -5 ºC to +50 ºC.
- Cable line requirements:
- type of cable: mining teletechnical;
- loop resistance: < 880 Ω;
- insulation resistance between wires: >1 MΩ;
- Insulation resistance between wire and ground: >2 MΩ.
- Flameproof operating conditions

The DLM 2001 Measuring Probe has been designed for ground motion recording and seismic data transmission and is along with its circuit's flameproof and obtained ATEX certification.

6.3.1.2 Description of the DLM-SO Seismic Signal Receiving Station

The one block of seismic signal receiving station DLM-SO has been designed based on 16 seismic receivers station panels operating with 16 DLM probes and transmission lines. Two blocks can be connected in to 32 channels or four blocks can be connected in to 64-channel equipment.

A current-modulated signal in the measuring probe passes through the transmission line before entering the receiver. The signal turns separated there in the opto-isolating barrier and then is

transferred to the transmission line current detection circuit. The current detection circuit designed based on the operational amplifier and two transistors has a task to accurately reproduce the transmission line current and convert it into a proportional voltage signal. The current level in the transmission line is controlled by a two-colour light-emitting diode mounted on the front panel of the receiver. The orange colour gives evidence of the zero, factually 12 mA, current (supply current of probe) passing through the transmission line. A change in colour onto red or green shows an increase or a decrease in the current (modulation), respectively. The voltage signal separated in the detection circuit passes further to the filter –amplifier system, where the amplitude – frequency response of the receiver can be determined, that is the frequency bandwidth and signal level. The signal, properly formed, passes further to the output amplifier circuit, where it is amplified using x1, x2, x5, x10 amplification factors related to the switch positions on the printed circuit board.

Figure 6.3.1–2 : Seismic signal receiver station DLM-SO
Designed by GIG

To eliminate mains cable noise in transmission lines, a switch-controlled 50 Hz band-pass filter is used. In the receiver circuitry, a flameproof power supply providing D.C. 42 V and peak current 20 mA is used for feeding the transmission line. If the power supply load exceeded 20 mA, the current would be reduced, up to 11 mA in the case of a short-circuit. The voltage of 55 Vrms (for each panel of the receiver) is fed from the mains transformer plate to the sparkproof power supply unit. The other transformer is used for injecting power to all the remaining receiver circuits, e.g. amplifiers, filters

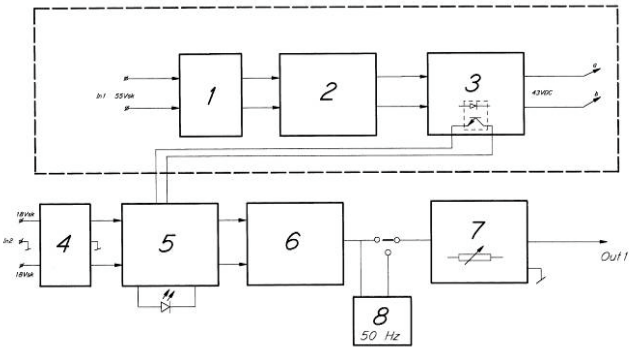

Figure 5 – Block diagram of one channel DLM-SO receiver
Designed by GIG. 1) rectifier circuit 2) constant voltage regulator and current limiter circuit 3) current limiter and short circuit current 4) rectifier and stabiliser circuit 5)current detection circuit of transmission line 6) filter-amplifier circuit 7) output amplifier circuit 8) band-pass filter

Functional and Technical Parameters

- Type of transmission: current.
- Sensitivity: ranging from 1.66 V/mA to 16.66 V/mA, depending upon gain selection x1, x2, x5, x10.
- Output voltage range: ±10 V.
- Frequency bandwidth: 0.8 to 250 Hz (-3 dB).
- Zero current: 12 mA.
- Modulation: ±6 mA.

- 50 Hz signal attenuation: -40 dB (filter switched on).
- Power supply: 230 V / 50 Hz.
- Power consumption: about 100 VA.
- Number of receiver panels (channels): 16.

Operating Conditions

- Humidity: 30% to 85% at a temperature of 20 ºC.
- Operating temperature: +10 ºC to +40 ºC.
- Atmosphere: non-aggressive, free of coal and metal dust as well as of acid vapors.
- Earthing system: elements grounded at one point.
- Power supply: 230 V ±10% 50 Hz.

The DLM-SO seismic signal receivers and their circuits have been designed so as to be sparkproof and obtained ATEX certification.

6.3.1.3 Description of the AS-Seisgram Seismic Recording System

The AS-Seisgram Seismic Recording System has been designed based on the IBM PC Class Computer with the built-in analogue-to-digital converter card (32 or 64 channels). The AS-Seisgram system for recording mining tremors has been designed for working in mine-operated seismic networks. Although its autonomous working is possible, it is intended for use in conjunction with another IBM PC Computer using the network. The purpose of the instrument is to continuously and automatically detect, collect and record seismic data from the DLM-SO receivers. Its basic advantages are the following software programs used with Microsoft Windows operating system:

- Seisgram for analysis of seismic signals;
- MultiLok for modern analysis of mine tremor parameters.
- Functional and Technical Parameters
- Number of input channels: 32, 64.
- Input voltage range: programmable, max ±10 V.
- Sampling frequency: programmable, up to 1000 Hz.
- A/D converter: 12 bits.
- Recording frequency bandwidth: programmable, D.C. to 1000 Hz.
- Operational system: WINDOWS.
- Type of mine tremor detection: seismic background analysis.
- Information transfer rate: 100 kB/s.
- User software programmes: Seisgram, MultiLok.

Operating Conditions

- Power supply: 230 V (+10/-15)%, f = 50 Hz (+/- 10%).
- Earthing system: elements grounded at one point.
- Vibrations: no vibrations.
- Environmental operating conditions:
  (a) Humidity: 30% to 85% at a temperature of 20 ºC.
  (b) Operating temperature: +10 ºC to +30 ºC.
  (c) Atmosphere: non-aggressive, free of coal and metal dust as well as of acid vapours

6.3.2 Appendix to Task 3.2

6.3.2.1 An Evolutionary Algorithm for Tomographic Calculation in Mines – Description

The proposed approach to solve passive tomography calculations will be performed using a misfit function based on the L1 norm. The L1 norm was selected over the least squares norm L2 as it is much less sensitive to the effects of large errors in outlier data (Tarantola, 1986).

$$L_1(\hat{v},\hat{h}) = \sum_{i=1}^{n}\sum_{j=1}^{m}\left|t_{ij}^{obs} - t_{ij}^{theor}\right| \qquad (8.1.2)$$

where: $\hat{v}$ = vector of velocity model parameters, $\hat{h}$ = vector of seismic sources parameters (co-ordinates and origin times), n = number of seismic events, m = number of seismic stations, t_{ij}^{obs} = observed P-wave travel time, t_{ij}^{theor} = P-wave travel time described by model.

The number of variables of the tomographic misfit function is a few hundred or more for typical passive tomography problems. To find the minimum of this function (3.2.1), evolutionary algorithms are used that are well adapted for optimisation problems with a large number of variables (Schwefel, 1995). Evolutionary algorithms use the principles of biological progression and try to mimic organic evolution that nature constructed during millions of years (Schwefel, 1995). Short and very simplified scheme of evolutionary algorithms can be described as follows, Schwefel (1995):

Step 0, initialisation: There should be storage in a digital computer for two points of an n-dimensional Euclidean space

Step 1, variation: Iteration g. Starting from point E(g) (position signed as a vector xE(g)) a second point N(g) (position signed as a vector xN,i(g)) is generated by using random perturbations. This point differs slightly from E(g).

Step 2, filtration: The two points are associated with different values of objective function F(x). Only one of them serves as a starting point in the next iteration g+1. In such case, the question is: how to choose random vector of disturbance $z^{(g)}_1$? For such continuous problems, multi-dimensional Gaussian distribution was assumed.

$$w(z_1,\ldots z_n) = \frac{1}{(2\pi)^{n/2}\prod_{i=1}^{n}\sigma_i} Exp\left(-\frac{1}{2}\sum_{i=1}^{n}\left(\frac{z_i}{\sigma_i}\right)^2\right) \qquad (6.3.2\text{-}1)$$

The evolutionary algorithm performance was compared with that of algebraic reconstruction (SIRT) algorithm. There is clear superiority of the velocity images using the evolutionary algorithm (see the *Figures* below).

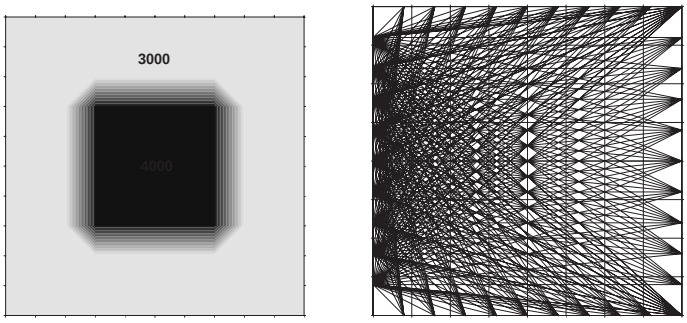

Figure 6.3.2–1 : Theoretical seismic velocity and seismic rays path coverage

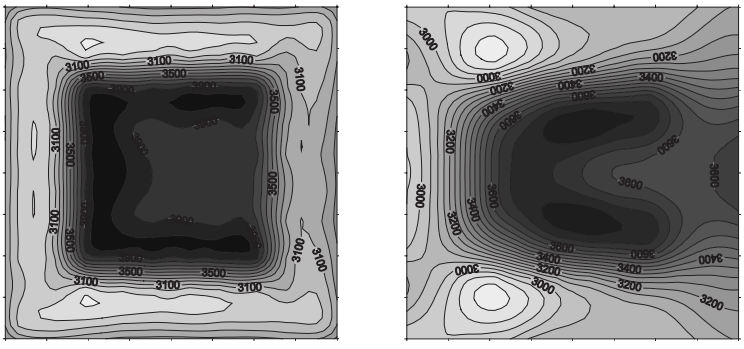

Figure 6.3.2–2 : Results of evolutionary and ART algorithms
Results of seismic velocity image obtained using evolutionary algorithm (left) and ART algorithm (right)

Description of parameters used in the software

- ielter – number of parents of a generation
- bkomma (true or false) – selection criterion applied to parents and descendants or only to descendants
- nachko – number of descendants in a generation
- irekom – switch for recombination type consisting of three digits each of which has values between 1 and 5; the first digit applies to the object variables X, the second one to step sizes and the third one to the correlation angles P
- bkorrl (true or fase) – false the hyper-ellipsoid can not rotate, true the hyper-ellipsoid can not rotate
- konvkr – switch for the convergence criterion:
- =1 the difference in the objective function values between the best and worst parents at the start of each generation is used to determine whether to terminate the search before the time limit is reached >1 the change in the mean of all the parental objective function values in konvkr generations is used as the search termination criterion
- tgrenz – used in monitoring the computation time i.e. the maximum CPU time in seconds
- deltas – factor used in step size change; all standard deviations(=step sizes) S(I) are multiplied by a common random number EXP(GAUSSN(deltas)), where GAUSSN(deltas) is a normally distributed random number with zero mean and standard deviation deltas
- deltai – as for deltas, but each S(I) is multiplied by its own random factor EXP(GAUSSN(deltai))

6.3.3 Appendix to Task 3.3

6.3.3.1 Backward Analysis of Velocity Images for Panel 2JD Before Rock-Burst Event

The velocity images were calculated using all seismic events recorded in longwall panel 2JD from 1 July 2007 to 30 April 2008. The idea of this study was that P-wave velocity increase with higher pressure in the rock and seismic events in the rock are more extensive in zone of higher pressure. In the *Figure* below the relation between P-wave velocity and pressure is shown (laboratory study on samples of rock – left site picture, and field study under edge – right site picture).

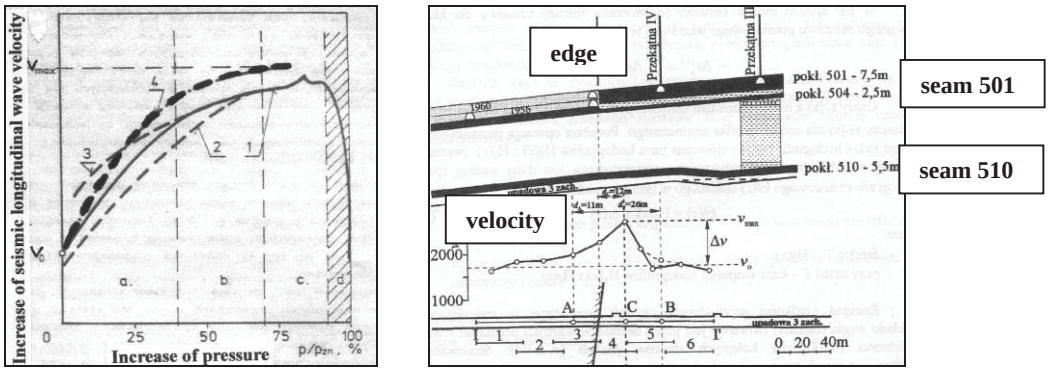

Figure 6.3.3–1 : Relation between P-wave velocity and pressure
Left: laboratory relation between pressure and P–wave velocity (study on samples – according to Dubinski 1989). Right: P-wave velocity profiling under edge (note velocity increase under edge where pressure is highest)

The first image of P-wave field velocity calculated in December 2007 showed the existence of a few zones with high value of velocity. The greatest magnitude and highest velocity events appeared 200 m in front of line of the coal face. The second image was calculated on 15 April 2008. The highest seismic anomaly appeared just before line of coal face and 200 m north-west of coal face at the boundary between a mined and un-mined area near the gallery 1JD. On 16 April 2008 collapse took place in the longwall panel 2JD (*Figure 6.3.3–2*). The rock-burst event allowed verification the effectiveness of the tomographic forecast. It turned out that damage had occurred in the gallery 1JD generally in the location of the greatest seismic anomaly calculated on 15 April 2008. The hypercentre of the rock-burst was situated on the high velocity gradient located to the north-east from the area of damage. A study of the P-wave velocity in longwall panel area 2JD has shown that the seismic

velocity anomaly is moving in time. Epicentres of shocks were located in the area of highest velocity anomaly as calculated in December 2007 and in April 2008 (see *Figure 6.3.3–3*).

Figure 6.3.3–2 : Picture of rock-burst effect in tunnel
after tremor with seismic energy $9 \cdot 10^7$ J, (M_L=3.3), which occurred on 16 April 2008. The gallery was damaged on segment of 85 metres and the floor was lifted up 1.5 m.

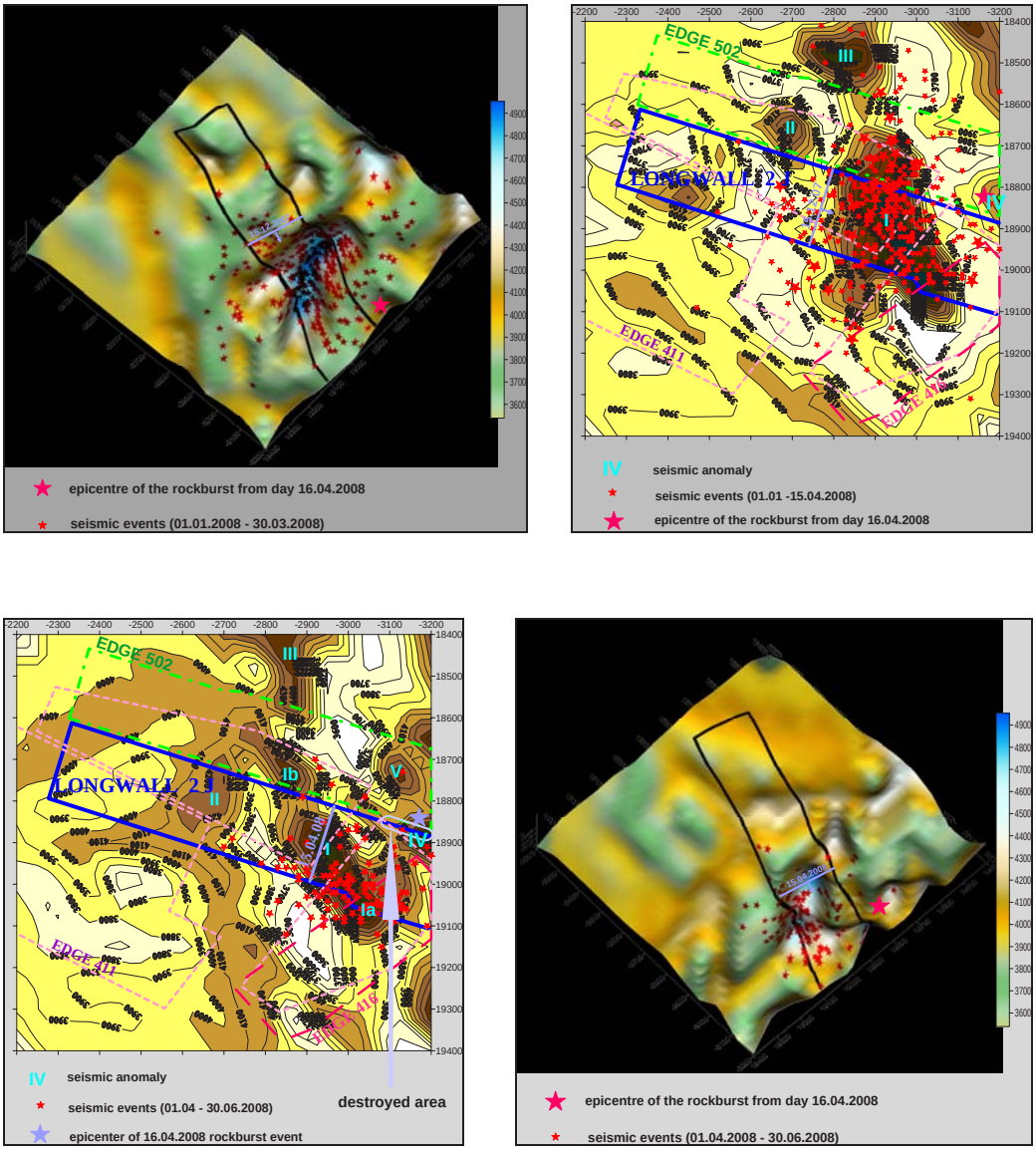

Figure 6.3.3–3 : Longwall 2JD – velocity image results from passive tomography
Left: based on tremors recorded July–Dec 2007 (stars indicate tremors during the next 3 months)
Right: Jan–April 2008 (stars indicate tremors during next 3 months, April–June 2008)

The seismic hazard zones depend on high seismic wave velocity, high gradient of seismic wave velocity and the location of mining activity. Backward analysis showed that passive tomography was providing new and improved quality into forecasting of zones of seismic hazard. Images of the P-wave velocity and real-time seismic monitoring also allow for testing applied effectiveness of rock-burst prevention methods. The application of evolutionary algorithms in tomography calculations is a completely novel approach and undoubtedly is an innovation in safe working in mines.

The velocity image results from passive tomography based on tremors recorded from July 2007 to April 2008 in longwall 2JD – seam 502 is shown on *Figure 6.3.3–3*. The stars indicate tremors that occurred in longwall panel 2JD during the next 3 months after calculation sessions. Almost all the seismic events took places in the highest velocity (see 2D pictures) or high gradient velocity zones (see 3D pictures).

The average P-wave seismic velocity in the area of study amounted to 3950 m/s. The image on see *Figure 6.3.3–3* shows that the highest velocity reaches value more than 4700 m/s in zones I, Ia and IV. This zone I was moved forward comparing to the previous picture. In this zone a lot of seismic events took places. The zone IV developed in the first quarter of a year of 2008. In this zone the rock-burst event took place on 16 April 2008. The rock-burst caused collapsing of gallery 1JD on the length of 85 m (*Figure 6.3.3–2*) on the southern site of the IV zone. The serious damaging effects in the gallery 1JD took place in the high velocity zone IV. It can be seen that seismic hazard zones depend on high seismic wave velocity (zones I and IV), high gradient of seismic wave velocity and area of mining.

Backward analysis of seismic activity in the longwall panel 2JD has shown that velocity images are appropriate to identify areas of high rock-mass instability. The task is to study temporal changes in images of P-wave field velocity. This method enables to estimate over-stressed zones in the rock strata with time

The results of passive tomography interpretation show that changes in the velocity images are related to migration of the high stress zones, because of the geology is the same in the area of study. Potentially seismic-prone zones allow an estimation to be made of the distance between the potential seismic sources and underground openings. This parameter is necessary to estimate rock-burst risk level in galleries, McGarr (1991), Mutke (2007). To do this empirical correlation can be used between normalised parameter, PPV·*R*, and the scalar seismic moment, M_0 , Mutke (2008). The calculated value of peak particle velocity (PPV) in the damaging area reached value 0.3 m/s.

6.3.4 Appendix to Task 3.4

6.3.4.1 Seisgram and Multilok software

The real-time seismic system was installed in Wujek-Slask mine. During almost two years of continuously measurements, from 1 July 2007 to 30 April 2008 , more than 700 seismic events from the area of longwall 2JD seam 502 were recorded and from June 2006 to July 2007 more than 1000 seismic events from the area of longwall 8 L seam 510 (seismic energy: Es > 1kJ, local magnitude $M_L > 0.6$).

A new method of processing the seismic data was developed and implemented to SOS pilot system. The software is based on the network architecture of all variants of the WINDOWS system. Its basic advantage is the software for the analysis of seismic signals Seisgram and the software for the modern analysis of tremor parameters – MultiLok.

The Seisgram software is designed for comprehensive analysis of digital seismograms recorded on the recorder, and also for the control of the registration and detection process of seismological events.

The MultiLok software includes the procedures of tremor focus location and assessment of the seismic energy. The location of tremor foci is based on methods relating to the first arrivals of

longitudinal P-waves and first arrivals of shear S-waves. Some new conceptions were used, such as the L-1 standard apart from the L-2 standard. Moreover, several mini-maximisation algorithms were used: Simplex, modified Powell algorithm and Davidon-Fletcher-Powell algorithm. The MultiLok program allows the collection of recorded data in database sheets. Furthermore, the software has a built-in module performing seismic source parameters calculations.

A few pictures from Seisgram software and MultiLok software to processing and analysis of mining seismic events are shown in the *Figures* below.

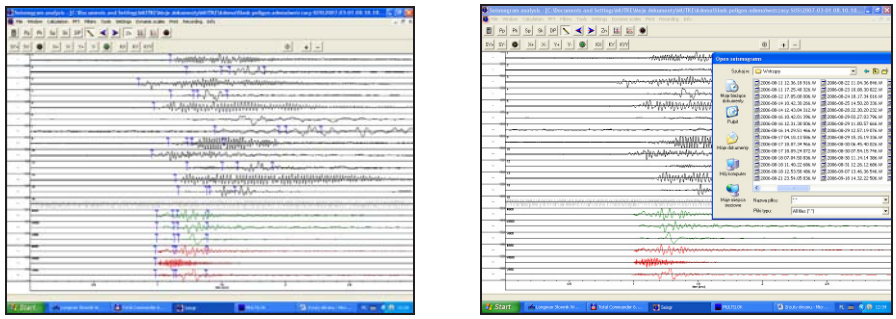

Figure 6.3.4–1 : Import of seismic event from recorded files
and auto pick time arrive of Pp and Sp wave, using Seisgram software and SOS pilot seismic network

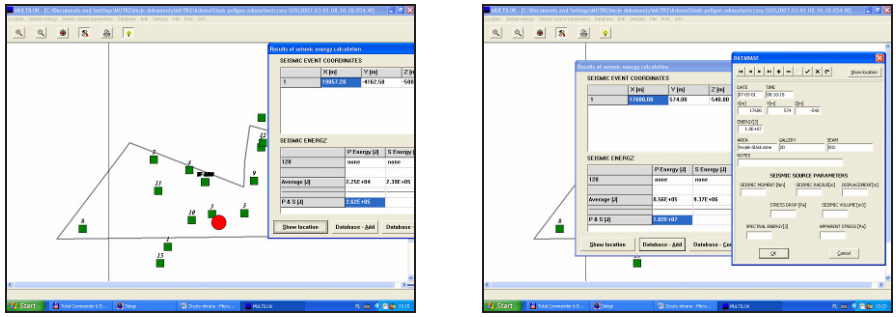

Figure 6.3.4–2 : Location of seismic event and database sheet
of interpreted seismic parameters, using MultiLok software and SOS pilot seismic network

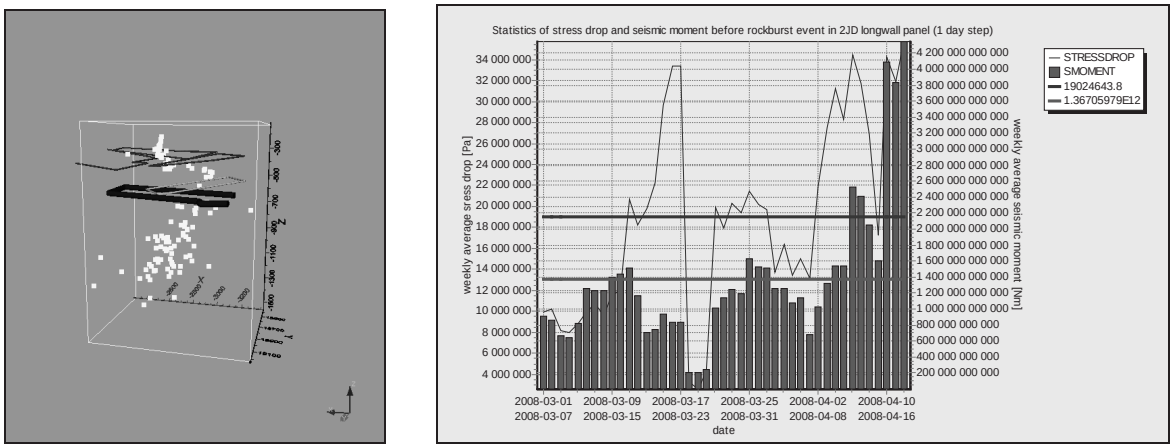

Figure 6.3.4–3 : Example of 3D location of seismic events
In Wujek-Slask mine. Left: gray dots show hypercentre of seismic events, thick line shows contour of longwall 2JD, thin lines show edges). Right: statistics of stress drop and seismic moment before rock-burst event in 2JD longwall panel (weekly average with 1 day step).

The database contains 3D co-ordinates of each seismic event, time of origin and seismic energy. 3D locations of seismic events have shown that approximately 70% of the source locations had been identified to lie beneath the coal seam, whilst 20% lay above the seam. These seismic events occurred far from tunnels and face of longwall 2JD. Only a few strong seismic events were located in seam 502 on either side of longwall 2JD, close to face of longwall 2JD. One of them turned out rock-burst event.

3 D location of seismic events from longwall panel 2JD and statistics of seismic moment and stress drop before rock-burst event are shown in the *Figure* above. On the pictures are shown that stress drop and seismic moment calculated as weekly average with 1 day step increase just before rock-burst dated 16 April 2008.

A key conclusion from the near field study in Upper Silesia Coal Basin was that damage effects in excavations only occur where the tremor source location is within 100 m from a mine opening (Mutke 2007, 2008). The 3D location presented in this project is very important, and can be used in both the spatial-temporary planning of mining operations under predicted high seismicity conditions and the rational choice of support and preventive actions ensuring functionality of mine workings and improvement in work safety level.

6.4 WP4 IN SITU DRILLING AND GEOPHYSICAL LOGGING

6.4.1 Appendix to Task 4.1

a) Drilling parameters

Technology regarding the measurement of drilling parameters consists of measuring and recording physical values at real time. The variations of which can be correlated with geomechanical properties of crossed ground. There are several kinds of recording devices. The one purchased by Geocontrol is the Jean Lutz LT3.

Figure 6.4.1–1 : Recording parameters, Jean Lutz LT3

The drilling parameters measured in one borehole are the following:

- Depth
- Drilling speed, V (m/s)
- Thrust on bit, F (kN)
- Fluid pressure, (bar)
- Torque, T (kN·m)
- Rotary speed, N (rps)

The combination of these parameters permits to obtain the specific energy, which can be defined as energy required excavating unit volume of rock. It is a useful parameter that may also be taken as an index of the mechanical efficiency of a rock-working process. The equation of specific energy, for a borehole with a section A (m^2), can expressed as follows:

$$E = \frac{F}{A} + \frac{\pi \cdot N \cdot T}{A \cdot V} \qquad (6.4.1\text{-}1)$$

In order to start the correlations between drilling parameter and geomechanical properties, a specific test borehole was drilled in Subhullero Formation, aged Westfalian, in the North Carboniferous of Spain (Asturias).

In the *Figure* below (BH-1) it can be observed the different drilling parameters measured and the specific energy obtained with depth.

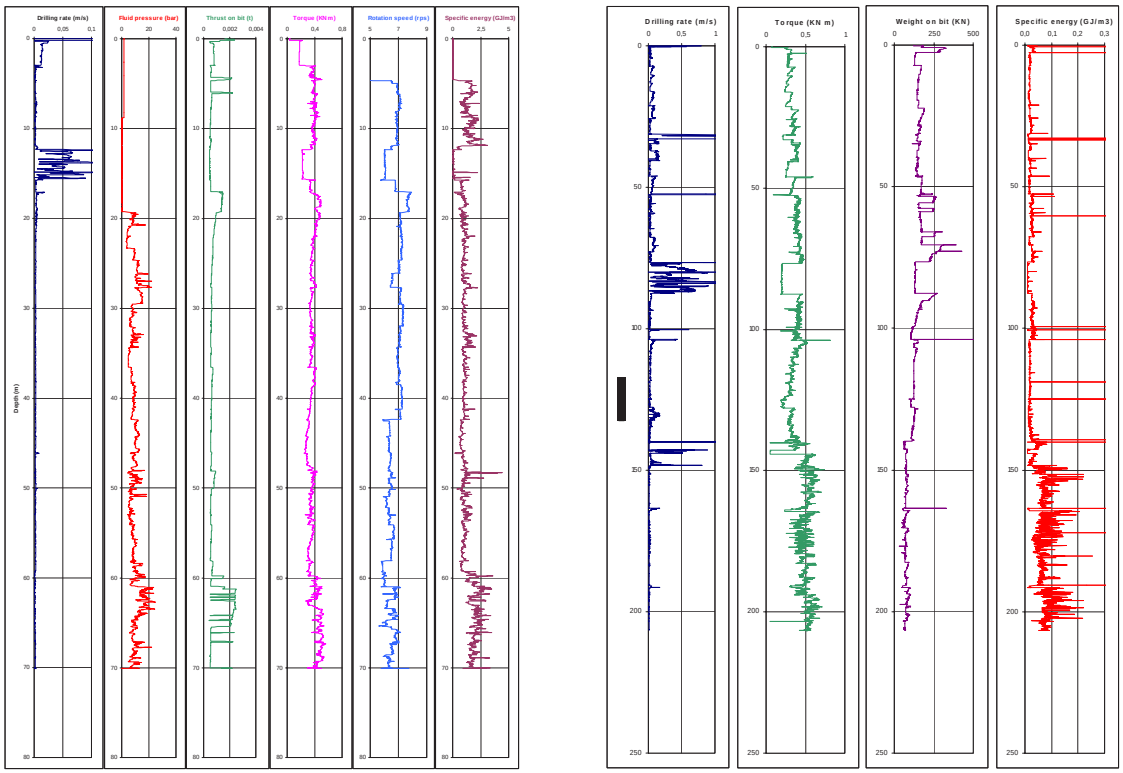

Figure 6.4.1–2 : Drilling parameters and specific energy obtained with depth
Left: BH-1. Right BH-2

It can be observed how all of the parameters show a relatively constant value along the borehole BH-1, with two zones in which data are clearly different of the average value. The first zone is situated between 12 and 16 metres, and it is represented by an increase in the drilling rate accompanied with a decrease of the values of torque and rotation speed. The lithology is almost the same along the borehole, siltstones with different rate of weathering and fracture with fine levels of sandstones. These sandstone levels are two of three metres thick although at 60 m depth, a level of one metre thick has been detected.

The first zone corresponds approximately in the borehole with a highly fractured and weathering material situated between 6 and 15.65 metres. The second section is located between 61 and 65 metre, and it is characterised by an increase of the thrust on bit and slightly higher values of the torque. In the borehole, this zone is represented by a low weathering material, with a high strength and a RMR of 50. Specific energy reflects these results with a minimum between 12 and 16 metres corresponding to the highly fractured zone, and a maximum from 61 to 65 metres corresponding to better materials.

Another borehole (BH-2) was instrumented in the South of Spain for the measurements of drilling parameters and correlation with rock mechanical properties. The borehole BH-2 was drilled from the surface to 139.75 metres depth and it was cored from this depth to 223 m. The first 139 metres correspond to Miocene materials that cover Palaeozoic (Devonian -Carboniferous) metamorphic rocks with high content of sulphurs. In *Figure 6.4.1–2* it is shown the log of drilling parameters recorded. It can be observed an increase in torque and specific energy, and a decrease of drilling rate and weight on bit from 139.75 metres when the Palaeozoic rocks are bored.

b) Acoustic televiewer

Once an acoustic televiewer Mount Sopris SLT ABI-40 was acquired, two main researches were developed. The first one was related with the geometry of the borehole while the second one was related with the discontinuities characterisation (structure) in open boreholes. Following, it is shown the first application considering the borehole ovalisation analysis and its use for the estimation of the

existing natural stress field. To make this research some intensive televiewer measurements were carried out at Borehole BH-8+970 (227.5 m depth) located at the Southeast of Spain (Almería).

This borehole was drilled for a new railway line, in a schist formation. Its depth is 227.50 m, and it has been registered between 65 and 227.5 m. After a detailed analysis of the travel time data, the following sections have been chosen, for an ovalisation study: 74.00, 87.00, 96.10, 104.50, 182.40, 217.70 and 218.50 depth. The following *Figures* show the section at 74.20 m and 182.40 m depth.

In ECSC 7220-PR/135 (Improved Rock Stress Measurement and Analysis for Planning of Underground Mines), a specific methodology to determine the natural stress field was developed (Galera, 2006) and its results compared with hydrofrac measurements. Using this methodology the *Table* below contains the:

- maximum radio (r_b)
- breakout angle (θ)
- strike of the minimum diameter (S_H)

DEPTH	r_b (mm)	BREAKOUT ANGLE			RATIO $\sigma_{h\text{-}H}/\sigma_V$		STRIKE S_H		
		θ_1 (º)	θ_2 (º)	θ (º)	Ko (S_H)	Ko (Sh)	α_1	α_2	
74.20	52.70	33	35	34	2.52	2.20	33	17	N-155 º-E
87.00	52.20	38	34	36	2.52	2.20	14	15	N-165 º-E
96.10	52.03	47	43	45	1.77	1.56	75	68	N-108 º-E
104.50	51.30	43	44	43	1.77	1.56	60	44	N-128 º-E
182.40	51.40	38	32	35	0.989	0.89	17	19	N-162 º-E
217.70	50.70	41	37	39	0.81	0.73	29	37	N-147 º-E
218.50	51.60	38	44	41	0.80	0.72	50	46	N-132 º-E

Table 6.4.1–1 : Results of the estimation of natural stress field in BH-8+970

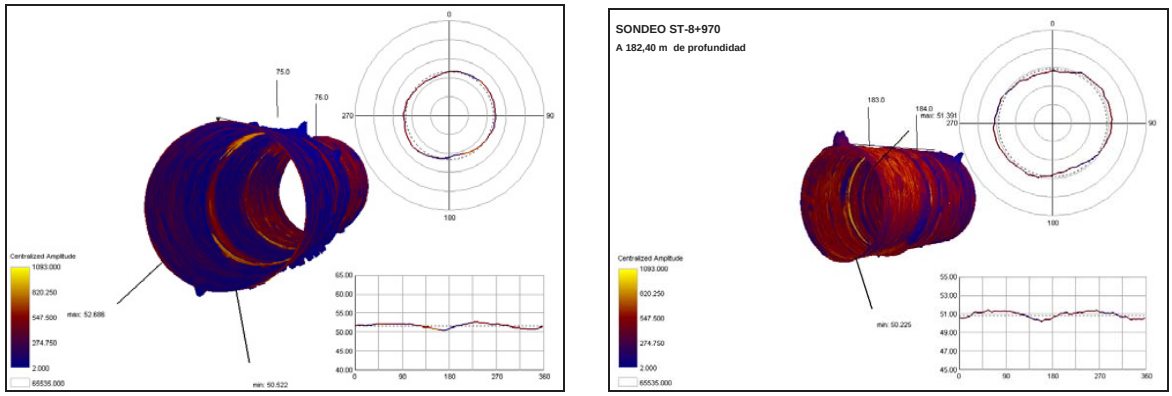

Figure 6.4.1–3 : Borehole results
a) 8+970 section at 74.20 m depth b) Borehole 8+970 at 182.40

c) Geophysical methods, Sonic Log

Geophysical logs were developed mainly for petroleum industry, but sonic log also has been used in recent years for geotechnical purposes due to the good correlation between deformational properties of the rock and the velocity of P and S waves. For this reason sonic log has been used in several holes bored in different types of rocks to compare the values obtained, and to correlate the elastic properties of the rock with the results obtained.

Three boreholes were drilled in the North of Spain; the materials obtained in these boreholes were Cretaceous formations with shale and sandstones (BH-01). Other tests were made in granitic rocks in

the Central System of Spain (BH-02). The tool used is the Mount Sopris Instrument sonic log model 2 SAA-1000 F which it is shown in the *Figure* below.

Figure 6.4.1–4 : Sonic log 2 S AA-1000 F of Mount Sopris

Qualitatively, sonic log can be used for the identification of lithology, in drilled wells. There is much variation within sedimentary rocks; however, high velocities are more likely to be associated with carbonates, middle velocities with sands and shales and low velocities with shales.

In the *Figure* below is shown a sequence of a well bored in the north of Spain. It can be observed a good correlation between the wave velocities and the lithology obtained. The lithology has been determined by the samples cored on the borehole.

It can be observed that the highest values of S and P waves velocity correspond to calcareous rocks (dolomite). The dynamic modulus also reflects this. A very clear reduction in velocity and dynamic modulus marks the limit of calcareous formation and shales. The transit from sand to dolomite is not so evident although it can be observed an increase in P wave velocity and dynamic modulus. The Poisson's ratio shows an almost constant value along the borehole but in shales these values suffer a slight reduction.

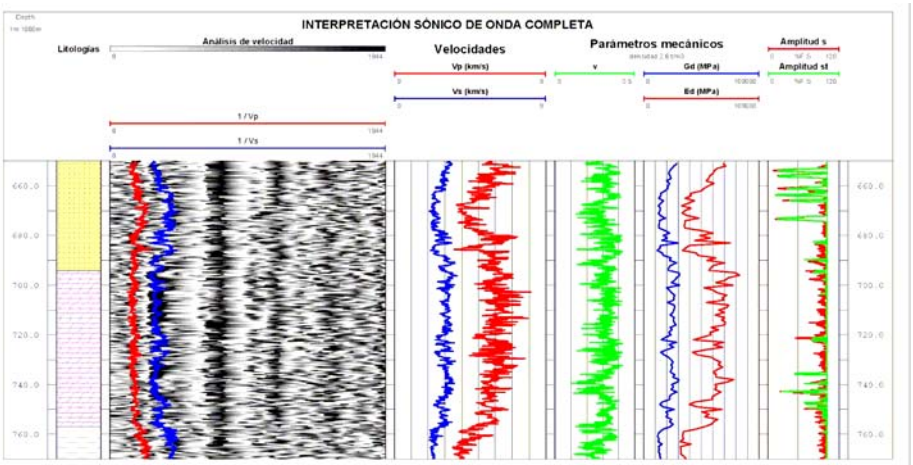

Figure 6.4.1–5 : Sonic log and borehole samples
Relationship between wave velocities of the sonic log and the lithology obtained in the samples cored in the borehole.

6.4.2 Appendix to Task 4.3

The borehole BH4 was drilled in the Coto Minero del Sil Mine, in Fabero Subzone, located in Bierzo Coal Basin, at north-western Spain.

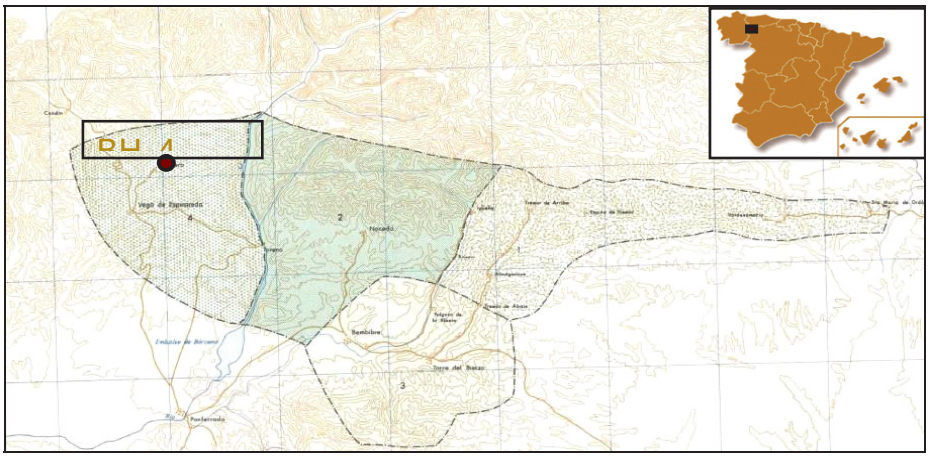

Figure 6.4.2–1 : Location of Bierzo Coal Basin

The section of the BH4 is situated in the Stephaniense Facies, belongs to the Upper Carboniferous Period, its lithology consist in sandstones and shales with layers of coal, these seams are 0.5 to 2 m thick. The next *Figure* shows the stratigraphic column and geological situation of Fabero.

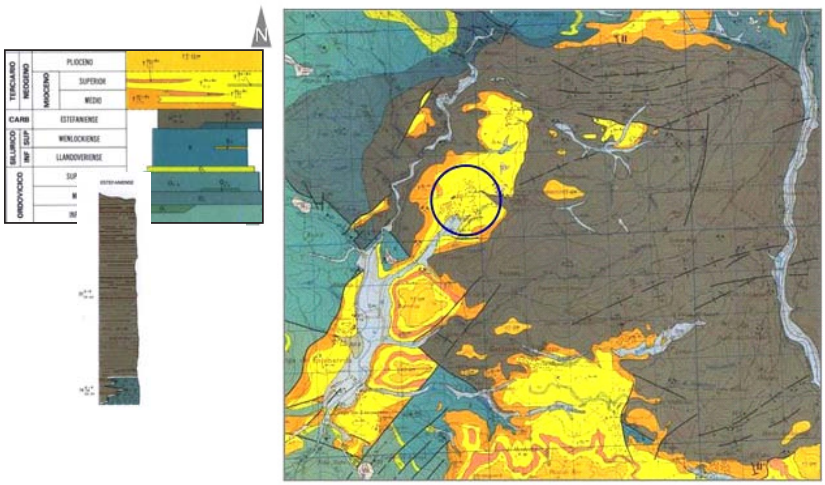

Figure 6.4.2–2 : Geological situation of Fabero

The BH4 was testified according to the test model used in Geocontrol, principally shows:

- Lithology and description
- Recovery (%)
- Weathering
- RQD (%)
- Nº Joints/m
- RMR

Below, it shows an example of this test model, between 30 and 40 metres.

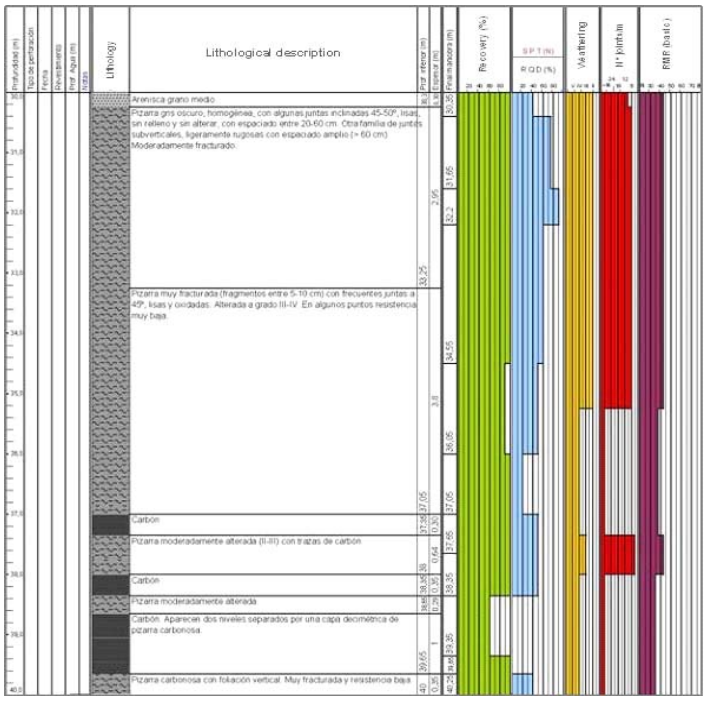

Figure 6.4.2–3 : Geotechnical logging model

Besides, drilling parameters and geophysical logging were carried out, the different parameters obtained, were contrasted with the lithology. Drilling parameters, Specific energy and lithology obtained with depth are showed in the next graphics.

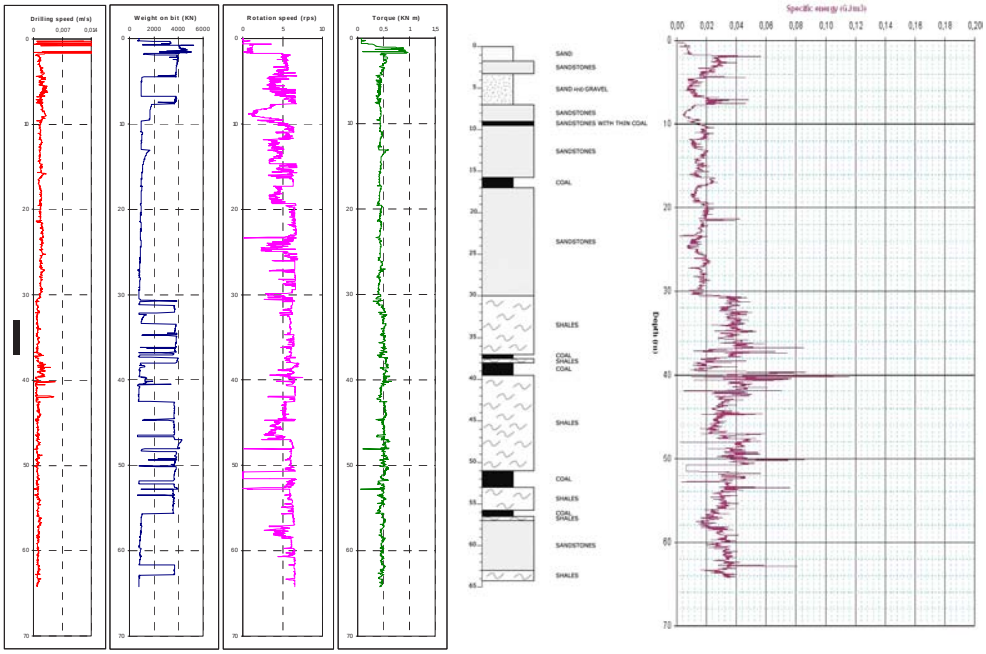

Figure 6.4.2–4 : Drilling parameters, lithology and specific energy

A different response is observed for sandstones and shales, specially in these parameters of drilling speed, weight on bit (WOB) and specific energy. A brief conclusion would be that the drilling speed decreases for shales, while Specific energy and Weight on bit increases. In the thicker coal seams (like between 37-40 m), drilling speed increases. Also a good agreement between the Specific energy and the main Rock Mass geomechanical parameters (RMR and Joints/m) has been observed, by the way, as in previous BHs a high scatter has been obtained considering RQD value.

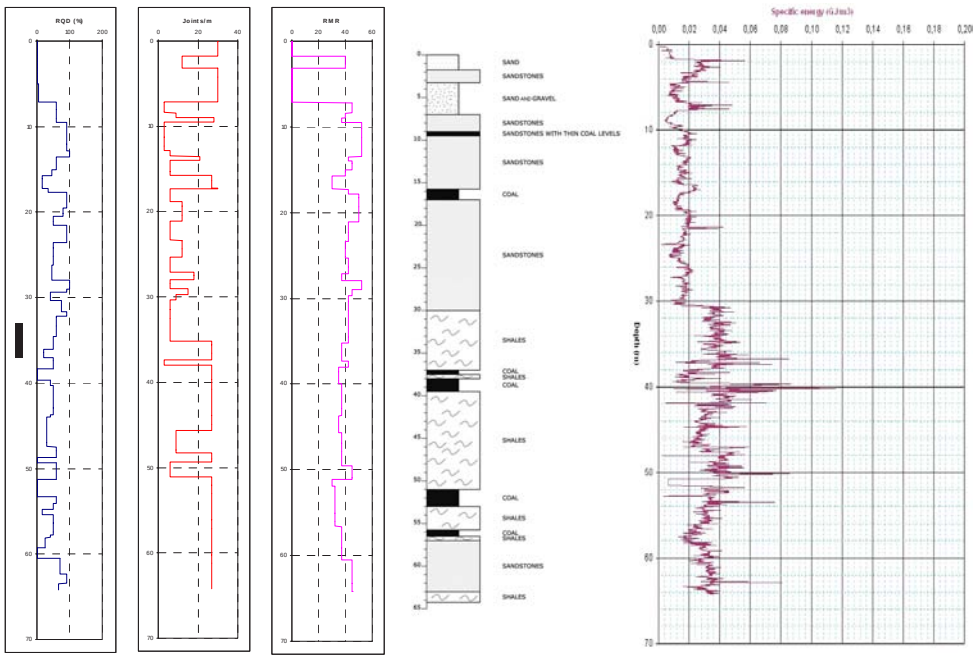

Figure 6.4.2–5 : Rock mass geomechanical parameters, lithology and Specific energy

With regard to the lithology, geophysical well logging parameters proportionate clear information, natural gamma ray shows low values for sandstones and coal, while for shales show high values. The SPR (punctual resistivity) shows high values for sandstones and low values for shales, while for coal the values are moderate low.

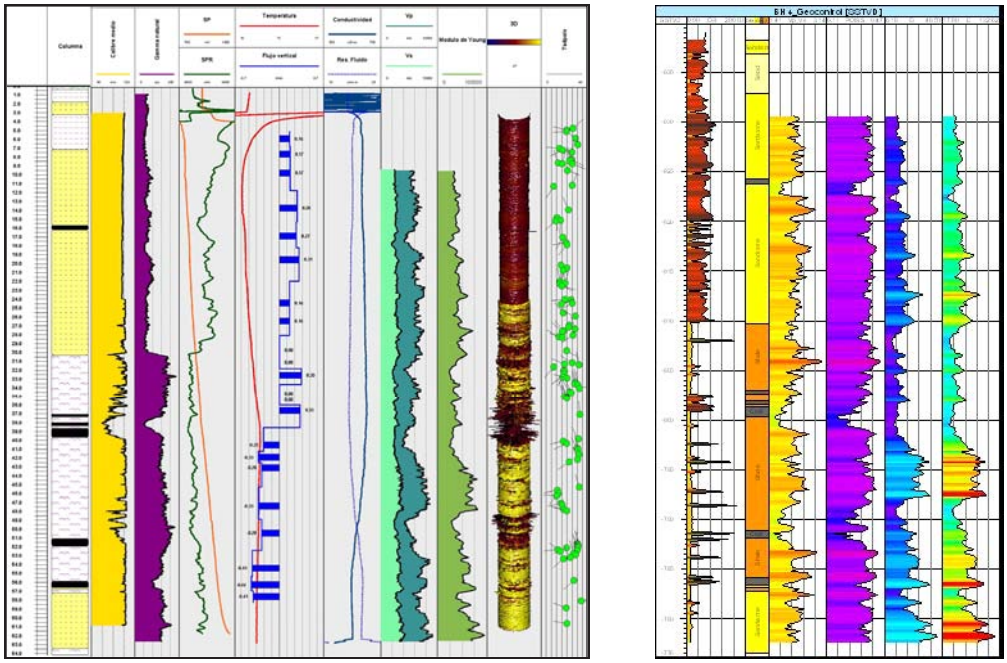

Figure 6.4.2–6 : Geophysical well logging and lithology (left)

Figure 6.4.2–7 : Calculated elastic parameters for BH-4 borehole (right)
The logs shown comprise, form left to right: gamma ray, lithology, and calculated Vp/Vs ratio, Poisson´s ratio, Shear modulus (GPa) and Young´s modulus (GPa)

In relation with dynamic modulus, a new analysis using Petrel code was done, with data from Spanish borehole (BH-4). For this borehole, the elastic parameters were calculated along their total length from the compression and shear wave velocity logs. Resulting logs are displayed in *Figure 6.4.2–7*.

6.5 WP5 RADIO IMAGING (SIGNAL TRANSMISSION AND ACQUISITION)

6.5.1 Appendices to Task 5.1

6.5.1.1 Principles of RIM technique

Introduction

This appendix describes the operation of the RIM technique in further detail, and should be read in the context of the corresponding section of the main report. The salient points of a conventional radio imaging system are shown in the diagrams below.

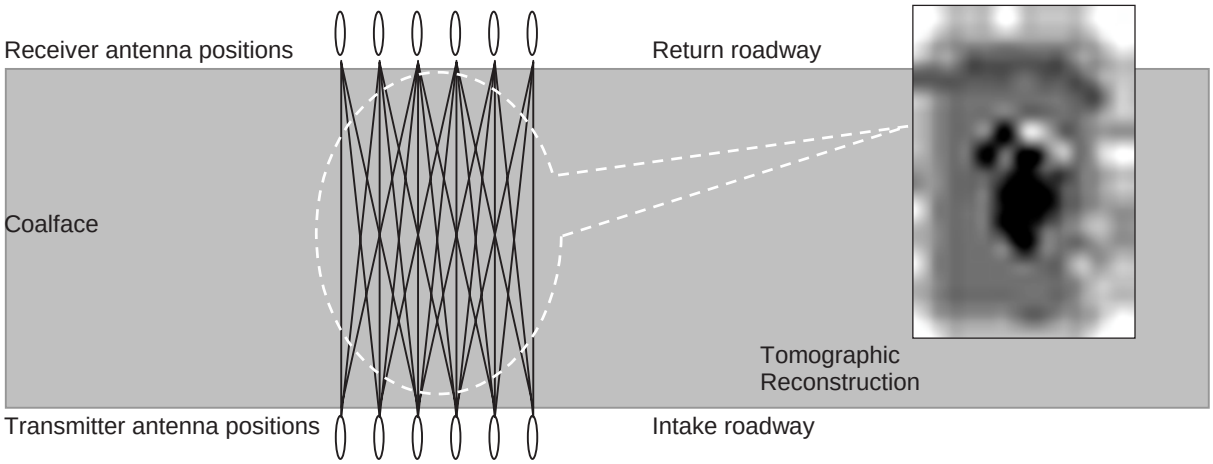

Figure 6.5.1–1 : Plan view of a coal panel, showing RIM operation

The conventional 'radio imaging method' utilises vertical magnetic loop antennas in a co-planar orientation. A number of 'ray paths' are measured across the seam. A more complex tomographic reconstruction would not assume straight-line ray paths, but incorporate the complete field behaviour.

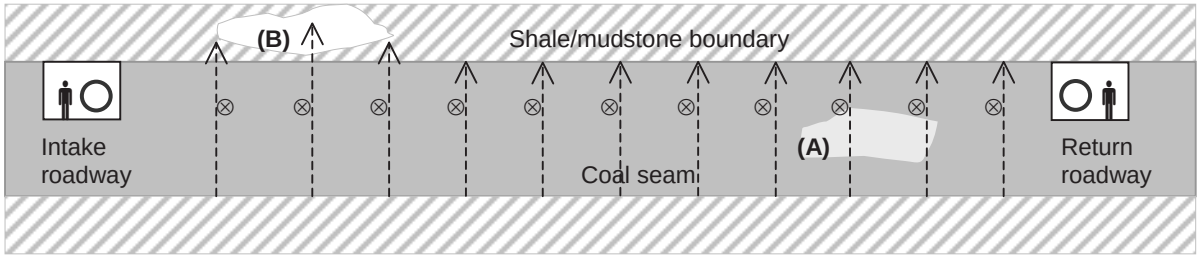

Figure 6.5.1–2 : Elevation across a coal panel, showing RIM operation

The co-planar orientation of the antennas can be observed. This induces a 'quasi-TEM' wave, which is similar to that which would be produced by direct current injection. The shale/mudstone conductive layer behaves like a transmission line, so there is a vertical electric field between the 'plates' (indicated by the vertical arrows and a horizontal magnetic field (indicated by ⊗). The anomaly at (A) affects the attenuation and phase of the signal. An anomaly at (B) can affect the signal if the skin depth in the boundary rock is too large, thereby allowing the signals to escape from the seam.

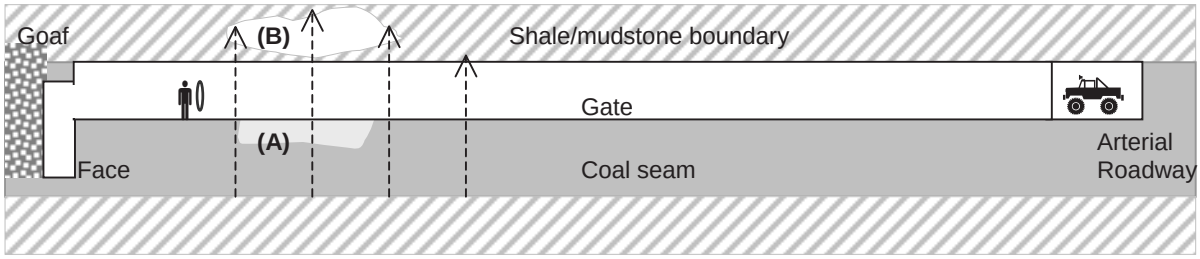

Figure 6.5.1–3 : Elevation along roadway, showing RIM operation

A modelling of the RIM technique is essentially a description of the fields within a low-conductivity layer, bounded by high conductivity layers. The model is well-described by [Delogne, 1982]. Additionally, either of the papers [Lagace *et al.*, 1975] or [Emslie and Lagace, 1976] gives a useful description of the propagation. From a knowledge of the fields in a semi-infinite medium, it should be apparent that a homogenous earth model is not appropriate for such a stratified medium. This is confirmed by [Lagace *et al.*, 1975], who report that measurements indicated that the signal attenuation was lower with the magnetic loop antennas in a co-planar vertical alignment than a co-planar horizontal alignment. (No mention is made of a co-axial arrangement). The authors also dismiss their experimental results as being due to an infrastructure-guided mode (e.g. utilising the metal roof bolts) because such a wave would be difficult to excite. However, it should be noted that extensive and *continuous* metal infrastructure (such as rails, pipes and braided hoses) is commonly perceived and stated to be significant problem in RIM surveys. The practical deployment of cross-panel electromagnetic survey techniques currently requires that cross-panel electrical connections are disconnected over a distance of 25 m or more (to prevent significant mode coupling).

The most obvious mode of propagation to a lay person is probably a ‘waveguide’. However, Lagace *et al.* dismissed a lossy rectangular waveguide mode, operating below cutoff, because it predicted a far higher attenuation than was observed. The model which was settled on, which is described by subsequent authors including [Hill, 1984] and [Shope, 1986] is that of a transverse magnetic wave and an ‘almost transverse’ electric wave, so the mode is referred to as a quasi-TEM mode. This is depicted in the Figure below. Although the wave is largely constrained by the conductive boundaries to the coal seam, this is not entirely the case, and an analysis shows that the attenuation coefficient in the coal seam is dependent both on the skin depth on the coal seam *and* the skin depth in the surrounding strata.

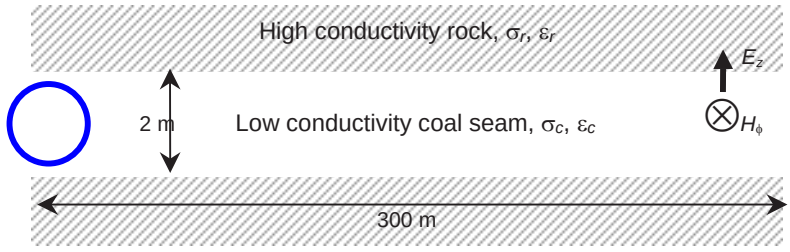

Figure 6.5.1–4 : TEM model of coal-seam propagation
Vertical co-planar induction loop antennas result in transverse electric and magnetic fields

Because this mode operates below the waveguide cutoff frequency, the mode is sometimes referred to as a ‘zero order transverse waveguide mode’. However, in the opinion of the ADEMA report authors, this terminology is highly misleading. Partly, this is a matter of semantics – when is a wave ‘guided’; and, if it is ‘guided’, can it be definitely said to be travelling in a ‘wave guide’? Clearly the answer is that it would be misleading to refer to a pair of wires or a co-axial cable as a waveguide; such structures are more properly termed ‘transmission lines’. Moreover, it is well understood that transmission lines support TEM modes, but not TE or TM modes and that, conversely, a hollow-tube waveguide cannot support a TEM mode. Additionally, the phase velocity in a hollow-tube waveguide is greater than the speed of light whereas, in a transmission line this cannot be the case.

It is therefore suggested that the term ‘waveguide’ should not be used in the context of coal-seam propagation. The main danger of referring to the coal seam as a waveguide is, perhaps, in imagining it to be a conventional low-loss structure, which will operate at a high frequency.

Mathematical Modelling

An analytical propagation model was derived by [Lagace *et al.*, 1975], who compared the predictions of this model with the actual measured behaviour of signals in a coal seam and demonstrated a good agreement of theory and practice. A typical result quoted in the paper is as follows...

Coal conductivity	140	μS/m
Coal permittivity (relative)	7	
Rock conductivity	1	S/m
Seam height	2	m
Frequency of transmission	57.5	kHz
Transmitter moment	0.7	Am^2
Transmission distance	380	m
Signal strength at receiver	60	nA/m

Some detail of the modelling used to obtain this result is given in the later appendix, *Modelling a Coal Seam as a Transmission Line*.

The salient point is that the transmitter is much smaller than that used for Shope's experiments and is therefore considerably smaller than that considered necessary for tests within the ADEMA project. A moment of 0.7 Am^2 could be realised, for example, by a loop antenna with a specific aperture of just 0.8 $m^2/\sqrt{\Omega}$ ([1]) and a power dissipation of just 0.7 W. A loop antenna with a specific aperture of 50 $m^2/\sqrt{\Omega}$ ([2]), could achieve the same moment with a dissipation of only 200 μW.

Given that the coal in this example has a relatively low conductivity compared to the boundary rock, it may be a valid assumption to assume a radome diameter of 2 m; that being the seam height in the above example. Using relationships derived in [Gibson, 2003], it can be stated that, even for the large antenna described above, R_r / R_d – the ratio of radiation resistance to 'dissipative' resistance of the antenna – is of the order of 10^{-7} and R_e / R_d – the ratio of external to 'dissipative' resistance – is only 0.7%. In other words, the radiated power is entirely negligible and the power dissipated in the conducting medium is less than 1% of the power dissipated in the antenna.

Another highly significant point that emerges from this simple example is that the power dissipation in the conducting medium is essentially *independent* of the magnetic moment and the signal strength at the receiver. It is therefore wrong to analyse such systems in terms of power. This may seem to be counter-intuitive, and it is easier to understand if one considers the case of a current injection antenna.

Example: Consider the voltage that is present across two sense electrodes due to a current injected via another two electrodes. Clearly the sense voltage is proportional to the injected current. An analysis will also show that it is proportional to the distance between the electrodes, so it is proportional to an electric dipole moment. The same analysis will show that the sensed voltage is *not* proportional to the size of the electrodes themselves. However, the size of the electrodes changes the resistance between them, and therefore the power drawn from the 'transmitter' and dissipated in the medium. This is precisely the situation described above – the power dissipation in the conducting medium is essentially *independent* of the transmitter's dipole moment and the signal strength at the receiver.

The signal strength at the receiver can be related to the received voltage via the law of induction, $v = \mu_0 N A \, d\omega/dt \, H$ showing that, for the larger antenna quoted above, it is about 4.5 μV. Of course, what is more significant is the signal/noise ratio. A typical Figure for background noise, taken from practical measurements reported in the same paper, is around 10 nA/m/√Hz at 100 kHz. Graphs of the noise at a number of mine locations show that it obeys a rough $1/f$ variation and a large ±30 dB variation depending on location within the mine and mine activity. It is important to stress that the magnetic noise field spectral density *cannot* be converted into an equivalent electric field merely by multiplying by the wave impedance Z_0. The measured noise is the vector sum of different noise sources and so it cannot be equated to a single electromagnetic wave with E and H-fields related by the wave impedance.

---

1 e.g. 10 turns of 7/0.2 equip. wire on a 300 mm dia. former , resistance 0.7 Ω (excluding skin losses etc)

2 e.g. 30 turns of 30/0.2 equip. wire on a 1000 mm dia. former , resistance 60 Ω (excluding skin losses etc)

The salient point about the above example is that the coal and the boundary rock form a transmission line with relatively good conducting walls and relatively low losses within. This is not the case for geological conditions in the UK. Moreover, it is inadequate to assume, during modelling, that the boundaries are perfectly-conducting because their finite conductivity has a significant effect on the propagation. Expressions for in-seam propagation, as derived by [Delogne, 1982; Emslie and Lagace, 1976; Hill, 1984; Lagace *et al.*, 1975; Shope, 1987; Wait, 1976], require both in-seam and boundary-rock electrical parameters.

RIM in the Context of the ADEMA project

Some considerable efforts were made within the ADEMA project in order to gauge the criticality of RIM parameters and methods within Work Package 5 that might have a bearing on the focussing of resources within Work Package 6. The discussion that follows examines the parameters that were considered to likely to materially affect how RIM may be deployed and how this would, in turn, influence the tomographic approach to be used.

One of the objectives of the radio-imaging module of the ADEMA project was to determine the factors that affected the deployment of radio imaging methods. Broadly, these were considered to be i) factors affecting signal transmission and acquisition (WP5) and ii) factors affecting tomographic reconstruction (WP6). The two are closely related and inter-dependent. Work Package 1 assessed in some detail the use of RIM world-wide, including a historical perspective on UK use. The literature indicated that some mining companies were well-satisfied with RIM and had preferred it to in-seam seismic surveys. However, on other occasions, RIM surveys have produced less satisfactory results. Unfortunately, reports describing UK RIM trials in the 1980 s were not available, although two facts were known, namely that...

- The particular geological conditions in the UK (high electrical conductivity, long ‘probing’ distance) had required a lowering of the probe frequency from 80 kHz to around 20 kHz.
- The *perceived* need to disconnect the metallic infrastructure had resulted in RIM surveys being an expensive and time-consuming exercise.

The reduction in probe frequency reportedly required for UK work does not indicate *of necessity* that there will be a worsening of the spatial resolution of anomalous features that can be detected. Commonly, it is assumed that spatial resolution is related to wavelength. This ‘classical’ or Rayleigh limitation on resolution is caused by diffraction around an object of dimensions comparable with a wavelength and means that there is a lower limit on the frequency of the illuminating source. This limitation does not apply to RIM surveys because they are not focussed ‘lens-based’ configurations. In support of this, can be cited the obvious fact that zero-frequency electrical resistivity tomography is an established technique. It can therefore be stated, with certainty that spatial resolution is not fundamentally related to frequency. However, one of the effects of a reduced probe frequency is that the phase shift and changes in attenuation caused by an anomaly will be smaller, requiring the instrumentation to have a lower bandwidth and a higher resolution.

More recent application of the latest RIM techniques [Stolarczyk, 2003], in the UK, in 2003 had the salient features of...

- the use of two RF signals, one for imaging and the other for synchronisation, for phase coherent detection by the receiver,
- a method of achieving receiver phase coherency with a transmitter to achieve maximum receiver threshold sensitivity,
- measurement of attenuation and phase shift,
- the use of the full wave inversion method for image reconstruction.

A significant result of this project has been to deduce the likely effect of a variation in the conductivity contrast between the coal and the surrounding rock. Clearly, if the signal is not to be affected by out-of-seam anomalies then there must be minimal geological anomalies within, say, a

skin depth of the coal/rock boundary. Thus it is not solely the conductivity *contrast* that is significant, but the conductivity of the boundary rock *alone*. Literature describing RIM methods frequently quotes the rock conductivity as being as high as 1 S/m, corresponding to a skin depth of 1.8 m at 80 kHz. If the rock has a much lower conductivity of, say, 10 mS/m then the skin depth is 18 m at 80 kHz resulting in the possibility that anomalies will have a noticeably greater significance.

A further detrimental effect arises if the coal seam is too conductive, resulting in a lower skin depth and reducing the strength of the signals at the receiver. Literature describing RIM methods frequently quotes the coal conductivity as being as low as 0.5 mS/m, corresponding to a skin depth of 80 m at 80 kHz. However, measurements at Daw Mill suggest that the coal conductivity is ten times higher than this, resulting in a skin depth of only 25 m. Given that the oblique ray paths may be 400 m or more, this is a clear indication of the necessity to reduce the probing frequency. However, as noted above, this reduction in the probing frequency allows anomalies in the boundary rocks to have a far greater impact on the signals.

Summary of Discussion

The above discussion can be summarised as follows.

- The coal in the UK (in Daw Mill colliery) has a higher conductivity than reported for previous uses of RIM, resulting in a lower skin depth.
- The large size of the coal panels, coupled with the necessity for oblique ray-path measurements and the lower skin depth in the coal requires a lower probing frequency.
- The use of a lower probing frequency coupled with the lower than previously-reported conductivity of the boundary rock results in a large skin depth in the boundary rock, such that anomalies in the boundary rock have a greater effect on the signal strength.
- The use of a lower probing frequency also results in lower phase shift and amplitude variations which, if they are below the resolution of the receivers, will affect the success of the reconstructed image.
- However, the use of a lower probing frequency probably reduces the effect of any spurious signals that are propagated along the metallic infrastructure. It should be pointed out that there does not appear to be any sound documentary evidence that spurious signals are a problem, even with higher-frequency operations.

From the above, it is questionable whether a reduction in probe frequency could be successful. Existing state-of-the-art tomographic algorithms already make use of phase and amplitude measurements, and use a full wave inversion (FWI) technique [Stolarczyk, 2003; Stolarczyk and Stolarczyk, 1999]. It is not known whether proprietary algorithms assume an in-seam TEM mode of propagation, although that would appear likely. Any enhancements to these algorithms that allowed for a finite skin depth in the boundary rock would, it is anticipated, result in a rather intractable mathematical problem.

Regarding the signals, it seems that there is a difficult trade-off between better propagation at low frequencies and a better selective elimination of out-of-seam anomalies at higher frequencies. This confirms ADEMA's aim of studying methods of improving signal detection, which will allow the retention of a higher probing frequency.

Tomographic Reconstruction

In his PhD thesis, [Shope, 1987] considered three algorithms that are well-known in the literature – the back-plane projection technique (BPT), the algebraic reconstruction technique (ART) and the simultaneous iterative reconstruction technique (SIRT). He concluded that the latter is best. In [Stolarczyk and Peng, 2003; Stolarczyk and Stolarczyk, 1999] the use of the full-wave inversion (FWI) technique is described. This system achieves a greater imaging resolution by not relying on the straight ray path assumption, and claims to be able to resolve multiple anomalies. In [Stolarczyk and Peng, 2003] the comment is made that "The comparison of reconstructed images shows that the algebraic reconstruction technique (ART) produces a smeared image in the direction of wave propagation. The ART algorithm assumes that the coal seam waveguide signal travels on a straight ray path. Severe geologic anomalies cause refraction of the signal, and the ray path assumption fails. This is the cause of the smeared image. In mild anomalies in the Pittsburgh coal seam, the image is

not significantly distorted. Cross-panel RIM tomography has proven effective in detecting geologic anomalies within longwall panels. The full-wave algorithm processes the RIM receiver magnitude and phase data to reconstruct the image with much higher resolution than ART."

One facet of the RIM technique, which applies equally to ERT measurements, is that it utilises multi-pair tomographic measurements with a large number of averaged measurements, such that the process of statistical ensemble averaging occurs. Shope discussed the ability of multiple measurements to reduce the noise, which he demonstrates with forward modelling using the SIRT technique.

A further salient point related to the incorrect assumption of a straight ray path is that the conductivity of the medium gives rise to fields that are out of phase and in a different orientation to the energising field. One analysis, in [Burrows, 1978], shows that it is the rate-of-change of conductivity with distance that gives rise to a component of the secondary field at the receiver. It is most probable that these secondary fields contain useful information, and so the orientation of the antennas becomes an issue. However, this was considered outside the scope of the ADEMA project as it would require some highly-specialised mathematical analysis, well beyond the current state-of-the-art, to adapt currently-used tomographic algorithms.

6.5.1.2 Modelling a Coal Seam as a Transmission Line

This appendix gives some detail of the analytical modelling that was used to investigate the RIM technique. Prior experimental evidence, backed by theory, has shown that low frequency electromagnetic waves propagate through a coal seam as if it were a lossy transmission line – that is, a zero-order TEM wave. Theoretical modelling of the coal seam as a lossy transmission line has reportedly [Lagace *et al.*, 1975] produced results that are closer to practical observations than a model that assumed a below-cutoff evanescent waveguide mode, a uniform medium or an infrastructure-guided wave.

A lossy transmission line occurs because the rocks (e.g. shales, mudstones) that form a boundary with the coal seam are usually relatively highly conducting. Sandwiched between them is the coal with a relatively low conductivity. Because of skin depth attenuation in the shale, the signal is mostly restricted to a region close to the coal, and so the shales therefore take the role of conducting plates with a lossy dielectric between them. The structure can be considered either as an electromagnetic wave travelling in the coal and bounded by induced charges in the 'plates' of the transmission line, or as a conventional electric current flowing in the conducting 'plates', which gives rise to a field between them. Both views are 'correct' and represent different ways of considering the problem.

Transmission Line Model

The transmission line can be modelled quite adequately using conventional circuit techniques. It is assumed that the conducting plates have effective thickness h and conductivity σ_r (r = rock). The coal has conductivity σ_c (c = coal). It is assumed assume that the plates are separated by a distance 2 b (the height of the coal seam) and have a width w. Provided that sensible assumptions are made concerning skin depth, the parameters of this transmission line are given, by well-known formulas, to be

inductance,	$L = \mu_0\, 2\, b / w$	[H/m]	
wall resistance,	$R = 2 / \sigma_r\, h\, w$	[Ω/m]	
dielectric conductance,	$G = \sigma_c\, w / 2\, b$	[S/m]	
capacitance,	$C = \varepsilon c\ w / 2\ b$	[F/m]	(6.5.1-1)

[Bannister, 1973], quoted in [Lagace *et al.*, 1975], showed that, for sensible assumptions about skin depth, the penetration of a field into a conducting wall could be modelled by ascribing a 'complex thickness' to the wall, of $\delta_r / (1 + j)$ so this can be substituted for h in the above equations. The standard transmission line formula (e.g. see [Davidson, 1978]) then describes the propagation coefficient, k as

$$jk = \alpha + j\beta = \sqrt{(R + j\omega L)(G + j\omega C)} \qquad (6.5.1\text{-}2)$$

and so expressions for α and β may be derived. The attenuation, rather than the phase characteristic, is of primary interest and so it is the value of α that is important, because the attenuation with distance r is given by $\exp(-\alpha r)$. This means that α is associated with a type of skin depth, which Lagace calls the "radial skin depth", and which is defined as $\delta = 1/\alpha$. Assuming a good conductor and the several other conditions, the attenuation coefficient is

$$\alpha \approx \frac{1}{\delta_c} + \frac{1}{2b\sqrt{\sigma_r/\sigma_c}} \qquad (6.5.1\text{-}3)$$

which shows that the propagation coefficient is modified by the seam height and the conductivity ratio, which is an important result.

If the plates of the transmission line were perfect conductors ($\sigma_r = \infty$) the propagation would be governed by the skin depth of the coal δ_c. But it can be seen can see that if the walls are not perfectly conducting then the seam height $2b$ has an effect on the attenuation *and so also does the conductivity ratio*. The former effect is the central point of RIM – that a seam thinning increases the attenuation of the signal. But the latter effect could give rise to an unwanted sensitivity to non-uniformity in the roof strata. This will be greater at low frequencies because of the smaller contribution of δ_c. Equation (6.5.1-3) must be interpreted with care because of the conditions necessary for it to be a good approximation.

The above model is not complete as it does not explain how the signal arrives in the coal – and clearly no useful calculations of attenuation can be made without a knowledge of what is being attenuated. Clearly, since the signal is propagating outwards from a point source, there must be some term to demonstrate this. Equally, it is well-known that the fields close to a point-source transmitter are 'distorted' in terms of the apparent wavelength. The complete description of the transmitted wave – again, with some sensible assumptions made – is given, according to [Lagace *et al.*, 1975] by

$$\mathbf{H}_\phi = \frac{jm_d k^2}{8\left(b + \frac{1}{2}\delta_r\right)} H_1^{(2)\prime}(kr) \qquad (6.5.1\text{-}4)$$

where $\mathbf{H}_\phi$ is the transverse magnetic field, m_d is the magnetic dipole moment of the transmitter, k is the propagation constant derived above, r is the radial distance from the transmitter and H is the derivative of the Hankel function. This function is not straightforward to model in MatLab and so the graphs below compare the MatLab modelling with the graphs reproduced in [Lagace *et al.*, 1975].

In the graphs of Figure 6.5.1–5 below, the circles are points measured on Lagace's published graphs; the joined black dots are points from the MatLab calculation, for which there is a close agreement. Lagace considered a 2 m seam with $\sigma_c = 140$ μS/m and $\sigma_r = 1$ S/m. On the same Figure are three graphs relating to Daw Mill; a 7 m seam with $\sigma_c = 5$ mS/m and $\sigma_r = 150$ mS/m. The attenuation is vastly larger – even at 2 kHz, but these graphs all use Lagace's 0.7 Am^2 antenna, which is very small.

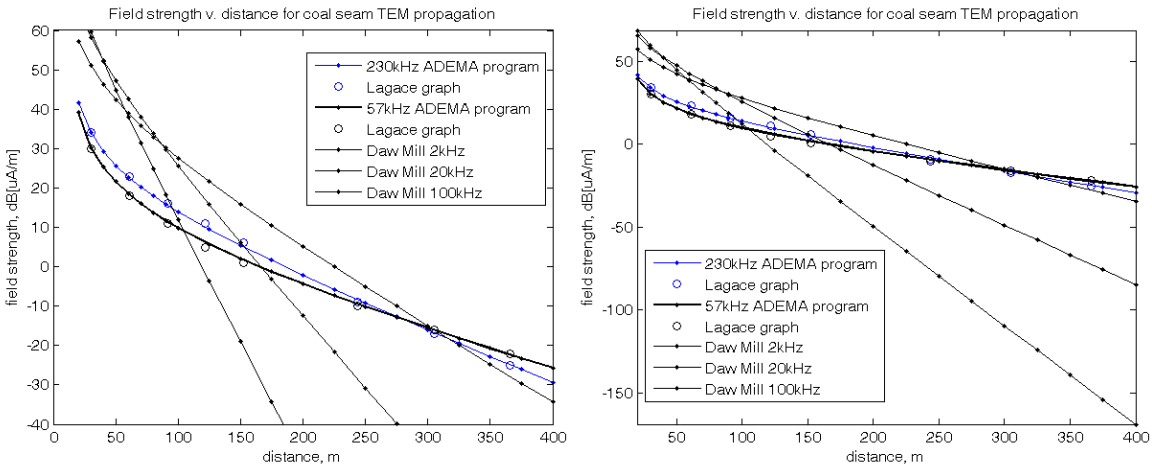

Figure 6.5.1–5 : Field strength v. distance; analytical model of TEM propagation
These graphs compare the results of a MatLab model with the data given in [Lagace et al.*, 1975].*

The graphs in Figure 6.5.1–5 show magnetic signal strength. However, for an induction loop system it is also relevant to look at induced signal, which increases with frequency. *Figure 6.5.1–6*, below left, assumes a receiver loop of diameter 1 m with 100 turns of wire. It also assumes a magnetic moment of 70 Am^2 for ADEMA's experiments. A further refinement would be to look at signal/noise ratio. But if it is assumed – as Lagace suggests – that the mine noise varies as $1/f$ then there is no net effect if an induction loop antenna is used.

For the situation where the signal is injected via electrodes, a simplification assumes that the model is that of a lossy transmission line with a 30 V source. A graph showing only the transmission line attenuation is given in *Figure 6.5.1–7*, below right. For example, if a signal of 30 V is injected and there is an attenuation of 180 dB, the receiver signal would be 30 nV.

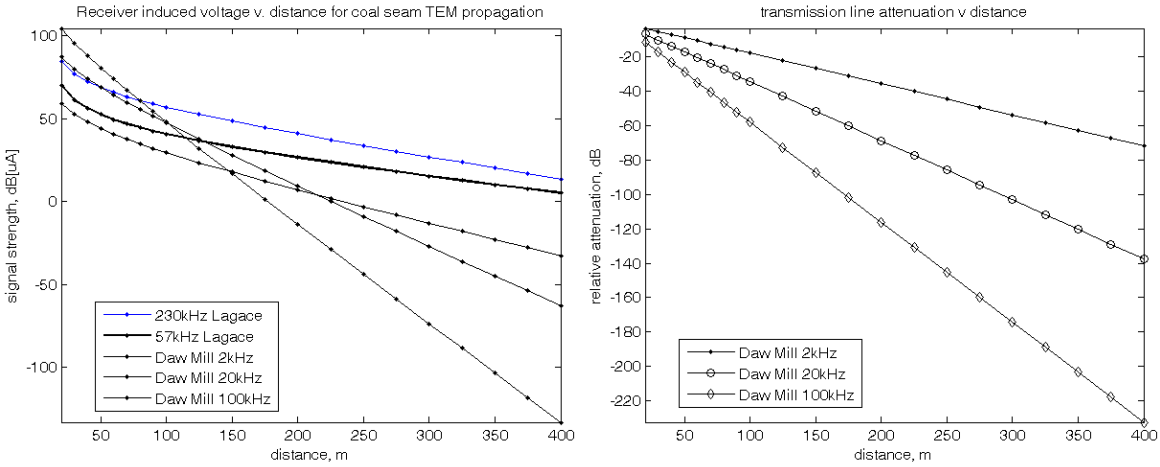

Figure 6.5.1–6 : Induced voltage v. distance; analytical model of TEM propagation

Figure 6.5.1–7 : Attenuation v. distance; current-injected TEM mode
Left: induced voltage in a receiver loop due to an induction loop transmitter. The model allows for the coupling into the system. Right: the attenuation due to a directly injected signal.

6.5.2 Appendices to Task 5.2

6.5.2.1 A Conductive Pad J-field Antenna

This appendix describes current injection antennas in further detail, and should be read in the context of the corresponding section of the main report.

The use of disposable plastic electrodes is described in the annex, *Electrodes for Resistivity Tomography in Coal Mines*. For field tests of this technique it was considered to be convenient to use drilled holes for electrodes. Additionally, there may be difficulty in ensuring good electrical conduction to the walls of the drilled hole unless a conductive grout were used. For these reasons, and also to allow rapid deployment of a RIM surveying tool, the use of compressible foam pads was investigated as a means of coupling the signal without requiring holes to be drilled for electrodes.

Vermason (**vermason.co.uk**) are manufacturers of conductive cushioning foam used for the transport of electronic devices. One of their products is a polyurethane foam impregnated with rigid conductive latex. It has a volume resistivity of 250 Ωm and a compression deflection (at 50% compression) of 3.3 kPa. A 300 mm square of such material will, if it is 100 mm thick, have a resistance across the faces of 280 Ω. To compress this to 50 mm will require a force of 300 N, corresponding to a gravity-assisted mass of 30 kg. Clearly, the resistance is inversely proportional to the *square* of the compressed thickness – a force of 600 N will compress it to 50 mm thickness and a resistance of 70 Ω. The capacitive reactance across the faces of the material is negligible.

The resistance of the compressed foam must now be compared with the resistance of the coal. For this, it can be noted that the electrode resistance between buried hemispheres of radius a is $1/\pi\sigma a$. It might be supposed that a disc-like surface electrode would have a roughly similar resistance which, for coal of conductivity $\sigma = 5$ mS/m and for a disc of radius $a = 150$ mm, suggests a resistance of around 420 Ω. ([Williams, 1951] calculates the resistance between two flat discs placed on a conducting half-space to be $1/4\sigma a$. The formula for a hemisphere was used in calculations; the difference is not significant).

The foam resistance of $2 \times 70\Omega$ (two electrodes) will therefore account for around 25% of the power dissipation. For rods that approximate to an ellipsoid in section, a becomes $\ell/\ln(4\ell/d)$, so a cylindrical rod of length $\ell = 900$ mm and diameter $d = 9$ mm would result in a similar resistance.

The conclusion to be drawn is that a modest size of conductive pad and a modest size of electrode have a similar resistance, which is only a small fraction of the resistance of the coal. However, it should be noted that since the circuit has a resistance of around 560 Ω then a driving current of, say, 40 mA would require a voltage of 22 V and would draw around 1 W of power.

Whilst it is recognised that such a device might not meet intrinsic safety requirements, equipment trials are possible in accordance with regulation 19(2) (g) of the UK's Electricity at Work Regulations 1989, which allows non-certified, non-approved electrical apparatus to be used underground in a coal mine under certain conditions (commonly referred to as 'Manager's Rules'). Furthermore, the important observation can be made that it is not the actual current, or power that is important, but the signal to noise ratio. With advanced signal processing resulting in a processing gain of, say, 20 dB, the power requirement could be reduced from (say) 1 W to 10 mW and the voltage from (say) 22 V to only 2 V.

The driving requirements could be eased by using a larger conductive pad, although the force needed to compress a large pad might be difficult to achieve without mechanical assistance. Conversely, for a smaller pad, the increased resistance reduces the dipole moment obtainable for a given driving voltage. The salient point is that the power needed to achieve a certain dipole moment depends on the size of the electrodes. It is not possible to relate the transmitter output power to the dipole moment in any meaningful way and it is therefore wrong to discuss such a system in terms of power dissipation.

Clearly, for a given antenna, the more power that can be provided the better. However, it can be seen that it is difficult to inject a large amount of power without requiring either a large driving voltage or a large electrode. Rather than demonstrating a problem with this type of antenna, this is actually a demonstration of the efficiency of such a system compared with electric and magnetic dipole systems – that is, it requires only a low amount of power to achieve an adequate signal. This is also a manifestation of common sense – that the best way to inject a signal into the coal is to place it there directly, rather than to have to couple it inductively or electrostatically.

6.5.2.2 A Novel Ceramic Tile Antenna

Introduction

This appendix describes the principles of a ceramic tile antenna in further detail, and should be read in the context of the corresponding section of the main report.

It has been noted that [Wait, 1995 a; b] had observed that there were advantages to using a vertical electric dipole for geophysical measurements. This observation was supported by an analysis of thin-layer propagation in [Delogne, 1982]. The advantage of an *E*-field antenna – in addition to the significant point put forward by Wait – is the possibility of a greater specific length (i.e. the dipole moment obtained for a given power dissipation and mass of material) than a loop antenna. This is due to the absence of a multi-turn winding with its potentially severe skin and proximity effects and inter-winding capacitance. The analysis undertaken revealed that, following a similar line of argument to that used with induction loop antennas, the performance of the dielectric disc antenna depends on the mass of the dielectric and not on the area of the plates or their separation. These are mere 'operational' constraints that govern the voltage and current that might be required.

Derivation of a Figure of Merit

The electric dipole moment of a linear wire antenna can be expressed as the product of the current and the length, $p_d = I\,\ell$. Obviously it is impractical to use a long wire antenna but, just as a magnetic loop antenna may be transformed into a solenoid filled with a material of high magnetic permeability, so may a long wire be transformed into a pair of discs separated by a material with a high permittivity. In this situation the capacitance of the antenna is more easily calculable than for a wire dipole and the dipole moment can be derived in terms of frequency, permittivity, radius and voltage to be

$$p_d = \omega\varepsilon \cdot \pi r^2 \cdot U \qquad (6.5.2\text{-}1)$$

There are some important observations to make regarding this result. Firstly, the dipole moment depends on the area of the plates, but not on their separation. (The separation affects the current that is necessary to sustain the voltage in the above formula). Secondly, there is a trade-off of permittivity against voltage. (If an air dielectric would require 1000 V across the plates, a dielectric with $\varepsilon_r = 200$ would require only 5 V).

Recalling that the magnetic moment m_d of an air-cored magnetic loop antenna can be expressed in terms of its specific aperture Φ_m and the power dissipation P in its winding, as

$$m_d = \Phi_m \sqrt{P} \ , \text{ with } \Phi_m = \tfrac{1}{2} a \sqrt{M \frac{\sigma}{\rho}} \qquad (6.5.2\text{-}2)$$

(where a is the radius of the loop, σ is the conductivity of the wire and ρ is the mass density of the wire) this can be compared with an expression – assumed to be novel – for the electric dipole moment of a dielectric disc antenna, which, in terms of its *specific length* Φ_e, is

$$m_d = \Phi_e \sqrt{P} \ , \text{ with } \Phi_e = \sqrt{M \frac{\sigma_d}{\rho}} \ , \text{ with } \sigma_d = \frac{\omega\varepsilon}{d} \qquad (6.5.2\text{-}3)$$

(For which σ_d now represents a property of the dielectric rather than the metal wires comprising the antenna and there is, of course, the implicit assumption that the dielectric loss exceeds the copper loss). Here, d is the dissipation or loss factor of the dielectric, ω is the angular frequency and ε is the permittivity of the dielectric. Some further significant observations can now be made.

The performance of the antenna depends on the ratio $\varepsilon_r/\rho d$. For most common materials, this is quite low e.g. for polyethylene (with $\varepsilon_r = 2.3$, $d = 2\times10^{-4}$, $\rho = 1000$ kg/m^3) it is 12 m^2/kgΩ. However, with specialised ceramics the Figure may rise to 300.

Following a similar line of argument to that used with induction loop antennas, the performance of the dielectric disc antenna depends on the mass of the dielectric and not on the area of the plates or their separation. These are 'operational' constraints that govern the voltage and current that might be required.

Whilst the Q-factor of an air-cored induction loop is proportional to Φ^2 / a^3, the Q-factor of a dielectric disc is simply $1/ d$ and can easily be very high.

A Practical Design

From the assumption that the mass is the limiting factor, an experimental dielectric disc antenna requires finding a material with the highest possible ratio $\varepsilon_r / \rho d$ where ρ is the mass density and d is the loss factor of the dielectric. The first candidate to eliminate is, of course, air. For air, the ratio ε_r / ρ is only about 0.8 kg/m^3, but the loss factor is essentially zero, making σ_d infinite. The reasons that air cannot be used as the dielectric are that

- the low capacitance would require too high a voltage for safety,
- the low capacitance would mean that stray capacitance would have a large effect on performance,
- the construction would require metal plates in order for it to be self-supporting, so the mass would be high.

The design is therefore constrained to using solid dielectrics that will allow the use of thin metal foil electrodes and that have a 'reasonable' permittivity, to keep the voltage low. Unfortunately, most substances only have a low permittivity and a moderate dissipation factor. Polyethylene, for example, has $\varepsilon_r \approx 2.3$ and $d \approx 0.0002$, giving rise to an $\varepsilon_r / \rho d$ Figure of just 12.

A supposedly-readily-available material with a somewhat better performance is high-purity alumina (aluminium oxide) which is manufactured in the form of ceramic tiles for a number of engineering applications. For a very high-purity material, ε_r approaches 10 and d can be as low as 0.0001. With a specific gravity of about 3.9 the Figure of merit $\varepsilon_r / \rho d$ is about 25.

Materials used for making capacitors can achieve still-higher Figures of merit – capacitors using barium strontium titanate can achieve a Figure of 300 from $\varepsilon_r = 2500$, $d = 0.0015$ and $\rho = 5550$ kg/m^3. Research materials with an even higher permittivity exist, but these tend also to have a higher loss factor and so the overall Figure of merit tends to be only 100 or lower.

Arrangements were made with a manufacturer of ceramic capacitors to supply 16 tiles, 4 mm × 50 mm × 50 mm, of a high-permittivity $Ba_{1-x}Sr_xTiO_3$ perovskite ceramic. The total mass was about 1 kg and the tiles were constructed with top and bottom metallisation. The individual tiles can be connected in a number of ways including a conventional multi-layer configuration and a series connection, without affecting the specific length of the antenna (i.e. the moment produced for a given power dissipation). For a series connection, the metallisation serves to steer the field along the column of tiles and thereby reduce the severity of the edge effects.

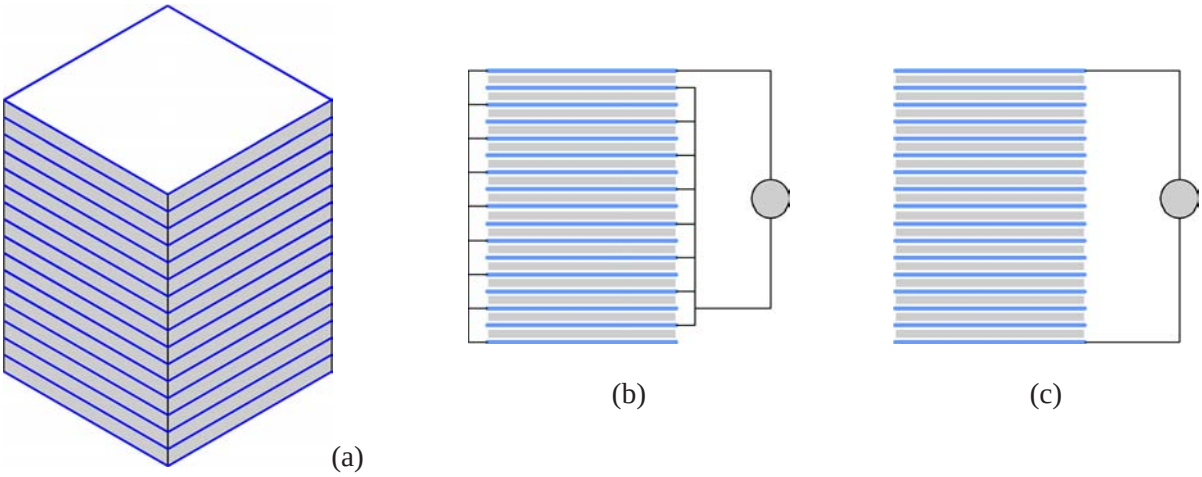

Figure 6.5.2–1 : A multi-layer capacitor formed from ceramic tiles
(a) isometric view of 16 tiles; (b) schematic showing connections for multi-layer device;
(c) schematic connections for single-layer device showing metallisation that reduces edge effects

The intended power dissipation of this device was 1 W, resulting in an electric dipole moment of around 40 mAm (see *Table* below). This figure is relatively low but the inherent losses in a magnetic loop antenna (skin and proximity effects) give support to the assertion suggest that an *E*-field antenna will demonstrate some merit.

Design Parameters			**Performance**						
Dielectric density	***5550***	kg/m^3	Effective tiles		***1***	***4***	***8***	***16***	
Dissipation factor	***1.50E-03***		Tile thickness		72.1	18.0	9.0	4.5	mm
Rel. Permittivity	***2500***		Capacitance		0.8	12.3	49.1	196	nF
Dielectric mass	***1***	kg	Reactive current		0.6	2.3	4.5	9.1	A
Frequency	***100***	kHz	Reactive voltage		1176	294	147	73	V
Design power dissipation	***1***	W	Current at parallel resonance		0.9	3.4	6.8	13.6	mA
Reactive power figure	667	VA	Voltage at series resonance		1.76	0.44	0.22	0.11	V
Energy storage	0.53	mJ							
Specific length	0.041	m/√Ω							
Dipole moment	40.9	mAm							

Table 6.5.2–1 : Parameters for a ceramic tile antenna
*The design parameters are indicated in **blue-bold italic** and the resulting outputs from the spreadsheet are indicated in unembellished typescript*

6.5.3 Appendices to Task 5.5

6.5.3.1 Experimental Equipment

This appendix describes some items of experimental equipment in further detail, and should be read in the context of the corresponding section of the main report.

Several items of experimental equipment were constructed for laboratory-based tests, and some items were submitted to a UK company, Health, Safety and Engineering Consultants Limited (HSEC), for inspection prior to being used underground. However, as noted above, the restrictions on the use of non-approved equipment still caused considerable difficulties. During initial experiments in Daw Mill colliery, for example, it was not possible to locate exposed areas of coal where the conductive pad electrodes could be properly deployed. Additionally, none of the areas of the mine where regulations allowed deployment of the equipment were close to the coalface and access to the return roadway was similarly restricted. Although initial experiments were undertaken, such were the difficulties in gaining access to appropriate test areas underground that several tests could not be undertaken. It was the considered view that obtaining detailed practical results would require a significant additional amount of design work that was not envisaged at the outset of the project. There are perhaps two possibilities for resolving this problem in future projects, namely (i) extending the project support period to allow equipment to be I.S. certified or otherwise approved for use, and (ii) identifying at a

European level whether there are underground test mine facilities which might lend themselves to experimentation purposes, including providing access for non-approved apparatus to workings that are the equivalent of a modern coalface.

The equipment that was built included...

1. A low-power transmitter for initial experiments with wideband sounding sequences. This was based around a microprocessor and an H-bridge driver using MOSFET transistors.
2. A data-capture module suitable for sampling the received signal, and a mass-storage device capable of storing 30 M samples at a sustained rate of 1 M sample/second. Initially this was based around a PIC18F8720 microprocessor, from **microchip.com**. For convenience, this device was used on a demonstration board supplied by Microchip. However, problems with data throughput meant that for initial field tests it was decided to use a data logger module from Measurement Computing (type USB-1616HS). A separate front-end differential amplifier and 12th-order Butterworth anti-aliasing filter were used. This approach required a separate ruggedised laptop to collect the data, and so would be unsuitable for full field implementation.
3. Loop antennas constructed from computer ribbon cable.
4. Conductive foam pad electrodes comprising a 40 mm layer of conductive foam, a copper foil bleed wire and a backing board made from medium density fibreboard (MDF).
5. A ceramic disc antenna was constructed from the 16 tiles that were specially manufactured. This was used for laboratory measurements in an un-tuned and tuned configuration.

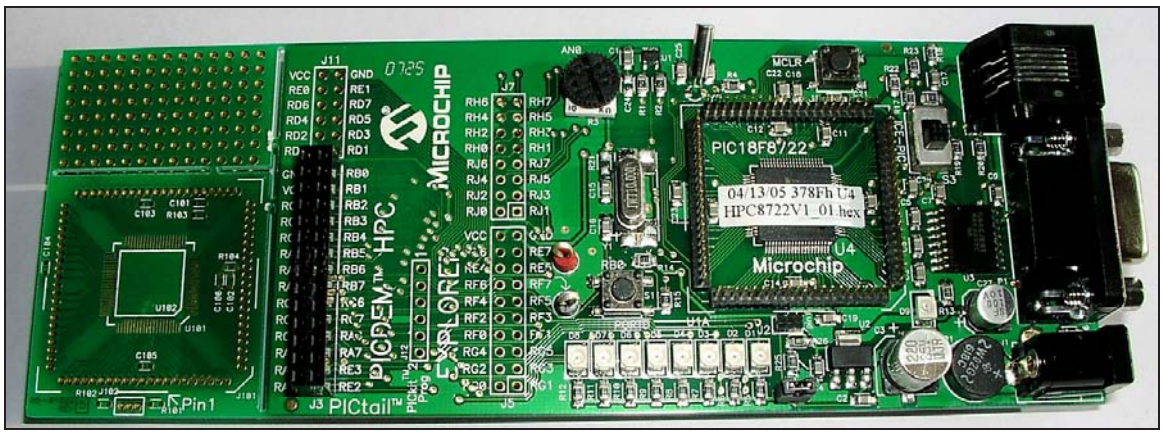

Figure 6.5.3–1 : Demo board for the PIC18 F8722
Used for laboratory experiments with data capture

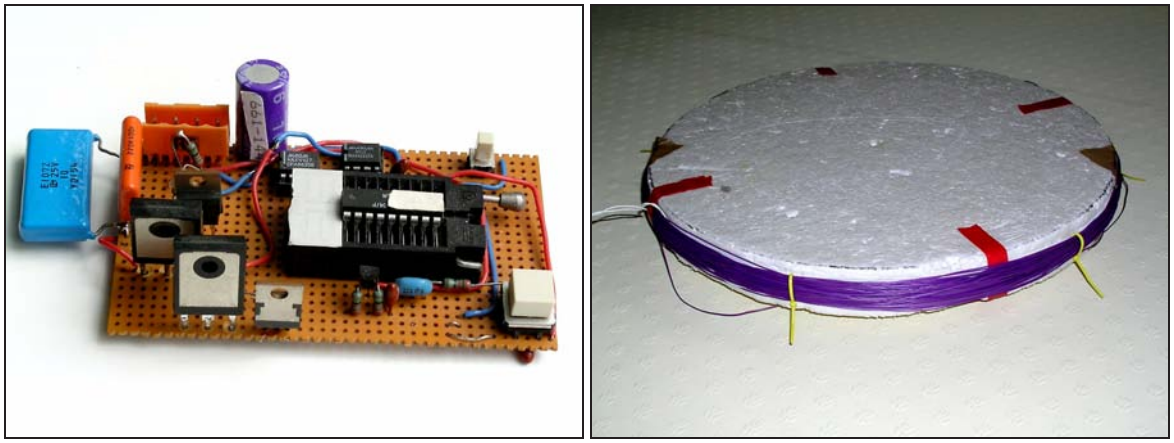

Figure 6.5.3–2 : Experimental wideband digital transmitter and untuned loop antenna

Figure 6.5.3–3 : Experimental data-capture module and ruggedised laptop computer

6.5.3.2 Electrodes for Resistivity Tomography in Coal Mines

This appendix describes the use of ERT electrodes in further detail, and should be read in the context of the corresponding section of the main report.

A study into the feasibility of using an array of ERT electrodes resulted in a patent application, of which the essential details are summarised below.

One significant problem with the RIM method of imaging the geological structure of the coal panel is the need to avoid spurious signals by disconnecting or removing all metalwork in the vicinity of the equipment for the duration of the measurements. Other difficulties arise because of the need to synchronise the transmitter and receiver signals, and because of the time and man-power needed to undertake a surveying operation that requires the co-ordinated movement of two pieces of equipment in different areas of the mine.

These difficulties can be resolved by replacing the portable transmitter and receiver by an array of electrodes. The basis of this method is to make multiple readings of conductivity either by moving the four-electrode array or using a large array of perhaps 100 electrodes. In such a scheme, all possible pairs of electrodes may be energised in turn, and for each such instance, the potential difference between all possible combinations of the remaining electrodes may be recorded.

Instead of connecting each electrode to a multiplexer, which requires an extensive amount of cabling, state-of-the-art resistivity tomography equipment utilises a serial bus. Each electrode is attached to an addressable switch, controlled by a microprocessor, that connects it to one of the two current-injection buses or to one of the two voltage-sensing buses.

As a result of an investigation of this method, the following enhancements are proposed.

- The electrodes could be manufactured from a conductive plastic so that they could be left in position during the mining operation without causing damage to the coal cutting equipment; and so that the lightweight electrode material could be removed from the coal during the washing process.
- In a resistivity tomography system, the resolution is dependent on the electrode spacing and so it is proposed that the electrodes be positioned at distances as close as two metres. This can be contrasted with the spacing of receiver measurements in a RIM survey, which may be 15 m.
- The electrodes could form an extensive array, which might extend for many kilometres along the roadways.
- The GRP rib bolts commonly used in the UK to support the walls of the roadways on either side of the coal panel could be adapted to perform the additional function of an electrode for resistivity tomography.
- An alternative electrode could be used, comprising a flat disc placed against the coal panel and attached by means of a pin and plug. Construction using conductive plastic components will convey the same benefits outlined above. Coupling to the coal seam would be capacitive in nature.

As a consequence of the above design points, a means of disconnecting and reconnecting the addressable switches to the electrodes and the cable is required, so that it is possible to re-deploy the system at will, whilst leaving the electrodes placed in the coal seam. The design exercise has also

considered how the number of wires in the bus may be reduced; the advantages of such a system including the lower weight of cable and connectors and the lower cost of building the necessary intrinsically-safe connectors.

It will be appreciated that the large width of the coal seam imparts significant performance limitations, especially if it is desired to perform a measurement with both current-injection electrodes situated on the intake roadway and both voltage-sensing electrodes in the return roadway. An increased performance can be achieved by positioning one current injection electrode on either side of the coal panel, and one voltage sensing electrode likewise. The disadvantage of this is that the cable joining the electrodes has to traverse the coal panel. However, this cable can be routed via the district arterial roadway and permanently fixed in place.

It will also be appreciated that the signal levels are very low and so the use of long cable runs will cause problems due to electrical noise. Additionally, in general (but also specifically if the electrode contact resistance is high) the receiver measurements have to be made at a high impedance, which can also give rise to problems of electrical noise. These difficulties are exacerbated by the Intrinsic Safety requirements of a coal mine, which will limit the voltage across the driven electrodes to a far lower value that would normally be used for resistivity measurements. Ultimately, it is not the signal level that is the limiting factor, but the signal-noise ratio.

For reasons of noise immunity the voltage measurements will therefore have to take place in an extremely low bandwidth which, with a large number of electrodes, could result in a very lengthy operation. However, a significant benefit of the permanently *in situ* disposable electrodes will now be clear – namely that a lengthy tomography ‘scan’ can take place without disrupting coal production and that repeated scans may be made to further investigate an anomaly in the coal panel. Moreover, since the operation is largely automatic, it is not necessary to re-deploy personnel for such repeated scans.

It is clear that the same techniques being investigated for RIM, including signal detection using synchronous detection, spread-spectrum transmission and the use of filters based on digital signal processing techniques, can all be used to increase the signal/noise ratio of the detected voltage in an ERT system, thereby allowing it to operate in an intrinsically-safe environment.

6.6 WP6 RADIO IMAGING (TOMOGRAPHIC RECONSTRUCTION)

6.6.1 Introduction

In this research the wave propagation phenomenon of a Radio Imaging (RIM) signal through a coal seam was fully modelled to assess the effectiveness of the RIM technique for detecting flaws or anomalies in coal panels. The range of coal and shale losses (electrical conductivity) for productive use of RIM was determined. For the typical range of coal and shale conductivity encountered in European mines, the power dissipation in the coal and the shale layers has been reported. For a low loss coal mine scenario RIM signal sensing has been performed with various modelled flaws. The influence of any metalwork in the road ways of coal mine on the RIM signal distribution has also been modelled.

A novel GEM (Guided Electro Magnetic wave) technique has been developed which uses conducting boundaries along coal panel faces in the roadways to form a rectangular waveguide. The GEM principle is shown for certain modelled flaws in regular and lossless coal seams. The excitation issues for GEM are studied in detail. Typical results are presented to determine the range of electrical conductivity of the coal and shale to establish undistorted model field distribution in a coal seam for the applicability of the GEM technique. The power levels required to establish resonance for the GEM technique are reported.

6.6.2 RIM Modelling

In the modelling it is assumed that the coal seam is regularly shaped and sandwiched between layers of shale. The dimensions are considered to be those of the U.K. Daw Mill coal panel, i.e. 10 m thick × 300 m wide × 2000 m long. The shale layers are 10 m thick. The views of the coal panel, roadways, over- and under-burden shale layer arrangement in the model are illustrated in the *Figure* below.

Figure 6.6.2–1 : Coal seam model used to study RIM propagation
Left: top view, Right: isotropic view

Due to the complexity of the EM model and the limitation of available computing power the coal panel length is limited to ~667 m. It should be noted that the coal seam lengths reported for various model runs are rounded for convenience (e.g. 666.66 m is changed to 667 m), although the modelling work employed the high precision panel dimensions.

To study the effects of coal and shale losses on RIM signal propagation across the coal seam simulations were initially run for an ideal case where the coal is lossless (σ_{coal} = 0 S/m) and shale is a perfect conductor. The losses were then gradually increased by increasing coal conductivity and decreasing shale conductivity. Typical results for signal propagation for a low loss and a lossy scenario are presented in the *Figures* below.

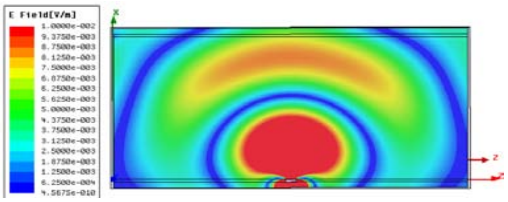

Figure 6.6.2–2 : Low loss model result for E-field distribution
Seam length 667 m (XZ plane), σ_{coal} = 10μS/m, $\varepsilon_{r\text{-}coal}$ = 10, σ_{shale} = 10 S/m, $\varepsilon_{r\text{-}shale}$= 20, 1 W input power

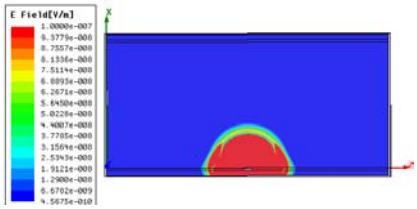

Figure 6.6.2–3 : High loss model result for E-field distribution
Seam length 667 m (XZ plane), σ_{coal} = 10 mS/m, $\varepsilon_{r\text{-}coal}$ = 10, σ_{shale} = 100 mS/m, $\varepsilon_{r\text{-}shale}$= 20, 1 W input power

In the low loss scenario much of the input EM signal/power from the transmitter propagates across the coal seam as shown in *Figure 6.6.2–2* and the EM energy leakage into the shale layers is low. The coal seam waveguide losses are increased either by an increase in the bulk electrical conductivity of the coal seam and/or by a decease in the bulk electrical conductivity of the shale. This causes a rise in the EM leakage into the shale. The required transmitter power is increased with the increase of losses in order to obtain minimum field levels across coal seam. Beyond certain levels of losses in the coal seam waveguide, the EM signal propagation across the coal seam from the RIM transmitter is distorted. The RIM signal distortion gets more serious as the coal seam waveguide losses are excessively increased, as shown in *Figure 6.6.2–3*. The distortion in the RIM signal is attributed to two factors; (1) excessive losses and attenuation in the coal and shale layers and (2) local non-modal fields stored near the excitation wave port. When more energy is transmitted (e.g., high sensitivity in *Figure 6.6.2–3*) to achieve minimum RIM signal across the coal seam in lossy scenarios, then near the excitation wave port the local source fields (non-modal stored energy fields and radiation fields) are strong enough to distort the RIM signal. In the model results it was seen that the field propagation distortion in the vicinity of the excitation wave port is aggravated owing to the increased losses in the coal and/or shale layers. The field propagation across a coal seam with typical UK coal and shale conductivity is shown in the *Figure* below.

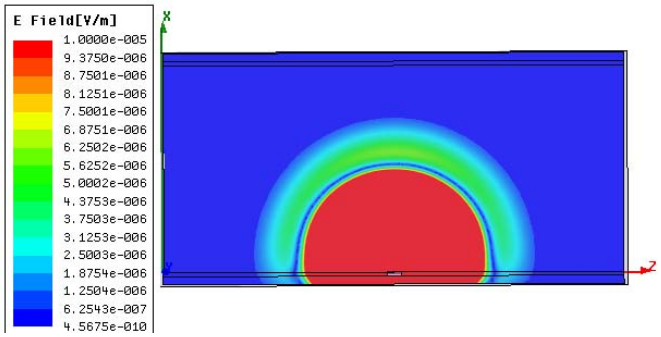

Figure 6.6.2–4 : Typical UK conductivity model result for E-field distribution
σ_{coal} = 1 mS/m, $\varepsilon_{r\text{-}coal}$ = 10, σ_{shale} = 100 mS/m, $\varepsilon_{r\text{-}shale}$= 20 and 1 W input.

By comparing the results illustrated in this *Figure* with those of *Figure 6.6.2–2*, it is evident that an increase in the bulk coal conductivity and a decrease in shale conductivity increased the attenuation of the EM signal. The change in the E-field distribution due to excessive attenuation can also be observed. The modelling results show that with realistic values (see *Table* below) of conductivity for shale and coal (e.g., U.K.), the coal seam waveguide will be very lossy and the attenuation is so high that the application of RIM technique is not feasible.

The RIM technique is applicable to low loss coal seam waveguide scenarios with a certain contrast between the bulk conductivity of coal and shale, where the losses do not introduce distortion in the RIM signal propagation across the coal panel.

Electrical Conductivity	Typical Signal Propagation Across Seam	Comments
σ_{coal} < 0.00001 S/m σ_{shale} > 5 S/m	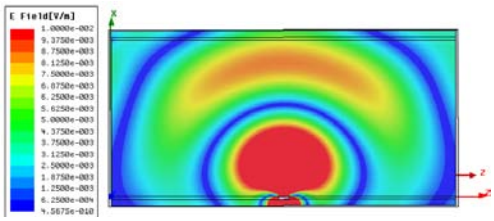	Losses in the coal and leakage into shale layers are negligible. In this scenario RIM technique is applicable.
σ_{coal} ~100 μS/m 1 S/m > σ_{shale} > 100 mS/m	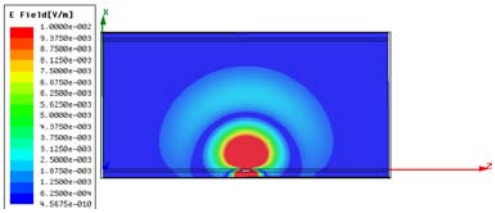	Losses in the coal and leakage into shale layers are high. Very high input power is required to establish detectable signal levels at the sensing regions. In this case RIM technique might be possible.
σ_{coal} > 1 mS/m σ_{shale} < 100 mS/m	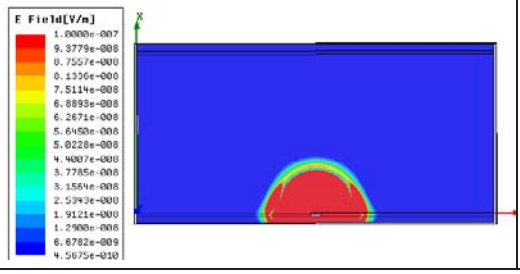	Signal distortion due to excessive losses and extremely high attenuation. An increase in the input power distorts the RIM signal due to strong local non-modal source fields. In such cases the RIM technique is not applicable.

Table 6.6.2–1 : Applicability of RIM for a range of coal and shale conductivity

In such cases, due to the presence of coal seam flaws or anomalies, the sensing signals across the seam will produce scattering signals that are amenable to analysis using inversion techniques. However in the lossy scenarios it is difficult to predict the EM propagation. Thus the RIM signal being sensed across the coal does not provide productive input to the tomographic inversion process, as the signal itself is distorted due to the losses. The range of coal and shale electrical conductivity and their implications on the RIM capability are summarised in the *Table* above.

6.6.2.1 Power Dissipation in Coal versus Shale Layers in RIM

When a coal panel waveguide 667 m long × 300 m wide × 6 m high is excited with 1 W input, the resultant power distribution between the coal panel and shale layers is as presented in the *Table* below as a function of coal and shale conductivity. Even when the excitation wave port is in contact with the coal seam, the net forward power flow into the coal seam is only 3% to 5% of the input power.

Coal / Shale Bulk Conductivity in S/m		Net Power Flow (+X direction) into the Coal Seam from Wave Port in mW	Power Flow into the Shale in mW		
Coal	Shale		Top Shale (+Y direction)	Bottom Shale (-Y direction)	Total Power Flow into Shale
0.00001	1.0	21.80	5.45	5.22	10.67
0.0001	0.1	27.35	9.27	9.27	18.54
0.001	0.1	55.38	10.20	10.00	20.20
0.01	0.1	233.3	13.37	13.13	26.50

Table 6.6.2–2 : Power levels in coal and shale for various bulk conductivity combinations

In a coal seam waveguide with realistic values of conductivity for shale and coal (e.g., in U.K.) as shown in the above *Table*, about 37% to 67% of the net power entered into the coal seam escapes into the shale layers. However due to further losses in the shale layers the field levels in the shale layers are many orders less than that in the coal seam.

6.6.2.2 Sensing the RIM Signal across Coal Seam

A number of simulations were performed with a variety of different model flaws (size, shape and locations) in the coal seam. The coal panel dimensions were 667 m length × 300 m width × 6 m height and shale layers are 10 m thick and sandwich the coal. The model flaws as considered to be shale material with σ_{shale} = 100 mS/m. When the bulk conductivity of coal and shale are 100 μS/m and 100 mS/m respectively, the results demonstrated that the RIM technique provides productive sensing data across coal seam.

6.6.2.3 Influence of Conducting Side Walls in Roadways

As a generalisation, there can be significant use of steel mesh to contain spalling from the rib-side walls of coal seam roadways. Even if the coal seam waveguide is considered as lossless, the introduction of any metal work or conducting boundaries on the coal seam lateral faces (front, back, and side) induces distortion in the EM signal propagation across the seam. Model results for field propagation across a coal panel from a transmitter in a lossless coal seam waveguide for two different cases (1) Presence of metal work at Z = 0 m (Face A in *Figure 6.6.2–1*) and Z = 667 m (Face C in that figure) and (2) metal work at Z = 0 m (Face A) and Z = 667 m (Face C) and X = 300 m (Face D) are shown in the two *Figures* that follow.

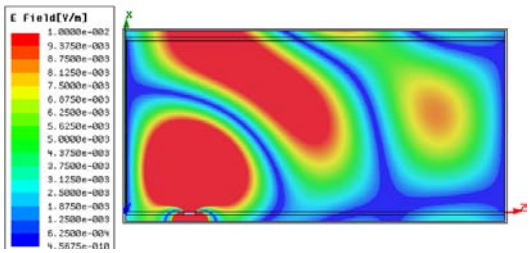

Figure 6.6.2–5 : E-field distribution in lossless seam (example i)
Metalwork at Z = 0 m and Z = 667 m

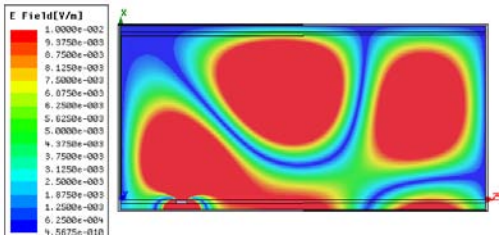

Figure 6.6.2–6 : E-field distribution in lossless seam (example ii)
Metalwork at Z = 0 m, Z = 667 m and Z = 300 m

Comparison of the two *Figures* above with the results shown in *Figure 6.6.2–2* illustrates the effect of the metal work presence on the field propagation from the transmitter across the coal panel. In the real mine situations the coal seam / shale layers are lossy and therefore the distortion in the EM signal is much more complex. If the side walls in the road ways are even remotely electrically conducting the direct propagation of RIM signal across the width of coal seam may no longer be possible. The amount of distortion in the EM signal is dependent on the conductivity, size and locations of the metal work in the mine.

6.6.3 A Novel Technique Using Guided Electromagnetic Waves (GEM)

A novel alternative to RIM for coal seam imaging known as GEM (Guided Electromagnetic Wave) was proposed. In comparison to RIM, GEM uses an identical deployment strategy except for three important factors. First, the GEM technique uses conducting boundaries along coal panel faces in the roadways to form a rectangular waveguide. Second, in GEM the transmitter will be inserted into the coal seam, to give maximum coupling and hence power input to the waveguide. Third, GEM does not necessarily operate at any ‘standard’ transmitter frequency; rather it sweeps the input frequency until the waveguide is set into a resonance mode.

A 2D schematic of the GEM technique is depicted in the *Figure* below, where a number of possible modes are set up in the waveguide. Each mode is a direct function of the waveguide dimensions. The coal seam is continuously excited with a loop antenna embedded into the coal seam to enforce a fundamental TE_{10} mode (the easiest) to be set up in the coal seam. As the GEM resonance frequency(s) are related to coal seam dimensions, any discontinuity (fault or roof/floor material

ingress into the seam) will change the expected resonance frequency and will thus pre-warn that a fault exists in the seam.

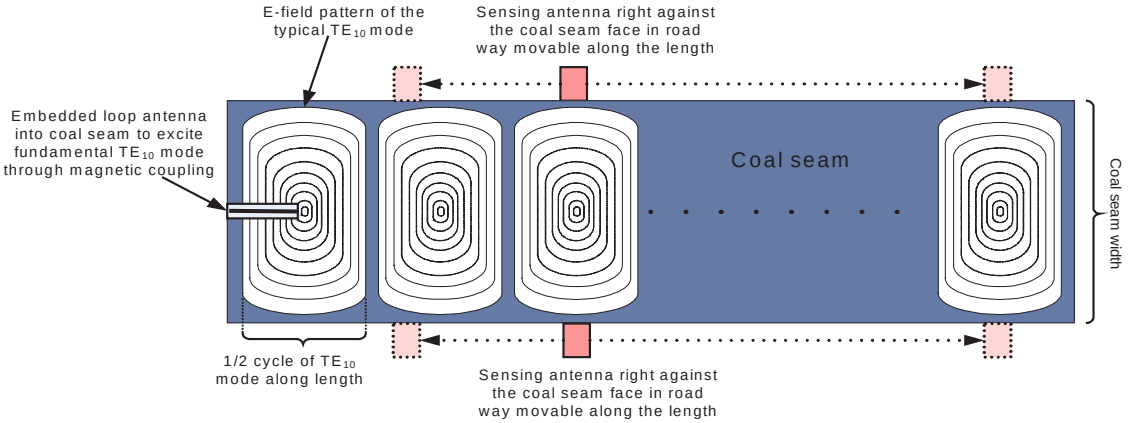

Figure 6.6.3–1 : Schematic of the proposed GEM (guided electromagnetic wave) technique

With further analysis of the EM field of the resonance modes in the coal seam and the use of the standard tomographic image construction algorithms the information (electrical nature, size, shape, location) of the anomalies in the coal seam can be obtained.

6.6.3.1 GEM Principle Demonstration by Modelling

The GEM technique has been modelled to determine its ability to detect the presence of anomalies in a coal seam. In the simplest case the coal seam was considered to be lossless and bounded by perfectly conducting shale. For computational simplicity the coal panel of 1333 m long (Δz) and the other two dimensions are the same as those of the coal panel at Daw Mill [300 m wide (Δx) × 6 m high (Δy)]. The conducting shale layers are modelled as conducting boundaries. For the regularly shaped lossless coal seam, the simulated results for scattering parameter 'S_{11}' versus frequency and the E-field (magnitude) of the TE_{10} mode in coal seam are shown in the *Figure* below.

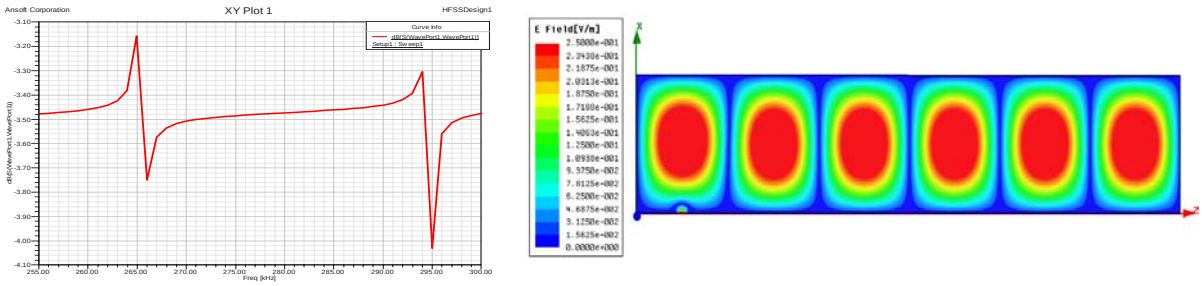

Figure 6.6.3–2 : Model result for scattering parameter 'S_{11}' versus frequency and E-field
This is for the TE_{10} mode in a uniform lossless coal seam 300 m wide × 6 m high × 1333 m long bounded by perfect conducting shale

Various model flaws were then introduced into the regular lossless coal seam to demonstrate the GEM principle. The results for the field distribution and scattering parameter S_{11} versus frequency at the feed port are presented for certain model flaws in a lossless coal seam; (a) a shale finger 300 m wide (Δx) × 3 m long (Δz) between shale layers at Z = 700 m (b) shale flaw 150 m wide (Δx) × 6 m thick (Δy) × 5 m long (Δz) at Z = 556 m, Y = 0 m and X = 0 m in the coal seam and (c) 150 m wide (Δx) × 6 m high (Δy) × 5 m long (Δz) at X = 25 m, Y = 0 m and Z = 556 m in the three *Figures* that follow. In all models the flaw material is assumed as shale with σ_{shale} = 10 mS/m and $\varepsilon_{r\ shale}$ = 20.

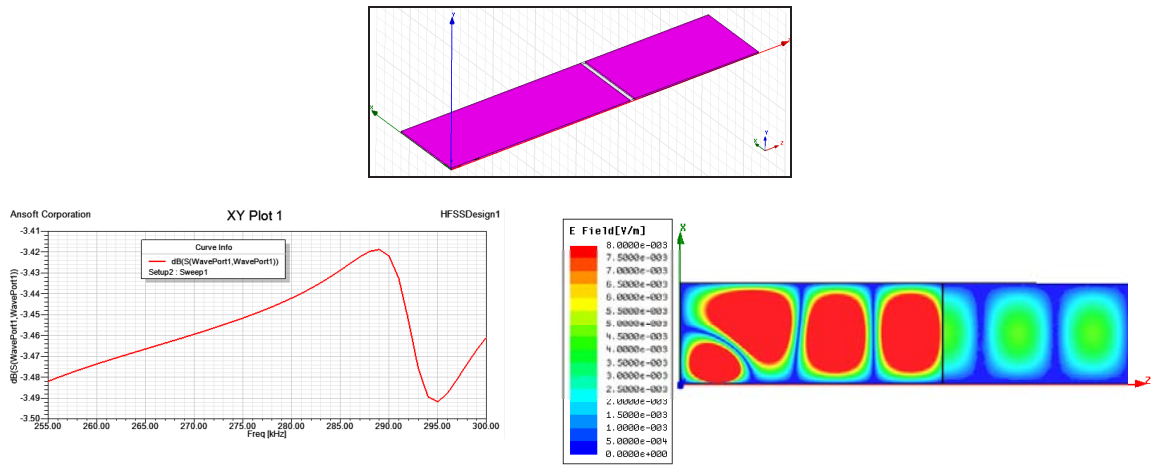

Figure 6.6.3–3 : Modelling of shale finger (example i)
Shale finger 300 m wide × 6 m thick × 3 m long at Z = 778 m
Top: Geometrical arrangement, Bottom-left: resulting scattering parameter 'S$_{11}$' versus frequency, Bottom-right: E-field of TE$_{10}$ mode in coal panel

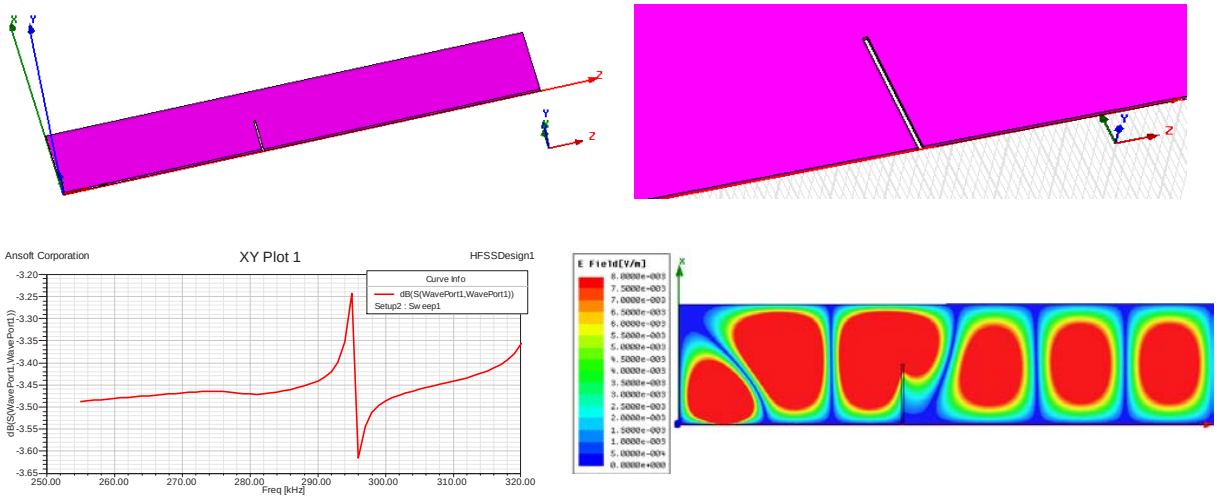

Figure 6.6.3–4 : Modelling of shale finger (example ii)
Shale finger 150 m wide × 6 m thick × 5 m long at Z = 556 m, Y = 0 m and X = 0 m
Top: Geometrical arrangement, Bottom-left: Resulting scattering parameter 'S$_{11}$' versus frequency, Bottom-right: E-field of TE$_{10}$ mode in coal panel

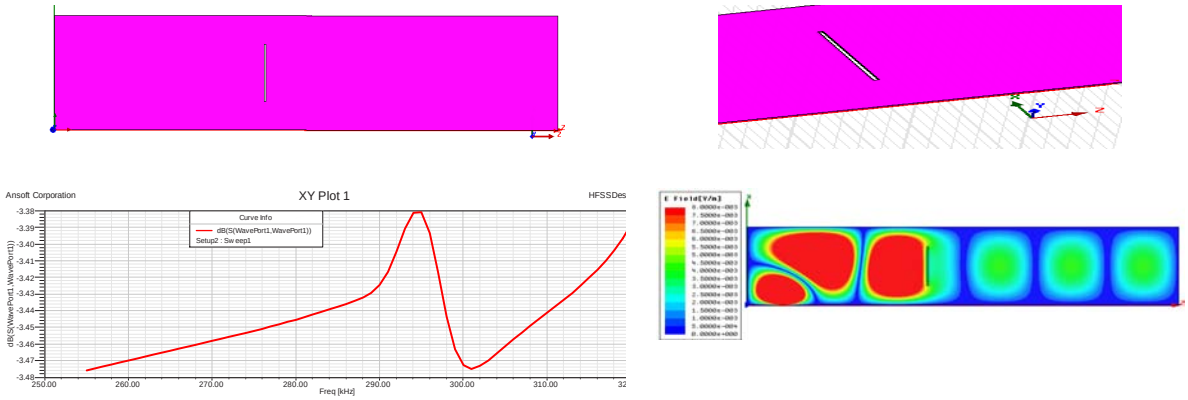

Figure 6.6.3–5 : Modelling of shale finger (example iii)
Shale finger 150 m wide × 6 m thick × 5 m long at x = 25 m, y = 0 m and z = 556 m
Top: Geometrical arrangement, Bottom-right: Resulting scattering parameter 'S$_{11}$' versus frequency, Bottom-right: the E-field of TE$_{10}$ mode in coal panel

The initial results with various modelled flaws demonstrated that each different flaw in the lossless uniform coal seam introduced a unique change in the resonant response and the modal (TE_{10} mode) field in the coal seam. The deviation in the resonance frequency of the mode indicates the irregularity or presence of flaws in the coal seam. By sensing model field distribution in the coal seam and using standard tomographic algorithms the information of flaw type, location and shape can be obtained.

6.6.3.2 Coal-seam Waveguide Excitation Investigation for GEM

The excitation issues for GEM, such as excitation from the bottom of the coal seam, adjacent excitation, the influence of the location of excitation port to signal levels along the coal panel length, coupling slot orientation, side wall conductivity, shale conductivity and shale relative permittivity were all studied in detail.

It was determined that the coal seam waveguide can be excited through magnetic coupling either from the bottom or adjacent to the coal seam. With seam losses there is a demand for more input power in order to overcome the attenuation and achieve adequate field levels for detection. Moreover, an increase in the excitation power also increases the distortion region due to the enhanced non-modal field strength near the excitation source. However it was apparent that the local distortion region due to the source is sensitive to the location of excitation port to a certain extent, see *Figure* below.

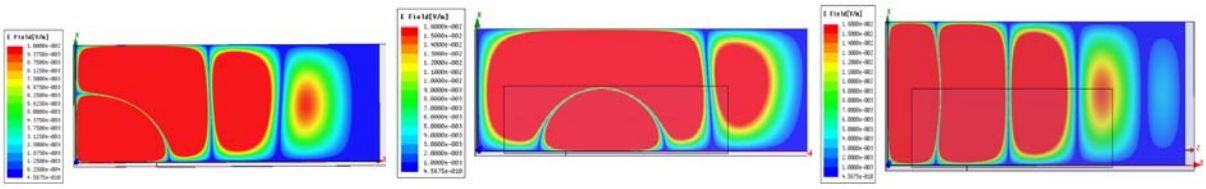

Figure 6.6.3–6 : Modelling of excitation slot
E-field of TE_{10} mode in panel with excitation slot in middle of the seam thickness
Left: at X = 0 m and Z=111 m, Centre: at X = 0 and Z = 333 m, Right: at X = 150 m and Z = 0 m

There is a 'GEM operating window' along the length of the coal seam beyond the region of the local source distortion but prior to the point where the GEM signal is swamped by noise. This is the length along the coal seam where the GEM signal is available for the tomographic reconstruction to find the presence of anomalies in the coal. This GEM operating window can be moved along the coal panel length by repositioning the location of the transmitter and/or its power level.

The model results confirm that the EM coupling is a maximum when the excitation port orientation is horizontal and negligible when the port orientation is vertical. The modelling results also confirm that with coal conductivity $\sigma_{coal} = 1$ mS/m and shale conductivity in the range $10\ \text{mS/m} \leq \sigma_{shale} \leq 100$ mS/m, the TE_{10} modal fields in the coal panel are not particularly sensitive to the conductivity in the range $1.03\times10^7\ \text{S/m} \leq \sigma_{sidewall} \leq 5.8\times10^7$ S/m of the roadway metal supports which form the electromagnetic wave boundaries at the edges of the panel.

The modelling results demonstrate that, at a given coal conductivity, the increases in shale conductivity improves the modal field strength in the coal seam due to decreased EM energy leakage into the shale layers. In the GEM modelling, when the coal conductivity is $\sigma_{coal} = 1$ mS/m and $\varepsilon_{r\text{-}coal} = 10$, and shale conductivity is in the range of $10\ \text{mS/m} \leq \sigma_{shale} \leq 100$ mS/m, the change in shale permittivity in the range $1 \leq \varepsilon_r \leq 40$ does not have any noticeable influence on the modal field in the coal panel.

The practical design issues regards the loop antenna required for GEM excitation were also investigated and the design relationship with respect to wavelengths in the coal and field mode cut-off wavelengths were established.

6.6.3.3 Operating Condition to Set up Resonant Modes for GEM

In this section we illustrate the modelling results used to determine the ranges of the electrical conductivity of the coal and the associated shale strata to establish undistorted model field distribution

in a coal seam. Simulations are performed using a 300 m width × 6 m thick coal seam as a function of coal conductivity (σ_{coal} = 10 nS/m to σ_{coal} = 1 mS/m and $\varepsilon_{r\text{-}coal}$ =10) with shale conductivity as parameter σ_{shale} = 10 S/m, 5 S/m, 1 S/m, 100 mS/m, 10 mS/m and $\varepsilon_{r\text{-}shale}$ = 20). The length of the coal panel was varied from 222 m to 888 m and side faces of coal seam are assumed as conductive with $\sigma_{coal} = 1.03\times10^{7}$ S/m to represent steel support structures. The excitation slot dimensions are 10 m long × 1 m high located at the coal panel face at X = 0 in the middle its thickness, with 1 kW input power. A few typical results for the E-field distribution of TE_{10} mode in the coal seam have been presented with various coal and shale conductivity in the four *Figures* that follow.

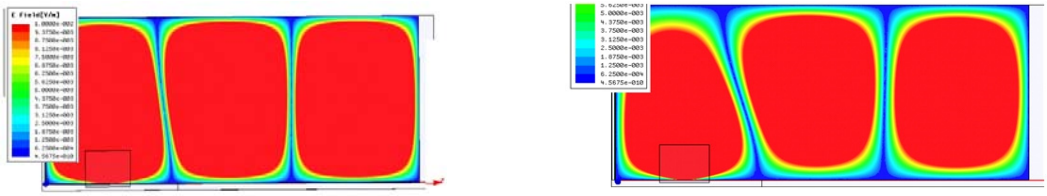

Figure 6.6.3–7 : E-field distribution, for various coal and shale conductivity (example i)
E_y- field distribution in seam when σ_{shale} = 10 S/m and $\varepsilon_{r\text{-}shale}$ = 20 with $\varepsilon_{r\text{-}coal}$ = 10
Left: σ_{coal} = 1μS/m, Right: σ_{coal} = 10μS/m

The distortion of the pattern close to the wave-portion in *Figure 6.6.3–7* is caused by the direct radiation fields and the reactive stored energy (near) fields of the port. For a low-loss waveguide the power required to strongly excite the mode is very small and hence the port local fields are weak by comparison with the modal fields, except very close to the port.

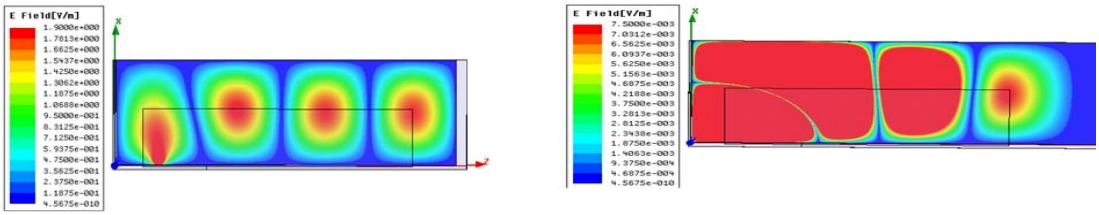

Figure 6.6.3–8 : E-field distribution, for various coal and shale conductivity (example ii)
E_y- field distribution in seam when σ_{shale} = 5 S/m and $\varepsilon_{r\text{-}shale}$ = 20 with $\varepsilon_{r\text{-}coal}$ = 10
Left: σ_{coal} = 1μS/m, Right: σ_{coal} = 100μS/m

In *Figure 6.6.3–8* (right), the material forming the panel displays a tan$\delta \approx 1$ and a rapid rate of field attenuation is evident. Even when the wave propagating medium is only slightly lossy (σ_{coal} > 100μS/m) (U.K. coal is usually much lossier than this) significant power is required at the source to establish and sustain the waveguide mode at any significant distance from the source. Power is now disappearing into the coal as resistive heating and the coupling to the TE_{10} mode is greatly weakened. For high input power, the directly radiating (non-modal) and stored energy fields near the source are more dominant than in *Figure 6.6.3–7* because of the high power level needed to excite the mode in the guide. In this x-z plane field presentation, if the field sensitivity scaling were set at the same level as *Figure 6.6.3–7*, the right hand lobe in *Figure 6.6.3–8* (right) would no longer be in evidence. The TE_{10} modal fields, although present, are swamped by the source fields and the field combination produces the distorted pattern shown (*Figure 6.6.3–8*). For an input power level of 1 kW the distortion extends about 600 m into the panel.

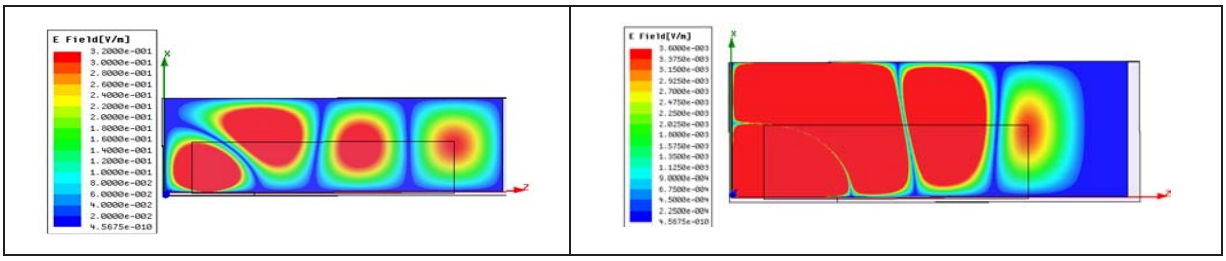

Figure 6.6.3–9 : E-field distribution, for various coal and shale conductivity (example iii)
E_y- field distribution in seam when σ_{shale} = 1 S/m and $\varepsilon_{r\text{-}shale}$ = 20 with $\varepsilon_{r\text{-}coal}$ = 10
Left: σ_{coal} = 1μS/m, Right: σ_{coal} = 100μS/m

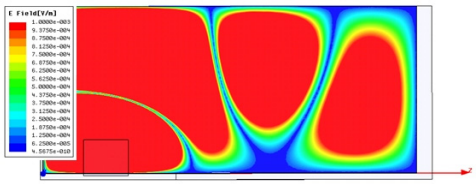

Figure 6.6.3–10 : E-field distribution, for various coal and shale conductivity (example iv)
E_y- field distribution in seam when σ_{shale} = 100 mS/m and $\varepsilon_{r\text{-}shale}$ = 20
with σ_{coal} = 1μS/m and $\varepsilon_{r\text{-}coal}$ = 10 (667 m long)

From the above results it is clear that for high coal conductivity (tanδ ≥ 1.0) the modal pattern in the panel waveguide becomes very weak. This is not surprising. More unexpectedly however is that the modal pattern can be swamped by non-modal fields, particularly close to the port or the source of the EM excitation. On the basis of fundamental propagation studies, supported by full-wave electromagnetic simulations of a lossy panel waveguide, the following conclusions have been drawn.

1) The set up of the modal fields in the coal seam waveguide depends on the electrical conductivity of coal and shale layers. TE_{10} mode propagation is predicted to be detectable 1000 m into a 300 m wide by 6 m high rectangular coal panel for which ε_r = 10 at a frequency f > 158 kHz, and at an injected power level of ~1 kW, provided the conductivity of the coal (σ) is less than 100 μS/m (tanδ ≈ 1) and the shale layers' conductivity forming the coal seam waveguide is about 5 S/m. This implies that the coal cannot be too wet. When the shale is less conductive, i.e. < 1 S/m and/or the coal seam is more conductive, i.e., > 100 μS/m, the energy losses into the shale and coal layers prevent the formation of the TE_{10} mode. Any increase in the excitation power to compensate for the shale and coal losses introduces distortion by the local non-modal source field near the excitation region. The field results in *Figure 6.6.3–9* and *Figure 6.6.3–10* demonstrate that at a given coal conductivity (or loss) a decrease in the shale conductivity increases the distortion due to the increased EM field leakage into the shale layers.

2) The modelling evidence is that there is an injected power level 'window' within which a detectable or discernible mode can be set up in a lossy geological stratum such as a coal seam. If the injected power is too low the modal fields are lost in noise; if they are too high, in order to overcome high power loss, the modal fields may be undetectable because they are swamped by the local non-modal source fields. For example with 1 kW of injected power, for a panel with σ_{coal} > 100 μS/m and σ_{shale} = 5.0 S/m, the TE_{10} mode will be distorted at < 600 m and no longer detectable at > 900 m, see *Figure 6.6.3–8* (right).

3) For a panel with reflecting end walls a longitudinal standing wave pattern is predicted for the 300 m wide by 6 m high by 1000 m long panel provided the conductivity of the coal is less than 100 μS/m. This Figure will depend on the particular standing wave pattern which is formed. For a coal panel with the above dimensions and for which ε_r = 10 and σ = 100 μS/m the TE_{10} standing wave resonance occurs at 260 kHz, and at a power level in the range 1 kW to 10 kW

4) In a very wet or electrically lossy geological layer (σ > 0.003 S/m), TE_{10} mode formation will not occur in a layer which is more than ~50 m wide.

6.6.3.4 Excitation Power Levels to Establish Resonance

This section presents model results for the power requirements to establish resonance in the coal seam waveguide using the GEM technique with an E-field of 1 mV/m (panel length 1000 m for 300 m × 6 m × 1000 m) coal seam waveguide as a function of coal conductivity, (σ_{coal} = 100 μS/m to 0.1 μ S/m, $\varepsilon_{r\text{-}coal}$ = 10) with shale conductivity (σ_{shale} = 5.0 S/m and 1.0 S/m and $\varepsilon_{r\text{-}shale}$ = 20). See *Figure 6.6.3–11*.

The results demonstrate that for lossy coal (σ > 100 μS/m) sandwiched between layers of shale (5 S/m and 1 S/m respectively) it will not be possible to detect the presence of the TE_{10} mode at the far end of a 2000 m coal panel (e.g., Daw Mill) unless a very high level of power can be injected into the seam. But, as we have seen (see the coal/shale conductivity study section), at these kinds of power levels the modal fields are liable to be swamped by the source near fields closer to the port. An increase in the coal conductivity increases the EM field attenuation in coal seam. Thus for a given length the required power to establish resonance in a coal panel significantly increases with the increase of coal conductivity. Excessive losses in the coal introduce distortion in the resonance modal pattern.

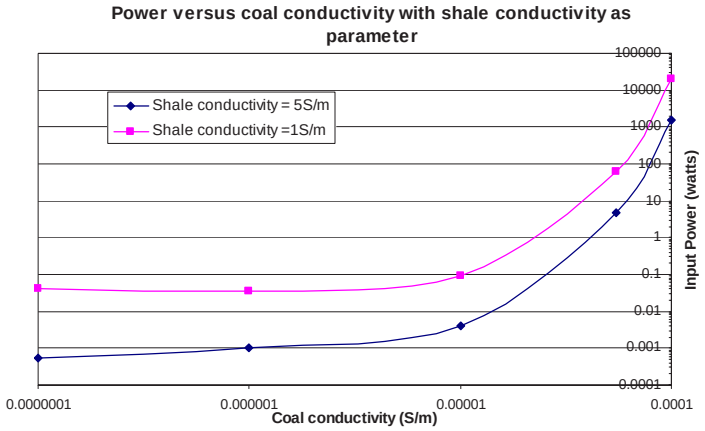

Figure 6.6.3–11 : to establish resonance for GEM versus coal conductivity
E-field Magnitude = 1 mV/m at 1000 m from Input, Panel 300 m Wide × 6 m Thick, ($\varepsilon_{r\text{-}coal}$= 10 and $\varepsilon_{r\text{-}shale}$ = 20

For a panel with reflecting end walls a longitudinal standing wave pattern is predicted for the 300 m wide by 6 m high by 1000 m long panel provided the conductivity of the coal is less than 100 μS/m. For a coal panel with the above dimensions and for which ε_r = 10 and σ = 100 μS/m the TE_{10} standing wave resonance occurs at 260 kHz, and at a power level in the range 1 kW to 10 kW. In low coal conductivity (low coal loss) regime the required power to establish resonance exponentially increases with the length of the coal panel. An increase in shale conductivity decreases the power required to establish resonance in the coal panel by decreased the power loss into the shale.

6.7 WP 7 MODELLING

6.7.1 Appendix to Task 7.1

Geomechanical numerical models were constructed to predict mining induced stress changes around an underground cavity as well as associated subsurface and ground surface deformations. Two benchmark models were defined relevant to two main mining application areas: conventional long-wall extraction and underground coal gasification. The benchmarks are not site-specific; however, the geological settings and the material (i.e. geomechanical) properties have been inspired by the interpreted data from the Daw Mill Colliery (Task 7.3). Task 7.1 comprises a tool comparison component as each of the three project partners involved in this work package (Heriot-Watt, Geocontrol and TNO) used a different numerical tool for geomechanical simulations.

6.7.1.1 Case 1: Subsidence Above Longwall Coal Mine

Case 1 is a synthetic case of subsidence prediction above a longwall coal mine based on subsidence prediction example 1 from the Subsidence Engineers' Handbook (SEH; National Coal Board, 1975). SEH provides subsidence solutions based on empirical data from the extensive history of longwall coal mining operations in UK. The existing empirical solutions from the UK practice were used to evaluate the predictive capability of different numerical tools used for subsidence prediction. Subsidence calculations following the SEH approach have been automated by the program called MulPan (Multiple Panel) Ground Movement Prediction System (British Coal HQTD, 1987), which was made available to the present study. The subsidence profiles obtained by numerical modeling were compared with the solutions given by SEH/MulPan.

The modelling objective in Case 1 was to calculate subsidence profiles above a longwall coal mine for a full face advance of 420 m (See *Figure* below). An optional task considered subsidence prediction for a face advance of 150 m. The material properties of coal were given (density ρ=1.7 t/m^3, Young's modulus E=3.5 GPa, Poisson's coefficient υ=0.3, cohesion c=1.1 MPa and friction angle ϕ=34°). The material properties of overburden were not prescribed. The sensitivity of subsidence to the material properties of overburden was investigated in several calculation scenarios.

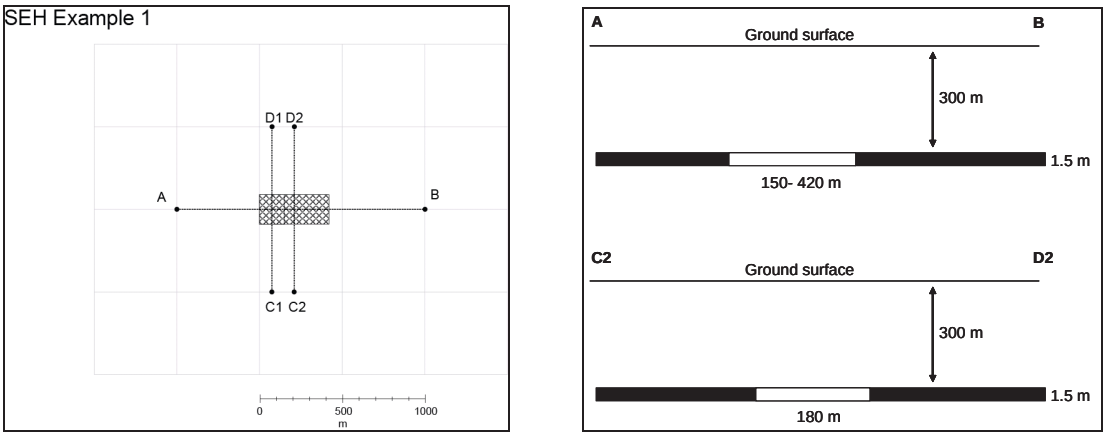

Figure 6.7.1–1 : Test case 1: subsidence above longwall coal mine
left: Top view of a longwall coal mine for a full face advance of 420 m.
right: Profiles A-B and C2-D2 through a longwall coal mine.

Numerical tools used for subsidence calculations were: (i) two finite element (FE) codes called SavFem (SavFem, -) and Diana (Diana, 2008); (ii) a finite difference code FLAC3D (FLAC, 2007); and (iii) the program called AEsubs, which is a semi-analytic tool for subsidence prediction (Fokker and Orlic, 2006). HWU and TNO used a two-dimensional (2D) finite element modelling approach since in the case of a full face advance (420 m) the plane strain conditions apply and modelling can be performed in two dimensions. Geocontrol used a full 3D finite difference FLAC3D model for subsidence calculations (because of the symmetry, only a quarter of the mine was modelled).

The following assumptions were used in all the numerical models: (i) three zones of disturbance with different material properties were differentiated over a mine cavity: the caved zone, the fractured zone and the undisturbed zone; (ii) the cavity and the caved out zone were completely filled in with the caved waste material (goaf) which supports the roof of the caved zone; (iii) the material properties for the models were developed from the relationships and factors given by Wilson (1981) for typical UK Coal Measures rocks and the data from the Daw Mill Colliery; (iv) the material properties and the stress-strain relations for the goaf were obtained from literature (Yavuz, 2004). Three scenarios were developed for each of the typical geological settings assuming: (i) strong and hard strata lithology (Unconfined Compressive Strength UCS ~ 50 MPa); (ii) medium strong strata lithology (UCS ~ 30 MPa); and (iii) soft and weak strata lithology (UCS ~ 15 MPa). The Mohr-Coulomb material model was used in Diana models and the Drucker-Prager criterion in SavFem models. In FLAC models, a Double Yield (DY) material model was used for the goaf, while a Mohr-Coulomb material model was used for other materials.

The results in the *Figure* below show a comparison between the individual numerical modelling results and the empirical solution obtained by using SEH/MulPan. The SavFem's results (top) and the Diana's results (middle) show increasing surface subsidence with reducing strength of the strata lithology. However, in all cases the magnitude of the modelled subsidence is less than predicted by SEH/MulPan. In addition, the subsidence profiles do not exhibit the more localised maxima directly over the panel. This is mainly due to the arching effect which causes re-distribution of the overburden load above the excavation to the abutting undisturbed strata. It may still be possible to improve the finite element model results by reducing the stiffness of the overburden, but the overall shape of the profile is difficult to match to the SEH/MulPan empirical profile, which depicts the maximum possible subsidence compiled from numerous field observations. The subsidence profiles similar to the SavFem's results (*Figure 6.7.1–2*, left) with the shallow subsidence profiles were also obtained by AEsubs (*Figure 6.7.1–2*, middle), which has been developed for subsidence prediction above compacting hydrocarbon reservoirs. FLAC 3D simulations, carried out with the large strain hypothesis, resulted in the best match with the SEH/MulPan subsidence profile (*Figure 6.7.1–2*, right). Using a Double Yield material model for the goaf, which can cope with significant irreversible compaction, and iteratively changing the input parameters for this material model, it was possible to obtain a good match between the SEH/MulPan and FLAC 3D subsidence profiles (case 3a in *Figure 6.7.1–2*, right).

6.7.1.2 Case 2: Induced Changes in Stresses and Deformations Around Mining Caverns in Coal

Case 2 investigated the influence of different roof strata lithologies on stress distribution and deformation around a cavern in coal. In particular, it was investigated how the inhomogeneous roof lithology affects the spatial extent of stress perturbation and plastic deformation around a cavern.

The induced stress and deformation were calculated for a 6 ×3 m cavern (excavation phase 1) and a 30 ×3 m cavern (excavation phase 2) assuming that the roof consists of a horizontal sequence of alternating, 2 m-thick layers of mudstone, sandstone and coal. Because of the symmetry, only a half of the cavern had to be modelled (Figure 6.7.1–3).

Different values of geomechanical properties were assigned to various lithologies: (i) coal: density ρ=1.7 t/m3, Young's modulus E=3.5 GPa, Poisson's coefficient υ=0.3, cohesion c=1.1 MPa and friction angle ϕ=34°; (ii) sandstone: ρ=2.3 t/m3, E=15.5 GPa, υ=0.2, c=6.3 MPa and ϕ=35°; and (iii) mudstone: ρ=2.3 t/m3, E=12.4 GPa, υ=0.25, c=2.8 MPa and ϕ=19°.

The numerical tools used for calculations were the same as in the case of Test case 1: Herriot Watt used finite element code SavFem (SavFem, -), TNO used finite element code Diana (Diana, 2008), and Geocontrol used a two-dimensional version of the finite difference code FLAC (FLAC, 2007). The numerical models were developed as plane strain models. In the FLAC model, the large strain

hypothesis was used and interface elements were introduced along all edges of the cavern in order to simulate correctly potential roof collapse.

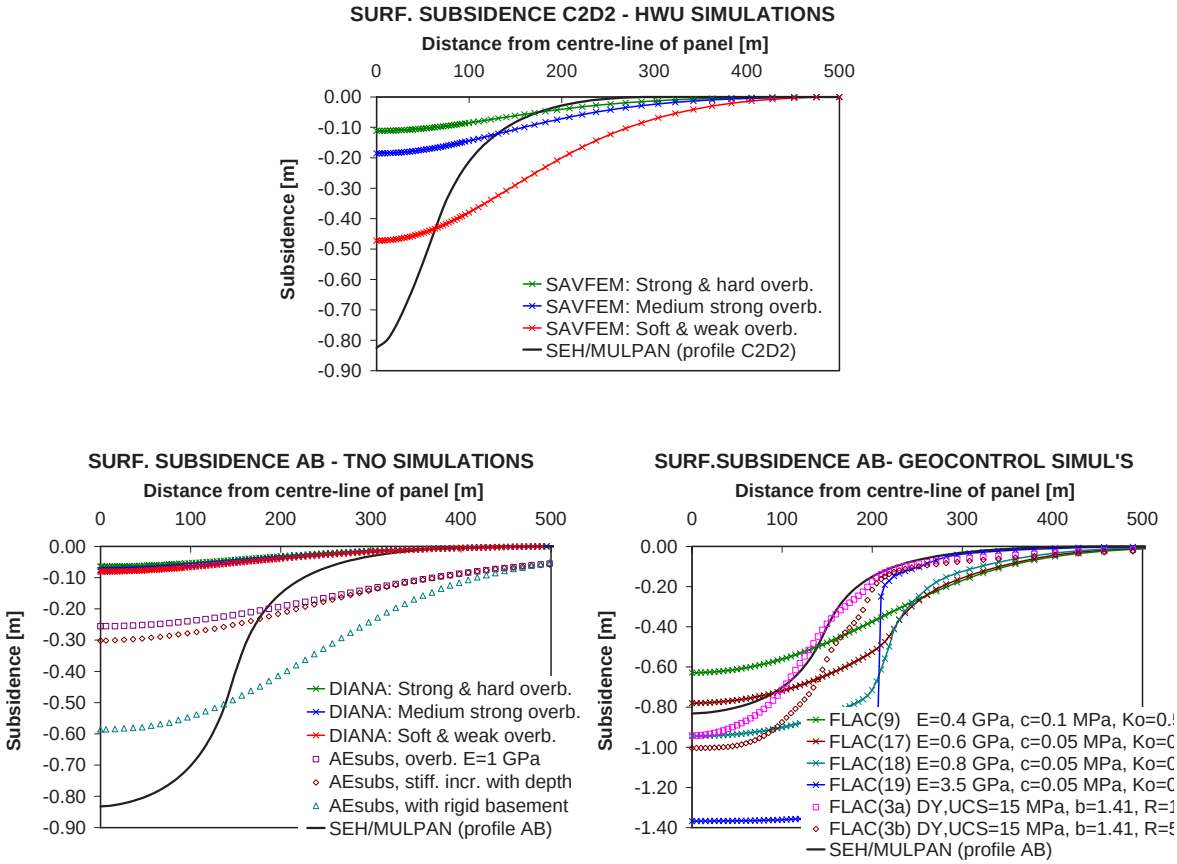

Figure 6.7.1–2 : Surface subsidence
along profile A-B calculated by Herriot-Watt (top), TNO (bottom left) and GEOCONTROL (bottom right). Legend: E-Young's modulus, DY-Double Yield model, UCS-Unconfined Compressive Strength, b-bulking factor, R-ratio of elastic to plastic bulk modulus.

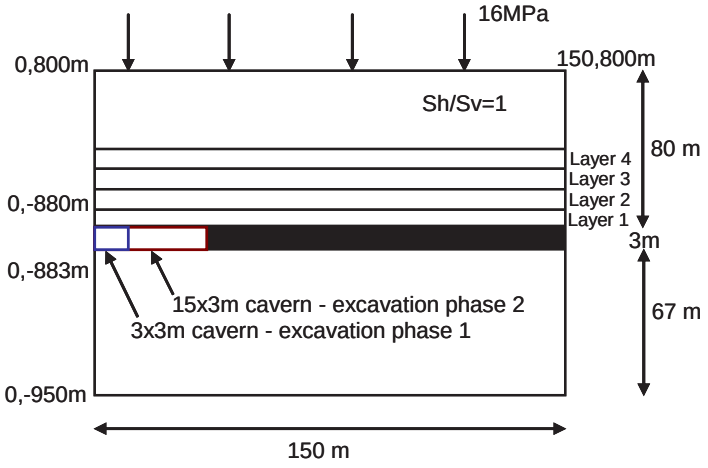

Figure 6.7.1–3 : Test case 2. changes in stresses and deformation
Left hand edge represents the centre-line of a mining cavity in coal

The models represent detailed roof strata geometry in the surrounding of the mine cavity and do not extend towards the ground surface. A uniformly distributed load of 16 MPa acting on top of the models was prescribed to compensate for the weight of overburden not included in the numerical models. Horizontal displacements were not allowed on lateral edges of the models, while vertical displacements were not allowed on the bottom boundary.

The models were loaded in three phases (load steps): (i) stress initialisation with the applied gravity load and the prescribed distributed load (the initial vertical and horizontal stresses were equal); (ii) creation of 3 m wide cavity with applied internal hydrostatic pressure; and (iii) creation of 15 m wide cavity with applied internal hydrostatic pressure.

Several scenarios were calculated to investigate how the variation in roof strata lithology influences the spatial pattern of stress and deformation around the cavity. Two reference cases were defined without variations in roof lithology: one with a sequence of mudstone layers and another with a sequence of sandstone layers. Other scenarios considered possible combinations of one or two coal layers inter-layered between either mudstone or sandstone layers.

The calculation results were presented in the form of: (i) stress profiles, one vertical profile along the centre-line of the cavern and one horizontal profile through the middle of the cavern; and (ii) contour plots showing the extent of the induced stress, strain and plasticity zone around the cavern.

The results in the *Figure* below show a comparison of stress profiles along the centre-line of the model for both excavation phases for the Reference case with mudstone sequence. The prediction obtained by using the FE packages SavFem and Diana were very similar. However, the FLAC results were very different from the other two due to the lack of the internal hydrostatic load in cavern. Other important observations were that inhomogeneous roof strata lithology largely affects the extent of plasticity and fractured zones above the cavity. Mudstones are generally weaker than sandstones and promote development of more extensive plasticity zones in the roof than sandstones, especially in scenarios with sequences of coal layers in-between mudstones. The key material properties that largely determine the extent of plasticity and fractured zones around the modelled cavity are the tensile and shear strength of each rock type in the roof strata sequence.

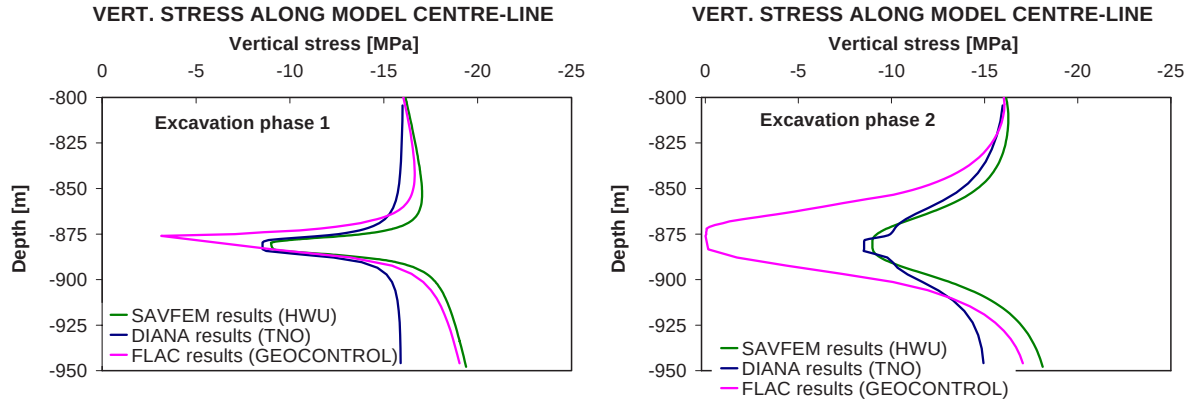

Figure 6.7.1–4 : Vertical stress along the model centre-line
for excavation phase 1 (left) and excavation phase 2 (right). Reference case with mudstone sequence without variation in roof strata lithology

6.7.2 Appendix to Task 7.3

6.7.2.1 Shared Earth Model

During the course of the project, continuously new information has become available. In order to efficiently and conveniently incorporate data from the exploration techniques being investigated in this project, the oilfield approach of a shared earth model has been applied to as described by Pringle *et al.* (2004) and Olden *et al.* (2001). Interpreted geo-scientific data and simulation results are integrated in the initial 3D geological model, for efficient communication, data sharing and visualisation of the results among the project partners.

A shared earth model (SEM) of the Daw Mill Colliery was initially constructed by TNO in Petrel 2005 and subsequently updated to Petrel 2007 upon its release during the course of the project. TNO co-ordinated all activities regarding this task. Throughout the project's lifetime an up-to-date version

of the Petrel shared earth model has been available to all project partners on the password-protected ADEMA web site.

Multiple 1D, 2D and 3D datasets have been integrated into a single 3D digital geological model, representing both in-situ as well as remote-sensing information. UK Coal provided a comprehensive data set of the Daw Mill mining area, consisting of a digital elevation model and topographic maps (indicating the extent of present workings and information on borehole and fault locations), as well as a 3D seismic cube and velocity and depth maps. During the course of the project additional data was produced and imported in the model, such as the acoustic impedance cube used by SIP. Data on roof boreholes and stress tests from UK Coal were introduced to the model, as is illustrated in the *Figure* below. The boreholes investigated in more detail are indicated as well.

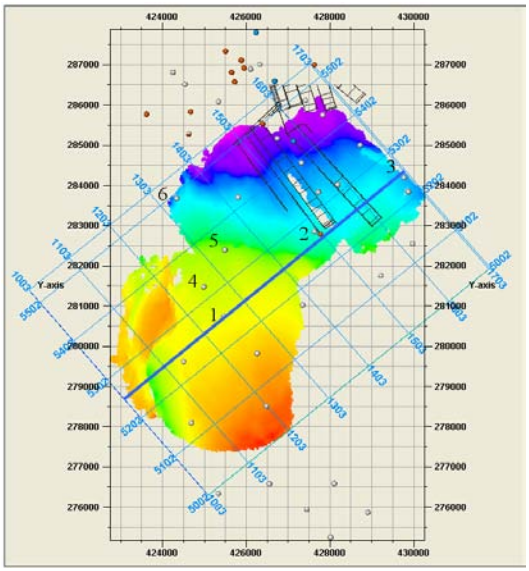

Figure 6.7.2–1 : Depth map of the Thick Coal Seam at Daw Mill (time domain), showing Inline 5250 in blue. Dots indicate well tops (grey), stress test locations (orange) and roof boreholes (blue). Boreholes: 1) Greenways Farm, 2) Hillfields, 3) Long Lady Wood, 4) Berryfield Farm, 5) Eaves Green Lane, 6) Keatleys Pool

6.7.2.2 Well Logs

Available well data on some 50 boreholes from the Daw Mill area was provided by UK Coal to TNO, comprising digital well logs (DLIS and TIF formats) as well as hardcopy drilling reports. However, only DLIS files were imported in the shared earth model, due to digital format incompatibility associated with the binary tape image files (TIF). Contribution of the latter to the quality and extent of the data set would be limited. Therefore, the laborious task of format conversion of these files to Petrel-compatible DLIS files was not further pursued. Moreover, the available digital well log headers typically lack information on well parameter units and rotary Table elevation above ordnance datum. With respect to the parameter units, standard industry units are presumed to be applied, legitimated by communication on this part with the British Geological Survey (BGS) and the general good agreement with typical log values in relation to certain lithologies. In order to obtain information on the relative elevation of the rotary Table level, the British Geological Survey was requested (through UK Coal) to provide TNO with additional ordnance datum information for the Daw Mill boreholes. This data was subsequently incorporated in the shared earth model. Data on ground level and/or drilling Table was gathered for all 22 targeted wells, enabling vertical referencing of the well log data.

6.7.2.3 Lithological Data

Specific attention was paid to three boreholes (Long Lady Wood, Hillfields and Greenways Farm boreholes) along inline 5250, which was used for seismic analysis and construction of the 2D

geomechanical model. Also Berryfields Farm, Eaves Green Lane and Keatleys Pool boreholes, situated off this inline. Lithological information for the six wells was derived from lithological descriptions and recognized formation boundaries based on reported drilling cuttings. The four main lithologies are defined as sandstone, siltstone, mudstone and coal. Rare occurrences of conglomerate and ironstone are neglected.

High resolution data was obtained especially for the lower part of the section, comprising the coal-bearing strata, while the upper part of the section is described in a more general manner. The typical time-lag and consequential misfit with true depth associated with cutting transport along the borehole was corrected using the coal spike of the Thick Coal Seam. Lithological distributions for these wells are confirmed by discrimination based on gamma ray, sonic and/or bulk density logs.

6.7.2.4 Geomechanical Parameters

Long Lady Wood and Hillfields boreholes show a complete set of relevant log types required for further evaluation. Therefore these wells were selected to derive a representative simplified lithological column and to estimate the elastic properties and strength of the overburden, which subsequently was used to construct the geomechanical model. Based on general experiences, Poisson's ratio (ν) was estimated at 0.4 for coal and at 0.33 for the clastic sediments. P- and S-wave velocities (V_p, V_s, in m/s) and Young's modulus (E, static and dynamic, in kPa) were derived using sonic (Δt, in μs/ft) and bulk density (ρ, in g/cm^3) logs according to the formulas stated below (Eissa and Kazi, 1988). Subsequently, the calculated values were differentiated per lithology, *Table* below.

$$V_P = \frac{10^6}{\Delta t \cdot 3.280839}, \quad V_S = V_P \sqrt{\frac{\nu - 0.5}{\nu - 1}}, \quad E_{dyn} = \rho V_s^2 \frac{3V_p^2 - 4V_s^2}{V_p^2 - V_s^2}, \quad E_{stat} = 0.64 \cdot E_{dyn} - 3.2 \cdot 10^5 \qquad (6.7.2\text{-}1)$$

Lithology	**Dynamic Young's modulus (GPa)**		***Static Young's modulus (GPa)***	
	mean	st. dev.	*mean*	*st. dev.*
Sandstone	27.05	13.34	17.31	8.54
Siltstone	24.31	6.72	15.56	4.30
Mudstone	18.37	5.10	11.76	3.27
Coal	6.08	2.28	3.89	1.46

Table 6.7.2–1 : Geomechanical parameters per lithology calculated from well log data

6.7.2.5 Seismic and P-Impedance Volume

Additionally, the comprehensive well database for the Daw Mill colliery was applied to derive a P-wave and density volume through the process of seismic inversion by SIP (for details see WP2). The increase in resolution achieved using the simultaneous inversion technology has allowed a revised Thick Coal Seam pick to be made. This was completed by hand in order to yield a high resolution top coal surface, which is incorporated in the Petrel shared earth model (*Figure 6.7.2–2*).

Figure 6.7.2–3 depicts a P-impedance map generated using a 10 ms mean amplitude window below the revised top thick coal pick. A general decrease in impedance to the south can be observed. The potential correlation of this phenomenon to improved or reduced coal quality or seismic tuning effects was investigated in more detail in Task 2.4 (Extraction of Rock Properties from Seismic data).

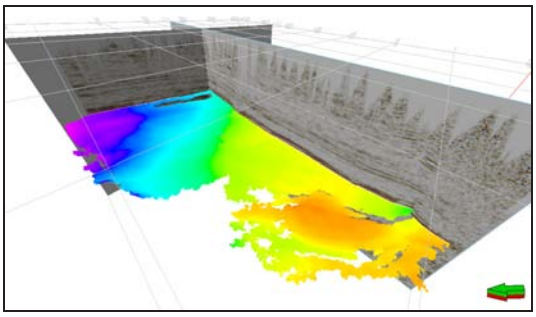

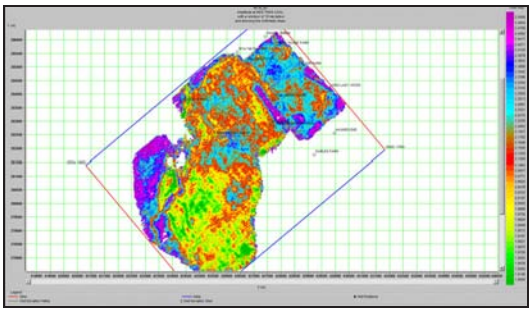

Figure 6.7.2–2 : seismic reflection of Thick Coal Seam
Automatically picked seismic reflection of Thick Coal Seam, inline 5250 and xline 1550 (in time domain).

Figure 6.7.2–3 : Post-stack inversion
of pre-conditioned seismic derivative density result for a window approximately corresponding to the Thick Coal Seam.

6.8 WP 8

There are no appendices to this work package.

6.9 WP 9

There are no appendices to this work package.

European Commission

EUR 24217 — ADEMA: Advances in exploration methods and applications

J. Wilson, T. Jowitt, J. Galera, C. Munoz, A. Lurka, G. Mutke, S. Lavu, R. Limacher, R. McHugh, P. Olden, R. Westerman, M. Bedford, D. Brenkley, J. Ford, D. Gibson, A. Fogg, T. Benedictus, S. Dortland, B. Orlic, F. van Bergen, B. Wassing, P. Winthaegen

Luxembourg: Publications Office of the European Union

2009 — 143 pp. — 21 × 29.7 cm

Research Fund for Coal and Steel series

ISBN 978-92-79-14549-0

doi:10.2777/884

ISSN 1018-5593

Price (excluding VAT) in Luxembourg: EUR 7